Technische Universität München

Exzellenzcluster "Origin and Structure of the Universe"

Study of rare B decays in the Standard Model and Beyond: The role of power corrections in global fits

Stefan J. Vickers

Vollständiger Abdruck der von der Fakultät für Physik der Technischen Universität München zur Erlangung des akademischen Grades eines

Doktors der Naturwissenschaften (Dr. rer. nat.)

genehmigten Dissertation.

Vorsitzender:		Univ.-Prof. Dr. Shawn Bishop
Prüfer der Dissertation:	1.	Senior Lecturer Dr. Martin Gorbahn University of Liverpool, United Kingdom
	2.	Univ.-Prof. Dr. Alejandro Ibarra

Die Dissertation wurde am 21.07.2014 bei der Technischen Universität München eingereicht und durch die Fakultät für Physik am 02.09.2014 angenommen.

Technische Universität München

Doctoral Thesis

Study of rare B decays in the Standard Model and Beyond: The role of power corrections in global fits

Author:
Stefan J. Vickers

Supervisor:
Dr. Martin Gorbahn

at the

Excellence Cluster Universe
Technische Universität München
D-85774 Garching

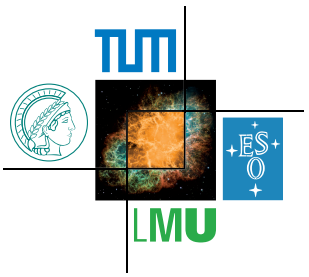

September 2014

ABSTRACT

We infer the size of weak-annihilation contributions in the framework of QCD factorisation from latest data of decay rates, strong phases and CP asymmetries of charmless hadronic $B \to M_1 M_2$ decays that are mediated by $b \to (d, s)$ QCD- and QED-penguin operators, such as $B \to (K\pi, K\eta^{(\prime)}, KK)$, $B \to (K\rho, K\phi, K\omega, K^*\pi, K^*\eta^{(\prime)})$, $B \to (K^*\rho,\, K^*\phi,\, K^*\omega,\, K^*K^*)$ and, $B_s \to (\pi\pi,\, K\pi,\, KK,\, K^*\phi,\, K^*K^*,\, \phi\phi)$, admitting one phenomenological parameter per final state system $M_1 M_2$. Beyond the Standard Model, we study the possibility to determine simultaneously the phenomenological weak-annihilation and new-physics parameters from data, employing model-independent scenarios with an enhanced electroweak Standard Model sector, an enhanced Z-penguin coupling and an extended operator basis, with $\mathcal{O}^b = (\bar{s}b)\,(\bar{b}b)$ as well as including complementary constraints from $b \to s\gamma$ and $b \to s\ell^+\ell^-$. The impact of these scenarios on so far unmeasured CP-violating observables in, for instance, $\bar{B}_s \to \phi\phi$ and $\bar{B}_s \to \bar{K}^{*0}K^{*0}$, which will become available in the foreseeable future from the LHCb and Belle II collaborations, is discussed.

ZUSAMMENFASSUNG

Wir leiten die Größe von weak-annihilation Beiträgen im Kontext von QCD Faktorisierung anhand aktueller Daten bezüglich Zerfallsraten, starken Phasen und CP Asymmetrien für charmlose, hadronische $B \to M_1 M_2$ Zerfälle, welche mittels $b \to (d, s)$ QCD- und QED-Pinguinoperatoren vermittelt werden, wie zum Beispiel $B \to (K\pi, K\eta^{(\prime)}, KK)$, $B \to (K\rho, K\phi, K\omega, K^*\pi, K^*\eta^{(\prime)})$, $B \to (K^*\rho,\, K^*\phi,\, K^*\omega,\, K^*K^*)$ sowie auch $B_s \to (\pi\pi,\, K\pi,\, KK,\, K^*\phi,\, K^*K^*,\, \phi\phi)$, ab, wobei jeweils ein phenomenologischer Parameter für jedes Endzustandssystem angenommen wird. Jenseits des Standard Models studieren wir die Möglichkeit, die phenomenologischen weak-annihilation und Neuen Physik Parameter gleichzeitig aus den Daten zu bestimmen, wobei wir modelunabhängige Szenarien mit einem verstärkten elektroschwachen Standard Model Sektor, einer verstärkten Z-Pinguin Kopplung, sowie einer erweiterten Operatorbasis mit $\mathcal{O}^b = (\bar{s}b)\,(\bar{b}b)$, verwenden, als auch die Hinzunahme von komplementären Einschränkungen von $b \to s\gamma$ und $b \to s\ell^+\ell^-$. Die Auswirkungen dieser Szenarien auf bisweilen ungemessenen CP verletzenden Observablen für z.B., $\bar{B}_s \to \phi\phi$ und $\bar{B}_s \to \bar{K}^{*0}K^{*0}$, die in absehbarer Zeit vom LHCb und Belle II Experiment verfügbar sein werden, werden diskutiert.

Contents

List of Figures

List of Tables

Abbreviations

ADM	**A**nomalous **D**imension **M**atrix
ATLAS	**A** **T**oroidal **L**HC **A**pparatu**s**
CERN	**C**onseil **e**uropéen pour la **r**echerche **n**ucléaire
CKM-matrix	**C**abibbo-**K**obayashi-**M**askawa-matrix
CLEO	**Cleo**patra collaboration
CMS	**C**ompact **M**uon **S**olenoid
CR	**c**redibility **r**egion
DONUT	**D**irect **O**bservation of the **NU** **T**au
EFT	**E**ffective **F**ield **T**heory
EWH	**E**ffective **W**eak **H**amiltonian
FCNC	**f**lavour-**c**hanging **n**eutral **c**urrent
HS	**h**ard-**s**pectator scattering
LCDA	**l**ight-**c**one **d**istribution **a**mplitude
LCSR	**l**ight-**c**one **s**um **r**ules
LHC	**L**arge **H**adron **C**ollider
LHCb	**L**arge **H**adron **C**ollider **b**eauty
NP	**n**ew-**p**hysics
QCD	**q**uantum **c**hromo**d**ynamics
QCDF	**QCD** **f**actorisation
QED	**q**uantum **e**lectro**d**ynamics
RGE	**r**enormalisation **g**roup **e**quation
SM	**S**tandard **M**odel of particle physics
WA	**w**eak **a**nnihilation

Dedicated to my family.

Chapter 1

Introduction

The Standard Model of particle physics (SM) describes successfully the interactions of fundamental particles under the strong, weak, and electromagnetic forces, which are embedded through local gauge invariance under the gauge group $G_{\mathrm{SM}} = \mathrm{SU(3)_C} \times \mathrm{SU(2)_I} \times \mathrm{U(1)_Y}$. This symmetry group can be separated into two distinct sectors. The strong interaction give rise to hadronic bound states, such as mesons, baryons, and nuclei. The dynamics of the constituents, quarks and gluons, is created by the colour charge they carry and determined by the local $\mathrm{SU(3)_C}$ gauge group, usually denoted by the theory of quantum chromodynamics (QCD). Due to its non-Abelian nature, QCD is asymptotically free, which means that it becomes strongly coupled below and weakly coupled above some energy scale Λ_{QCD}. As a consequence of this, colour charged objects, like quarks and gluons, cannot be separated and only occur in colour-singlet combinations as mesons and baryons, which is known as colour confinement. Strongly coupled theories do in principle not allow to calculate scattering amplitudes at low energies in ordinary perturbation theory. This implies that determining observables of processes in which QCD interactions at small momentum transfer are involved become a rather complicated problem.

The residual symmetry is part of the electroweak theory from Glashow, Weinberg, and Salam [5–7]. It successfully describes the unification of the weak and electromagnetic interaction of particles through the spontaneously symmetry breaking of $\mathrm{SU(2)_I} \times \mathrm{U(1)_Y} \rightarrow \mathrm{U(1)_Q}$ by the vacuum expectation value of a scalar field. This mechanism is known as the Brout-Englert-Higgs mechanism [8–13], which predicts the existence of a fundamental scalar particle and was originally invented to obtain fermion masses in a local gauged theory. The fermion masses are obtained from the interaction terms in the Lagrangian between two fermions and a scalar, so called Yukawa interactions, when the scalar field takes on its vacuum expectation value and are sources of interesting observations in the SM. For instance, the rotation of the quark fields into

their physical mass eigenbasis generates, on the one hand, a CP-violating phase, represented through the Cabibbo-Kobayashi-Maskawa-matrix (CKM-matrix), and on the other hand, flavour-violating charged currents which subsequently introduce flavour-violating neutral currents (FCNCs) at the loop level.

After the discovery of the top quark in 1995 [14, 15] and the tau neutrino in 2000 [16], both at the Tevatron, the scalar particle of the SM — the Higgs particle — was for a long time the solely unobserved piece of this theory. Roughly 50 years after its postulation, finally a boson with spin 0 and mass $m_S \simeq 126\,\text{GeV}$ was found in 2012 by the two experiments CMS [17] and ATLAS [18] of the large hadron collider (LHC) at CERN. Experimental effort was made on the measurement of its coupling to the known particle content and will carry on in the future. Due to the confirmation of its SM-like nature within today's available precision, the discovery of the Higgs particle was claimed, whereupon Englert and Higgs were awarded with the Nobel Prize in 2013. Due to the outstanding success of the SM in describing the fundamental nature of particle interactions and after it had been experimentally fully established, the question arises whether this is the end of the story about particle physics. The answer to this is no.

Apart from the above-described forces, we also know of gravitation, which is not included into the SM. This force is extremely weak at energies accessible at particle accelerators, but becomes strongly coupled at the Planck scale, $\Lambda_{\text{Pl.}} \sim 10^{19}\,\text{GeV}$. This implies that the SM can only be an effective description, valid within a certain energy range. Therefore, the question that physicists are concerned with nowadays is not whether the SM has to be extended, but rather at which scale. One hint towards the scale of new-physics, Λ_{NP}, delivers the stability condition of the Higgs particle vacuum expectation value against the age of the universe. However, this was studied with the quoted experimental value for the Higgs particle mass [19] and no additional new-physics (NP) below the Planck scale seems to be required. Further intriguing hints can be grouped into either conceptional or observational issues. Examples for the latter are the observation of neutrino oscillation, which implies that neutrinos necessarily have to be massive, the existence of dark matter and dark energy in the universe, for which no appropriate candidate in the SM exists, and, the matter anti-matter asymmetry, which requires more CP violation (Sakharov conditions [20]) than present in the SM.

All these observational facts are indeed true deficits of the theory, but unfortunately do also not require NP to enter below the Planck scale. Contrary, conceptional issues are somehow more vague and it is not clear if these problems should be treated seriously. They mainly concern the question whether certain parameters or patterns of the theory are just needed to be put in by hand or can be generated through dynamical assumptions. Lets discuss here two examples, whereas indeed more can be found. The existence of exactly three generations of leptons and quarks and the fact that the order of magnitude of their Yukawa couplings, which determine the masses of the fermions,

ranges for example for the masses of the quarks from $m_u \sim 2\,\text{MeV}$ up to $m_t \sim 173\,\text{GeV}$ is often referred to the flavour puzzle of the SM. The separation of scales by five orders of magnitude might hint towards a more fundamental theory that could explain this puzzle. Also the mass of the Higgs particle obeys a naturalness problem. Whereas the masses of the fermions and gauge bosons are protected from quantum corrections by the chiral, respectively gauge symmetry of the SM, the mass of the scalar is not. It is linked to the largest scale involved in the fundamental theory and connected to the scalar sector. If the largest scale is indeed given by $\Lambda_{\text{Pl.}}$, some miracle cancellation between 17 orders of magnitude has to be present to obtain a Higgs particle mass of the electroweak scale.

The most promising extensions of the SM which addresses the hierarchy problem are Composite Higgs Models, postulating the Higgs particle to be not fundamental (inspired by QCD with pions as light scalar particles), as well as supersymmetric models. Due to the strong coupling of the top quark to the Higgs particle field, the former class of models imply that the top quark necessarily has to be a composite particle, too. These theories typically require a top partner with $m_{t'} \lesssim 1\,\text{TeV}$. Supersymmetric models imposes a symmetry between fermions and bosons which, in case of an exact symmetry, lead to a complete cancellation of radiative corrections to the Higgs particle mass. We know that supersymmetry must be broken, but if the mass splitting between SM particles and their super-partners ($m_{susy} \sim$ TeV) is not too far from the electroweak symmetry breaking scale, quantum corrections still sufficiently cancel to explain the hierarchy problem. Both theories then imply the extension of the SM spectrum with sub-TeV particles, which can be directly searched for in high-energy collisions, as it is done at the LHC. So far, no further resonances have been found and bounds for masses of exotic particles are being pushed towards the TeV scale.

Complementary to direct searches of new particles are the indirect footprints of potential NP at high-energies in low-energy phenomena as, for instance, in electroweak precision observables, higgs, and flavour physics. Although the impact of a particular model on those observables strongly depend on the underlying dynamics, they have been extremely successful in constraining the structure and energy scale of physics beyond the SM. Observables in flavour physics, in particular from loop- and CKM-suppressed FCNC processes, are interesting because NP could become competitive to the SM contribution. B mesons, which contain one b quark, are the heaviest mesons. They offer the richest phenomenological playground in flavour physics. Their rare decays are triggered at the quark level by $b \to (d,\, s)$ transitions and were extensively studied in the past for various, radiative, (semi-)leptonic and hadronic decay modes. Most observables concerning these decay systems were measured during the last decade by the two electron-positron collider experiments BaBar at PEP-II (USA) and Belle at KEKB (Japan), taking data with an integrated luminosity of $\mathcal{L} = 424\,fb^{-1}$, respectively $\mathcal{L} = 1\,ab^{-1}$. At the end of 2009, also LHC entered the stage of flavour physics with a B physics program at the LHCb

detector. So far, data according to an integrated luminosity of $\mathcal{L} = 1\, fb^{-1}$ at a centre-of-mass energy $\sqrt{s} = 7\,\text{TeV}$ and $\mathcal{L} = 2\, fb^{-1}$ at $\sqrt{s} = 8\,\text{TeV}$ were recorded. Due to the higher production cross section, the experiments at LHC were already able to quote some most precise measurements for decay modes that can be measured despite the "dirty environment" at a hadron-collider. Examples are $\bar{B}_s \to \bar{K}^{*0} K^{*0}$ and $\bar{B}_s \to K^+\pi^-$. The experimental efforts will continue at the LHC, running between 2015–2018 at the designed centre-of-mass energy of 14 TeV and taking data at the LHCb experiment with an expected integrated luminosity of $2\, fb^{-1}$. After a main shutdown in 2018 and major LHCb detector upgrades, in order to collect data with a higher luminosity, further $\mathcal{L} = 45\, fb^{-1}$ are expected after roughly ten years. Together with the continuation of the Belle experiment by Belle II at SuperKEKB, with an expected 50 times larger integrated Luminosity of $50\, ab^{-1}$ until 2021/2022, observables in heavy flavour physics will become precisely measured.

With regard to the upcoming experimental precision, the key issue to indirect searches of new fundamental interactions is a profound control of SM contributions on the theory side. The source of uncertainties for both leptonic and semi-leptonic observables mainly originate from hadronic inputs, like the decay constant of the B meson or form factors for which substantially improvements are expected in the future from lattice calculations. However, for hadronic decays we rely on calculations in the framework of QCD factorisation (QCDF) which suffers from some conceptual issues. In this framework, certain corrections to the decay amplitude elude from a consistent description in ordinary perturbation theory due to low-scale QCD interactions and are, although subleading in a power expansion of Λ_{QCD}/m_b, essential for a reliable phenomenological analysis. The most relevant power corrections are classified according to their Feynman diagram topologies. There are weak annihilation (WA) and hard-spectator scattering (HS) interactions. The attempt of a perturbative calculation results in a infrared divergence which is regularised by some uncontrolled soft gluon interaction and needs to be estimated through power counting arguments. These contributions are modelled through additional phenomenological parameters $\rho_{A,H}$ and typically included into the observables as uncorrelated source of uncertainty due to which NP contributions are hardly distinguishable from SM background. The present thesis addresses this problem through a simultaneous fit of NP and WA parameters under the assumption of universal WA among decay systems that are related via $(u \leftrightarrow d)$ quark exchange. We give our results according to this assumption within the SM in Chapter 5. Even though such a test does not rely on first principle calculations, but it can still be checked, whether the data renders power corrections subleading, as postulated by QCDF. We therefore introduce the ratio $\xi_3^A(M_1 M_2)$ which describes the relative amount of power corrections to the leading decay amplitude and determined its value from data for each decay system. Since we almost exclusively investigate QCD-penguin-dominated decay modes,

one naively expect similar contour regions from the individual decay systems. That this does not to be the case in general is discussed among pure WA-dominated decays in Section 5.2. Typically, a decay system contains up to eight observables which can be utilised to infer one complex WA parameter. Most fits are therefore tightly over-constrained and we would expect to observe discrepancies in the data if the assumption of universality were unjustified. Currently $B \to K\pi$ is the only decay system with serious tensions. Our prediction and the measured value for the difference of the two CP asymmetries in $\bar{B}^0 \to K^-\pi^+$ and $B^- \to K^-\pi^0$ differ significantly from each other. This result confirms the $\Delta A_{\rm CP}^{K\pi}$ puzzle, known from the literature. The discrepancy also occurs in other approaches that determine decay amplitudes as for example through symmetry arguments and is unlikely to be caused by underestimated WA contributions only. A potential solution to this due to other power corrections (HS) will be discussed in Section 5.1.4. Because our approach of fitting power corrections eliminates the largest source of uncertainty, we gain an additional tension in the ratio of branching ratios $R_n^B(K\pi)$.

This motivated us to confront hadronic data with model-independent contributions to certain effective couplings in the SM, in particular, to the Wilson Coefficients of the 4-quark QED-penguin operators in Section 6.1, to the effective Z-boson coupling to the flavour violating $b \to s$ transition in Section 6.2 and, at last, through an extended operator basis, $\mathcal{O}^b = (\bar{s}b)\,(\bar{b}b)$, in Section 6.3. The latter two scenarios can also be related to the above-mentioned (semi-)leptonic decays. We exclusively choose NP in $b \to s$ transition because these decay systems offer more data to infer NP and WA parameter simultaneously. The advantage of a model-independent approach is the tremendous simplification of the analysis. Whereas a specific model can obtain a large number of various new parameters, we concentrate on a rather small subset that can effectively account for the impact of several particular NP models on hadronic decays without the need of concerning constraints from for example direct searches. We quantify our results through bounds on these effective couplings and check whether the above-denoted tensions can be resolved. Because contributions to CP asymmetries naively requires new CP-violating phases, the NP couplings are left complex. This will have visible effects in certain not-yet-measured observables of semi-leptonic and hadronic decays which will be predicted for each considered scenario.

The concept and technical details of the Effective Weak Hamiltonian and QCDF approach, needed for the calculation of (semi-)leptonic and hadronic B-meson decays, are reviewed in Chapter 2 and Chapter 3, whereas the phenomenological interested reader might like to skip these chapters. An overview of the experimental data, available for (semi-)leptonic and hadronic decays, and the definition of the corresponding observables as well as the sets, used in our fits, are summarised in Chapter 4. Various technical details are collected in the appendices, describing the statistical treatment of our fit in

Appendix A and the anomalous dimension matrix (ADM) and NLO QCDF corrections for the new introduced operators $\mathcal{O}^b$ in Appendix C. Studying a total of twenty different QCD-penguin- and WA-dominated hadronic decay systems, we moved for the sake of clarity the SM fits of certain decay modes into Appendix B.

Part I

Theory

Chapter 2

Effective Weak Hamiltonian

The main work of solving physical problems is to find a theory that describes the underlying physics at its intrinsic scale (length, energy, velocity, ...) and to adopt the right approximations when discarding irrelevant physical phenomena at different scales, thereby simplifying also calculations. The energy E of a car, moving with velocity v, can be calculated by means of classical mechanics. Although we know that special relativity is a more fundamental theory in nature, classical mechanics can be seen as an effective description to lowest order in $\mathcal{O}(|v/c|)$, where c is the speed of light. As long as our desired precision does not undershoot this order parameter, the effective description prevents us from calculating tiny, unimportant corrections.

Similar simplifications for the calculation of low-energy amplitudes in Quantum Field Theory can be made by means of *Effective Field Theory* (EFT). Typically, the physical process of interest can be separated by a certain energy threshold Λ, which divides heavy degrees-of-freedom χ with masses $M_\chi > \Lambda$ from light degrees-of-freedom ϕ with masses $m_\phi < \Lambda$. If the fundamental theory is known, we can write down the Hamiltonian

$$\mathcal{H}_{\text{fund.}} = \mathcal{H}(\chi, \phi). \tag{2.1}$$

Being interested in processes taking place at energy scales much below the scale Λ, we can *integrate out* the heavy spectrum from the theory and write down the most general Hamiltonian respecting the symmetries of the underlying fundamental theory and containing only the light degrees-of-freedom

$$\mathcal{H}_{\text{eff.}} = \mathcal{H}_{\text{eff.}}(\phi) = \lim_{E<M_\chi} \mathcal{H}(\chi, \phi). \tag{2.2}$$

An expansion in powers of external momenta of the light fields ϕ introduces a finite number of local operators with dimension $d \leq 4$ (*relevant/marginal*) and an infinite number of local operators with dimension $d > 4$, *irrelevant*. At energies below the

threshold the *irrelevant* operators become less important with increasing dimension, such that we can truncate the series for a given accuracy [21]. The remnant of the high-energy physics manifest itself by the choice of allowed operators (symmetry) and the magnitude of their coefficients (energy scale), determined by a *matching calculation* or taken from data.

There are typically two reasons for the use of an EFT, for which Chiral Perturbation Theory [22, 23] and Fermi's Theory of Weak Interactions [24] are cited here as examples. The former is the low-energy EFT of Quantum Chromodynamics (QCD) and permits in many cases reliable calculations of decay properties for pions and kaons [25]. Although the fundamental theory of hadrons is known, perturbative QCD does not provide insights into the physics at energies below the charm quark mass due to the non-perturbative nature of its coupling constant α_s at low energies which necessitates the use of the effective description. Contrary to that, the underlying fundamental forces of the decay rate of a neutron into a proton, electron, and anti-electron neutrino were not known at the beginning of the last century, but could be correctly described by Fermi through the introduction of a local 4-fermion interaction in the Hamiltonian, written in a modern perspective,

$$\mathcal{H}_{\text{eff}} = \frac{G_F}{\sqrt{2}} \left(\bar{u}\,\gamma_\mu(1-\gamma_5)\,V_{ud}\,d\right)\,\left(\bar{\nu}_l\,\gamma^\mu(1-\gamma_5)\,l\right), \tag{2.3}$$

with V_{ud} the first element of the Cabibbo-Kobayashi-Maskawa (CKM) matrix [26, 27] and the effective coupling constant $G_F = 1.16637 \times 10^{-5}\,\text{GeV}^{-2}$ (Fermi constant) with mass dimension $[G_F] = -2$. Because Fermi's theory was yet a suitable, but effective description of some low-energy phenomena, identifying G_F with the energy scale up to which its effective description is valid

$$\frac{G_F}{\sqrt{2}} = \frac{1}{M_\Lambda^2}, \tag{2.4}$$

Fermi would have claimed the existence of a fundamental theory at the scale of $\mathcal{O}(10^2)\,\text{GeV}$ — the scale of electroweak symmetry breaking of the Standard Model (SM). The advantages of effective theories can be summarised as follows:

- Effective theories separate the dynamics at different distance scales and as such simplify — or enable — practical calculations.
- Effective theories allow to facilitate a bottom up approach. Instead of modelling physics at some high scale and investigating its effects on low-energy observables, we can use measurements to extrapolate to the high-energy regime.

EFT can also be applied to the physics of weakly-decaying B mesons. At least — restricting to the SM — three different energy scales are involved. The necessary flavour

change $b \to (d, s)$ takes place at the energy scale of the W-boson mass, $M_W \sim 80\,\text{GeV}$, whereas the energy of the decay in the rest-frame of the B meson is provided by $m_B \sim 5\,\text{GeV}$. The energy of binding quarks into mesons is given by the QCD cut-off scale $\Lambda_{\text{QCD}} \sim 0.2\,\text{GeV}$ at which QCD becomes strongly coupled. This implies the following hierarchy of scales

$$\Lambda_{\text{QCD}} \ll m_B \ll M_W. \tag{2.5}$$

Due to the separation between the electroweak scale and m_B, large logarithms will occur in calculations of QCD- and QED-radiative corrections, which spoil the convergence of the perturbation series and reliability of predictions. Rephrasing the problem through an EWH, a consistent resummation of large logarithms to all orders in perturbation theory can be achieved by means of *renormalisation group equations* (RGE). This is discussed in Section 2.1. We use Section 2.2 to define the EWH, needed in the present work, and to set up our notations. Chapter 3 is designated to the discussion of hadronic matrix elements. Here we will make use of the *QCD factorisation* framework (QCDF) [1, 28, 29], in which the hierarchy between m_B and Λ_{QCD} is utilised to show that a systematic calculation of higher-order corrections can be made reliably in the case of a 2-body B-meson decay into either two light or one light and one heavy meson.

A pedagogical introduction to EFT and their application in Particle Physics can be found in [30, 31] and references therein. The EWH formalism for B-meson decays are worked out in the publications of [32, 33] from which many aspects of the following discussion are inspired.

2.1 Renormalisation Group improved perturbation theory

The weak decay of a B meson is triggered by a flavour-changing process, taking place at the scale M_W. Because the maximal energy release in the decay is provided by the mass of the B meson, $p \sim m_B$, a low-energy effective theory of weak interactions seems to be desirable. Due to $m_B/M_W \ll 1$, we can expand any amplitudes in the full theory in powers of external momenta, p/M_W, and safely drop terms beyond leading order. Unfortunately, after taking QCD corrections into account, our calculation will contain terms of the form $\alpha_s^n\ (\alpha_s\ \ln(M_W/m_b))^k$. Though the strong coupling constant being not too large for energies above the hadronic scale, the product $\alpha_s\ \ln(M_W/m_b) \sim \mathcal{O}(1)$ spoils the convergence of our perturbation series.

In order to restore its validity, we will disentangle in a first step the two different energy regimes with the help of an EWH. This is achieved by integrating out all degrees-of-freedom with masses $M_\chi \geq \mu$ from the SM Hamiltonian and adding the arising local

operators that respect the symmetry of the SM gauge group $\mathrm{SU(3)_C \times SU(2)_L \times U(1)_Y}$

$$\mathcal{H}_{\mathrm{SM}}(\chi\,,\phi) \longrightarrow \mathcal{H}_{\mathrm{QCD\times QED}}(\phi) + \sum_i C_i(\mu)\mathcal{O}_i(\mu). \tag{2.6}$$

The described procedure introduces the renormalisation scale μ, which can be interpreted as the scale that separates short-distance from long-distance physics or as the validity limit for our low-energy effective theory. The infinite sum of local operators completely reproduces the features of the full Hamiltonian, but according to the above mentioned expansion in momenta of external fields, it will be sufficient to order the series by the dimension of the operators and keep up to dimension $d = 6$.

The Wilson Coefficients C_i are effective coupling constants and multiply the effective operators. They are obtained from a matching calculation at the separation scale μ. Under the requirement that the *amplitudes* — in the sense of amputated Green functions — in the full and effective theory are equal, the Wilson Coefficients can be computed to the desired accuracy in the strong and electromagnetic coupling constant and solely depend on the heavy degrees-of-freedom, parametrised through mixing angles and masses.

The truncation of higher-dimensional operators leads to the observation that the effective theory does not correctly reproduce the UV behaviour of the full theory implying additional divergence that need to be renormalised by an *operator renormalisation*

$$\mathcal{O}_i^{(0)} = Z_{ij}\mathcal{O}_j, \tag{2.7}$$

where $\mathcal{O}_i^{(0)}$ is the unrenormalised operator. As can be seen from Equation 2.7, the operator renormalisation constant Z_{ij} is given as a matrix with in general non-vanishing off-diagonal elements. As a consequence of renormalisation, the operators $\mathcal{O}_j$ mix into each other. A set of operators, needed to render all amplitudes finite, is called *closed under renormalisation*. It is worth to mention that the actual operator renormalisation is not affected from the specific choice of the physics beyond the high-energy scale.

The additional operator renormalisation can also be reinterpreted as the usual renormalisation of coupling constants as it is done for example in the renormalisation of the α_s in QCD. The according matrix-valued renormalisation constant for the Wilson Coefficients is defined as follows

$$C_i^{(0)} = Z_{ij}^c\, C_j. \tag{2.8}$$

Comparing the expressions for the effective amplitudes after renormalising either the operators or the coefficients, we find the relation

$$Z^c_{ij} = Z^{-1}_{ji}. \tag{2.9}$$

After the renormalisation of the full and effective amplitudes, we can determine the Wilson Coefficients, which include all information of the physics above μ and contain terms proportional to $\alpha_s \ln(M_W/\mu)$. The matching scale μ is typically chosen in the vicinity of M_W in order to guarantee that the Wilson Coefficients can be calculated in perturbation theory. However, because matrix elements of the local operators should be evaluated at $\mu \sim m_b$, we require a tool to evolve the Wilson Coefficients from the high-energy scale down to the low-energy scale. This can be achieved by means of RGE, which describes the dependence of renormalised quantities on the renormalisation scale μ and adds automatically large logarithms up to all orders in couplings. From the fact that bare quantities do not depend on the renormalisation scale, we can derive from Equation 2.8

$$\frac{d}{d\ln\mu} C_i(\mu) = \gamma_{ji}(\alpha_s)\, C_j(\mu), \tag{2.10}$$

where the *anomalous dimension matrix* (ADM) γ is defined in terms of the renormalisation constant Z from Equation 2.7

$$\gamma_{ij} \equiv Z^{-1}_{ij} \frac{d}{d\ln\mu} Z_{ij}. \tag{2.11}$$

The solution to Equation 2.10 automatically adds up the large logarithms in the Wilson Coefficients and can be expressed in a simple form

$$C_j(\mu_b) = U_{ij}(\mu_b, \mu_W)\, C_j(\mu_W), \tag{2.12}$$

where U_{ij} is the Evolution Matrix describing the dependence of the Wilson Coefficients between two different energy scales μ_W and μ_b.
At leading order the Evolution Matrix is given by

$$U^{(0)}(\mu_b, \mu_W) = \left(\frac{\alpha_s(\mu_W)}{\alpha_s(\mu_b)}\right)^{\frac{\gamma^0}{2\beta_0}}, \tag{2.13}$$

where β_0 is the leading order coefficient of the QCD β-function and γ^0 the leading order ADM in the expansion $\gamma = \frac{\alpha_s}{4\pi}\gamma^0 + \mathcal{O}(\alpha_s^2)$. The logarithm in $\alpha_s^{n=0}\ (\alpha_s \ln(M_W/m_b))^k$ are implicitly summed up and the Wilson Coefficients are obtained to the *leading log approximation*. A resumation of higher-order corrections, $\alpha_s^{n=j}\ (\alpha_s \ln(M_W/m_b))^k$, can

	C_1	C_2	C_3	C_4	C_5	C_6
$\mu = M_W$	0.983	0.052	0.001	-0.002	0.001	-0.002
$\mu = m_b$	1.08	-0.188	0.013	-0.035	0.009	-0.041
	C_7/α	C_8/α	C_9/α	C_{10}/α	$C_{7\gamma}$	C_{8g}
$\mu = M_W$	0.112	0.002	-1.009	-0.020	-0.188	-0.095
$\mu = m_b$	-0.016	0.057	-1.229	0.215	-0.304	-0.152

TABLE 2.1: Next-to-leading order 4-quark and dipole Wilson Coefficients given at the matching scale $\mu_W = M_W$ and the hadronic scale $\mu_b = m_b$ for $m_t(m_t) = 164\,\text{GeV}$, $\alpha_s(M_W) = 0.119$, and $1/\alpha(m_b) = 132$.

be obtained from the ADM $\gamma^j \sim (\frac{\alpha_s}{4\pi})^{j+1}$. A clear presentation of how the large logarithms are resumed can be found in [34]. At last, performing the matching calculation at the scale M_W, we find the necessary initial conditions $C_j(\mu_W)$ for the solution in Equation 2.12.

2.2 Effective Weak Hamiltonian for B decays

In the following we will define the EWH for B mesons decaying into two hadrons, into leptons/photons and at most one hadron, as well as the EWH for B^0-$\bar{B}^0$ mixing. While the focus of this work will reside on the phenomenology of hadronic decays, we want to set the stage to discuss correlations of a wider class of flavour observables in models beyond the SM. For the moment, our discussion is kept generic, concerning the two possible flavour-changing processes $b \to d$ and $b \to s$. Both transitions are investigated for the SM hypothesis in Chapter 5. In the case of physics beyond the SM, discussed in Chapter 6, we exclusively elaborate on $b \to s$ transitions.

2.2.1 $|\Delta B| = 1$ hadronic B decays

Restricting to the SM, the EWH for hadronic B-meson decays can be written in terms of twelve operators with non-vanishing Wilson Coefficients

$$\mathcal{H}_{\text{eff}} = \frac{G_F}{\sqrt{2}} \sum_{p=u,c} \lambda_p^{(D)} \left(C_1^p O_1^p + C_2^p O_2^p + \sum_{i=3}^{10} C_i O_i + C_{7\gamma} O_{7\gamma} + C_{8g} O_{8g} \right) + \text{h.c.}, \quad (2.14)$$

where $D = (d, s)$ and $\lambda_p^{(D)}$ is introduced as the short notation for the involved product of CKM-matrix elements, $\lambda_p^{(D)} \equiv V_{pb} V_{pD}^*$. In principal, the CKM-matrix elements are parts of the Wilson Coefficients, but in the SM it is common practice to factorise them. In writing Equation 2.14, we explicitly used the unitarity of the CKM-matrix, $-\lambda_t =$

$\lambda_u + \lambda_c$. The flavor-changing 4-quark and dipole operators are

$$\begin{aligned}
\mathcal{O}_1^p &= (\bar{p}_\alpha\, b_\alpha)_{V-A}(\bar{D}_\beta\, p_\beta)_{V-A}, & \mathcal{O}_2^p &= (\bar{p}_\beta\, b_\alpha)_{V-A}(\bar{D}_\alpha\, p_\beta)_{V-A},\\
\mathcal{O}_3 &= (\bar{D}_\alpha\, b_\alpha)_{V-A}\sum\nolimits_q (\bar{q}_\beta\, q_\beta)_{V-A}, & \mathcal{O}_4 &= (\bar{D}_\alpha\, b_\beta)_{V-A}\sum\nolimits_q (\bar{q}_\beta\, q_\alpha)_{V-A},\\
\mathcal{O}_5 &= (\bar{D}_\alpha\, b_\alpha)_{V-A}\sum\nolimits_q (\bar{q}_\beta\, q_\beta)_{V+A}, & \mathcal{O}_6 &= (\bar{D}_\alpha\, b_\beta)_{V-A}\sum\nolimits_q (\bar{q}_\beta\, q_\alpha)_{V+A},\\
\mathcal{O}_7 &= (\bar{D}_\alpha\, b_\alpha)_{V-A}\sum\nolimits_q \frac{3}{2}e_q(\bar{q}_\beta\, q_\beta)_{V+A}, & \mathcal{O}_8 &= (\bar{D}_\alpha\, b_\beta)_{V-A}\sum\nolimits_q \frac{3}{2}e_q(\bar{q}_\beta\, q_\alpha)_{V+A},\\
\mathcal{O}_9 &= (\bar{D}_\alpha\, b_\alpha)_{V-A}\sum\nolimits_q \frac{3}{2}e_q(\bar{q}_\beta\, q_\beta)_{V-A}, & \mathcal{O}_{10} &= (\bar{D}_\alpha\, b_\beta)_{V-A}\sum\nolimits_q \frac{3}{2}e_q(\bar{q}_\beta\, q_\alpha)_{V-A},\\
\mathcal{O}_{7\gamma} &= -\frac{em_b}{8\pi^2}\bar{D}_\alpha\,\sigma^{\mu\nu}(1+\gamma_5)F_{\mu\nu}\, b_\alpha, & \mathcal{O}_{8g} &= -\frac{g_s m_b}{8\pi^2}\bar{D}_\alpha\,\sigma^{\mu\nu}(1+\gamma_5)T^a_{\alpha\beta}G^a_{\mu\nu}\, b_\beta,
\end{aligned} \tag{2.15}$$

where $(\bar{q}\, q)_{V\pm A} = \bar{q}\gamma_\mu(1\pm\gamma_5)q$, the sum is over active quarks $q = (u, d, s, c, b)$, with e_q denoting their electric charge in units of $|e|$, and α, β denoting colour indices. $\mathcal{O}^p_{1,2}$ are known as *current-current* operators, $\mathcal{O}_{3-6}$ as *QCD-penguin* operators, $\mathcal{O}_{7-10}$ as *QED-penguin* operators, and $\mathcal{O}_{7\gamma,8g}$ as *electro- and chromo-magnetic dipole* operators.

The analytic formulas of the initial Wilson Coefficients as well as the ADMs for the present choice of operator basis can be found in [32, 33]. The Wilson Coefficients are calculated up to next-to-leading order in the strong and electromagnetic coupling constants. The RGEs are solved within the next-to-leading log approximation. As described in [29], we will use the modified counting scheme, in which the dominant part of the QED-penguin Wilson Coefficients, scaling with either $x_t = m_t^2/m_W^2$, with m_t the mass of the top quark, or with inverse powers of the weak mixing angle $1/s^2_{\mathrm{W}}$, are treated as a leading-order effect. The numerical values for the next-to-leading-order Wilson Coefficients are summarised in Table 2.1 at $\mu = M_W$ and $\mu = m_b$.

In general, new-physics (NP) scenarios can give additional contributions to the SM Wilson Coefficients or generate different additional operators as the ones given in Equation 2.15. Because the SM operator basis is closed under QCD and QED renormalisation, only new operators can mix into the SM operators, but not vice versa. A special class of operators are the χ-flipped operators. They are obtained by a global interchange of the projectors $\frac{1}{2}(1-\gamma_5) \leftrightarrow \frac{1}{2}(1+\gamma_5)$. We will denote these operators with a prime. Since the unbroken part of the SM symmetry, $\mathrm{SU(3)_C} \times \mathrm{U(1)_Q}$, does not distinguish between the left- and right-handed components of the fermionic fields, the solution to the RGE is equivalent. As we will see in Chapter 3, similar relations, up to an overall sign, can be found for the matrix elements of these operators.

In later parts of this work we will introduce different operators at the electroweak scale $\mu = M_W$ in order to study the impact of NP on B-meson decays in a model-independent way. As it is evident from the previous discussion, the Wilson Coefficients at the hadronic scale are just a linear combination of the Wilson Coefficients at the

electroweak scale. Therefore, it can be useful to quantify the impact of the high-scale onto the low-scale Wilson Coefficients. We introduce the normalised Evolution Matrix $\widetilde{U}$, defined as

$$\widetilde{U}_{ij}(\mu_b, \mu_W) = U_{ij}(\mu_b, \mu_W)\, \frac{C_j(\mu_W)}{C_i(\mu_b)}, \tag{2.16}$$

where no sum over the indices is understood.
As it is implicit from the definition, $\sum_j \widetilde{U}_{ij}(\mu_b, \mu_W) = 1$. The entries of the normalised Evolution Matrix describe the relative change of the low-scale Wilson Coefficient according to a relative change of the high-scale Wilson Coefficient by 1.

Referring to the four different kind of operators in the Standard Model basis mentioned above, we find the following sub-matrices $\widetilde{U}_{\text{c.c.}}$ with $(i,j) = (1,2)$, $\widetilde{U}_{\text{dip}}$ with $(i,j) = (7\gamma, 8g; 1, 2, 7\gamma, 8g;)$, $\widetilde{U}_{\text{QCD}}$ with $(i,j) = (3-6; 1-6)$ and, $\widetilde{U}_{\text{QED}}$ with $(i,j) = (7-10; 1, 2, 7-10)$, evaluated at the scales $\mu_W = M_W$ and $\mu_b = m_b$

$$\widetilde{U}_{\text{c.c.}} = \begin{pmatrix} 1.01 & 0 \\ 1.31 & -0.31 \end{pmatrix}, \qquad \widetilde{U}_{\text{QCD}} = \begin{pmatrix} 0.93 & 0 & 0.05 & 0 & 0 & 0 \\ 0.95 & 0 & 0 & 0.05 & 0 & 0 \\ 0.96 & 0 & 0 & 0 & 0.07 & 0 \\ 0.94 & 0 & 0 & 0 & 0. & 0.08 \end{pmatrix},$$

$$\widetilde{U}_{\text{dip}} = \begin{pmatrix} 0.56 & 0 & 0.41 & 0 \\ 0.52 & 0 & 0 & 0.44 \end{pmatrix}, \quad \widetilde{U}_{\text{QED}} = \begin{pmatrix} 6.20 & 1.42 & -6.69 & 0 & 0 & 0 \\ 0.26 & -0.09 & 0.71 & 0.06 & 0 & 0 \\ 0.07 & 0 & 0 & 0 & 0.91 & 0 \\ -0.07 & 0 & 0 & 0 & 1.17 & -0.10 \end{pmatrix}, \tag{2.17}$$

where only those entries are non-vanishing for which $|\widetilde{U}_{ij}| \geq 0.05$.
The following observation can be made from the normalised Evolution Matrix $\widetilde{U}$:

- The mixing of $C_1^p(M_W)$ into the other operator classes is a dominant effect. A subtle difference arises for the two possible flavour transitions. In the case of $|\Delta S| = 1$ decays, a large hierarchy between the CKM-matrix elements $\lambda_u^{(s)}/\lambda_c^{(s)} \sim 0.02$ is encountered. Only a modification of $C_1^c(M_W)$ implies large corrections to other Wilson Coefficients at the scale $\mu = m_b$. For $|\Delta D| = 1$, the CKM-matrix elements are of the same order $\lambda_u^{(d)} \sim \lambda_c^{(d)}$, such that both Wilson Coefficients $C_1^p(M_W)$ can influence the low-scale Wilson Coefficients through mixing effects.

- The impact of the colour-suppressed coefficient $C_2^p(M_W)$ on the other classes of operators is small, except for $C_7(m_b)$.

- The impact of the colour-allowed current-current coefficient $C_1^p(M_W)$ on the dipole operators is of the same order as their self-mixing.

	C_{9V}/α	C_{10A}/α
$\mu = M_W$	0.156	-0.330
$\mu = m_b$	0.324	

TABLE 2.2: Next-to-leading order semi-leptonic Wilson Coefficients given at the matching scale $\mu_W = M_W$ and the hadronic scale $\mu_b = m_b$ for $m_t(m_t) = 164\,\text{GeV}$, $\alpha_s(M_W) = 0.119$, and $1/\alpha(m_b) = 132$.

- The mixing of the colour-allowed current-current coefficient $C_1^p(M_W)$ into the QCD-penguin coefficients is the dominant effect. An $\mathcal{O}(1)$ modification of $C_3(M_W)-C_6(M_W)$ can almost be neglected.
- For the mixing into $C_7(m_b)$, a cancellation occurs between the contributions from $C_1^p(M_W)$ and $C_7(M_W)$, explaining its small value, which then mainly originates from the colour-suppressed current-current coefficient $C_2^p(M_W)$. $C_9(m_b)$ is dominated by its self-mixing and the colour-suppressed QED-penguin coefficients $C_{8,10}(m_b)$ are dominated by their colour-allowed counter-parts $C_{7,9}(M_W)$.

2.2.2 $|\Delta B| = 1$ (semi-)leptonic B decays

Many extensions of the SM provide additional contributions to the physics of B-meson decays. Within a concrete model, we can work out the Wilson Coefficients in terms of the fundamental parameters of the model. Correlations among all kinds of observables arise automatically. However, a model-independent analysis such as the modification of Wilson Coefficients can also introduce correlations: First, both decays depend on a common subset of the SM Wilson Coefficients $\{C_1(M_W) - C_6(M_W),\, C_{7\gamma}(M_W),\, C_{8g}(M_W)\}$. Second, additional operators can arise that influence the observables via mixing effects and contribute to both decay classes. In order to account for such effects we need to add to the EWH in Equation 2.14 the following terms

$$\mathcal{H}_{\text{eff}}^{\text{s.l.}} = 4\frac{G_F}{\sqrt{2}} \sum_{p=u,c} \lambda_p^{(D)} \left(C_{9V}\mathcal{O}_{9V} + C_{10A}\mathcal{O}_{10A}\right) + \text{h.c.}, \tag{2.18}$$

with the flavour-changing semi-leptonic operators

$$\mathcal{O}_{9V} = (\bar{D}\gamma_\mu P_L b)(\bar{l}\gamma^\mu l), \qquad \mathcal{O}_{10A} = (\bar{D}\gamma_\mu P_L b)(\bar{l}\gamma^\mu\gamma_5 l), \tag{2.19}$$

where we have used the abbreviation $P_L = \frac{1}{2}(1-\gamma_5)$.
The values of the Wilson Coefficients are given for the two renormalisation scales M_W and m_b in Table 2.2. The μ-dependence for C_{10A} is trivial because non of the operators mix into $\mathcal{O}_{10A}$ and as a conserved current under QCD there is even no self-mixing.

As in the previous subsection, we give the non-vanishing entries for the normalised Evolution Matrix $\widetilde{U}_{\text{s.l.}}(\mu_b, \mu_W)$ with $(i,j) = (9V;\, 1, 2, 9V)$,

$$\widetilde{U}_{\text{s.l.}} = \begin{pmatrix} 0.41 & 0.11 & 0.48 \end{pmatrix}. \tag{2.20}$$

The leading contributions to $C_{9V}(m_b)$ are almost equally provided by $C_1(M_W)$ and $C_{9V}(M_W)$. The mixing effect from $C_2(M_W)$ is rather small as in the case of the mixing into the 4-quark QED-penguin operators.

2.2.3 $|\Delta B| = 2$ B^0-$\bar{B}^0$ mixing

For completeness, we also specify the relevant EWH for B^0-$\bar{B}^0$ mixing

$$\mathcal{H}_{\text{eff}}^{|\Delta B|=2} = \frac{G_F^2}{4\pi^2} M_W^2 \left(\lambda_t^{(D)}\right)^2 \sum_i C_i \mathcal{O}_i + \text{h.c.}, \tag{2.21}$$

with the operators [35]

$$\begin{aligned}
\mathcal{O}_V^{LL} &= (\bar{D}_\alpha \gamma_\mu P_L b_\alpha)(\bar{D}_\beta \gamma^\mu P_L b_\beta), \\
\mathcal{O}_S^{LL} &= (\bar{D}_\alpha P_L b_\alpha)(\bar{D}_\beta P_L b_\beta), \qquad & \tilde{\mathcal{O}}_S^{LL} &= (\bar{D}_\alpha P_L b_\beta)(\bar{D}_\beta P_L b_\alpha), \\
\mathcal{O}_S^{LR} &= (\bar{D}_\alpha P_L b_\alpha)(\bar{D}_\beta P_R b_\beta), \qquad & \tilde{\mathcal{O}}_S^{LR} &= (\bar{D}_\alpha P_L b_\beta)(\bar{D}_\beta P_R b_\alpha).
\end{aligned} \tag{2.22}$$

Along with the χ-flipped operators $\mathcal{O}_V^{RR}$, $\mathcal{O}_S^{RR}$, $\tilde{\mathcal{O}}_S^{RR}$, a complete set of possible $|\Delta B| = 2$ operators is defined. Only the Wilson Coefficient C_V^{LL} receives contributions in the SM from box diagrams. Since the total number of operators is manageable, we already quoted operators that might arise only after the inclusion of physics beyond the SM, contrary to the previous subsections.

Chapter 3

Hadronic Matrix Elements

In the previous section, we discussed the necessity to introduce the EWH formalism for weakly-decaying B mesons. The Wilson Coefficients were calculated at the matching scale $\mu_W \sim M_W$ and evolved down by means of RGEs to $\mu_b \sim m_b$. In order to obtain physical decay amplitudes, we still have to calculate the matrix elements of the operators included in $\mathcal{H}_{\text{eff}}$ of Equation 2.14

$$\mathcal{A}_{\bar{B}\to M_1 M_2} = \langle M_1 M_2 | \mathcal{H}_{\text{eff}} | \bar{B} \rangle = \frac{G_F}{\sqrt{2}} \sum_{i,p} \lambda_p \, C_i^p(\mu_b) \, \langle M_1 M_2 | \, \mathcal{O}_i^p \, | \bar{B} \rangle \, (\mu_b). \tag{3.1}$$

The matrix elements describe how the quarks hadronise into the final-state mesons. The bound-state dynamics typically takes place at an energy scale Λ_{QCD}, at which the strong interaction cannot be treated in perturbation theory, which makes the determination of hadronic matrix elements a formidable exercise. Fortunately, for the decay of a B meson, we can utilise the hierarchy $\Lambda_{\text{QCD}} \ll m_b$. To lowest order in a expansion in Λ_{QCD}/m_b, one can show that QCD contributions to the matrix elements, $\langle M_1 M_2 | \, Q_i^p \, | \bar{B} \rangle$, factorise into universal, simpler, non-perturbative objects, like form factors and decay constants and non-factorisable corrections are dominated by the exchange of hard gluons. The above statement is valid for a B meson decaying into either two light or one light and one heavy meson, where the heavy meson has absorbed the spectator quark. This formulation was systematically worked out in the framework of *QCD factorisation* (QCDF) [1, 28, 29, 36]. Previously, the factorisation ansatz itself, which we will call *naive factorisation*, was already discussed in the literature [37, 38], but it was far from clear why radiative corrections below m_b should be suppressed. QCDF provides a systematic way to calculate hadronic matrix elements to leading power in Λ_{QCD}/m_b and to all orders in perturbation theory in α_s. Naive factorisation is automatically recovered as the matrix elements to leading order in α_s and explains its phenomenological success in the past. Hadronic matrix elements were also calculated by means of QCD-sum rules. But to our knowledge, only the decays $B \to \pi\pi$ has been investigated so far [39–41]. In

some cases it is possible to use appropriate symmetries to circumvent the problem of calculating hadronic matrix elements. The decay amplitudes are usually decomposed into different topological contributions and related via for example isospin or flavour symmetries ($\mathrm{SU(2)_I}$, $\mathrm{SU(3)_F}$) to amplitudes of other decays, which then can be extracted from experiment. Potential drawbacks are non-factorisable symmetry breaking effects, which cannot be calculated from first principle and need to be modelled in some way. In addition, the explicit dependence on the Wilson Coefficients, worked out in the EWH, becomes lost and analyses that exclusively rely on symmetry arguments are usually unsuitable for testing specific NP scenarios. Under the assumption of the validity of the SM, such analysis usually allow to determine parameters like CKM-matrix elements or to predict observables like branching ratios and CP asymmetries. If measurements for these quantities exist, the SM hypothesis can be falsified. Though many studies can be found in the literature, we want to mention just a few examples: An isospin analysis for $B \to K\pi$ was worked out in [42], the decay $\bar{B}_s \to K^+K^-$ has been related to $\bar{B} \to \pi^+\pi^-$ in [43, 44] and the authors in [34, 45] combined flavour symmetry arguments with QCDF.

In the first part of this chapter, we will introduce the main concepts of QCDF in Subsection 3.1.1 and define all necessary quantities for our analysis in Subsection 3.1.2. A parametrisation of the decay amplitudes in terms of form factors, decay constants and amplitude coefficients is given in Subsection 3.1.3, encoding the underlying hard QCD-dynamics. The main goal of the present thesis is a analysis of subleading power corrections within the SM and beyond. We define a quantitative measure of necessary power-suppressed corrections compared to the leading decay amplitude in Subsection 3.1.3, which can be compared between different models. Section 3.2 summarises our numerical input.

3.1 QCD factorisation

3.1.1 Conceptual aspects

The calculation of hadronic matrix elements is due to their non-perturbative nature rather challenging. With regard to a lacking systematic treatment, one might be forced to rely on more heuristic arguments. In the case of a B-meson decaying into two mesons, $B \to M_1M_2$, it was assumed that the hadronisation process decouples into the transition of the B meson into M_1 and the ejection of M_2 from the vacuum

$$\langle M_1M_2|j_1 \times j_2|\bar{B}\rangle \longrightarrow \langle M_1|j_1|\bar{B}\rangle \, \langle M_2|j_2|0\rangle \sim F^{B\to M_1}(q^2)\, f_{M_2}, \tag{3.2}$$

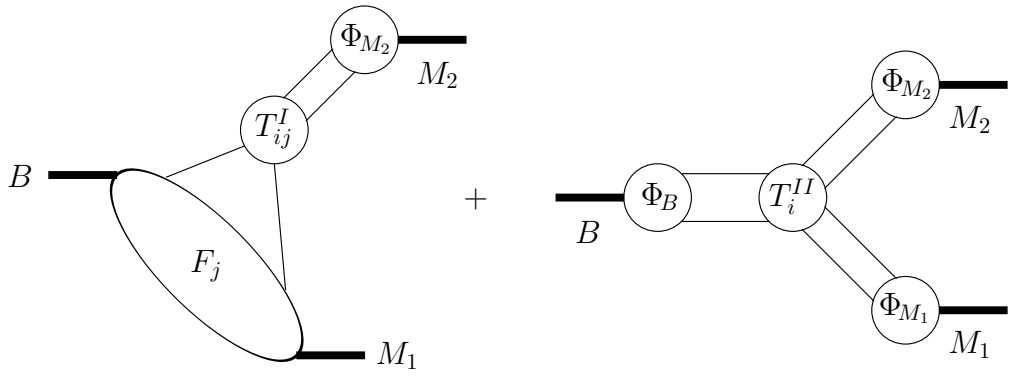

FIGURE 3.1: Graphical representation of the factorisation formula in QCDF. [Graphic taken from [1]].

with the bilinear quark current $j_i = \bar{q}'\Gamma_i q$ and Γ_i representing some Dirac structure. In the following discussion, M_1 will always refer to the meson that picks up the spectator quark and M_2 to the ejected meson.

The physical interpretation can be understood by recalling the specific kinematic situation and Bjorken's colour transparency argument [46, 47]: The b quark decays at the weak vertex into three quarks. Because their masses are much lighter than the mass of the b quark, they will leave the vertex with high momentum in the b-quark rest frame. One of the light quarks picks up the spectator quark from the B meson to hadronise into M_1. In order to hadronise into M_2, the residual two quarks are necessarily produced in a highly collinear configuration with small transverse extension of order Λ_{QCD}, forming a compact object. Since the ejected meson is fast, its intrinsic colour structure cannot be resolved by a soft gluon. These radiative corrections only interact with the colour-dipole moment of the ejected meson, which is suppressed for a compact object (colour-transparent).

The expectation that hadronic matrix elements naively factorise does not account for a proper cancellation of the residual scale dependence of the Wilson Coefficients. Hence the naive factorisation picture is incomplete. In further developments, it was possible to show that the colour transparency argument and factorisation can be incorporated in a systematic way to hadronic B-meson decays by a consistent power expansion in Λ_{QCD}/m_b, resulting in the framework of QCDF [1, 28, 29]. Even further, the authors claimed that to leading power in Λ_{QCD}/m_b only the exchange of hard gluons dominates the non-factorisable contributions to the decay amplitude, whereas soft contributions are confined to either the $(B \to M_1)$ or the ejected-meson system. This allows us to calculate radiative corrections perturbatively to the naive factorisation ansatz and results

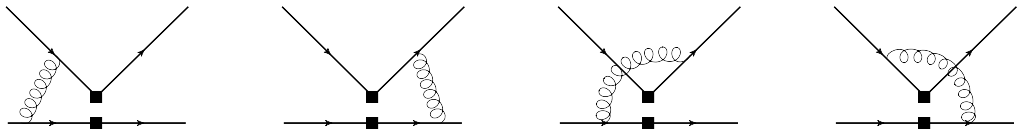

FIGURE 3.2: Non-factorisable vertex corrections to the decay amplitudes $a_{i,\mathrm{I}}$

into the formula

$$\begin{aligned}\langle M_1 M_2|\mathcal{O}_i|\bar{B}\rangle = \sum_j F_j^{B\to M_1}(m_2^2)\int_0^1 du\, T_{ij}^{\mathrm{I}}(u)\,\Phi_{M_2}(u) \;+\; (M_1 \leftrightarrow M_2) \\ + \int_0^1 d\xi dv du\, T_i^{\mathrm{II}}(\xi,v,u)\,\Phi_B(\xi)\,\Phi_{M_1}(v)\,\Phi_{M_2}(u) \;+\; \mathcal{O}\left(\frac{\Lambda_{\mathrm{QCD}}}{m_b}\right),\end{aligned} \tag{3.3}$$

where $\Phi_{M_i}(x)$ are light-cone distribution amplitudes (LCDA) of the mesons. They describe the probability that the constituent quarks of the meson carry the longitudinal momentum fraction x, respectively $\bar{x} = 1 - x$ and are defined later. $T^{\mathrm{I,II}}$ are hard-scattering kernels, which contain the radiative corrections to naive factorisation. Equation 3.3 is expected to hold to all orders in perturbation theory and was formally proven to $\mathcal{O}(\alpha_s^2)$ in [1]. A graphical presentation of factorisation is shown in Figure 3.1.

The main task now is to identify the leading contributions to the hard-scattering kernels. To lowest order, we will have to calculate the insertion of operators into diagrams without radiative corrections. They will set the leading scaling property of our decay amplitude. After the weak decay of the b quark, no momentum transfer takes place between $(B \to M_1)$ transition and the ejected meson and the hard-scattering kernel obey a trivial dependence on the momentum fraction u

$$T^{\mathrm{I}}(u) = 1 + \mathcal{O}(\alpha_s), \qquad\qquad T^{\mathrm{II}} = \mathcal{O}(\alpha_s). \tag{3.4}$$

The integral over Φ_{M_2} results in the meson decay constant f_{M_2}, as the proper normalisation of the LCDA, and naive factorisation in Equation 3.2 emerges as the leading order contribution in $\Lambda_{\mathrm{QCD}}/m_b$ and α_s in Equation 3.3. One should remark the following difference between the case of the decay into either two light or one light and one heavy meson: The momentum of the spectator quark is of the order Λ_{QCD}. Hence M_2 is formed in the case of light-light final states in an asymmetric momentum configuration. The hadronisation of a light meson with one quark carrying almost all of the longitudinal momentum fraction, $u \sim 1$, is suppressed by $(\Lambda_{\mathrm{QCD}}/m_b)^{3/2}$ compared to the decay into heavy-light final states, which will give rise to corrections to the former case, being absent in the latter.

The first non-factorisable corrections arise from vertex and penguin correction, shown in Figures 3.2 and 3.3 and contribute to the hard-scattering kernel $T^{\mathrm{I}}(u)$. The

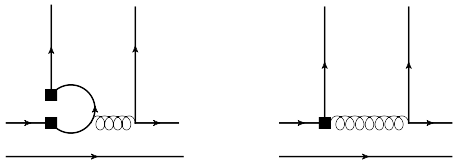

FIGURE 3.3: Non-factorisable penguin corrections to the decay amplitudes $a_{i,\mathrm{I}}$

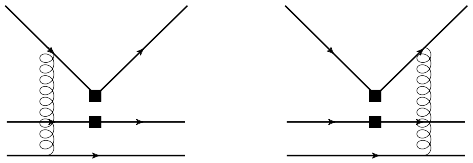

FIGURE 3.4: Non-factorisable hard-spectator scattering corrections to the decay amplitudes $a_{i,\mathrm{II}}$

success of QCDF was to show that these corrections are dominated by hard-gluon exchange and are therefore calculable in perturbation theory. Because momentum is transferred between the $(B \to M_1)$-system and M_2, the hard-scattering kernel depends on the longitudinal momentum fraction u and its convolution with the LCDA become mode dependent. As we will see in Subsection 3.1.3, these corrections introduce strong interaction phases, which occur in QCDF first at order α_s. CP asymmetries arise through the interplay of weak phases, given through the CKM-matrix in the SM, and strong phases of the decay amplitudes, making CP asymmetries especially sensitive to these radiative corrections. To leading order in $\Lambda_{\mathrm{QCD}}/m_b$, it is sufficient to work in the leading-twist approximation for the LCDA, which is equivalent to omit contributions from non-leading Fock states. However, higher twist contributions, though being formally subleading, can become numerically important and will be considered in our analysis (see Chapter 3.1.2). Fortunately, in the case of vertex and penguin corrections these contributions factorise.

The first corrections to the hard-scattering kernel $T^{\mathrm{II}}(\xi, v, u)$, which is given by the second line of Equation 3.3, arise from interactions between M_2 and the spectator quark, shown in Figure 3.4 and called hard-spectator scattering (HS). Whereas these contributions are subleading in the case of heavy-light, they have to be considered for light-light final states. Again, soft gluon contributions are suppressed by the colour transparency argument, but the exchange of hard gluon scales like the leading amplitude and has to be considered as a perturbative, radiative correction to the factorisation formula. HS violates naive factorisation because it cannot be cast into a form factor and decay constant. As in the case for the vertex and penguin corrections, chiral-enhanced contributions also occur for the HS. These contributions cannot be calculated reliably due to logarithmic divergences. These originate from soft-gluon exchange between the quarks in M_2 and the spectator quark and cannot be sufficiently suppressed by higher-twist contributions in the LCDA. In nature, such effects will be smeared out by uncontrollable QCD effects and need to be regularised by a soft cut-off scale to obtain an estimate for the order of magnitude that can be expected from those contributions.

The last class of contributions arises through weak annihilation (WA), shown in Figure 3.5. The spectator quark annihilates with the b quark and the residual two quarks from the weak interaction vertex hadronise into the final state mesons together with a

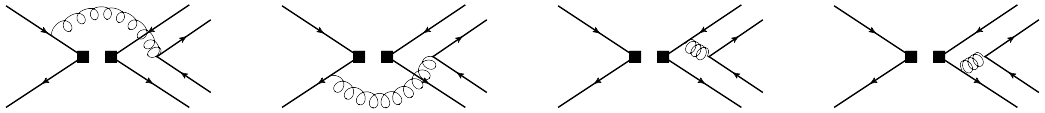

FIGURE 3.5: Non-factorisable weak-annihilation corrections to the decay amplitudes b_i.

quark pair emitted from a gluon vertex. Although WA is power-suppressed relative to the leading amplitude, it is chiral enhanced and might be numerically relevant for a sensible phenomenological analysis. Unfortunately, WA cannot be consistently calculated in a hard-scattering approach, which reflects the occurrence of logarithmic divergence already at leading twist.

3.1.2 Non-perturbative quantities

In the following section, we define the relevant non-perturbative quantities needed for hadronic B-meson decays, in particular, transition form factors and LCDAs for light and heavy mesons.

We will use the definition for the form factors given in [48]. The transition of a B meson into a pseudoscalar meson P can be described by the two form factors F_+, F_0

$$\langle P(p')|\bar{q}\gamma^\mu b|\bar{B}(p)\rangle = F_+(q^2)\left[p^\mu + p'^\mu - \frac{M_B^2 - m_P^2}{q^2}q^\mu\right] + F_0(q^2)\frac{M_B^2 - m_P^2}{q^2}q^\mu, \quad (3.5)$$

where $q = p - p'$ and m_P denotes the mass of the meson P. At large recoil ($q^2 \to 0$) the two form factors coincide in the heavy quark limit [49]

$$F_0(q^2 = 0) = F_+(q^2 = 0) + \mathcal{O}(\Lambda_{\text{QCD}}/m_b), \quad (3.6)$$

and in the case of $B \to PP$, PV decays, it suffices to only consider F_0. The relevant form factors for the transition into a vector meson are parametrised by V, A_0, A_1, A_2[1]

$$\begin{aligned}
\langle V(p',\varepsilon^*)|\bar{q}\gamma^\mu b|\bar{B}(p)\rangle = &\quad V(q^2)\frac{2i}{M_B + m_V}\epsilon^{\mu\nu\rho\sigma}\varepsilon^*_\nu p'_\rho p_\sigma, \\
\langle V(p',\varepsilon^*)|\bar{q}\gamma^\mu\gamma_5 b|\bar{B}(p)\rangle = &\quad 2m_V A_0(q^2)\frac{\varepsilon^*\cdot q}{q^2}q^\mu + (M_B + m_V)A_1(q^2)\left[\varepsilon^{*\mu} - \frac{\varepsilon^*\cdot q}{q^2}q^\mu\right] \\
&- A_2(q^2)\frac{\varepsilon^*\cdot q}{M_B + m_V}\left[p^\mu + p'^\mu - \frac{M_B^2 - m_V^2}{q^2}q^\mu\right], \quad (3.7)
\end{aligned}$$

where ε^* is the polarisation vector and m_V the mass of the vector meson. The convention $\epsilon^{0123} = -1$ has been used.

The form factor A_0 occurs in $B \to VP$ and $B \to V^0V^0$ decays, where V^0 is the longitudinal polarisation mode of the vector meson. The decay amplitude into the

[1] In principle also tensor form factors exists for $B \to P, V$, but those are irrelevant for our analysis.

positive/negative helicity states $B \to V^{\pm}V^{\pm}$ depends on a linear combination of A_1 and V

$$F_{\pm}(q^2) = \left(1 + \frac{m_V}{m_B}\right) A_1(q^2) \mp \left(1 - \frac{m_V}{m_B}\right) V(q^2). \tag{3.8}$$

The special kinematic of a two-body decay can again be utilised to also employ form-factor relations for $B \to V$ decays in the heavy-quark limit [49]

$$V(q^2 = 0) = A_1(q^2 = 0) + \mathcal{O}(\Lambda_{\text{QCD}}/m_b), \tag{3.9}$$

and together with Equation 3.8 the form factors obey the following scaling properties

$$\frac{F_-}{A_0} \sim 1, \qquad \frac{F_+}{A_0} \sim \mathcal{O}(\Lambda_{\text{QCD}}/m_b). \tag{3.10}$$

LCDAs of light mesons are formally needed in QCDF at leading-twist order. Higher twist-3 contributions are suppressed relative to the leading twist, but can be proportional to the chiral quark condensate and therefore numerically enhanced. Nevertheless, it is sufficient to consider only two-particle distribution amplitudes, although 3-particle quark-antiquark-gluon distribution amplitudes contribute also to the twist-3 corrections, but are not enhanced and can therefore be neglected. The defining equations for the relevant twist-2, ϕ_P, and twist-3, ϕ_p, LCDAs for a light pseudoscalar meson are [48, 50]

$$\begin{aligned} \langle P(p')|\bar{q}(y)\gamma_\mu\gamma_5[y,x]q(x)|0\rangle &= -if_P p'_\mu \int_0^1 du\, e^{i(u\,p'\cdot y + \bar{u}\,p'\cdot x)}\phi_P(u,\mu), \\ \langle P(p')|\bar{q}(y)i\gamma_5[y,x]q(x)|0\rangle &= f_P\mu_P \int_0^1 du\, e^{i(u\,p'\cdot y + \bar{u}\,p'\cdot x)}\phi_p(u,\mu), \end{aligned} \tag{3.11}$$

with f_P the decay constant of the light meson P and the chiral enhanced factor $\mu_P = m_P^2/(m_{q_1} + m_{q_2})$. The longitudinal momentum of the constituent valence quarks is parametrised by the fraction $u, \bar{u} = 1 - u$ of the momentum of the pseudoscalar meson, p', and μ is the renormalisation scale of the light-cone operators. $(x - y)^2 = 0$ obey a light-like separation and the expression $[y, x]$ indicates that the quark fields between x and y are connected via a path-ordered exponential of gluon fields in order to guarantee an gauge-invariant definition of the distribution amplitudes. The twist-3 projection occurs in corrections from, for instance, scalar penguins, hard-spectator scattering, and weak annihilation interactions, for which a common chiral-enhanced factor emerge

$$r_\chi^P(\mu) = \frac{2m_P^2}{m_b(\mu)(m_{q_1}(\mu) + m_{q_2}(\mu))}, \tag{3.12}$$

and though formally power-suppressed, numerically of order 1. All distribution amplitudes are normalised to $\int_0^1 du\, \phi(u,\mu) = 1$, as can be seen from taking $x \to y$. In the

limit, where the renormalisation scale is sent to infinity, the distribution amplitudes obey the asymptotic form

$$\phi_P(u,\mu\to\infty) = 6u\bar{u}, \qquad \phi_p(u,\mu\to\infty) = 1. \tag{3.13}$$

In practical calculations, it is convenient to express the LCDA in a Gegenbauer expansion

$$\phi_P(u,\mu) = 6u\bar{u}\left(1+\sum_{n=1}^{\infty}\alpha_n^P(\mu)C_n^{(3/2)}(2u-1)\right), \tag{3.14}$$

which is usually truncated after $n = 2$ and the Gegenbauer polynomials are given by $C_1^{(3/2)}(u) = 3u$ and $C_1^{(3/2)}(u) = \frac{3}{2}(5u^2-1)$.

Similar relations are obtained for light vector mesons. The relevant twist-2 and twist-3 LCDAs are defined through [48, 51]

$$\begin{aligned}\langle V(p',\varepsilon_\parallel^*)|\bar{q}(y)\gamma_\mu[y,x]q(x)|0\rangle &= -if_V p'_\mu\int_0^1 du\, e^{i(u\,p'\cdot y+\bar{u}\,p'\cdot x)}\phi_V(u,\mu),\\ \langle V(p',\varepsilon_\parallel^*)|\bar{q}(y)\sigma_{\mu\nu}[y,x]q(x)|0\rangle &= -if_V^\perp(\mu)m_V\int_0^1 du\, e^{i(u\,p'\cdot y+\bar{u}\,p'\cdot x)}\frac{p'_\mu z_\nu - p'_\nu z_\mu}{p'\cdot z}\phi_v(u,\mu),\end{aligned} \tag{3.15}$$

where Wandzura-Wilczek relations [51] can be utilised to express all twist-3 amplitudes into the single function $\phi_v(u,\mu)$. The chiral-enhanced factor for vector mesons is defined through

$$r_\chi^V(\mu) = \frac{2m_V}{m_b(\mu)}\frac{f_V^\perp(\mu)}{f_V}, \tag{3.16}$$

and the Gegenbauer expansion for $\phi_V(u,\mu)$ is analogue to Equation 3.14 with the substitution $\alpha_n^P(\mu)\to\alpha_n^V(\mu)$. The twist-3 amplitudes $\phi_v(u,\mu)$, however, are parametrised by an expansion in Legendre polynomials

$$\phi_v(u,,\mu) = 3\left(1+\sum_{n=1}^{\infty}\alpha_{n,\perp}^V(u,\mu)P_{n+1}(2u-1)\right), \tag{3.17}$$

which is again truncated after $n = 2$. The normalisation of the twist-3 distribution amplitudes is $\int_0^1 du\,\phi_v(u,\mu) = 0$, contrary to the normalisation of $\phi_p(u,\mu)$.

The LCDA of the B meson occurs in the second part of the factorisation formula in Equation 3.3. The exchange of a hard gluon between the emitted meson M_2 and the spectator quarks q_s (HS interaction) can resolve the inner momentum structure of the B meson. In contrast to the LCDA of light mesons, the momentum is mostly carried by the momentum of the heavy b quark, $p_b\sim p$, and the momentum of the light spectator quark, l, is of the order $\mathcal{O}(\Lambda_{\text{QCD}})$. Since the spectator quark is neither heavy nor energetic, no

further restrictions can be made on the momentum components of l. Nevertheless, it turns out that the HS amplitude at leading order in α_s only depends on the light-cone component $l_+ = \xi p_+$, where we have introduced the longitudinal momentum fraction ξ. The integration over $l_\perp$ and l_- can be preformed over the B-meson wave function and introduces the necessity of the B-meson LCDA in hadronic decays with light-light final states. To leading order in Λ_{QCD}/m_b, the LCDA can be decomposed into two scalar wave functions Φ_{B_1,B_2} [52]

$$\langle 0|\bar{q}(z)[z,0]b(0)|\bar{B}(p)\rangle = -\frac{if_B}{4}[(\not{p}+m_b)\gamma_5]\int_0^1 d\xi e^{-i\xi_+ z_-}[\Phi_{B_1}(\xi)+\not{n}_-\Phi_{B_2}(\xi)], \quad (3.18)$$

where we chose the light-like vector $n_- = (1,0,0,-1)$. The normalisation conditions are given by

$$\int_0^1 d\xi \Phi_{B_1}(\xi) = 1, \qquad \int_0^1 d\xi \Phi_{B_2}(\xi) = 0. \quad (3.19)$$

Actually, only the first inverse moment of the B meson LCDA Φ_{B_1} occurs in QCDF calculations

$$\int_0^1 \frac{d\xi}{\xi}\Phi_B(\xi) \equiv \frac{m_B}{\lambda_B}. \quad (3.20)$$

The quantity λ_B is theoretically purely known. It can be either obtained from QCD-sum rule calculations or extracted from experimental measurements of, for instance the decay $B \to \gamma\ell\nu$, which will be discussed later on in Subsection 3.2.1.

3.1.3 Parameterisation of the decay amplitudes

The following section shall be used to present the parametrisation of the hadronic B-meson decay amplitudes, which have been calculated first in [29, 36, 53]. As was argued in the previous subsections, the matrix elements in the decay amplitudes in Equation 3.1 factorises in a naive way via Equation 3.2 and, radiative corrections are perturbatively calculable to leading order in Λ_{QCD}/m_b. These corrections are parametrised by effective coefficients $a_i(M_1M_2)$

$$\begin{aligned}\mathcal{A}_{\bar{B}\to M_1M_2} = \frac{G_F}{\sqrt{2}}\sum_{i=1}^{10}\sum_{p=u,c}\lambda_p\big(&a_i^p(M_1M_2)\ \langle M_1|j_{1,i}|\bar{B}\rangle\langle M_2|j_{2,i}|0\rangle + \\ &a_i^p(M_2M_1)\ \langle M_2|j_{1,i}|\bar{B}\rangle\langle M_1|j_{2,i}|0\rangle\big),\end{aligned} \quad (3.21)$$

where we absorbed the explicit dependence on Wilson Coefficients into $a_i(M_1M_2)$ and $j_{1,i}$, $j_{2,i}$ correspond to the bilinear quark current of the operators defined in Equation 2.14, where the odd-numbered operators have to be fierzed into a colour-singlet

structure. Note that the sum over i extends to 10 because the dipole operators only contribute via penguin contributions to the decay amplitudes.

The effective coefficients $a_i(M_1M_2)$ depend on the Wilson Coefficients and on the convolution of the hard-scattering kernel with the mode dependent LCDAs, which introduces strong rescattering phases [36]

$$\begin{aligned} a_i^p(M_1M_2) &= a_{i,\mathrm{I}}^p(M_1M_2) + a_{i,\mathrm{II}}(M_1M_2), \\ a_{i,\mathrm{I}}^p(M_1M_2) &= \left(C_i + \frac{C_{i\pm1}}{N_c}\right) N_i(M_2) + \frac{C_{i\pm1}}{N_c}\frac{C_F\alpha_s}{4\pi}\, V_i(M_2) + P_i^p(M_2), \\ a_{i,\mathrm{II}}(M_1M_2) &= \frac{C_{i\pm1}}{N_c^2} C_F\alpha_s\pi\, H_i(M_1M_2), \end{aligned} \tag{3.22}$$

where the upper (lower) sign in the Wilson Coefficients apply for i odd (even). N_c is the number of colours and the colour factor $C_F = 4/3$ for $N_c = 3$. Analytically formulas for the vertex corrections, $V(M_2)$ (Figure 3.2), the penguin contractions, $P^p(M_2)$ (Figure 3.3), and for HS interactions, $H(M_1, M_2)$ (Figure 3.4), can be found in [36, 53].

In accordance to the $a_i(M_1M_2)$, additional coefficients $b_i(M_1M_2)$ can be defined to account for WA contributions. Before introducing them, we would like to mention some aspects on end-point singularities: As it was already discussed in the previous Subsection 3.1.1, contributions from HS and WA topologies elude from a systematic treatment in QCDF. However, such subleading corrections can be chiral enhanced and yield sizeable contributions in predictions. Due to the ignorance of the respective QCD mechanisms, additional phenomenological parameters with the according power counting arguments are introduced

$$X_{A,H} = (1 + \rho_{A,H}) \ln \frac{m_b}{\Lambda_{\mathrm{QCD}}}, \qquad \rho_{A,H} \equiv |\rho_{A,H}| e^{i\phi_{A,H}} \tag{3.23}$$

with the complex parameters $\rho_{A,H}$.

In HS, they originate from terms involving twist-3 LCDAs, $\Phi_{m1}(y) \neq 0$ for $y \to 1$, in convolutions

$$\int_0^1 \frac{dy}{1-y}\Phi_{m1}(y) \equiv \Phi_{m1}(1)X_H + \int_0^1 \frac{dy}{[1-y]_+}\Phi_{m1}(y) \tag{3.24}$$

that are regulated by the introduction of the phenomenological parameter X_H[2], which represents a soft-gluon interaction with the spectator quark. As indicated above, it is expected that $X_H \sim \ln(m_b/\Lambda_{\mathrm{QCD}})$ because it arises in a perturbative calculation of these soft interactions that are regulated in principle latest by a physical scale of order Λ_{QCD}.

[2] In principle one might introduce a separate X_H for each meson M_1 and M_2 as well as for each operator insertion. Because most decay amplitudes are numerically dominated by one X_H, we will treat them as universal at least for decays that are related via $(u \leftrightarrow d)$ quark exchange. Similar arguments will be adopted to the discussion of WA contributions.

Neither the adequate degrees-of-freedom nor their interactions that should be used in an effective theory below this scale are known. It is also conceivable that factorisation might be achieved at some intermediate scale between m_b and $\Lambda_{\rm QCD}$. The factor $(1+\rho_H)$ summarises the remainder of an unknown matrix element, including the possibility of a strong phase that affects especially the predictions of CP asymmetries. The numerical size of the complex parameter ρ_H is unknown, however too large values will give rise to numerically enhanced subleading $\Lambda_{\rm QCD}/m_b$ contributions compared to the formally leading terms putting to question the validity of the $\Lambda_{\rm QCD}/m_b$ expansion of QCDF.

WA is entirely subleading in $\Lambda_{\rm QCD}/m_b$ and consists in principle of six different building blocks $A_k^{i,f}$ $(k=1,2,3)$, which are characterised by gluon emission from the initial (i) and final (f) states (Figure 3.5) and the three possible Dirac structures that are involved: $k=1$ for $(V-A)\otimes(V-A)$, $k=2$ for $(V-A)\otimes(V+A)$ and $k=3$ for $(-2)(S-P)\otimes(S+P)$. They contribute to non-singlet annihilation amplitudes with specific combinations of Wilson Coefficients of the 4-quark operators [29, 36, 54]

$$\begin{aligned} b_1 &= \frac{C_F}{N_c^2} C_1 A_1^i\,, & b_2 &= \frac{C_F}{N_c^2} C_2 A_1^i\,, \\ b_3^p &= \frac{C_F}{N_c^2}\left[C_3 A_1^i + C_5(A_3^i + A_3^f) + N_c C_6 A_3^f\right]\,, & b_4^p &= \frac{C_F}{N_c^2}\left[C_4 A_1^i + C_6 A_2^i\right]\,, \\ b_{3,\rm EW}^p &= \frac{C_F}{N_c^2}\left[C_9 A_1^i + C_7(A_3^i + A_3^f) + N_c C_8 A_3^f\right]\,, & b_{4,\rm EW}^p &= \frac{C_F}{N_c^2}\left[C_{10} A_1^i + C_8 A_2^i\right]\,, \end{aligned} \tag{3.25}$$

and depend on the argument M_1 and M_2. In particular, they correspond to the amplitudes due to current-current (b_1, b_2), QCD-penguin (b_3^p, b_4^p) and QED-penguin ($b_{3\rm EW}^p$, $b_{4\rm EW}^p$) annihilation. When ignoring end-point singularities, results for WA contributions can be derived in terms of convolutions of hard-scattering kernels with LCDAs of twist-2 and chiral-enhanced twist-3. In analogy to HS, the end-point singularities are then regulated in a model-dependent fashion

$$\int_0^1 \frac{dy}{y} \to X_A\,, \qquad\qquad \int_0^1 dy \frac{\ln y}{y} \to -\frac{1}{2}(X_A)^2, \tag{3.26}$$

introducing phenomenological parameters X_A that depend in principle on the meson and are different for each building block $A_k^{i,f}$. Explicit expressions for $A_k^{i,f}$ in terms of X_A are given for $M_1M_2 = PP,\, PV,\, VP,\, VV$ in the literature [36, 54], but independently one has $A_{1,2}^f = 0$. As a further simplification, it is assumed in the literature that there is only one phenomenological parameter, independent of meson type and Dirac structure, such that $A_k^{i,f}(X_A)$ are functions of the same parameter. It should be noted that the WA amplitudes Equation 3.25 in the light-cone sum rule (LCSR) approach exhibit the same dependence on the products of Wilson Coefficients and building blocks [41], however in this approach the calculation of $A_k^{i,f}$ does not suffer from end-point singularities due to different assumptions and approximations. With the latter in mind, a more general

approach would be to interpret the building blocks themselves as phenomenological parameters, or equivalently introduce one X_A for each of them. When investigating NP effects in a concrete extension of the SM or model-independently in the framework of the effective theory, it is desirable to keep the explicit dependence on the Wilson Coefficients in Equation 3.25 because they depend on non-standard parameters, including new weak phases. In the case of non-negligible WA contributions, the CP asymmetries and, to less extend branching ratios, will be sensitive to the interference of NP and strong phases due to X_A.

It is common practice to combine effective decay coefficients into flavour amplitudes if their quark flavour in the factorised matrix elements (Equation 3.2) coincide. Though both decay coefficients contribute to the same decay amplitudes, their linear combination depend on the spin of the final state meson

$$\alpha^p_{3,\mathrm{EW}}(M_1M_2) = \begin{cases} a^p_9(M_1M_2) \;\; - a^p_7(M_1M_2) & M_1M_2 = PP\,, VP, \\ a^p_9(M_1M_2) \;\; + a^p_7(M_1M_2) & M_1M_2 = PV\,, VV, \end{cases} \tag{3.27}$$

$$\alpha^p_{4,\mathrm{EW}}(M_1M_2) = \begin{cases} a^p_{10}(M_1M_2) - r^{M_2}_\chi a^p_8(M_1M_2) & M_1M_2 = VP,\, VV, \\ a^p_{10}(M_1M_2) + r^{M_2}_\chi a^p_8(M_1M_2) & M_1M_2 = PP,\, PV. \end{cases} \tag{3.28}$$

The current-current coefficients are simply obtained through the replacement $a_{1,2} \to \alpha_{1,2}$. The relations for the QCD-penguin coefficients can be obtained from Equation 3.27 by appropriate replacements for the a_i's. The flavour amplitude for the WA coefficients are obtained by the normalisation

$$\beta_i(M_1M_2) = \begin{cases} \frac{1}{m_{M_2}} \frac{f_B f_{M_1}}{m_B F^{B\to M_1}} b_i(M_1M_2) & M_1M_2 = V^\pm V^\pm, \\ \frac{1}{m_B} \frac{f_B f_{M_1}}{m_B F^{B\to M_1}} b_i(M_1M_2) & \text{others} \end{cases} \tag{3.29}$$

The corresponding matrix elements for the χ-flipped operators, which will be used in the phenomenological section of this work, can be obtained from the decay amplitudes $a_i(M_1M_2)$, exploiting parity transformations [55]

$$\langle M_1M_2|\mathcal{O}'_i|\bar{B}\rangle = -\eta_{M_1M_2}\,\langle M_1M_2|\mathcal{O}_i|\bar{B}\rangle\,, \qquad a'_i(M_1M_2) \overset{C_i\to C'_i}{=} a_i(M_1M_2), \tag{3.30}$$

with the parity of the final state $\eta_{M_1M_2} = 1$ for PP, VV and $\eta_{M_1M_2} = -1$ for PV, VP. Analogue relations can be derived for the WA coefficients $b_i(M_1M_2)$. In the case of positive/negative polarised final states, form factors and decay amplitudes have to be replaced in Equation 3.30 by their helicity counterpart: $F_\pm \leftrightarrow F_\mp$ and $a_\pm(M_1M_2) \leftrightarrow a_\mp(M_1M_2)$.

Now we defined all necessary quantities to write the decay amplitude of a B meson into two mesons in the compact form

$$\begin{aligned}\mathcal{A}_{\bar{B}\to M_1M_2} = \sum_{p=u,c}\lambda_p\Big[A_{M_1M_2}\Big(\sum_i \alpha_i(M_1M_2)+\sum_j\beta_j(M_1M_2)\Big)+\\ A_{M_2M_1}\Big(\sum_i \alpha_i(M_2M_1)+\sum_j\beta_j(M_2M_1)\Big)\Big],\end{aligned} \tag{3.31}$$

where the sums over the index i, j include only those coefficients for which the quark flavour of the operators in Equation 3.21 matches those of the initial and final state mesons. The corresponding operators for β_j can be found in [36]. The naive factorisation amplitude is given by

$$A_{M_1M_2} = i\frac{G_F}{\sqrt{2}}m_B^2\begin{cases} f_{P_2}F_0^{B\to P_1} & \text{for } M_1M_2 = PP,\\ -f_{V_2}F_0^{B\to P_1} & \text{for } M_1M_2 = PV,\\ -f_{P_2}A_0^{B\to V_1} & \text{for } M_1M_2 = VP,\\ f_{V_2}A_0^{B\to V_1} & \text{for } M_1M_2 = V^0V^0,\\ \frac{m_{M_2}}{m_B}f_{V_2}F_+^{B\to V_1} & \text{for } M_1M_2 = V^+V^+,\\ \frac{m_{M_2}}{m_B}f_{V_2}F_-^{B\to V_1} & \text{for } M_1M_2 = V^-V^-.\end{cases} \tag{3.32}$$

The positive/negative decay amplitudes are suppressed by m_{M_2}/m_B compared to the longitudinal polarised decay amplitude. Together with the scaling properties of the form factors in Equation 3.10, the following hierarchy is on hand

$$\mathcal{A}_{\bar{B}}^0 : \mathcal{A}_{\bar{B}}^- : \mathcal{A}_{\bar{B}}^+, \qquad 1 : \left(\frac{\Lambda_{\text{QCD}}}{m_b}\right) : \left(\frac{\Lambda_{\text{QCD}}}{m_b}\right)^2. \tag{3.33}$$

This is a consequence of the left-handedness of the SM. Taking χ-flipped operators into account, the hierarchy between A^- and A^+ gets inverted,

$$\mathcal{A}_{\bar{B}}'^0 : \mathcal{A}_{\bar{B}}'^+ : \mathcal{A}_{\bar{B}}'^-, \qquad 1 : \left(\frac{\Lambda_{\text{QCD}}}{m_b}\right) : \left(\frac{\Lambda_{\text{QCD}}}{m_b}\right)^2, \tag{3.34}$$

which qualitatively allows to study potential effects of right-handed currents in the transverse helicity basis

$$\mathcal{A}_\perp = \frac{1}{\sqrt{2}}(\mathcal{A}_+ + \mathcal{A}_-), \qquad \mathcal{A}_\parallel = \frac{1}{\sqrt{2}}(\mathcal{A}_+ - \mathcal{A}_-). \tag{3.35}$$

3.1.4 Power-suppressed corrections

As already indicated, the phenomenological parameters $X_{A,H}$ are unknown and the size of $|\rho_{A,H}|$ is typically adjusted to reproduce data of branching fractions assuming the SM. The phase $\phi_{A,H}$ is kept arbitrary and by varying it freely an uncertainty estimate

within "conventional QCDF" due to WA (HS) is obtained for the theoretical prediction of observables under consideration. This procedure shows that WA is important and constitutes a major source of theoretical uncertainty in predictions. In this thesis, we instead determine the phenomenological parameter $\rho_{A,H}$ — and for $B \to K\pi$ also ρ_H — from the data in the framework of the SM and scenarios beyond, simultaneously with additional NP parameters. In the latter case, the determination of the NP parameters will take into account the uncertainty of WA (HS) when marginalising over $\rho_{A,H}$. As a consequence, no predictions will be possible for those observables that are used in the fit to determine $\rho_{A,H}$.

This procedure is different to conventional QCDF in as much as it assumes one universal parameter ρ_A for all observables in one specific decay mode. Indeed, in conventional QCDF the independent variation of $\rho_{A,H}$ for each observable in a specific decay assumes in principle also different WA (and HS) contributions for each observable. However, since the parameters $\rho_{A,H}$ are introduced in QCDF at the level of decay amplitudes one would expect that they are the same for all observables of a specific decay mode. Consequently, conventional QCDF allows for situations where experimental measurements and theory predictions for two observables are in agreement, although for the first observable the agreement is reached for values of $\phi_{A,H}$ that might be much different from those where the agreement is reached for the second observable.

In the lack of precise data for most of the decays, we make the further assumption of a WA parameter that is even universal for decay modes that are related by the exchange of $(u \leftrightarrow d)$ quarks. As an example, this allows to combine observables of the four decay channels $\bar{B}^0 \to \bar{K}^0\pi^0$, $K^-\pi^+$ and $B^- \to K^-\pi^0$, $\bar{K}^0\pi^-$, to which we refer as "decay system" $B \to K\pi$. All considered decay systems and the according measured observables are listed in Subsection 4.1.1. This assumption is motivated by the circumstance that the dominant contributions to the amplitude in all considered decays come actually from the linear combination $\hat{\alpha}_4^c(M_1M_2) = \alpha_4^c(M_1M_2) + \beta_3^c(M_1M_2)$, which is due to isospin-conserving QCD-penguin operators $O_{3,\dots,6}$. Furthermore, since $\beta_3^c(M_1M_2)$ is due to the large Wilson Coefficient C_6 and an additional colour enhancement numerically dominated by only one topology A_3^f, which parametrised WA with a gluon exchange at the final-state quark current, the introduction of only one WA parameter is reasonable.

As the credibility of QCDF crucially rely on a meaningful expansion in $\Lambda_{\rm QCD}/m_b$, we quantify the amount of power corrections needed to explain the measurements of branching ratios and CP asymmetries by

$$\xi_i^H(\rho_H) = \left|\frac{\alpha_{i,\rm II}^{\rm tw.3}(\rho_H)}{\alpha_{i,\rm I} + \alpha_{i,\rm II}^{\rm tw.2}}\right|, \qquad \xi_i^A(\rho_A) = \left|\frac{\beta_i(\rho_A)}{\alpha_{i+\delta_{i3},\rm I}}\right|. \tag{3.36}$$

In the case of two vector mesons in the final state, $\xi^{A,H}$ is defined by the mean value

of the corresponding ratios for longitudinal and negative polarised amplitudes $\xi_{i,VV}^{A,H} = \frac{1}{2}(\xi_i^{0,(A,H)} + \xi_i^{-,(A,H)})$[3]. In the SM, the power-suppressed ratios exclusively depend on the parameter $\rho_{A,H}$ and contour lines can easily be obtained for our fits. However, for fits which take effects from physics beyond the SM into account, the ratios $\xi_i^{A,H}$ additionally depend on the NP parameters — directly through the explicit dependence on the Wilson Coefficients and indirectly from data via the Likelihood — and should be evaluated for each value ρ_A at the best-fit point of the residual fit parameters. The exact statistical treatment will be discussed in Chapter A.5. The most important contribution from power-suppressed corrections are clearly obtained from HS in α_2, which is enhanced by the large Wilson Coefficient C_1 and from the WA correction β_3 in QCD-penguin dominated decays. Therefore ξ_2^H and ξ_3^A will play an important role in the phenomenological part of this work.

3.2 Input

After we discussed the main conceptual issues regarding hadronic B-meson decays, we complete the chapter with the definition of the numerical input, which will be used in the phenomenological part of this thesis, and briefly comment on the parameter λ_B.

3.2.1 Moments of the B-meson LCDA from $B \to \gamma\ell\nu$

The inverse moment of the LCDA of the B meson, λ_B, as defined in Equation 3.20, is of crucial importance for decays. It enters the decay amplitudes as an overall factor in HS

$$H_i(M_1 M_2) \sim \frac{1}{\lambda_B}, \tag{3.37}$$

and therefore, especially important for observables that depend on the colour-suppressed tree contribution $\alpha_2^u(M_1 M_2)$. Unfortunately, it is non-trivial to obtain reliable theoretical predictions for λ_B. The authors in [56], using means of QCD-sum rules, quoted

$$\lambda_B = 460 \pm 110\,\text{MeV} \qquad \text{(QCD-sum rules)}. \tag{3.38}$$

This calculation seems to be in contradiction to the analysis in [2], in which the impact of λ_B on the branching ratios of the tree-level-dominated decays $B \to \pi\pi\,(\rho\pi,\, \rho_L\rho_L)$ have been investigated. The analysis was performed within the framework of QCDF and at NNLO precision for the tree-level decay amplitudes $\alpha_{1,2}(M_1 M_2)$. The theory

[3] Due to their scaling property, the positive helicity amplitudes are calculated in naive factorisation and do not contribute to the $\xi_{i,VV}^{A,H}$

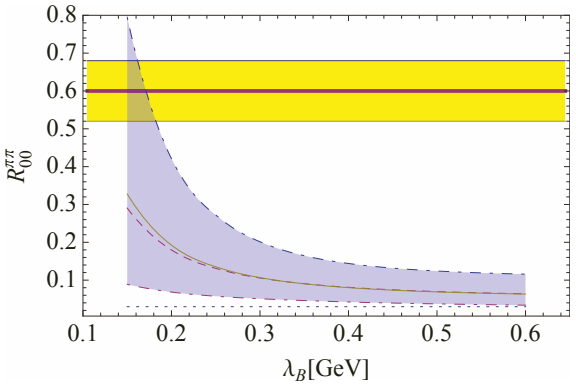

FIGURE 3.6: Theoretical prediction for $R_{00}^{\pi\pi}$ at LO (dotted), NLO (dashed) and NNLO (solid) vs. λ_B. The theoretical error band, according to the error estimate in [2], is shown in blue. The red solid line shows the central value of the measurement within the 1σ confidence level in yellow. [Plot taken from [2]].

prediction for the ratio

$$R_{00}^{\pi\pi} \equiv 2\frac{\Gamma(\bar{B}^0 \to \pi^0\pi^0)}{\Gamma(\bar{B}^0 \to \pi^+\pi^-)} \tag{3.39}$$

is shown in Figure 3.6 for $\lambda_B \in [0.1\,\text{GeV}; 0.6\,\text{GeV}]$. The ratio has been employed in order to reduce uncertainties from form factors, but the misalignment between experiment and theory is mainly caused by the branching ratio $\mathcal{B}(\bar{B}^0 \to \pi^0\pi^0)$, dominated by $\alpha_2^u(\pi\pi)$. Even for a low value of $\lambda_B = 200\,\text{MeV}$, theory and experiment only overlaps within their uncertainties. Larger values, as suggested from QCD-sum rules, cannot explain the observed branching ratios in tree-level-dominated B-meson decays, which lead to the hypothesis

$$\lambda_B = 200^{+250}_{-0}\,\text{MeV} \qquad \text{(QCDF)}. \tag{3.40}$$

As discussed in the previous section, the calculation of hadronic matrix elements involves incalculable power corrections, which have been estimated in this analysis through power counting arguments and finally incorporated into the total error budget. Therefore, the extraction of the inverse moment of the B-meson LCDA might be corrupted by underestimated soft QCD effects.

The decay $B \to \gamma\ell\nu$ seems to be a more robust candidate to extract λ_B from experiment. The differential decay rate with respect to the energy of the lepton pair, E_γ, factorises into a vector and a axial-vector form factor ([57], and references therein)

$$\frac{d\Gamma}{dE_\gamma} = \frac{G_F^2\alpha}{48\pi^2}\,|V_{ub}|^2\,m_B^4(1-x_\gamma)x_\gamma^3\,(F_A + F_V) \tag{3.41}$$

where $x_\gamma = \frac{E_\gamma}{2m_B}$. To leading order in heavy quark expansion and for energetic photons $E_\gamma \sim \mathcal{O}(m_B/2)$, the two form factors coincide and are given by

$$F_A = F_V = \frac{Q_u m_B f_B}{2E_\gamma} \frac{1}{\lambda_B}, \tag{3.42}$$

which can be used to extract λ_B from branching ratio measurements. The authors in [57] also calculated radiative and power corrections to the form-factor relation in Equation 3.42 and concluded a significant decrease for the branching ratio with respect to these corrections.

So far, only upper limits from CLEO [58] and BaBar [59, 60] exist on the branching ratio of $B \to \gamma\ell\nu$ and the current situation is still inconclusive, resulting only in a lower bound on

$$\lambda_B \geq 150\,\text{MeV} \qquad (B \to \gamma\ell\nu). \tag{3.43}$$

A decreasing upper limit on the branching-ratio measurement, which might be improved by the experiments Belle and Belle II, implies an increasing lower bound on λ_B.

3.2.2 Numerical input

Here we collect the numerical input, used in our analysis, in Table 3.1. Additional input, which will be used for (semi-)leptonic decays and B^0-$\bar{B}^0$ mixing, are postponed to Subsection 4.2.1. For the purpose of comparability, we also quote, in addition to our observable predictions, the results from a conventional error estimation in the phenomenological part. In that sense, the following input for $\rho_A^{M_1M_2}$ is used

$$|\rho_A^{M_1M_2}| = \begin{cases} 1.9 \pm 0.1 & \text{for } M_1M_2 = PP, \\ 1.7 \pm 0.3 & \text{for } M_1M_2 = PV, \\ 1.6 \pm 0.3 & \text{for } M_1M_2 = VV, \end{cases} \tag{3.44}$$

and $\phi_A^{M_1M_2} = 0$ to obtain central values of predictions. The error from WA contributions are then obtained from freely varying $\phi_A^{M_1M_2} \in [0; 2\pi]$ and $|\rho_A^{M_1M_2}|$ within its above defined error interval. In the case of HS corrections, $|\rho_H^{M_1M_2}| = 0 \pm 1$ for all final states and $\phi_H^{M_1M_2} = 0$ with the same error treatment as for WA. Inspired from our findings in Chapter 5, the input is chosen, such that most observables do not contradict existing measurements within the SM.

As shown in Equation 3.33, the positive helicity amplitudes, being power-suppressed compared to the longitudinal and negative polarised amplitudes, cannot be calculated in QCDF and will be set in our analysis to zero through $F_+^{B\to V} = 0$ according to the treatment in [61]. In order to obtain an estimate of potential corrections to this simplification,

we will employ naive factorisation and vary the form factors within $F_+^{B\to V} = \pm 0.06$. Since the experimental information on $\mathcal{B}(B \to \gamma\ell\nu)$ is still inconclusive, we will use the suggested input from tree-level-dominated B-meson decays, $\lambda_B = 0.200^{+0.250}_{-0}$ GeV [2].

Further, the input for the CKM-matrix elements are taken from the UTfit collaboration [62]. For the SM part, Chapter 5, we employ the results of the CKM "Standard Model fit", whereas in Chapter 6 we allow for additional contributions beyond the SM and results from the CKM "New Physics fit" are employed. Compared to the former, the latter fit allows for an additional generic correction to the $B - \bar{B}$ mixing amplitude, which is especially important for the analysis of CP asymmetries.

Electroweak input

$G_F[10^{-5}\,\text{GeV}^{-2}]$	$\Lambda^{(5)}_{\overline{\text{MS}}}[\text{GeV}]$	$M_Z[\text{GeV}]$	$\alpha_s^{(5)}(M_Z)$	$\alpha_e^{(5)}(m_b)$	
1.16638	0.213	91.1876	0.1184	1/132	[63, 64]

quark masses

m_t^{pole}	$m_b(m_b)$	$m_c(m_b)$	m_s	m_q/m_s	
(173.2 ± 0.9)	4.2	(1.3 ± 0.2)	(0.095 ± 0.005)	0.0370	[36, 63, 65]

CKM-matrix elements

	λ	$\lvert V_{cb}\rvert$	$\bar\rho$	$\bar\eta$	
SM	0.22535 ± 0.00065	0.04172 ± 0.00056	0.127 ± 0.023	0.353 ± 0.014	[62]
NP	0.22530 ± 0.00060	0.04061 ± 0.00097	0.147 ± 0.045	0.368 ± 0.048	

B meson input

	B_u	B_d	B_s	
$f_B[\text{MeV}]$	190.5 ± 4.2		227.7 ± 4.5	
$\lambda_B[\text{MeV}]$	200^{+250}_{-0}	200^{+250}_{-0}	200^{+250}_{-0}	[66]
$\tau_B[\text{ps}^{-1}]$	1.641	1.519	1.516	[63]
$M_B[\text{MeV}]$	5279.25	5279.58	5366.77	

Hadronic input — pseudoscalar mesons

	K	π	η	η'	
$f_P[\text{MeV}]$	160	131	$(1.07 \pm 0.02) f_\pi$	$(1.34 \pm 0.06) f_\pi$	[36, 67]
$F_0^{B\to P}$	$0.33 \pm 0.04^\dagger$	0.26 ± 0.02	0.23 ± 0.05	0.19 ± 0.12	[4, 67, 68]
$F^{B_s\to P}$	$0.30^{+0.04}_{-0.03}$	–	–	–	[69]
$\alpha_1(P)$	0.05 ± 0.02	0.00	0.00	0.00	[67, 70]
$\alpha_2(P)$	0.17 ± 0.10	0.17 ± 0.10	0.00 ± 0.3	0.00 ± 0.3	

Hadronic input — vector mesons

	K^*	ρ	ϕ	ω	
$f_V[\text{MeV}]$	218 ± 4	209 ± 1	221 ± 3	187 ± 3	[36]
$f_V^\perp[\text{MeV}]$	175 ± 10	156 ± 9	175 ± 9	142 ± 9	[71]
$A_0^{B\to V}$	0.34 ± 0.03	0.30 ± 0.03	–	0.28 ± 0.03	[61]
$F_-^{B\to V}$	0.62 ± 0.05	0.58 ± 0.04	–	0.55 ± 0.04	
$F_+^{B\to V}$	0.00 ± 0.06	0.00 ± 0.06	–	0.00 ± 0.06	[53]
$A_0^{B_s\to V}$	0.39 ± 0.03	–	0.47 ± 0.04	–	[61]
$F_-^{B_s\to V}$	0.59 ± 0.04	–	0.72 ± 0.04	–	
$F_+^{B_s\to V}$	0.00 ± 0.06	–	0.00 ± 0.06	–	[53]
$\alpha_1(V)$	0.02 ± 0.02	0.00	0.00	0.00	[72]
$\alpha_1^\perp(V)$	0.03 ± 0.03	0.00	0.00	0.00	
$\alpha_2(V)$	0.08 ± 0.06	0.10 ± 0.05	0.13 ± 0.06	0.10 ± 0.05	
$\alpha_2^\perp(V)$	0.08 ± 0.06	0.11 ± 0.05	0.11 ± 0.05	0.11 ± 0.05	

TABLE 3.1: Numerical input used in our analysis. Form factors are given at $q^2 = 0$. Other scale-dependent quantities are quoted at the scale $\mu = 2\,\text{GeV}$. †For the $B \to K$ form factor we used $\alpha_4^K(2.2\,\text{GeV}) = -0.0089$ [4] as additional input.

Chapter 4

Observables

This chapter defines all relevant observables that enter our analysis. We concentrate in the first part on hadronic decays as the main subject of interest in this work and begin with the definition of branching ratios and CP asymmetries in Subsection 4.1.1, from which certain isospin-sensitive observables are constructed. These combined observables are discussed in more detail in Subsection 4.1.2 for the decay system $B \to K\pi$. The non-negligible decay-rate difference of the heavy and light mass eigenstates of the B_s meson lead to some subtlety in the calculation of observables for B_s compared to B_d decays, considered in Subsection 4.1.3. The last part is dedicated to observables that might be correlated in certain NP models to those from hadronic decays, in particular, to (semi-)leptonic decays in Subsection 4.2.1 and neutral B-meson mixing in Subsection 4.2.3. Since the phenomenology of hadronic decays within the SM is exhaustively discussed in Chapter 5, we at least briefly discuss certain tensions in the data of (semi-)leptonic decays in Chapter 4.2.2.

4.1 Observables from hadronic 2-body decays

4.1.1 Definition of observables and observable sets

The 2-body decays of a B meson into final states $f = PP$, PV, V_hV_h with light charmless pseudo-scalar and/or vector mesons, given for a polarisation mode, $h = L, \perp, \parallel$, provide various observables. There are the CP-averaged branching fractions and direct rate CP asymmetries

$$\bar{\mathcal{B}}(\bar{B} \to \bar{f}) = \frac{\tau_B}{2}\left(\Gamma(\bar{B} \to \bar{f}) + \Gamma(B \to f)\right) = \tau_B\,\bar{\Gamma}(\bar{B} \to \bar{f}), \tag{4.1}$$

$$A^{\mathrm{CP}}(\bar{B} \to \bar{f}) = \frac{\Gamma(\bar{B} \to \bar{f}) - \Gamma(B \to f)}{2\bar{\Gamma}(\bar{B} \to \bar{f})}, \tag{4.2}$$

with τ_B the lifetime of the B meson and Γ the decay rates. Besides these, frequently combinations involving different combinations of charged and neutral B, M_1 and, M_2,

are used in the literature that are either ratios of branching fractions or differences of direct CP asymmetries. The complete set of ratios [73, 74] is

$$\begin{aligned}
R_c^B &\equiv 2\,\frac{\bar{\mathcal{B}}(B^-\to M_1^- M_2^0)}{\bar{\mathcal{B}}(B^-\to M_1^0 M_2^-)}, & R_n^B &\equiv \frac{1}{2}\,\frac{\bar{\mathcal{B}}(\bar{B}^0\to M_1^- M_2^+)}{\bar{\mathcal{B}}(\bar{B}^0\to M_1^0 M_2^0)},\\
R_c^{M_1} &\equiv 2\,\frac{\bar{\mathcal{B}}(B^-\to M_1^- M_2^0)}{\bar{\mathcal{B}}(\bar{B}^0\to M_1^- M_2^+)}, & R_n^{M_1} &\equiv \frac{1}{2}\,\frac{\bar{\mathcal{B}}(B^-\to M_1^0 M_2^-)}{\bar{\mathcal{B}}(\bar{B}^0\to M_1^0 M_2^0)},\\
R_c^{M_2} &\equiv \frac{\bar{\mathcal{B}}(B^-\to M_1^0 M_2^-)}{\bar{\mathcal{B}}(\bar{B}^0\to M_1^- M_2^+)}, & R_n^{M_2} &\equiv \frac{\bar{\mathcal{B}}(B^-\to M_1^- M_2^0)}{\bar{\mathcal{B}}(\bar{B}^0\to M_1^0 M_2^0)},
\end{aligned} \tag{4.3}$$

where factors of the life-time ratio τ_{B^0}/τ_{B^-} in $R_{c,n}^{B,M_1,M_2}$ [74] have not been included in the definition, anticipating that these ratios are extracted directly in experiment allowing for the cancellation of experimental systematic errors. Further, the following two differences of direct CP asymmetries are frequently considered

$$\begin{aligned}
\Delta A^{\rm CP} &\equiv A^{\rm CP}(\bar{B}^0\to M_1^- M_2^+) - A^{\rm CP}(B^-\to M_1^- M_2^0),\\
\Delta A_0^{\rm CP} &\equiv A^{\rm CP}(\bar{B}^0\to M_1^0 M_2^0) - A^{\rm CP}(B^-\to M_1^0 M_2^-).
\end{aligned} \tag{4.4}$$

In addition, two further CP asymmetries S_f and H_f arise for neutral $\bar{B}^0$ meson decays into a CP eigenstate f that can be extracted in time-dependent analysis

$$A^{\rm CP}(\bar{B}^0\to \bar{f})(t) = \frac{S_f\sin(\Delta m_B\,t) - C_f\cos(\Delta m_B\,t)}{\cosh\left(\frac{\Delta\Gamma_B}{2}t\right) - H_f\sinh\left(\frac{\Delta\Gamma_B}{2}t\right)}, \qquad (\bar{B}^0 = \bar{B}_d,\,\bar{B}_s), \tag{4.5}$$

where the mass and width differences of the heavy and light mass eigenstates are denoted as $\Delta m_B = m_{B,H} - m_{B,L} > 0$ and $\Delta\Gamma_B = \Gamma_{B,H} - \Gamma_{B,L}$, respectively. A measurement of the asymmetry H_f in the B_d system is unlikely in the foreseeable future since $\Delta\Gamma_{B_d}/\Gamma_{B_d} \ll 1$. All the CP asymmetries

$$S_f = \frac{2\,{\rm Im}(\lambda_f)}{1+|\lambda_f|^2}, \qquad H_f = \frac{2\,{\rm Re}(\lambda_f)}{1+|\lambda_f|^2}, \qquad C_f = -A^{\rm CP} = \frac{1-|\lambda_f|^2}{1+|\lambda_f|^2}, \tag{4.6}$$

can be expressed in terms of a single complex quantity [75]

$$\lambda_f \equiv \frac{q}{p}\frac{\overline{\mathcal{A}}_f}{\mathcal{A}_f}, \tag{4.7}$$

where q, p are the strong interaction eigenstate components of the mass eigenstates $B_{L,H}$ and the decay amplitudes $\overline{\mathcal{A}}_f \equiv \mathcal{A}(\bar{B}\to\bar{f})$ as well as $\mathcal{A}_f \equiv \mathcal{A}(B\to f)$.

In the case of 2 vector mesons in the final state, an angular analysis can moreover determine further quantities such as the strong phase differences between the individual

polarisation amplitudes

$$\varphi_{\perp,\parallel} = \arg \frac{\mathcal{A}_{f_{\perp,\parallel}}}{\mathcal{A}_{f_L}}, \qquad \bar{\varphi}_{\perp,\parallel} = \arg \frac{\overline{\mathcal{A}}_{f_{\perp,\parallel}}}{\overline{\mathcal{A}}_{f_L}}, \tag{4.8}$$

from which again two CP-averaged and two CP-violating observables can be constructed [53]

$$\begin{aligned} \phi_{\perp,\parallel}(B \to VV) &= \frac{1}{2}\left(\bar{\varphi}_{\perp,\parallel} + \varphi_{\perp,\parallel}\right) - \pi \,\text{sign}\,\left(\bar{\varphi}_{\perp,\parallel} + \varphi_{\perp,\parallel}\right)\,\theta\,\left(\bar{\varphi}_{\perp,\parallel} - \varphi_{\perp,\parallel} - \pi\right), \\ \Delta\phi_{\perp,\parallel}(B \to VV) &= \frac{1}{2}\left(\bar{\varphi}_{\perp,\parallel} - \varphi_{\perp,\parallel}\right) + \pi\,\theta\left(\bar{\varphi}_{\perp,\parallel} + \varphi_{\perp,\parallel}\right). \end{aligned} \tag{4.9}$$

The branching ratios of the single polarisation amplitudes are typically normalised to the total branching ratio $\mathcal{B}(B \to VV) = \sum_h \mathcal{B}(B \to V_h V_h)$ and parametrised by the so-called polarisation fraction, defined as

$$f_h(B \to VV) = \frac{\bar{\mathcal{B}}(B \to V_h V_h)}{\bar{\mathcal{B}}(B \to VV)}. \tag{4.10}$$

A complete set of independent observables in $B \to VV$ decays consists out of ten observables. We include in our fits, according to the usually quoted experimental results, the total branching ratio $\mathcal{B}$ and CP asymmetry C together with two out of the three polarisation fractions f_h and polarisation specific CP asymmetries C_h and the four relative strong phases $\phi_{\perp,\parallel}$ and $\Delta\phi_{\perp,\parallel}$ from Equation 4.9. So far, $B \to K^*\phi$ is the only hadronic decay mode for which a complete angular analysis could be performed.

We investigate mainly $B \to M_1 M_2$ decays mediated by $b \to s$ transitions, in particular for the NP analysis, where we can exploit the phenomenological richness of several well-measured decay systems, but $b \to d$ examples will be also considered in the analysis of the SM. The final state $M_1 M_2$ consists either out of two pseudo-scalars ($M_1 M_2 = PP$) or one pseudo-scalar and one vector ($M_1 M_2 = PV$) meson or two vector mesons ($M_1 M_2 = VV$), which are listed in Table 4.1, Table 4.2 and Table 4.3, respectively, together with the observables that have been measured. We use the most recent values from the HFAG 2012 compilation and updates from 2014 on the website [3]. Those observables that were updated meanwhile from the individual experiments, but not yet included from the HFAG collaboration, enter the likelihood function in Equation A.2 as single measurement and are explicitly mentioned in the tables (marked by an dagger). For each decay group, composed of $u \to$ quark-exchange related decay modes, we assume one universal WA parameter $\rho_A^{M_1 M_2}$.

In addition, we investigate the complementarity of composed observables, the ratios of branching fractions $R_{c,n}^{B,M_1,M_2}$ from Equation 4.3 and differences of CP asymmetries ΔA_{CP} in Equation 4.4. It is desirable to have direct experimental determinations of the uncertainties for these "composed" observables that already account for the cancellation

$b \to s$				
$B \to K\pi$	$B \to K\eta$	$B \to K\eta'$	$B_s \to KK$ [76]	$B_s \to \pi\pi$
$\bar{K}^0\pi^0$: $\mathcal{B}$, C, S	$\bar{K}^0\eta$: $\mathcal{B}$	$\bar{K}^0\eta'$: $\mathcal{B}$, C, S	K^+K^- : $\mathcal{B}$, C, S	$\pi^+\pi^-$: $\mathcal{B}$
$K^-\pi^+$: $\mathcal{B}$, C	$K^-\eta$: $\mathcal{B}$, C	$K^-\eta'$: $\mathcal{B}$, C		
$K^-\pi^0$: $\mathcal{B}$, C				
$\bar{K}^0\pi^-$: $\mathcal{B}$, C				
$b \to d$				
$B \to KK$	$B_s \to K\pi$			
$\bar{K}^0K^0$: $\mathcal{B}$	$K^+\pi^-$: $\mathcal{B}$, C			
K^+K^-: $\mathcal{B}$				
K^-K^0 : $\mathcal{B}$, C				

TABLE 4.1: Observables of $B \to PP$ decays mediated by $b \to (d, s)$ transitions that are used in the fit.

$b \to s$				
$B \to K^*\pi$	$B \to K\rho$	$B \to K^*\eta$	$B \to K^*\eta'$	$B \to K\phi$ [77–80]
$\bar{K}^{*0}\pi^0$: $\mathcal{B}$, C	$\bar{K}^0\rho^0$: $\mathcal{B}$, C, S	$\bar{K}^{*0}\eta$: $\mathcal{B}$, C	$\bar{K}^{*0}\eta'$: $\mathcal{B}$, C	$\bar{K}^0\phi$: $\mathcal{B}$, $C^\dagger$, S
$K^{*-}\pi^+$: $\mathcal{B}$, C	$K^-\rho^+$: $\mathcal{B}$, C	$K^{*-}\eta$: $\mathcal{B}$, C	$K^{*-}\eta'$: $\mathcal{B}$, C	$K^-\phi$: $\mathcal{B}$, C
$K^{*-}\pi^0$: $\mathcal{B}$, C	$K^-\rho^0$: $\mathcal{B}$, C			
$\bar{K}^{*0}\pi^-$: $\mathcal{B}$, C	$\bar{K}^0\rho^-$: $\mathcal{B}$, C			
$B \to K\omega$ [81, 82]				
$\bar{K}^0\omega$: $\mathcal{B}$, C, S				
$\bar{K}^-\omega$: $\mathcal{B}$, C				

TABLE 4.2: Observables of $B \to PV$ decays mediated by $b \to s$ transitions that are used in the fit.

of systematic uncertainties, which are only accessible to the experimental collaborations themselves. This is important because usually outsiders are not in the position to account retroactively for cancellations of systematic errors and are restricted to the application of rules of error propagation to the uncertainties of the measurements of the involved components, which then might result in too conservative estimates. Of course such a procedure on the experimental side requires that the according decay modes with charged and neutral final states can be analysed simultaneously, which is the case for BaBar, Belle, and also Belle II collaborations. In this context, it should be noted that ratios of Gaussian distributed quantities are not Gaussian distributed, although the differences are small as long as the tail regions of the distribution do not contribute. We account for this subtlety through adapting the correct distribution function for ratios of branching ratios as described in Appendix A.1.

The possibility of constructing composed observables are mostly effective for the

$b \to s$		
$B \to K^*\rho$	$B \to K^*\phi$ [83, 84]	$B \to K^*\omega$
$\bar{K}^{*0}\rho^0$: $\mathcal{B}$, C, f_L	$\bar{K}^{*0}\phi^\dagger$: $\mathcal{B}$, $f_{L,\perp}$, C, $C_{L,\perp}$, $\phi_{\perp,\parallel}$, $\Delta\phi_{\perp,\parallel}$	$\bar{K}^{*0}\omega$: $\mathcal{B}$, C, f_L
$K^{*-}\rho^+$: $\mathcal{B}$, C, f_L	$K^{*-}\phi$: $\mathcal{B}$, $f_{L,\perp}$, C, $C_{L,\perp}$, $\phi_{\perp,\parallel}$, $\Delta\phi_{\perp,\parallel}$	$K^{*-}\omega$: $\mathcal{B}$, C, f_L
$K^{*-}\rho^0$: $\mathcal{B}$, C, f_L		
$\bar{K}^{*0}\rho^-$: $\mathcal{B}$, C, f_L		
$B_s \to \phi\phi$	$B_s \to K^*K^*$[85]	
$\phi\phi$: $\mathcal{B}$, f_L	$\bar{K}^{*0}K^{*0}$: $\mathcal{B}$, $f_{L,\perp}$	
$b \to d$		
$B_s \to K^*\phi$	$B \to K^*K^*$	
	$\bar{K}^{*0}K^{*0}$: $\mathcal{B}$, f_L	
$K^{*0}\phi$: $\mathcal{B}$, f_L	$K^{*-}K^{*0}$: $\mathcal{B}$, f_L	

TABLE 4.3: Observables of $B \to VV$ decays mediated by $b \to (d, s)$ transitions that are used in the fit.

decay system $B \to K\pi$, $K\rho$, $K^*\pi$, $K^*\rho$ due to four individual decay modes. These will play the crucial role in constraining the NP parameter space in Chapter 6. For this purpose, we construct a full independent set of observables by three CP asymmetries, the difference in CP asymmetry $\Delta A_{\rm CP}$, one branching ratio and three specific chosen ratios of branching ratios (Set II). The fit results in the SM section will be compared with the observable set of four branching ratios and four CP asymmetries (Set I). In summary

$$\begin{aligned} \text{Set I}: &\quad (4\times\mathcal{B}) \quad + \quad (4\times C) \\ \text{Set II}: &\quad (1\times\mathcal{B}) \quad + \quad (3\times C) \; + \\ &\quad (3\times R_{n,c}) + \quad \Delta A_{CP}\,. \end{aligned} \tag{4.11}$$

Experimental data on the mixing-induced CP asymmetries S_f also exist for most decay systems, but are lacking of precision at the moment and will become very well measured by the Belle II collaboration in the near future [86, 87]. Our strategy will be to constrain the WA parameter $\rho_A^{M_1M_2}$ for each decay system together with the NP parameter space, from which we then predict S_f. In order to avoid including NP effects from B^0-$\bar{B}^0$ mixing in S_f that can typically not reliably be accounted for in a model-independent analysis, we instead predict the observable [88, 89]

$$\begin{aligned} \Delta S_f &\equiv S(\bar{B}_d \to \bar{f}) - \eta_f S(\bar{B}_d \to J/\psi\,\bar{K}_S), \\ \Delta S_f &\equiv S(\bar{B}_s \to \bar{f}) - \eta_f S(\bar{B}_s \to J/\psi\,\phi), \end{aligned} \tag{4.12}$$

with $\eta_f = \pm 1$ the CP eigenvalue of the final state f. The decay $\bar{B}_d \to J/\psi\,\bar{K}_S$ and

$\bar{B}_s \to J/\psi\,\phi$ are dominated by contributions from charm tree-level operators and CP violation in the decay is both parametrically (CKM) and topologically (loop) suppressed. We expect that the CP-violating phase in B^0-$\bar{B}^0$ mixing, ϕ_{B_d} and ϕ_{B_s}, can clearly be extract, even in the presence of most NP scenarios [75]

$$\begin{aligned} \lambda_{J/\psi\,\bar{K}_S} &\simeq e^{-\phi_{B_d}}, & S(\bar{B}_d \to J/\psi\,\bar{K}_S) &\simeq \sin 2\beta, \\ \lambda_{J/\psi\,\phi} &\simeq e^{-\phi_{B_s}}, & S(\bar{B}_s \to J/\psi\,\phi) &\simeq \sin 2\beta_s, \end{aligned} \tag{4.13}$$

in which the angles of the CKM unitarity triangle are defined as $\beta = \arg\left(\lambda_c^d/\lambda_t^d\right)$ and $\beta_s = \arg\left(\lambda_t^s/\lambda_c^s\right)$. This source of CP violation enters all mixing-induced CP asymmetries in the same way and can be eliminated by the construction of ΔS_f, which therefore exclusively measures the interference of CP violation in the decay and in mixing.

Further interesting candidates to predict are the direct and mixing-induced CP asymmetries in $\bar{B}_s \to \phi\phi$ and $\bar{B}_s \to \bar{K}^{*0}K^{*0}$. On the one hand, the SM predictions for CP violation are to a very good approximation zero (see Appendix B) and we do not have to struggle with SM background. On the other hand, no measurements, apart from branching ratios and polarisation fractions, exist at the moment, but could become available in the near future [90]. The latter aspect implies that the WA parameters, $\rho_A^{\phi\phi}$ and $\rho_A^{K^*K^*}$, cannot be well constrained at the moment and, in combination with CP-violating contributions beyond the SM, could lead to visible effects in these observables.

4.1.2 Anatomy of $B \to K\pi$

Various B meson decays are studied in the phenomenological part of this work. However, the observables for $B \to K\pi$ are particular interesting because they are experimentally quite well measured. We therefore clarify how the single observables depend on the flavour amplitudes to obtain a qualitative handle for the outcome of our fits in Chapters 5 and 6. All four decays of a B meson into a pion and kaon are dominated by the QCD-penguin flavour amplitude $\hat{\alpha}_4^c(\pi K)$, which can be used as an expansion parameter for the decay amplitudes. Thereby, the definition of the following ratios, which had been mentioned first in [74], proof useful:

$$r_{\rm T} \equiv -\left|\frac{\lambda_u^s}{\lambda_c^s}\right| \frac{\alpha_1(\pi K)}{\hat{\alpha}_4^c(\pi K)}, \qquad r_{\rm T^C} \equiv -\left|\frac{\lambda_u^s}{\lambda_c^s}\right| \frac{A_{K\pi}}{A_{\pi K}} \frac{\alpha_2(K\pi)}{\hat{\alpha}_4^c(\pi K)},$$

$$r_{\rm EW} \equiv \frac{3}{2}\frac{A_{K\pi}}{A_{\pi K}} \frac{\alpha_{3,\rm EW}^c(K\pi)}{\hat{\alpha}_4^c(\pi K)}, \qquad r_{\rm EW^C} \equiv \frac{3}{2} \frac{\alpha_{4,\rm EW}^c(\pi K)}{\hat{\alpha}_4^c(\pi K)}, \qquad r_{\rm EW^A} \equiv \frac{3}{2} \frac{\beta_{3,\rm EW}^c(\pi K)}{\hat{\alpha}_4^c(\pi K)}. \tag{4.14}$$

The absolute value of the QCD-penguin amplitude $|\hat{\alpha}_4^c(\pi K)|$ is well known from branching ratio measurements, but its strong phase, $\hat{\phi}_4^c(\pi K)$, is rather undetermined. Since the calculable part of $\hat{\phi}_4^c(\pi K)$ is small, receiving contributions first at $\mathcal{O}(\alpha_s)$, the

incalculable part can become compatible in size, but need to be extracted by the fits. It is therefore advisable, when trying to understand our fit results, to reparametrise the ratios in the following way

$$r_i \equiv \left(r_i^{\mathrm{R}} + i\, r_i^{\mathrm{I}}\right) e^{-i\hat{\phi}_4^c(\pi K)}, \qquad (i = \mathrm{T}, \mathrm{EW}), \tag{4.15}$$

with analogue expressions for the colour-suppressed and WA topologies. Similar expansion parameters can be constructed for the other decay chains $B \to PV, VP, VV$. Since their QCD-penguin amplitude is predicted to be smaller in QCDF, expanding observables in terms of the ratios suffer from less well convergence. The dependence on the real and imaginary parts are kept explicitly because they contribute to different observables. For example, the real parts enter in the expansions of the ratios of branching ratios, which are given in the SM

$$\begin{aligned}
R_n^B(K\pi) &\simeq 1 + 2\,\mathrm{Re}\left(\mathrm{r_{EW}} + \mathrm{r_{EW^C}}\right) - 2\,\mathrm{Re}\left(\mathrm{r_T} + \mathrm{r_{T^C}}\right)\cos\gamma,\\
R_c^B(K\pi) &\simeq 1 + 2\,\mathrm{Re}\left(\mathrm{r_{EW}} + \mathrm{r_{EW^C}}\right) - 2\,\mathrm{Re}\left(\mathrm{r_T} + \mathrm{r_{T^C}}\right)\cos\gamma,\\
\frac{\tau_{B^0}}{\tau_{B^-}} R_n^K(K\pi) &\simeq 1 + 2\,\mathrm{Re}\left(\mathrm{r_{EW}}\right) - 2\,\mathrm{Re}\left(\mathrm{r_{T^C}}\right)\cos\gamma,\\
\frac{\tau_{B^0}}{\tau_{B^-}} R_c^K(K\pi) &\simeq 1 + 2\,\mathrm{Re}\left(\mathrm{r_{EW}}\right) - 2\,\mathrm{Re}\left(\mathrm{r_{T^C}}\right)\cos\gamma,\\
\frac{\tau_{B^0}}{\tau_{B^-}} R_n^\pi(K\pi) &\simeq 1 + 2\,\mathrm{Re}\left(2\,\mathrm{r_{EW}} + \mathrm{r_{EW^C}}\right) - 2\,\mathrm{Re}\left(\mathrm{r_T} + 2\,\mathrm{r_{T^C}}\right)\cos\gamma,\\
\frac{\tau_{B^0}}{\tau_{B^-}} R_c^\pi(K\pi) &\simeq 1 - 2\,\mathrm{Re}\left(\mathrm{r_{EW^C}}\right) + 2\,\mathrm{Re}\left(\mathrm{r_T}\right)\cos\gamma,
\end{aligned} \tag{4.16}$$

with the weak phase $\gamma = \arg\left(\lambda_u^d/\lambda_c^d\right)$. We can now make use of the parametrisation in Equation 4.15, to rewrite the real parts of the ratios through

$$\mathrm{Re}\,(r_i) = r_i^{\mathrm{R}} \cos\hat{\phi}_4^c(\pi K) + r_i^{\mathrm{I}} \sin\hat{\phi}_4^c(\pi K). \tag{4.17}$$

We know from the arguments above that the imaginary parts of the flavour amplitudes are suppressed by either α_s or $\Lambda_{\mathrm{QCD}}/m_b$, which implies $r_i^{\mathrm{I}} \ll r_r^{\mathrm{R}}$. If $\hat{\phi}_4^c(\pi K)$ is not in the vicinity of $\pi/2$ or $3/2\pi$,[1] the second term in Equation 4.17 can be neglected for these observables and ratios of branching ratios mainly depend on $R_{c,n}^{B,K,\pi} \sim \cos\hat{\phi}_4^c(\pi K)$.

However, the CP asymmetries are dominated by the imaginary part of the ratios

$$\begin{aligned}
C(\bar{B}^0 \to K^-\pi^+) &\simeq 2\,\mathrm{Im}\left(\mathrm{r_T}\right)\sin\gamma, & C(\bar{B}^0 \to \bar{K}^0\pi^0) &\simeq -2\,\mathrm{Im}\left(\mathrm{r_{T^C}}\right)\sin\gamma,\\
C(B^- \to K^-\pi^0) &\simeq 2\,\mathrm{Im}\left(\mathrm{r_T} + \mathrm{r_{T^C}}\right)\sin\gamma, & C(B^- \to \bar{K}^0\pi^-) &\simeq 0,
\end{aligned} \tag{4.18}$$

[1] This would imply that the QCD-penguin amplitude become purely imaginary, which in principle is not excluded if we allow the WA parameter $\rho_A^{M_1M_2}$ to vary within large values. However, it turns out that such a scenario seems to be not preferred from the data — neither in the SM nor beyond.

which expansion can be, similar as above, written in

$$\mathrm{Im}\,(r_i) = -r_i^{\mathrm{R}} \sin\hat{\phi}_4^c(\pi K) + r_i^{\mathrm{I}} \cos\hat{\phi}_4^c(\pi K), \tag{4.19}$$

but no further simplifications can be made in general and statements depend on the model under consideration and the outcome of the fits. The expansion will be very useful in the forthcoming sections to qualitative discus the features of our results. Although the mixing-induced CP asymmetry, $\Delta S_{K\pi}$, is not going to be included into the set of observables, it can in complete analogue be expanded in terms of the ratios

$$\Delta S_{K\pi} \simeq 2\mathrm{Re}\,(r_{\mathrm{TC}})\,\cos 2\beta \sin\gamma. \tag{4.20}$$

As in the case for the ratios of branching ratios, the mixing-induced CP asymmetry is dominated by $\Delta S_{K\pi} \sim \cos\hat{\phi}_4^c$.

4.1.3 Implications of non-negligible $\Delta\Gamma_s$ on observables from B_s decays

A further subtlety arises for the decay of a B_s meson, which is going to be discussed here and was first noted in [91]. The lifetime differences between the light and heavy mass eigenstates of the B_s meson is, in contrast to the B_d meson, sizeable and leads to a relevant distinction between the usual theoretical and experimental definition of branching ratios and direct CP asymmetries. To understand this difference, we should be more careful in defining the branching ratio in Equation 4.1, which obeys a time dependence, similar as for the CP rate asymmetry in Equation 4.5,

$$\begin{aligned}
\frac{1}{2}\bar{\Gamma}(\bar{B}^0 \to \bar{f})(t) &= R_{\mathrm{H}}^f e^{-\Gamma_{\mathrm{H}} t} + R_{\mathrm{L}}^f e^{-\Gamma_{\mathrm{L}} t}, \\
\bar{\mathcal{B}}(\bar{B}^0 \to \bar{f})(t) &= \frac{\tau_B}{2}\left(R_{\mathrm{H}}^f + R_{\mathrm{L}}^f\right) e^{-t/\tau_B}\left[\cosh\left(\frac{\Delta\Gamma_B}{2}t\right) + H_f \sinh\left(\frac{\Delta\Gamma_B}{2}t\right)\right],
\end{aligned} \tag{4.21}$$

where $\bar{\Gamma}$ is expressed by the decay rates of the mass eigenstates, $R_{\mathrm{H,L}}^f e^{-\Gamma_{\mathrm{H,L}} t}$. Whereas the experimental branching ratio is given by the total event yield, which does not contain any information on the decay time, the theoretical branching ratio is defined in terms of the flavour eigenstates, given at $t = 0$

$$\begin{aligned}
\bar{\mathcal{B}}(\bar{B}^0 \to \bar{f})_{\mathrm{exp.}} &\equiv \int_0^\infty \bar{\Gamma}(\bar{B}^0 \to \bar{f})\, dt = \frac{\tau_B}{2}\left(R_{\mathrm{H}}^f + R_{\mathrm{L}}^f\right)\left[\frac{1 + H_f\, y}{1 - y^2}\right], \\
\bar{\mathcal{B}}(\bar{B}^0 \to \bar{f})_{\mathrm{the.}} &\equiv \bar{\mathcal{B}}(\bar{B}^0 \to \bar{f})\big|_{t=0} = \frac{\tau_B}{2}\left(R_{\mathrm{H}}^f + R_{\mathrm{L}}^f\right),
\end{aligned} \tag{4.22}$$

where $y \equiv \frac{\Delta\Gamma}{2\Gamma}$. These equations connect the measured branching ratio with its theoretical prediction

$$\bar{\mathcal{B}}(\bar{B}^0 \to \bar{f})_{\mathrm{exp.}} = \bar{\mathcal{B}}(\bar{B}^0 \to \bar{f})_{\mathrm{the.}}\left[\frac{1 + H_f\, y}{1 - y^2}\right]. \tag{4.23}$$

In the case of the B_d meson, we already mentioned above that $y_d \ll 1$ and both branching-ratio definition approximately coincide. The decay width difference for the B_s meson is sizeable, $y_s = 0.058 \pm 0.10$ [3], and the correction factor on the right-hand side cannot be neglected. If the final states are non-CP-eigenstates, $H_f = 0$ and the enhancement, $(1 - y_s^2)^{-1}$, is below 1%. However, the correction in the case of CP eigenstates can become significant and were estimated for some cases to be of $\mathcal{O}(10\%)$ [92]. The asymmetry H_f can in principle be measured and the rescaling could be preformed at the experimental side. This approach is desirable if the estimate of hadronic matrix elements relies on symmetry arguments and does not allow for an extraction of H_f. A systematic approach as QCDF does not suffer from this problem and the correction can be calculated, which is incorporated in our numerical analysis. To complete the actual discussion, we only need to generalise the presented formalism also to $B \to VV$ modes. The branching and polarisation fractions need to be corrected through

$$\bar{\mathcal{B}}(\bar{B}^0 \to VV)_{\text{exp.}} = \sum_{h=L,\perp\parallel} \bar{\mathcal{B}}(\bar{B}^0 \to V_h V_h)_{\text{the.}} \left[\frac{1 + H_{V_h V_h}\, y_s}{1 - y_s^2}\right], \tag{4.24}$$

$$f_h(\bar{B}^0 \to VV)_{\text{exp.}} = \frac{\bar{\mathcal{B}}(\bar{B}^0 \to V_h V_h)_{\text{the.}}}{\bar{\mathcal{B}}(\bar{B}^0 \to VV)_{\text{the.}}} \left[\frac{1 + H_{V_h V_h}\, y_s}{1 - y_s^2}\right]. \tag{4.25}$$

The corresponding formula for the direct CP asymmetries then follows from the definition in Equation 4.2.

4.2 Observables from (semi-)leptonic decays and B^0-$\bar{B}^0$ mixing

4.2.1 Observables from $B \to K^*\gamma$, $B \to (K,\, K^*)\,\ell^+\ell^-$, and $B_s \to \mu^+\mu^-$

Besides $B \to M_1 M_2$ decay channels, we in addition use complementary constraints from (semi-)leptonic FCNC decays, mediated by $b \to s(\gamma)\ell^+\ell^-$ to constrain the parameters of scenarios beyond the SM. The present subsection describes the details of experimental input and the evaluation of theory predictions of the relevant observables of the four exclusive decays $B \to K^*\gamma$, $B \to (K,\, K^*)\,\ell^+\ell^-$, and $B_s \to \mu^+\mu^-$, which are listed in Table 4.4.

The definitions of these observables can be found in [105] and theory predictions follow the procedure outlined in [106] for $B \to K^*\ell^+\ell^-$, [107] for $B \to K\,\ell^+\ell^-$, and [105] for $B \to K^*\gamma$ and $B_s \to \mu^+\mu^-$. As in the case of $B \to M_1 M_2$ decays, the various nuisance parameters are varied one at the time, keeping all others at their central value, and the according uncertainties are added in quadrature to yield a total theoretical uncertainty that is included into the likelihood function, following Chapter A.1. The list of relevant nuisance parameters can be found in [105].

Observable	q^2**-Binning** (if applicable)	**Ref.**
	$\boldsymbol{B \to K^*\gamma}$	
$\mathcal{B}$, S, C		[3]
	$\boldsymbol{B_s \to \mu^+\mu^-}$	
$\mathcal{B}$		[93, 94]
	$\boldsymbol{B \to K\ell^+\ell^-}$	
$\mathcal{B}$	$q^2 = [1, 6], [14.18, 16], [> 16]$ GeV^2	[95–97]
	$q^2 = [1, 6], [14.18, 16], [16, 18], [18, 22]$ GeV^2	[98]
$A_{\rm CP}$	$-$ " $-$	[99]
	$\boldsymbol{B \to K^*\ell^+\ell^-}$	
$\mathcal{B}$	$q^2 = [1, 6], [14.18, 16], [> 16]$ GeV^2	[95–97, 100, 101]
$A_{\rm FB}$, F_L	$-$ " $-$	[95–97, 100–102]
$A_T^{(2)}$, $A_T^{\rm (re)}$	$-$ " $-$	[100]
$A_{\rm CP}$	$-$ " $-$	[103]
$P'_{4,5,6,8}$	$-$ " $-$	[104]

TABLE 4.4: Observables of $B \to K^*\gamma$, $B_s \to \mu^+\mu^-$, and $B \to (K, K^*)\,\ell^+\ell^-$ that are used as constraints. To avoid double counting of data, either $A_{\rm FB}$ or $A_T^{\rm (re)}$ should be used in fits.

Concerning $B \to K^*$ form factors, we use the light-cone sum rule (LCSR) results from [61], including their extrapolation to large dilepton invariant masses, q^2. We do not make use of recent lattice results at high q^2 [108], which tend to predict to large branching ratios in this q^2 region compared to the measurements [109, 110].

The measurement of LHCb for $\mathcal{B}(B^- \to K^-\mu^+\mu^-)$ at low q^2 is lower than the theoretical predictions using LCSR form factors [111], as was recently also found in [112], yet after the inclusion of effects from $q\bar{q}$-resonances in this kinematic region. We remark that this persists even with the latest updates [113], based on a larger data set, but have not been used in this work. The values of $\mathcal{B}(B^- \to K^-\mu^+\mu^-)$ in the bin $q^2 = [1, 6]$ GeV^2, as used in this analysis, are tabulated in Table 4.5 for theory predictions based on different $B \to K$ form factors and compared to the LHCb measurement. In this work, we also account for lacking subleading corrections in QCDF [114, 115], following the procedure described in [105, 107], which yields larger uncertainties compared to [112] — the omission of these sources of uncertainty would yield the values given in brackets in Table 4.5, in good agreement with [112]. It can be seen that the use of form factors [4] at low q^2 can resolve this discrepancy in principle. Because both LCSR calculations [4, 112] are based on the same sum rule setup, we average both to determine a prior value of the form factor $f_+(q^2 = 0)$ as given in Table 3.1.

At high q^2, we use the first lattice results of $B \to K$ form factors [116], which have uncertainties below 10% in this q^2 region. The according SM predictions of $\mathcal{B}(B^- \to K^-\ell^+\ell^-)$ at high q^2 are in agreement with current measurements [117]. The

$10^7 \cdot \mathcal{B}(B^- \to K^-\mu^+\mu^-)_{[1,6]}$	pull value	form factors	
$1.82^{+0.62}_{-0.24}$	$3.4\,\sigma$	[111]	[112]
$1.79^{+0.71}_{-0.40}$ $(^{+0.59}_{-0.24})$	$1.6\,\sigma$ $(3.1\,\sigma)$	[111]	this work
$1.65^{+0.57}_{-0.49}$ $(^{+0.42}_{-0.38})$	$0.0\,\sigma$ $(0.5\,\sigma)$	[4]	this work
$1.67^{+0.60}_{-0.50}$ $(^{+0.46}_{-0.40})$	$0.0\,\sigma$ $(0.6\,\sigma)$	[4, 111]†	this work
1.21 ± 0.11	–	–	LHCb [98]

TABLE 4.5: The theory predictions of $\mathcal{B}(B^- \to K^-\mu^+\mu^-)$ in the bin $q^2 = [1, 6]$ GeV^2 based on different form factors from LCSR compared to the measurement of LHCb in the last row. †Average of both — see text for details.

extrapolation of the lattice form factors from high to low q^2 gives the similar high central values of $\mathcal{B}(B^- \to K^-\ell^+\ell^-)$ as the LCSR form factors [111] with large extrapolation errors.

As in the case of the hadronic decay into two vector meson, we can further construct additional observables due to the helicity structure in $B \to K^*(\to K\pi)\ell^+\ell^-$. We find for the differential decay rate of the decay mode $\bar{B} \to \bar{K}^*\ell^+\ell^-$

$$\begin{aligned}\frac{8\pi}{3}\frac{d^4\Gamma}{dq^2\, d\cos\theta_l\, d\cos\theta_K\, d\phi} = \\ (J_{1s} + J_{2s}\cos 2\theta_l + J_{6s}\cos\theta_l)\,\sin^2\theta_K + (J_{1c} + J_{2c}\cos 2\theta_l + J_{6c}\cos\theta_l)\,\cos^2\theta_K + \\ (J_3\cos 2\phi + J_9\sin 2\phi)\,\sin^2\theta_K\sin^2\theta_l + (J_4\cos\phi + J_8\sin\phi)\,\sin 2\theta_K\sin 2\theta_l + \\ (J_5\cos\phi + J_7\sin\phi)\,\sin 2\theta_K\sin\theta_l,\end{aligned} \tag{4.26}$$

where $\theta_{l,K}$ are defined as the angles between the $\bar{B}$ meson and the negative charged lepton, ℓ^-, respectively the kaon within the centre-of-mass system of $(\ell^+\ell^-)$, respectively $(K\pi)$. ϕ is the angle between the decay planes of $(\ell^+\ell^-)$ and $(K\pi)$, respectively spanned by their 3-momenta vectors, following the definition from [118]. 12 independent angular observables J_i are implicitly defined through Equation 4.26, from which, together with their CP counterparts $\bar{J}_i$, defined through the differential decay rate $d\bar{\Gamma}$ of the CP-conjugated decay mode, the individual observables in Table 4.4 are constructed. As described in [119], including solely the SM operators, defined in Equation 2.19, together with their χ-flipped counterparts and assuming massless leptons, the number of independent angular observables J_i reduces to eight, leaving a total of 16 observables. The measurements entering the fit are, apart from $A_{\rm CP}$ and $A_{\rm im}(= A_9)$ [97], all CP averaged and expected to be insensitive to CP-violating contributions beyond the SM. Other CP-violating observables could not be measured so far, which will be predicted for those NP scenarios that are related to semi-leptonic decays. Most attractive are observables that are constructed from the angular observables $J_{7,8,9}$. Their asymmetries are odd

under the transformation $\phi \to -\phi$ (T-odd) and therefore depend on $\cos\delta\theta$, in contrast to T-even CP asymmetries, depending on $\sin\delta\theta$ [120]. Because the relative strong phase $\delta\theta$ between the helicity amplitudes is, as for the hadronic decays, expected to be small, CP violation can still become large in the presence of contributions beyond the SM for the former and naturally smaller for the latter. Furthermore, $J_{8,9}$ being CP odd, their asymmetries can be obtained in the experiment from an untagged data sample. This advantage can be utilised for modes which K^* subsequently decays into the neutral final states $K^0\pi^0$ and, in principle, for the decay $B_s \to \phi\,\ell^+\ell^-$. Some effort has been made into the redefinition of these observables, such that the largest source of uncertainty from form factors drops out. We present predictions for observables, optimised for low q^2-bins [121]

$$\langle P_3^{\rm CP}\rangle = -\frac{1}{4}\frac{J_9-\bar{J}_9}{J_{2s}-\bar{J}_{2s}}, \qquad \langle P_{6,8}^{\prime\,\rm CP}\rangle = -\frac{1}{2}\frac{J_{7,8}-\bar{J}_{7,8}}{\sqrt{-(J_{2s}+\bar{J}_{2s})\,(J_{2c}+\bar{J}_{2c})}}, \tag{4.27}$$

and for high q^2-bins [118]

$$H_T^4 = \frac{2(J_8-\bar{J}_8)}{\sqrt{-2J_{2c}\,(2J_{2s}+J_3)}}, \qquad H_T^5 = \frac{-(J_9-\bar{J}_9)}{\sqrt{2J_{2s}^2-J_3^2}}. \tag{4.28}$$

The corresponding observable from the angular components J_7, $\bar{J}_7$ at high q^2 vanishes. In our approximation of massless leptons and only SM-like operators, $H_T^4 = H_T^5$. We complete the list of predicted observables by

$$A_{\rm im} = \frac{J_9-\bar{J}_9}{\Gamma+\overline{\Gamma}}, \tag{4.29}$$

which in fact was measured from the CDF collaboration, but still suffers from huge uncertainties, such that it is more reasonable to predict $A_{\rm im}$ rather than considering it as a constraint in the fit.

4.2.2 Recent tension in $P_5'\,(B \to K^*(\to K\pi)\,\ell^+\ell^-)$ at low-q^2

This work focus on $B \to M_1M_2$ decays, but it will be particular interesting for certain NP scenarios (see Chapters 6.2 and 6.3), where a combined analysis of hadronic and (semi-)leptonic observables is possible, to investigate, whether the data in both sectors can be explained simultaneously. Tensions in observables of the former decays will be extensively discussed in Chapter 5, whereas this subsection gives attention to the data of the latter decays. In contrast to hadronic observables, the experimental landscape is not summarised by the HFAG collaboration and the measurements of the single experiments enter our likelihood function in Equation A.2 individually. This implies that inconsistent measurements among each experiment automatically lead to large pull values, which however cannot be explained by theory, as it is the case for

$B \to K^*\ell^+\ell^-$	SM	$\mathcal{C}_{9,V}$	$\mathcal{C}'_{9,V}$	$\mathcal{C}_{9,V} - \mathcal{C}'_{9,V}$	$\mathcal{C}_{10,A}$	$\mathcal{C}'_{10,A}$	$\mathcal{C}_{10,A} - \mathcal{C}'_{10,A}$
A_{CP} [14, 16]	-1.9σ	(✓)	(✓)	(✓)	–	–	–
$\langle P'_4 \rangle_{[14,16]}$	-2.3σ	–	(✓)	(✓)	–	–	(✓)
$\langle P'_5 \rangle_{[1,6]}$	2.2σ	✓	–	✓	–	(✓)	(✓)

TABLE 4.6: Compilation of SM pull values for all "true" tensions in the data of semi-leptonic decays. The table illustrates the capability of solving these discrepancies within a model-independent fit of the vectorial and axial-vectorial Wilson Coefficients (see text for further explanation).

$\langle A_{\text{FB}} \rangle_{[>16]}\, B \to K^*\ell^+\ell^-$ and $\langle F_{\text{L}} \rangle_{[14,16]}\, B \to K^*\ell^+\ell^-$ from the Belle collaboration [95] compared to other experiments [96, 97, 100–102]. One of our methods to discuss the qualitative results of our NP fits are quoting significantly large pull values that exceed 1.6 standard deviations. Those observables, suffering from inconsistent individual measurements, are not accumulated. Additional inconsistent measurements also appear in the polarisation fraction $F_{\text{L}\,[1,6]} B \to K^*\ell^+\ell^-$. The disagreement between the BaBar [96], ATLAS [102], and other experiments [95–97, 100, 101] are indeed truly suspicious because the single results do not match at more than 4σ. Furthermore, the analysis from the ATLAS experiment only appeared as unpublished conference note, which convinced us, in order to be conservative, not to include these results in our fit.

Apart from these inconsistent measurements, there are also "true" tensions in the data. The SM predictions for the observables $\langle A_{\text{CP}} \rangle_{[14,16]}$, $\langle P'_4 \rangle_{[14,16]}$, and $\langle P'_5 \rangle_{[1,6]}$ of the decay $B \to K^*\ell^+\ell^-$ reveal discrepancies compared to the LHCb measurements [103, 104], as listed in Table 4.6. As we will discuss in detail later on, all NP scenarios, considered in this work, are restricted to the modification of either $\mathcal{C}^{(\prime)}_{9,V}$ or $\mathcal{C}^{(\prime)}_{10,A}$. In order to analyse whether it is in principle possible to resolve the tensions, ignoring constraints from hadronic decays at the moment, we preformed model-independent fits of all relevant semi-leptonic Wilson Coefficients, allowing for generic imaginary contributions. We used for these fits either the whole data set, as listed in Table 4.4, or exclusively one of the problematic observables, but for all q^2-bins. Scenarios that could not decrease the tension ($|\delta| \geq 1.6\sigma$) are marked with a dash in Table 4.6. Those scenarios that could in principle explain the discrepancy, ($|\delta| < 1.6\sigma$ for the reduced data set), but would spoil the residual observables ($|\delta| \geq 1.6\sigma$ for at least one observables in whole data set) are marked with (✓). At last, those scenarios that explain the tensions for both sets are indicated by ✓.

Inspecting Table 4.6, we can see that NP contributions to $\mathcal{C}^{(\prime)}_{10,A}$ do not help to relax any of the tensions. Furthermore, even for NP in $\mathcal{C}^{(\prime)}_{9,V}$, $\langle A_{\text{CP}} \rangle_{[14,16]}$ and $\langle P'_4 \rangle_{[14,16]}$ cannot be explained, too. These effects have to be traced back to statistical fluctuations in the

measurements. The only exception, which seems to be interesting from a phenomenological point of view, is $\langle P_5' \rangle_{[1,6]}$. Simultaneous contributions to $\mathcal{C}_{9,V}$ and $\mathcal{C}'_{9,V}$ ($p = 1.3\sigma$) can account for the observed discrepancy without violating the restrict constraints from other observables, whereas the following pattern can be observed

$$\mathcal{C}_{9,V} \simeq -\mathcal{C}'_{9,V}. \tag{4.30}$$

This effect is enhanced and decreases the pull values even further ($\delta = 1.0\sigma$) if we also include the doubtful longitudinal polarisation-fraction measurements from the ATLAS and BaBar collaborations as constrained into the fit. These observations are in agreement with the findings from the analysis in [122].

4.2.3 Model-independent parametrisation of M_{12}^s

In the case of a model-independent analysis, it is possible that also contributions to B^0-$\bar{B}^0$ mixing can occur. However, whereas the phenomenological impact of particular models to $\Delta F = 1$ observables can be correctly described by the effective enhancement of certain operators, this does not need not to be true for $\Delta F = 2$ observables, for which theses contributions are often just subleading. It is reasonable to not include constraints from meson mixing into the determination of the NP parameter space, but rather to check whether the additional contributions, demanded from (semi-)leptonic and hadronic decays, are still allowed. Our analysis exclusively concerns NP in $b \to s$ transitions, which only affects the mixing of the B_s meson. Due to that the following discussion is kept specific to this case.

The off-diagonal element of the B_s-$\bar{B}_s$ mass matrix is given by

$$M_{12}^s = \frac{1}{2m_{B_s}} \langle B_s | \mathcal{H}_{\text{eff}}^{|\Delta B|=2} | \bar{B}_s \rangle \,, \tag{4.31}$$

where the EWH, $\mathcal{H}_{\text{eff}}^{|\Delta B|=2}$, was already defined in Equation 2.21. The matrix elements of $\Delta B = 2$ operators in Equation 2.22 are typically parametrised through

$$\langle B_s | \mathcal{O}_V^{LL} | \bar{B}_s \rangle = \frac{32}{3} m_{B_s}^2 f_{B_s}^2 \mathcal{B}_{s,V}^{LL}(\mu_B), \qquad \langle B_s | \tilde{\mathcal{O}}_S^{LR} | \bar{B}_s \rangle = \frac{8}{3} m_{B_s}^2 f_{B_s}^2 \tilde{\mathcal{B}}_{s,S}^{LR}(\mu_B), \tag{4.32}$$

where f_{B_s} is the decay constant of the B_s meson, quoted in Table 3.1, and the bag factors $\mathcal{B}_V^{LL,s}(4.6\,\text{GeV}) = 0.87^{+0.05}_{-0.04}$ and $\tilde{\mathcal{B}}_S^{LR,s}(4.6\,\text{GeV}) = 1.75^{+0.21}_{-0.07}$ are obtained from lattice calculation in [35]. We only quoted those bag factors that are needed in this work.

As described in [62], although NP models can lead to different contributions to the operators in Equation 2.22, the new correction to the observable M_{12}^s can be specified

by only one complex quantity

$$M_{12}^{s} = M_{12}^{s,\mathrm{SM}}\, C_{B_s} e^{2i\phi_{B_s}}, \qquad C_{B_s} e^{2i\phi_{B_s}} = \frac{\langle B_s|\mathcal{H}_{\mathrm{eff,full}}^{|\Delta B|=2}|\bar{B}_s\rangle}{\langle B_s|\mathcal{H}_{\mathrm{eff,SM}}^{|\Delta B|=2}|\bar{B}_s\rangle}, \tag{4.33}$$

where in the case of the SM, $C_{B_s} = 1$ and $\phi_{B_s} = 0$ by construction. This parameter was measured in a model-independent fit and found to be well consistent with the SM expectation, $C_{B_s} = 1.066 \pm 0.083$ and $\phi_{B_s} = 0.6^\circ \pm 2.0^\circ$ [62]. Taking the latest SM prediction for M_{12}^{s} from [123], C_{B_s} and ϕ_{B_s} can then be expressed in terms of the NP parameters and will be fitted to this measurement.

Part II

Phenomenology

Chapter 5

Testing QCD factorisation within the Standard Model

In the present section, we discuss our results for QCD-penguin- and WA-dominated hadronic B-meson decays in the SM. The underlying soft QCD interaction, which appears in the framework of QCDF at order $\Lambda_{\rm QCD}/m_b$ and constitutes the main source of uncertainty, is extracted from a fit to the experimental data of branching ratios, CP asymmetries, polarisation fractions, and strong phase differences. The power-suppressed corrections from WA play a central role in the following analysis. The relative amount of subleading corrections, needed to explain the data, is quantified by the ratio $\xi_3^A(M_1M_2)$.

In Subsections 5.1.1 and 5.1.2, we summarise our findings under the assumption of universality among decay systems that are related via $(u \leftrightarrow d)$ quark exchange, which seems to be compatible with data. We mainly discuss the decay systems $B \to K\pi$, $K\rho$, $K^*\pi$, $K^*\rho$, but relevant results for other QCD-penguin-dominated decays are also mentioned. In addition to the $\Delta A_{\rm CP}^{K\pi}$ problem, which has already been discussed extensively in the literature [42, 74, 124–127], we also obtain a significant tension for the ratio of branching ratios $R_n^B(K\pi)$. We then further relax our approach of universality in Subsection 5.1.3, in which a common WA parameter for certain decay modes into the same final states is assumed. This can be already tested in, for instance, $B_s \to K\pi$ and $B_d \to K\pi$, for which data exist. Although universality might be justified under certain conditions, it will be clear from Subsection 5.2.1, where pure WA decays are concerned that this assumption does not hold in general. Similar fits for certain decay amplitudes have already been described in [128]. Contrary to our approach, the authors postulated one common WA parameter $\rho_A^{M_1M_2}$ for $B_s \to PP(VV)$ and for $B \to PP(VV)$.

In Subsection 5.1.4, we present a possible solution to the $\Delta A_{\rm CP}^{K\pi}$ problem relying on large power corrections from HS interactions. If such corrections are indeed responsible for the observed differences in CP asymmetries, they should cause visible effects in other observables.

5.1 QCD-penguin-dominated decays

5.1.1 Fit results for $B \to K\pi$

The most precise measurements in hadronic B-meson decays are available for $B \to K\pi$, from which we expect stringent bounds on the model parameter $\rho_A^{K\pi}$. The results of our analysis are condensed in Table 5.1, which lists p and pull values. Figure 5.1 shows the fit results in the $\rho_A^{K\pi}$ plane for the two different observable sets SI and SII, as defined in Subsection 4.1.1. Contours are plotted for the 68% (bright) and 95% (dark) credibility regions (CRs), taking into account data from branching ratio and CP asymmetry measurements separately and in combination.

The general shape of the branching-ratio contour can be understood in the following way: The leading contribution to the decay amplitude $\hat{\alpha}_4^c(\pi K) \equiv \alpha_4^c(\pi K) + \beta_3^c(\pi K)$, composed of a perturbatively-calculable QCD-penguin amplitude and an unknown WA contribution, is restricted to a circle in the complex plane

$$\Gamma(\bar{B} \to K\pi) \simeq V_{cb}V_{cs}^*\, F_0^{B\to\pi}(0)\, f_K\ \left|\hat{\alpha}_4^c(\pi K)\right|\, (1 + \mathcal{O}(r_i))\,, \tag{5.1}$$

where the r_i are defined in Equation 4.14. Depending on the phase, $\beta_3^c \equiv \beta_3^c(\rho_A^2, \rho_A)$ can interfere either constructively or destructively with the QCD-penguin amplitude $\alpha_4^c(\pi K)$, implying a strong correlation between phase and absolute value.

For $\phi_A^{K\pi}$ approximately 0 or π, the additional contribution from WA is mainly real and interferes constructively with the QCD-penguin amplitude. However, the contributions from the linear and quadratic WA terms in $\beta_3^c(\pi K)$ can interfere either constructively ($\phi_A^{K\pi} \sim 0$) or destructively ($\phi_A^{K\pi} \sim \pi$) with each other, leading to small $|\rho_A^{K\pi}| \sim 2.0$, respectively slightly larger $|\rho_A^{K\pi}| \sim 3.4$. This confirms the naive expectation from QCDF[1] that power-suppressed corrections should scale like $\ln(m_b/\Lambda_{\text{QCD}})$ times some unknown parameter of $\mathcal{O}(1)$. Large absolute values for WA contributions, $|\rho_A^{K\pi}| \sim 6$, are needed for $\phi_A^{K\pi}$ approximately $\frac{\pi}{2}$ or $3\frac{\pi}{2}$. In this case, the linear terms become mainly imaginary, whereas the quadratic terms are still real but now interfere destructively with the contributions from the QCD-penguin amplitude.

The left panel of Figure 5.1 shows that constraints from branching ratio measurements (blue) alone can already be satisfied by a small contribution from power corrections of $\xi_3^A(K\pi) \lesssim 0.25$. Nevertheless, $\left|\rho_A^{K\pi}\right|$ ($\lesssim 6$) is only weakly bounded and the fit does not reject solutions that raise the size of WA comparable to the leading order contribution in the decay amplitude. Such a *large weak-annihilation scenario* flips the

[1] As was mentioned in Chapter 3, we depart from the usual treatment of evaluating the Wilson Coefficients at the semi-hard scale $\mu_b = \mu_h$. Instead, we used $\mu_b = m_b$, which implies that the Wilson Coefficients in our analysis are smaller by a factor of roughly 1.5. With respect to this, we agree with the results in [74], where a parameter scan for the power-suppressed corrections was used and $\rho_A^{\text{PP}} = 1.5$ was fixed.

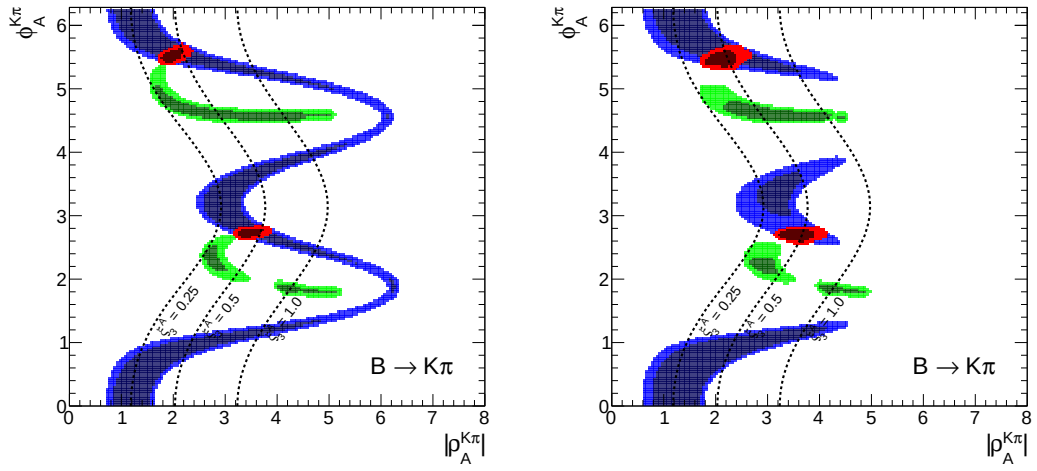

FIGURE 5.1: 68% and 95% CRs for the complex parameter $\rho_A^{K\pi}$ obtained from a fit with the observable set SI (left panel) and SII (right panel) for the decay system $B \to K\pi$ assuming the SM. Allowed regions are separately shown for branching ratios (blue), CP asymmetries (green), and the combination (red). The dashed lines correspond to $\xi_3^A(K\pi) = 0.25\,(0.5,\, 1.0)$.

sign of $\mathrm{Re}\,\hat{\alpha_4}^c(\pi K)$, which perturbative part is in fact predicted in QCDF to be positive, but in principle not forbidden by branching-ratio measurements to become negative. Additional information from ratios of branching ratios, shown on the right panel, are due to their sensitivity to $\cos\hat{\phi}_4^c(K\pi)$ (see Equation 4.16)

$$R_{n,c}^{B,K,\pi} \simeq 1 + \left(\sum_i c_i\, r_i^R\right) \cos\hat{\phi}_4^c(\pi K), \tag{5.2}$$

suitable to reject these points in parameter space. Since we abandon the idea of biased small WA with our large flat prior for $\rho_A^{M_1 M_2}$, it is a nontrivial result that the data prefer regions in parameter space that are favoured from a theoretical point of view (small corrections to the leading amplitude). Our fits support the assumptions of QCDF and power-suppressed corrections are confined to less than approximately 50%.

In addition to branching-ratio measurements, we also include information from direct CP asymmetries in $B \to K\pi$. The contours are shown in the plots by the green region. To observe CP violation, the decay amplitude must have non-vanishing weak and strong phases. The weak phase is parametrised in the SM by the CKM-matrix elements, and the strong phase arises in QCDF at $\mathcal{O}(\alpha_s)$, respectively at $\mathcal{O}(\Lambda_{\mathrm{QCD}}/m_b)$, which implies that CP asymmetries are formally known only to leading order. Since strong phases can either originate from radiative or power corrections, we expect a high sensitivity to our fit parameter in these observables. Whereas CP asymmetries with a neutral kaon in the final state are measured to be small with large uncertainties, the CP asymmetries with a charged kaon are observed to be large and with a relative opposite

sign. The leading contributions to the latter decay modes can be written in terms of the colour-allowed, $r_{\mathrm{T}}(\pi K)$, and the colour-suppressed, $r_{\mathrm{T^C}}(\pi K)$, penguin-to-tree ratios:

$$\begin{aligned} C(B^- \to K^-\pi^0) &\simeq 2\,\mathrm{Im}\,(\mathrm{r_T}(\pi\mathrm{K}) + \mathrm{r_{T^C}}(\pi\mathrm{K}))\,\sin\gamma &&= (-4.0 \pm 2.1)\,\%\ \text{(HFAG)}, \\ C(\bar{B}^0 \to K^-\pi^+) &\simeq 2\,\mathrm{Im}\,(\mathrm{r_T}(\pi\mathrm{K}))\,\sin\gamma &&= (+8.2 \pm 0.6)\,\%\ \text{(HFAG)}, \end{aligned} \tag{5.3}$$

from which the approximation for

$$\Delta A_{\mathrm{CP}}^{K\pi} \simeq 2\,\mathrm{Im}\,(\mathrm{r_{T^C}}(\pi\mathrm{K}))\,\sin\gamma = (-12.2 \pm 2.2)\,\%\ \text{(HFAG)}. \tag{5.4}$$

follows. The imaginary parts of the ratios can be expressed in terms of a single phase

$$\mathrm{Im}\,(\mathrm{r_T}(\pi\mathrm{K})) \propto -\underbrace{r_{\mathrm{T}}^{\mathrm{R}}(\pi K)}_{-17.4^{+1.0}_{-0.9}}\,\sin\hat{\phi}_4^c(\pi K) + \underbrace{r_{\mathrm{T}}^{\mathrm{I}}(\pi K)}_{-0.4^{+0.6}_{-0.5}}\,\cos\hat{\phi}_4^c(\pi K), \tag{5.5}$$

$$\mathrm{Im}\,(\mathrm{r_{T^C}}(\pi\mathrm{K})) \propto -\underbrace{r_{\mathrm{T^C}}^{\mathrm{R}}(\pi K)}_{-5.8^{+1.1}_{-3.4}-2.1^{+0.3}_{-1.2}\,\mathrm{Re}\,\rho_H}\,\sin\hat{\phi}_4^c(\pi K) + \underbrace{r_{\mathrm{T^C}}^{\mathrm{I}}(\pi K)}_{1.5^{+0.3}_{-0.5}-2.1^{+0.3}_{-1.2}\,\mathrm{Im}\,\rho_H}\,\cos\hat{\phi}_4^c(\pi K), \tag{5.6}$$

which need to be determined by the fits. The numerical results for the individual amplitude coefficients are quoted in % and calculated for $\rho_A^{K\pi}$ at the best-fit point of set SII, listed in Table 5.1. We explicitly kept the dependence of $r_{\mathrm{T^C}}(\pi K)$ on HS, parametrised through ρ_H, whereas it is numerical irrelevant for $r_{\mathrm{T}}(\pi K)$ and kept implicit. The particular choice of $\rho_A^{K\pi}$ was only needed for the determination of $|\alpha_4^c(\pi K)|$. Any other parameter point along the branching-ratio contour would have led to numerical equivalent results and likewise suited.

Because the measurement of $C(\bar{B}^0 \to K^-\pi^+)$ exhibit the smallest uncertainty, it will dominate the fits. The amount of CP violation originating from the second part in Equation 5.5 is insufficient to account for the data and can numerically be neglected, thus the first term determines $\sin\hat{\phi}_4^c(K\pi)$. With the sign of $\sin\hat{\phi}_4^c(K\pi)$ fixed, the direction of the CP violation from the first term of the colour-suppressed ratio in Equation 5.6 is also determined and disagrees with the measurements. The second term can compensate this effect for an appropriate choice of $\cos\hat{\phi}_4^c(K\pi)$, but in view of the numerical values, is unable to explain the large amount of CP violation in $\Delta A_{\mathrm{CP}}^{K\pi}$. The current situation can be summarised as follows: The absolute value of the leading decay amplitude in $B \to K\pi$ is well determined from branching ratio measurements. One of the two CP asymmetries can always be explained, if the strong phase is not restricted from theoretical prejudice, but a tension arises, when one tries to explained both simultaneously. This is known in the literature as the $\Delta A_{\mathrm{CP}}^{K\pi}$ puzzle, which is shown in our plots by disjoint contours from branching-ratio and CP-asymmetry measurements at 95% probability. Possible large NNLO corrections to the colour-suppressed tree amplitude $\alpha_2^u(K\pi)$ might relax the tension in case of destructive interference to the real part and constructive interference

M_1M_2	$K\pi$		$K^*\pi$		$K\rho$		$K^*\rho$	
set	SI	SII	SI	SII	SI	SII	SI	SII
p-value	0.44	0.04	0.95	0.90	1	1	1	0.97
$\lvert\rho_A\rvert$, ϕ_A	3.39; 2.73	3.34; 2.71	1.79; 5.85	1.61; 5.84	2.57; 2.79	2.69; 2.68	2.31; 2.74	1.56; 5.66
$\mathcal{B}(\bar{B}^0 \to M_1M_2)$	$+0.3\,\sigma$	–	$-0.3\,\sigma$	–	$0.0\,\sigma$	–	$0.0\,\sigma$	–
$\mathcal{B}(\bar{B}^0 \to M_1^+M_2^-)$	$0.0\,\sigma$	–	$0.0\,\sigma$	–	$0.0\,\sigma$	–	$+0.3\,\sigma$	$+0.1\,\sigma$
$\mathcal{B}(B^- \to M_1^-M_2)$	$0.0\,\sigma$	–	$+0.6\,\sigma$	–	$0.0\,\sigma$	–	$0.0\,\sigma$	–
$\mathcal{B}(B^- \to M_1M_2^-)$	$0.0\,\sigma$	$+0.2\,\sigma$	$0.0\,\sigma$	$+0.1\,\sigma$	$0.0\,\sigma$	$+0.1\,\sigma$	$0.0\,\sigma$	–
$R_c^B(M_1M_2)$	–	–	–	–	–	–	–	$-0.5\,\sigma$
$R_n^B(M_1M_2)$	–	$\mathbf{-1.9}\,\sigma$	–	$+0.6\,\sigma$	–	$0.0\,\sigma$	–	$+0.6\,\sigma$
$R_c^{M_1}(M_1M_2)$	–	$0.0\,\sigma$	–	$+0.8\,\sigma$	–	$+0.7\,\sigma$	–	$-0.8\,\sigma$
$R_c^{M_2}(M_1M_2)$	–	$+0.9\,\sigma$	–	$0.0\,\sigma$	–	$-0.2\,\sigma$	–	–
$\mathcal{C}(\bar{B}^0 \to M_1M_2)$	$0.0\,\sigma$	$0.0\,\sigma$	$+0.5\,\sigma$	$+0.4\,\sigma$	$0.0\,\sigma$	$0.0\,\sigma$	$0.0\,\sigma$	$0.0\,\sigma$
$\mathcal{C}(\bar{B}^0 \to M_1^+M_2^-)$	$+0.7\,\sigma$	$+0.1\,\sigma$	$+0.1\,\sigma$	$+0.1\,\sigma$	$0.0\,\sigma$	$+0.1\,\sigma$	$+0.5\,\sigma$	$+0.6\,\sigma$
$\mathcal{C}(B^- \to M_1^-M_2)$	$\mathbf{-2.1}\,\sigma$	–	$0.0\,\sigma$	–	$0.0\,\sigma$	–	$+0.3\,\sigma$	–
$\mathcal{C}(B^- \to M_1M_2^-)$	$\mathbf{+1.0}\,\sigma$	$\mathbf{+1.0}\,\sigma$	$+0.9\,\sigma$	$\mathbf{+1.0}\,\sigma$	$+0.7\,\sigma$	$+0.7\,\sigma$	$+0.1\,\sigma$	$0.0\,\sigma$
$\Delta A_{\rm CP}(M_1M_2)$	–	$\mathbf{-2.8}\,\sigma$	–	$-0.1\,\sigma$	–	$0.0\,\sigma$	–	$0.0\,\sigma$
$f_L(\bar{B}^0 \to M_1M_2)$	–	–	–	–	–	–	$0.0\,\sigma$	$0.0\,\sigma$
$f_L(\bar{B}^0 \to M_1^+M_2^-)$	–	–	–	–	–	–	$-0.6\,\sigma$	$-0.5\,\sigma$
$f_L(B^- \to M_1^-M_2)$	–	–	–	–	–	–	$+0.7\,\sigma$	$+0.9\,\sigma$
$f_L(B^- \to M_1M_2^-)$	–	–	–	–	–	–	$0.0\,\sigma$	$0.0\,\sigma$

TABLE 5.1: Compilation of p values and pulls of the SM fit evaluated at the best-fit point of $\rho_A^{M_1M_2}$ for the two different observable sets SI and SII of the decay systems $B \to K\pi$, $K\rho$, $K^*\pi$, $K^*\rho$.

to the imaginary part. Unfortunately, in view of current data, the authors in [2] have shown that the NNLO vertex corrections are cancelled by the NLO spectator scattering corrections in the case of $\alpha_2(\pi\pi)$. Because higher-order radiative corrections seem to be unsuitable to relax the observed tension, one might ask the question whether power-suppressed corrections from HS interactions can account for the above-described pattern of corrections to $\alpha_2^u(K\pi)$ and, if so, how large they need be. We addresses this question to Subsection 5.1.4.

Neglecting constraints from branching-ratio measurements, a best-fit point at $\rho_A^{K\pi} = 4.1\,e^{1.8i}$ (see Figure 5.1) is found, satisfying all constraints from direct CP asymmetries. This point in parameter space predict an accidental cancellation of the QCD-penguin amplitude $\alpha_4^c(\pi K)$ and $\beta_3^c(\pi K)$, and statistical confidence can only be achieved due to large theoretical uncertainties. Though branching-ratio measurements only become incompatible at more than 30σ, emerging numerical importance of unknown NNLO and subleading corrections cast doubt on predictions of CP asymmetries in that regime of parameter space.

The contour of the combined fit is displayed in the plots in red. Independent of the set of observables, two branching-ratio-compatible solutions remain with a relative power correction of roughly $\xi_3^A(\pi K) = 0.39$ to the QCD-penguin amplitude. Due to the quadratic dependence of $\beta_3^c(\pi K)$ on the fit parameter, an ambiguity arises that

is only slightly broken by other WA contributions, such that both solutions are almost degenerated. At the best-fit point of Set II, $\hat{\alpha}_4^c(\pi K) \equiv \alpha_4^c(\pi K) + \beta_3^c(\pi K) = (-0.101^{+0.006}_{-0.005} - 0.015^{+0.006}_{-0.007} i) + (-0.016^{+0.002}_{-0.001} + 0.037^{+0.003}_{-0.004} i)$. Our parametrisation of subleading corrections also accounts for higher-order α_s corrections to $\hat{\alpha}_4^c(\pi K)$. The calculation of NNLO QCD-penguin corrections become available in the foreseeable future [129] and could decrease $\xi_3^A(\pi K)$ in case of constructive interference to the real part and destructive interference to the imaginary part of $\alpha_4^c(\pi K)$. If, for instance, $\mathrm{Im}\,\alpha_4^{c,\mathrm{NNLO}}(\pi K) \simeq -\mathrm{Im}\,\alpha_4^{c,\mathrm{NLO}}(\pi K)$, $\xi_3^A(\pi K)$ would decrease to 0.27.

The goodness of the fit at the best-fit point is measured by the p value, which is of the order of reliable values for set SI ($p = 0.44$). Apart from a small discrepancy in $\mathcal{B}(\bar{B}^0 \to \bar{K}^0\pi^0)$ of $+0.3\sigma$, all pull values for branching ratios vanish, whereas, as explained above, direct CP asymmetries elude a suitable prescription. The pull values for $C(\bar{B}^0 \to K^-\pi^+)$ and $C(B^- \to K^-\pi^0)$ are $+0.7\sigma$, respectively -2.1σ and reflect the $\Delta A_{\mathrm{CP}}^{K\pi}$ puzzle, which is shifted into a pull for $\Delta A_{\mathrm{CP}}^{K\pi}$ of -2.8σ for the observable set SII. Both fits obtain a small deviation of $+1.0\sigma$ for the CP asymmetry $C(B^- \to \bar{K}^0\pi^-)$, which vanishes in the SM and is quite stable against power corrections.

Although the analysis of CP-violating observables for both sets do not differ significantly from each other, in the combination with ratios of branching ratios (SII), the fit cannot explain the measured value for $R_n^B(K\pi)$. A pull of -1.9σ in $R_n^B(K\pi)$ leads to a problematic p value of 0.04 for the SM. This additional discrepancy is already obtained in a fit without CP-violating observables: $\delta(R_n^B(K\pi)) = -1.2\sigma$, $\delta(R_c^K(K\pi)) = 0.4\sigma$ and, $\delta(R_c^\pi(K\pi)) = 0.6\sigma$. After contributions from WA are fitted and do not contribute to the error budget anymore, the largest uncertainty for branching-ratio predictions originates from form factors. This parametric dependence mostly cancels in ratios of branching ratios, which therefore become more suitable in testing the SM.

It is worthwhile to note the difference between the conventional treatment and our treatment of WA corrections. The disadvantage of fitting $\rho_A^{M_1M_2}$ is that we cannot predict those observables that are used in the fit. In the conventional QCDF, a central value for $\rho_A^{M_1M_2}$ is chosen, and typically, $\phi_A^{M_1M_2}$ is varied within a certain range to predict all observables. However, the choice of a central value for $\rho_A^{M_1M_2}$ is arbitrary, and the central values and uncertainties for the observables strongly depend on this selection, which might dispute the robustness of the predictions. That $\phi_A^{M_1M_2}$ is freely varied for each decay chain and each observable implies that WA contributions are taken uncorrelated into account, increasing uncertainties unreasonably large. Our approach correctly allows for these correlations and quantifies the assumption of universality among final state systems that are related via $(u \leftrightarrow d)$ quark exchange by the goodness of the fit. Under the potential drawback of less constrained contours, we can also remove certain observables from the fit, allowing us to predict them with a statistically weighted uncertainty from reasonable regions of WA automatically incorporated (see Appendix A.4).

PP								
		$B \to K\pi$	$B \to K\eta$	$B \to K\eta'$	$B \to KK$	$B_s \to KK$	$B_s \to \pi\pi$	$B_s \to K\pi$
$\lvert\rho_A^{PP}\rvert$	lower bound	> 1.8	> 0	> 0.9	$> 0\,(0.9)$	> 0	> 3.4	> 2.3
	upper bound	< 3.9	–	< 7.7	$< 6.1\,(8.6)$	< 5.5	< 10.9	< 4.8
ξ_3^A	best-fit point	0.39	0.08	1.83	0.58	1.83	–	0.96
	68% CR	[0.37; 0.54]	[0.00; –]	[0.18; 3.25]	[0.00; 2.07]	[0.02; 2.09]	–	[0.56; 1.54]
	95% CR	[0.34; 0.69]	[0.00; –]	[0.16; 3.34]	[0.00; 2.10]	[0.00; 2.13]	–	[0.44; 1.83]
PV								
		$B \to K^*\pi$	$B \to K\rho$	$B \to K^*\eta$	$B \to K^*\eta'$	$B \to K\phi$	$B \to K\omega$	
$\lvert\rho_A^{PV}\rvert$	lower bound	> 1.4	> 0.8	> 1.1	> 0	> 0.8	> 1.4	
	upper bound	< 3.4	< 3.4	< 4.4	< 6.1	< 3.6	< 4.5	
ξ_3^A	best-fit point	0.89	0.78	2.74	0.48	0.50	2.7	
	68% CR	[0.75; 1.40]	[0.39; 1.55]	[0.71; 3.77]	[0.02; 7.84]	[0.40; 2.41]	[0.70; 3.08]	
	95% CR	[0.69; 1.56]	[0.16; 2.18]	[0.64; 5.06]	[0.02; 8.41]	[0.32; 2.54]	[0.57; 3.15]	
VV								
		$B \to K^*\rho$	$B \to K^*\phi$	$B_s \to K^*\phi$	$B \to K^*K^*$	$B_s \to K^*K^*$	$B_s \to \phi\phi$	$B \to K^*\omega$
$\lvert\rho_A^{VV}\rvert$	lower bound	> 1.0	> 0.7	> 0.3	> 1.2	> 1.6	> 0.7	> 0.3
	upper bound	< 2.9	< 1.9	< 3.2	< 3.0	< 3.6	< 2.3	< 2.4
ξ_3^A	best-fit point	1.33	0.51	1.53	1.84	3.01	0.50	0.91
	68% CR	[0.84; 1.94]	[0.41; 0.59]	[0.30; 2.05]	[0.85; 2.68]	[1.94; 3.79]	[0.49; 1.11]	[0.20; 1.39]
	95% CR	[0.56; 2.33]	[0.34; 0.63]	[0.10; 2.15]	[0.09; 2.90]	[0.96; 4.17]	[0.41; 1.38]	[0.09; 1.46]

TABLE 5.2: Compilation of lower (upper) bounds at the 68% CR on the fit parameter $|\rho_A^{M_1M_2}|$ and of $\xi_3^A(M_1M_2)$ at the best-fit point, the 68% and, 95% CR, for observables set SII of the decay systems $B \to K\pi$, $K\rho$, $K^*\pi$, $K^*\rho$. The pure weak-annihilation decay $\bar{B}^0 \to K^+K^-$ is not included in the decay system $B \to KK$ and its bounds are given separately in parenthesis.

5.1.2 Fit results for $B \to K^*\pi$, $K\rho$, $K^*\rho$

We now analyse decay systems that are obtained from replacing a pseudoscalar in $B \to K\pi$ by its vector meson equivalent: ρ for π and K^* for K. Depending on the spin of the final states, QCDF implies qualitative differences between the decay modes, which will be discussed later on, but because the parametrisation of the decay amplitude in all four decay systems is identical, we expect observable effects, which are present in $B \to K\pi$, also in $B \to K^*\pi$ (PV), $B \to K\rho$ (VP)[2] and $B \to K^*\rho$ (VV). Unfortunately, experimental information for these decay systems are not as precise as for $K\pi$ final state. No striking tensions are expected, but restricted contour regions on the QCD model parameter $\rho_A^{M_1M_2}$ can be obtained.

Our fit results are shown in the plots of Figure 5.2 and pull and p values are collected in Table 5.1. There are no large deviations between experiment, and almost all pulls are below one standard deviation, leading to $p \sim 1$ for all three decay systems. We highlight the $+1.0\sigma$ tension for $C(B^- \to \bar{K}^{*0}\pi^-)$ and $+0.7\sigma$ tension for the same asymmetry with $K\rho$ in the final state. As just as for $C(B^- \to \bar{K}^0\pi^-)$, this CP asymmetry almost vanishes in the SM and it is difficult to increase this observable to become larger than

[2] The classification of $B \to K^*\pi$ as $(M_1M_2 = PV)$ and $B \to K\rho$ as $(M_1M_2 = VP)$ decay refers to the flavour amplitude $\alpha_4(M_1M_2)$, which indeed exclusively occurs in that combination for all decay amplitudes for a given decay system. Nevertheless, some decay amplitudes also contain contributions in which the role of the pseudoscalar and vector meson is interchanged.

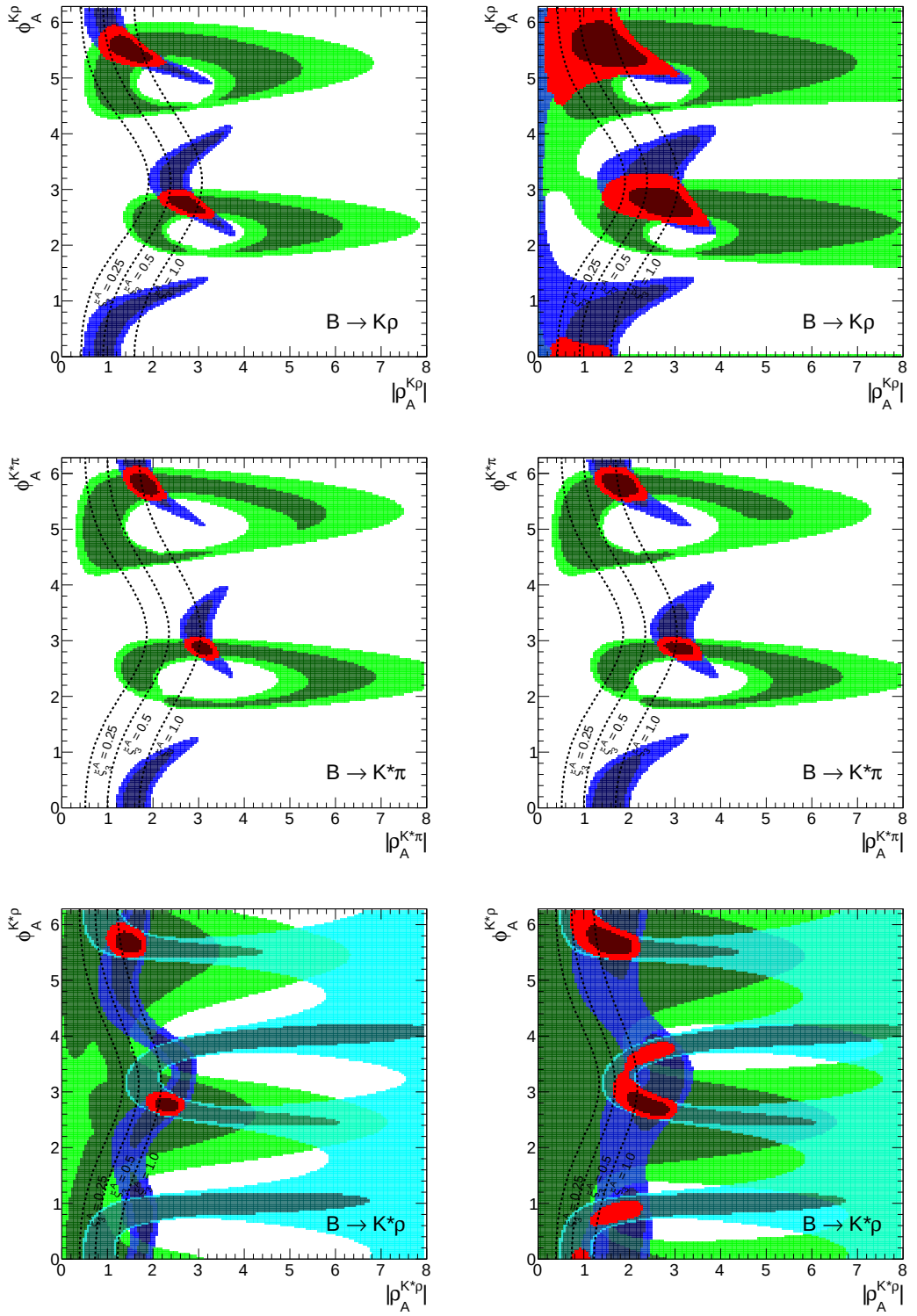

FIGURE 5.2: 68% and 95% CRs for the complex parameters $\rho_A^{K\rho}$, $\rho_A^{K^*\pi}$, $\rho_A^{K^*\rho}$ obtained from a fit with the observable set SI (left panel) and SII (right panel) for the decay systems $B \to K\rho$, $K^*\pi$, $K^*\rho$ assuming the SM. Allowed regions are separately shown for branching ratios (blue), CP asymmetries (green), polarisation fractions (cyan), and the combination (red). The dashed lines correspond to $\xi_3^A(M_1M_2) = 0.25\,(0.5,\,1.0)$.

1%, even in the presence of large power corrections. Therefore, this CP asymmetry is suitable to test the SM without relying too much on soft QCD interactions.

The qualitative features of the contour plots are similar to those in the previous section. For all three decay systems, independent of the observable set, we obtain two solutions when the restrictions from branching ratios and CP asymmetries are combined. One solution prefers small $|\rho_A^{M_1M_2}| \in [1;2]$ at $\phi_A^{M_1M_2}$ just below 2π; the other prefers larger values for $|\rho_A^{M_1M_2}| \in [2;3]$ at $\phi_A^{M_1M_2}$ just below π. Due to the quadratic dependence of the WA amplitude on $\rho_A^{M_1M_2}$, the two solutions are almost degenerate and only distinguishable through other, numerically subleading, WA topologies. As we detail in Section 5.2, assuming universality along all WA corrections might not be justified, and it is arguable if the ambiguity can be resolved by improved measurements.

Nevertheless, the contour regions for all three decay systems overlap within a probability of 68% for the small-$|\rho_A^{M_1M_2}|$ solution and at least for a probability of 95% for the large-$|\rho_A^{M_1M_2}|$ solution. Considering also the combined contour from $B \to K\pi$, a common contour region at the probability of at least 95% can be found for small $|\rho_A^{M_1M_2}|$. In the case of VV final states, we can exploit the three helicity amplitudes to construct further observables such as polarisation fractions to obtain additional constraints for our fit, which are shown in the lower panels in Figure 5.2 by the cyan contour. As can be seen from the plots, information from polarisation-fraction measurements are — at least in the case of $B \to K^*\rho$ — more restrictive than CP asymmetries and lead to orthogonal constraints compared to the contours from branching ratios. Although the contour regions for the decay modes $B \to K\pi\,(K\rho,\, K^*\pi)$ are obtained from branching fractions and CP asymmetries, whereas for $B \to K^*\rho$ from branching and polarisation fractions, the final contours are still rather similar.

Although no further tensions were obtained in our fits, we saw in the previous subsection that composed observables, like ratios of branching ratios, are more suitable to test the SM due to cancellation of uncertainties. Looking forward to more precise measurements from Belle II, we show the results for all six possible ratios of branching ratios at the according best-fit point for observable set SII in Figure 5.3. These should not be considered as predictions, but rather as indications whether our analysis will resist more accurate data.

The relative amount of power corrections compared to the leading contributions for PV, VP and VV final states are listed in Table 5.2. Although the lower bounds on $|\rho_A^{M_1M_2}|$ are weaker for decays with at least one vector meson in the final state, the power-suppressed ratio $\xi_3^A(M_1M_2)$ is typically larger by a factor of 2–3 compared to $B \to K\pi$, which is a qualitative feature of QCDF. As can be seen from Equation 3.27, the QCD-penguin flavour amplitude $\alpha_4(M_1M_2)$ is a linear combination of the vector and

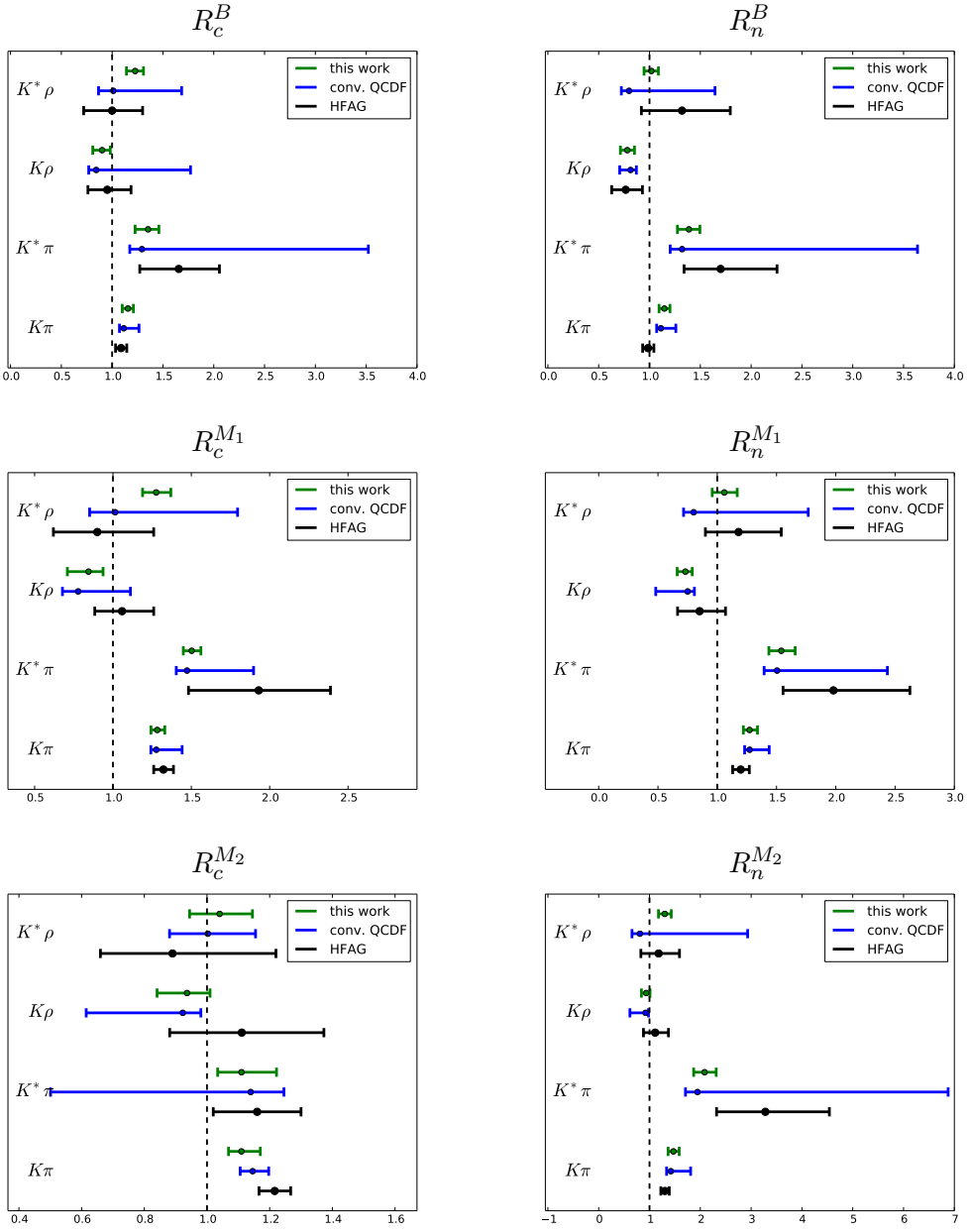

FIGURE 5.3: Experimental and theoretical results for all six possible combinations of ratios of branching ratios for the decays $B \to K\pi$, $K\rho$, $K^*\pi$, $K^*\rho$. The measurements (red) are taken from [3] with uncertainties added up quadratically (see Chapter A.1). Predictions are obtained either for $\rho_A^{M_1 M_2}$ at the best-fit point of set SII (green) or for conventional error estimation with $\rho_A^{M_1 M_2}$ as defined in Chapter 3.2.2 (black)

		this work	BaBar		Belle		HFAG	
$\bar{B}^0 \to \bar{K}^0\omega$	C	-0.08 ± 0.08	$-0.52^{+0.22}_{-0.20} \pm 0.03$	(2009) [130]	$0.09 \pm 0.29 \pm 0.06$ $0.36 \pm 0.19 \pm 0.05$	(2007) [131] (2013) [81]	$-0.32 \pm 0.17^{\dagger}$	(2012) [3]
$B^- \to K^{*-}\phi$	$\phi_\perp$ (rad.)	$2.07^{+0.27}_{-0.25}$	$2.69 \pm 0.20 \pm 0.03$	(2007) [132]	$2.31 \pm 0.30 \pm 0.07$	(2005) [133]	$2.58 \pm 0.17^{\dagger}$	(2012) [3]
	$\phi_\parallel$ (rad.)	$2.07^{+0.27}_{-0.25}$	$2.47 \pm 0.20 \pm 0.07$		$2.10 \pm 0.28 \pm 0.04$		$2.34 \pm 0.17^{\dagger}$	
$\bar{B}^0 \to \bar{K}^{*0}\phi$	$\phi_\perp$ (rad.)	$2.07^{+0.27}_{-0.25}$	$2.35 \pm 0.13 \pm 0.09^{\dagger}$	(2008) [83]	$2.37 \pm 0.10 \pm 0.04^{\dagger}$	(2013) [84]		
	$\phi_\parallel$ (rad.)	$2.07^{+0.27}_{-0.25}$	$2.40 \pm 0.13 \pm 0.08^{\dagger}$		$2.23 \pm 0.10 \pm 0.02^{\dagger}$			

TABLE 5.3: Collection of theoretical and experimental results for the CP asymmetry in $\bar{B}^0 \to \bar{K}^0\omega$ and the relative amplitude phases $\phi_{\perp,\parallel}$ for $B^{0(-)} \to K^{*0(-)}\phi$. Because the Belle collaboration recently published an update for the decay $\bar{B}^0 \to \bar{K}^{*0}\phi$, we used the individual results from BaBar and Belle in our fits, whereas for $B^- \to K^{*-}\phi$ the results from HFAG have been used. Values that are used in the fits are indicated with a †.

the chiral-enhanced scalar QCD-penguin amplitudes

$$\alpha_4(M_1M_2) = a_4(M_1M_2) \pm r_\chi^{M_2} a_6(M_1M_2). \tag{5.7}$$

In the case of $M_1M_2 = VP$, the two contributions interfere destructively, whereas for $M_2 = V$, the tree-level contribution to $a_6(M_1M_2)$ vanishes, leading to naturally smaller QCD-penguin amplitudes than for $M_1M_2 = PP$ and implicitly larger power-suppressed ratios $\xi_3^A(M_1M_2)$.

The contour plots for all other decay modes listed in Table 5.2 are either placed for completeness into Appendix B or are discussed in Subsection 5.1.3. In the following, we comment on the two decay systems:

$B \to K\omega$

The fit for the decay system $B \to K\omega$, shown on the left panel of Figure 5.4, produces a small tension for $C(\bar{B}^0 \to \bar{K}^0\omega)$ of about -1.0σ. We list the theoretical and experimental results in Table 5.3. Compared to the theory prediction at the best-fit point, the combined experimental result from HFAG can indeed not be explained within our fits; this tension arises from the large value from the BaBar collaboration. This decay system is interesting for two reasons: First, the fit prefers the large WA scenario, which have not been observed for the decays discussed above. The best-fit point has $\rho_A^{K\omega} = 4.1\, e^{4.6i}$, and power-suppressed corrections become suspiciously large $\xi_3^A(K\omega) = 2.7$. If we restrict the fit to $|\rho_A^{K\omega}| < 2$, the pull increases to 1.6σ. Second, the CP asymmetry is sensitive to the colour-suppressed tree amplitude $\alpha_2^u(K\omega)$. As we will see in Subsection 5.1.4, an enhanced colour-suppressed tree amplitude might provide a solution to the $\Delta A_{\rm CP}^{K\pi}$ problem and can be realised by larger HS interactions. If these power-suppressed corrections are enhanced in general, this effect would be clearly visible in this CP asymmetry, but the current experimental situation is inconclusive. The Belle collaboration recently updated its analysis [81], presented in the second column of Table 5.3, and unfortunately, the

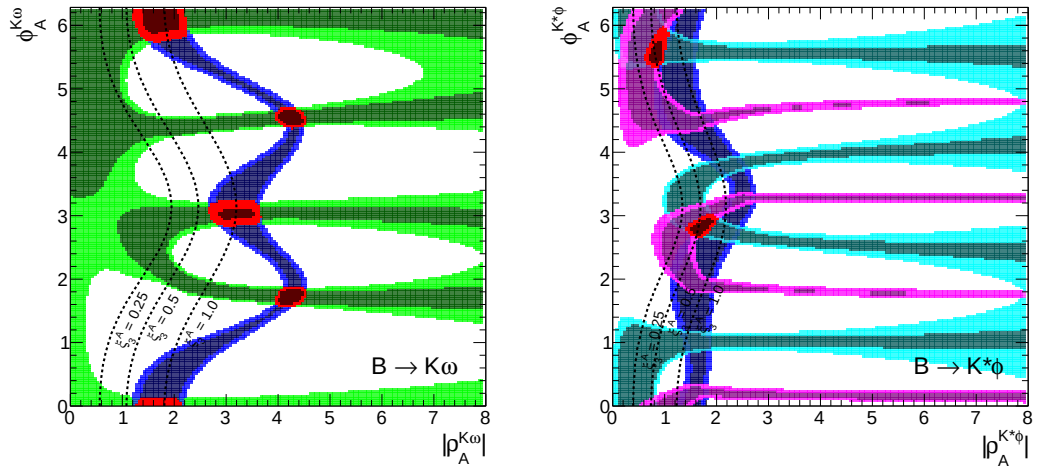

FIGURE 5.4: 68% and 95% CRs for the complex parameters $\rho_A^{K\omega}$ (left) and $\rho_A^{K^*\phi}$ (right) for the decay systems $B \to K\omega$, $K^*\phi$ assuming the SM. Allowed regions are separately shown for branching ratios (blue), CP asymmetries (green), polarisation fractions (cyan), relative amplitude phases (purple), and the combination (red). The dashed lines correspond to $\xi_3^A(M_1M_2) = 0.25\,(0.5,\,1.0)$.

new measurement is highly incompatible with that of the BaBar collaboration.

$B \to K^*\phi$

The combined contour for the decay system $B \to K^*\phi$, shown on the right panel of Figure 5.4, is restricted to a rather small region in parameter space and does not overlap with either the branching-ratio nor the amplitude-phase (purple) contour at the probability of 68%. The visible tension in the plot transfers to non-vanishing pulls for $\mathcal{B}(\bar{B}^0 \to \bar{K}^{*0}\phi)$ of 1.7σ and $\phi_\perp(B^- \to K^{*-}\phi)$ of 1.4σ. Since the decay amplitudes for the neutral and the charged decays do not differ significantly from each other, we expect that observables, $\hat{\mathcal{O}}$, for both decay channels should be almost equal, even in the presence of NP contributions

$$\hat{\mathcal{O}}(B^- \to K^{*-}\phi) \sim \hat{\mathcal{O}}(\bar{B}^0 \to \bar{K}^{*0}\phi). \tag{5.8}$$

Due to the hierarchy among the different helicity amplitudes (see Equation 3.33) the following relation should also hold

$$\phi_\perp = \phi_\parallel. \tag{5.9}$$

The experimental situation, as it is presented in Table 5.3, turns out to be inconsistent with the above findings. The amplitude phase $\phi_\perp$ from each decay is larger than $\phi_\parallel$[3], which explains the discrepancy mentioned above. The pattern in Equation 5.9, in contrast to Equation 5.8, is a particular outcome of the SM and can be broken through

[3]Except for the BaBar measurement in $\bar{B}^0 \to \bar{K}^{*0}\phi$, for which $\phi_\perp \sim \phi_\parallel$

right-handed currents in flavour-violating $b \to s$ transitions. χ-flipped operators could potentially relax the tension.

5.1.3 Universal weak annihilation for same final states

So far, we have assumed that QCD-penguin-dominated decay amplitudes can be parametrised by one WA contribution $X_A(M_1M_2)$ for those decay modes that are related via $(u \leftrightarrow d)$ quark exchange. In the following, we relax this assumption and also include those decay modes into a common decay system with different initial (B_s vs. B_d), but same final states, which implies relations between $|\Delta S| = 1$ and $|\Delta D| = 1$ decay modes. The assumption might be justified by the following reasoning: We have already argued that WA contributions in QCD-penguin-dominated decay amplitudes are numerically dictated by the topology in which the gluon is emitted from the quark current that hadronises into the final states (last 2 diagrams in Figure 3.5). This implies that momentum transfer from the initial B meson is only present at the weak interaction vertex and the uncontrollable soft QCD-interaction is triggered by the final-state quark currents that are, due to our assumption, equivalent. Furthermore, the emergent divergences in these topologies are expected to be regularised by some non-perturbative objects that are yet unknown but should replace the LCDA of the light mesons at the endpoints [134] and be equivalent for same final states. Therefore, one can expect that the hadronisation process of the final states might be universal and almost independent from the initial B meson and the difference between WA amplitudes in $B_d \to M_1M_2$ and $B_s \to M_1M_2$ should be of the order of the difference between the heavy meson masses $(m_{B_s} - m_{B_d})/m_{B_s}$. Similar arguments have been presented for the decays $\bar{B}_d \to K^-\pi^+$ and $\bar{B}_s \to K^+\pi^-$ in [135]. At the moment, experimental information for B_s decays is limited to at large six hadronic decay systems

$$\begin{aligned}
&B \to \pi\pi \quad \Longleftrightarrow \quad B_s \to \pi\pi, \\
&B \to KK \quad \Longleftrightarrow \quad B_s \to KK, \qquad B \to K^*K^* \quad \Longleftrightarrow \quad B_s \to K^*K^*, \\
&B \to K\pi \quad \Longleftrightarrow \quad B_s \to K\pi, \qquad B \to K^*\phi \quad \Longleftrightarrow \quad B_s \to K^*\phi,
\end{aligned} \tag{5.10}$$

whereas the corresponding measurements of the decay $B_s \to \phi\phi$ in the B_d system is lacking at the moment.

A relation between WA corrections in decay amplitudes with 2 pions in the final state might be not justified due to the fact that the B_d decay is driven by tree-level and the B_s decay by pure WA contributions. The latter will be further studied in Section 5.2. In the case of two kaons in the final state, one should be also cautious. Although the decay modes of both the B as well as the B_s meson are dominated by the QCD-penguin amplitude, the specific decay $B^- \to K^{(*)-}K^{(*)0}$ also receive corrections

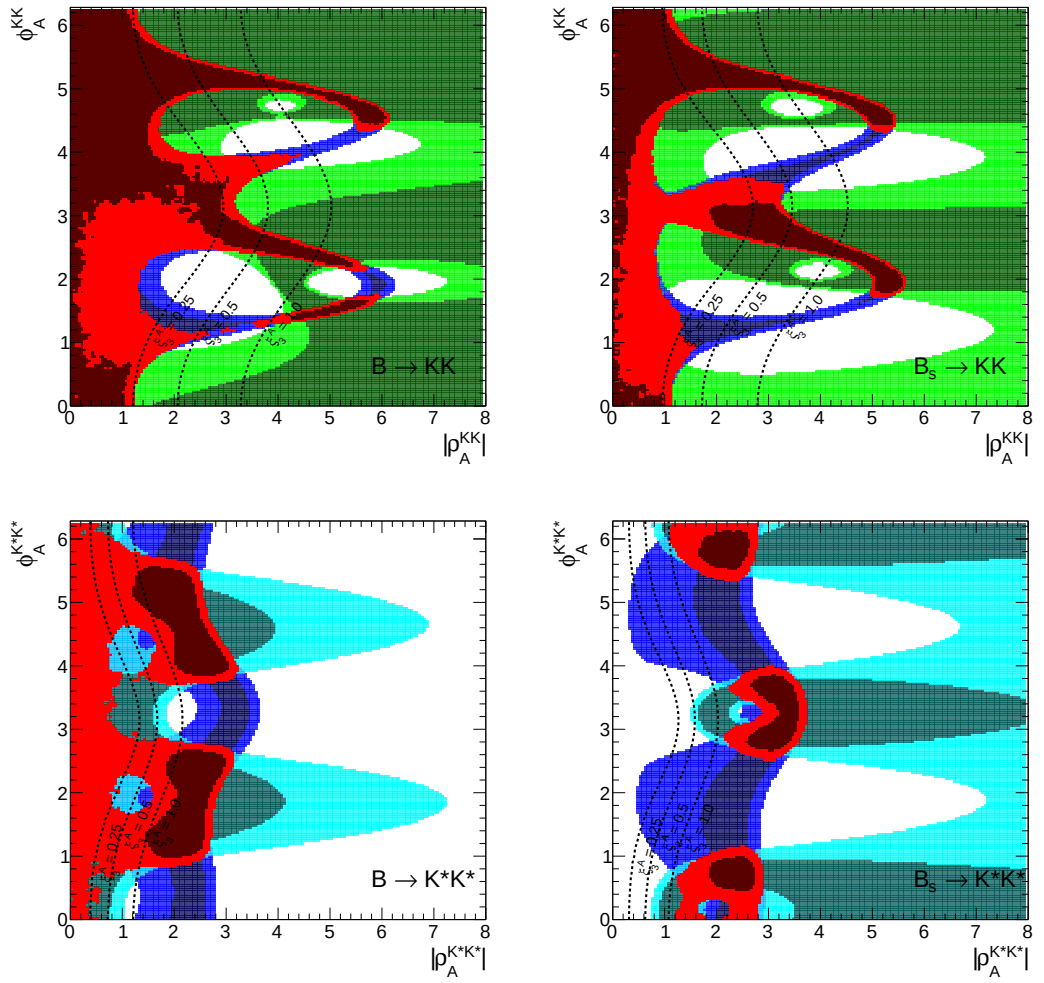

FIGURE 5.5: 68% and 95% CRs for the complex parameters ρ_A^{KK} (upper) and $\rho_A^{K^*K^*}$ (lower) for the decay systems $B \to K^{(*)}K^{(*)}$ (left) and $B_s \to K^{(*)}K^{(*)}$ (right) assuming the SM. Allowed regions are separately shown for branching ratios (blue), CP asymmetries (green), polarisation fractions (cyan), and the combination (red). The dashed lines correspond to $\xi_3^A(M_1M_2) = 0.25\,(0.5,\,1.0)$.

from tree-level WA. These contributions are parametrically suppressed by the CKM-elements $\lambda_u^{(s,d)}$, which is, however, less effective for $b \to d$ than $b \to s$ transitions and cannot be completely neglected for these modes. The contour plots for both PP and VV final states are presented in Figure 5.5. Whereas the contours for $B_{(s)} \to KK$ are still large and nicely overlap, they overlap for $B_{(s)} \to K^*K^*$ only marginally at a probability of 68%. It appears that those regions in parameter space that are favoured by the B decay are excluded for B_s, which mostly originate from polarisation-fraction measurements. If we omit observables from $B^- \to K^{*-}K^{*0}$ from the fit, the combined contour slightly increases and a coinciding region for both contours at $\phi_A^{K^*K^*} \sim 5.6$ can be found. Although the common area of both fits is considerably small compared to the residual allowed regions, it is not unlikely that at this phase, which was also favoured

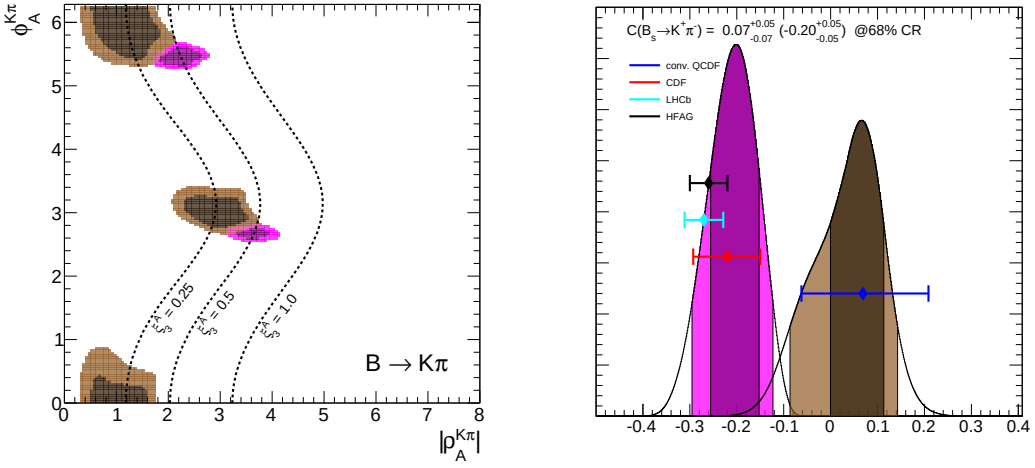

FIGURE 5.6: 68% and 95% CRs for the complex parameter $\rho_A^{K\pi}$ obtained from a fit with the reduced observable set for $B^- \to K^-\pi^0$ (brown) and $\bar{B}^0 \to K^-\pi^+$ (purple) assuming the SM. The dashed lines correspond to $\xi_3^A(K\pi) = 0.25\,(0.5,\,1.0)$. The right panel shows the corresponding predictions for the CP asymmetry $C(\bar{B}_s \to K^+\pi^-)$. Experimental results are drawn at the 1σ level and a prediction from QCDF within conventional error estimation is indicated by the label "conv. QCDF" .

from other decay systems, the data of both is correctly described. Further experimental improvements will clarify if different corrections from WA are needed.

The only remaining relations from Equation 5.10 to study are for the final states $K\pi$ and $K^*\phi$, whereas for the latter, experimental data for the B_s decay is not yet conclusive enough to judge on our assumptions. So our analysis will be restricted to $K\pi$ final states and we would like to test whether the CP asymmetry $C(\bar{B}_s \to K^+\pi^-)$, which was recently measured by the CDF [136] and LHCb [137] collaboration, can be predicted correctly, restricting WA contributions from a corresponding fit in the B_d system. Since the fit of $B \to K\pi$ data does not allow for a simultaneously explanation of the two CP asymmetries with a charged kaon in the final state, it might be reasonable to investigate them separately. Figure 5.6 shows the contours from branching-ratio and CP-asymmetry measurements of the two contradicting decay modes $\bar{B}^0 \to K^-\pi^+$ (purple) and $B^- \to K^-\pi^0$ (brown). In addition, we used $R_c^K(K\pi)$ to suppress solutions from the large weak-annihilation scenario. Due to the higher statistical weight of $C(\bar{B}^0 \to K^-\pi^+)$, the purple contour coincide nicely with the red contour in Figure 5.1 for which all constraints were taken into account. At this point, one should noticed that $|\rho_A^{K\pi}| > 1$ does not originate from the $\Delta A_{\rm CP}^{K\pi}$ problem, but rather from the precise measurement of the CP asymmetry $C(\bar{B}^0 \to K^-\pi^+)$. The resulting posterior probability was then used to predict the CP asymmetry $C(\bar{B}_s \to K^+\pi^-)$, as described in Appendix A.4, and is shown on the right panel in Figure 5.6. The measurement nicely agrees with the prediction from the $K^+\pi^-$-fit, whereas it fails at more than 4σ for the $K^+\pi^0$-fit. These results support, on the one hand, that $|\rho_A^{K\pi}| > 1$ is justified and, on the other hand, that universal WA among same

final states might be a reasonable approximation and should be further tested against improved measurements.

5.1.4 Possible solution to the $\Delta A_{\rm CP}^{K\pi}$ puzzle

We have seen that our theoretical prediction for $\Delta A_{\rm CP}^{K\pi}$ does not coincide with the corresponding measurements by about 2.8 standard deviations. The dominant source of CP violation in the SM originate from the weak phase of the CKM-matrix element V_{ub} in combination with the colour-suppressed and colour-allowed tree amplitudes, whereas the latter contribution cancels in the difference (see Equation 5.4). The residual CP-violating term in $\Delta A_{\rm CP}^{K\pi}$ is, at least in the SM, only proportional to $\alpha_2^u(K\pi)$. The colour-suppressed tree amplitude is sensitive to power corrections from HS interactions due to its dependence on the large Wilson Coefficient C_1 (see Equation 3.22). The following subsection shall clarify how far we have to abandon from the conventional error estimation in order to solve the $\Delta A_{\rm CP}^{K\pi}$ puzzle and what kind of implications we can expect for other observables. The fact that power corrections from HS interactions in colour-suppressed tree amplitudes might have been underestimated was also observed in the tree-level-dominated decay $\bar{B}^0 \to \pi^0\pi^0$ [2, 138], with the parametrisation of the decay amplitude

$$\mathcal{A}_{\bar{B}\to\pi^0\pi^0} = A_{\pi\pi} \sum_p \lambda_p^{(d)} \left(\delta_{pu}(-\alpha_2 + \beta_1) + \hat{\alpha}_4^p - 2\beta_4^p\right). \tag{5.11}$$

The measurement of the corresponding branching ratio is larger compared to the prediction form QCDF, indicating $|\rho_H^{\pi\pi}| > 1$ also for tree-level decays, which are assumed to be free of physics beyond the SM. The misalignment of the branching-ratio prediction was originally interpreted in [2, 138] as a hint towards a smaller value for λ_B as expected from QCD-sum rules (see Subsection 3.2.1). Once this parameter is precisely extracted from $\mathcal{B}(B \to \gamma\ell\nu)$, the justification of large power corrections from HS might be confirmed also in tree-level decays.

The upper panels of Figure 5.7 show contour regions for the parameters $\rho_H^{K\pi}$ (left) and $\rho_A^{K\pi}$ (right) from a simultaneous fit of HS and WA corrections. We used observable set SII to obtain the purple-coloured region, whereas the direct CP asymmetry $C(\bar{B}^0 \to \bar{K}^0\pi^0)$ and the ratio of branching ratios $R_n^B(K\pi)$ have been removed. Though the CP asymmetry strongly depends on power corrections from HS, it does not further constrain the fit due to lacking precision in the measurement, making it a suitable candidate to be predicted. In contrast, $R_n^B(K\pi)$ is indeed quite well measured and a tension of -1.9σ was already encountered for this observable in the previous fits, but because it is not sensitive to the HS corrections, it would spoil the fit to very large values for $\rho_H^{K\pi}$, which might be not necessary to explain $\Delta A_{\rm CP}^{K\pi}$. The brown contour is taken from the

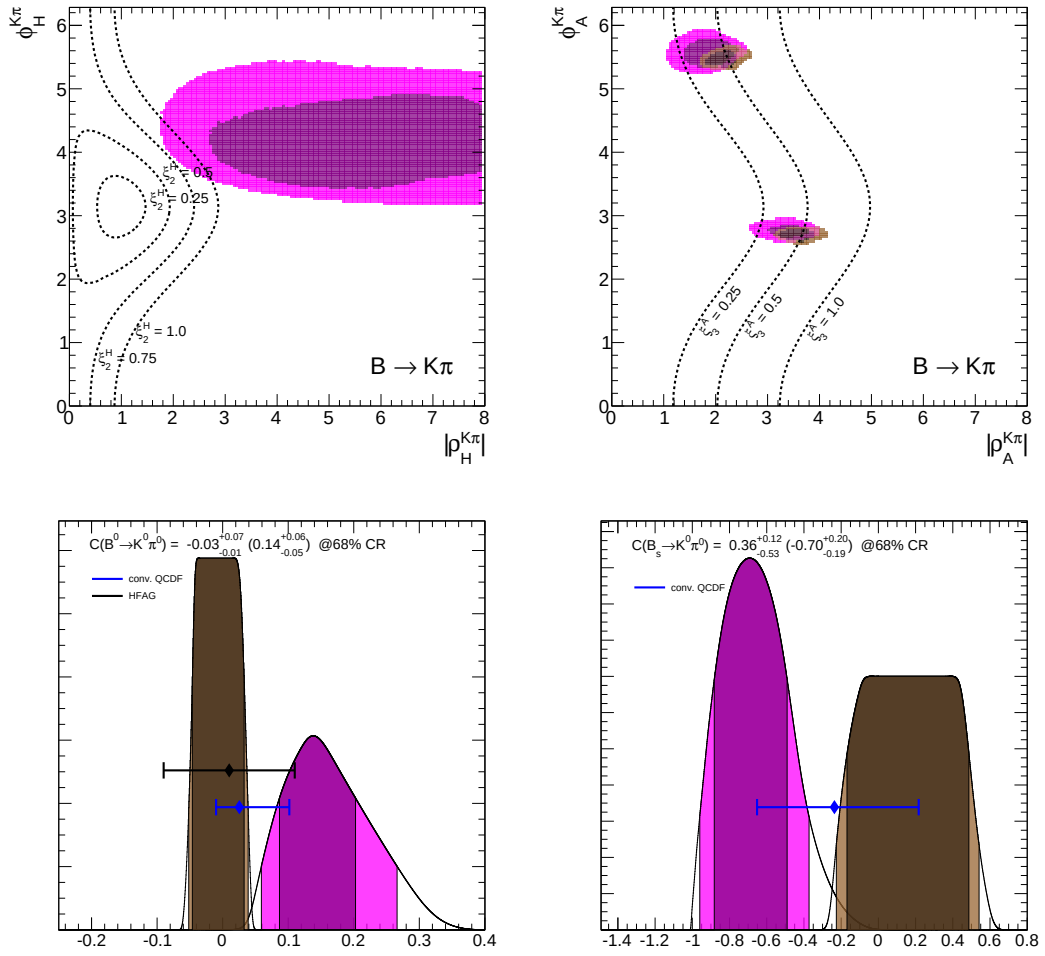

FIGURE 5.7: 68% and 95% CRs for the complex parameters $\rho_H^{K\pi}$ (upper left panel) and $\rho_A^{K\pi}$ (upper right panel) obtained from a fit with the observable set SII for the decay system $B \to K\pi$ assuming the SM and treating $\rho_H^{K\pi}$ as either fit parameter (purple) or nuisance parameter (brown). The dashed lines correspond to contour lines for $\xi_2^H(K\pi) = 0.25\,(0.5, 0.75, 1)$, respectively $\xi_3^A(K\pi) = 0.25\,(0.5, 1.0)$. The lower panels show the corresponding predictions for the CP asymmetries $C(\bar{B} \to \bar{K}^0\pi^0)$ (left) and $C(\bar{B}_s \to K^0\pi^0)$ (right). Experimental results, if available, are drawn at the 1σ level and a prediction from QCDF within conventional error estimation is indicated by the label "conv. QCDF".

findings in Figure 5.1, with all observable in set SII used as constraint and shall serve as comparison. In addition, contour lines for $\xi_2^H(K\pi)$ and $\xi_3^A(\pi K)$ are shown. The following results can be obtained from the plots.

- The prediction of $\Delta A_{\rm CP}^{K\pi}$ at the best-fit point for $\rho_H^{K\pi} = 3.3\,e^{3.7i}$ coincides with the measurement.

- The fit prefers $\phi_H \sim \frac{3}{2}\pi$, which implies that HS corrections to $\alpha_2^u(K\pi)$ should be mainly imaginary and interfere constructively with the imaginary part of the vertex corrections, following the desired pattern described in Chapter 5.1.1.

- In order to relax the tension in $\Delta A_{\rm CP}^{K\pi}$, $|\rho_H^{K\pi}|$ should be, at least, larger than 1.8 ($\rightarrow |\delta(\Delta A_{\rm CP}^{K\pi})| \leq 1.6\sigma$). Inspecting $\xi_2^H(K\pi)$, the relative amount of power corrections compared to the leading contribution at for instance $\rho_H^{K\pi} = 1.8\, e^{4.5i}$ is not larger than for parameter points that are usually included into the error budget ($\rho_H^{K\pi} = 1.0$). This is a remnant artefact of the parametrisation $X_H \sim (1 + \rho_H^{K\pi})$.
- The fit for the WA corrections is shifted in favour to smaller $|\rho_A^{K\pi}|$, which implies smaller values for $\xi_3^A(\pi K)$.[4]

If in fact large HS corrections are responsible for the observed discrepancy in $\Delta A_{\rm CP}^{K\pi}$, similar effects should be observable for other decay modes. For example, the CP asymmetries in $\bar{B}^0 \to \bar{K}^0\pi^0$ and also $\bar{B}_s \to K^0\pi^0$ should receive visible corrections, whereas in the latter case the effect would be enhanced compared to the former due to the different hierarchy of CKM-matrix elements

$$\left|\lambda_u^{(d)}/\lambda_c^{(d)}\right| \gg \left|\lambda_u^{(s)}/\lambda_c^{(s)}\right|. \tag{5.12}$$

The predictions for these observables are shown in the lower panels of Figure 5.7, whereas the colour code is in accordance with the upper panels. Once measured, respectively measured with higher precision, both observables will allow to test the assumption of *large hard-spectator scattering interactions* for $B \to K\pi$

$$\begin{aligned} C(\bar{B}^0 \to \bar{K}^0\pi^0)^{\rm fitX_H} &= 0.14^{+0.06}_{-0.05}, \quad C(\bar{B}^0 \to \bar{K}^0\pi^0)^{\rm scanX_H} = [-0.04,\, 0.04], \\ C(\bar{B}_s \to K^0\pi^0)^{\rm fitX_H} &= -0.70^{+0.20}_{-0.19}, \quad C(\bar{B}_s \to K^0\pi^0)^{\rm scanX_H} = [-0.17,\, 0.48]. \end{aligned} \tag{5.13}$$

From the previous discussion, we should keep in mind that even if additional NP contributions do not entirely account for solving the $\Delta A_{\rm CP}^{K\pi}$ problem, it might be reasonable that both soft QCD effects through HS and NP effects are needed to be taken into account. Therefore, observables like ratios of branching ratios seem to be an appropriate additional information to judge on the reliability of a NP model.

A similar analysis, concerning enhanced contributions from HS interactions, has been carried out in [139]. The authors found a best-fit point for $\rho_H^{K\pi} = 4.9\, e^{4.9i}$. With respect to deviating input values such as $\lambda_B = 0.35\,\text{GeV}$ and to the evaluation of HS at different renormalisation scales, their result lies in the ballpark of our 68% CR.

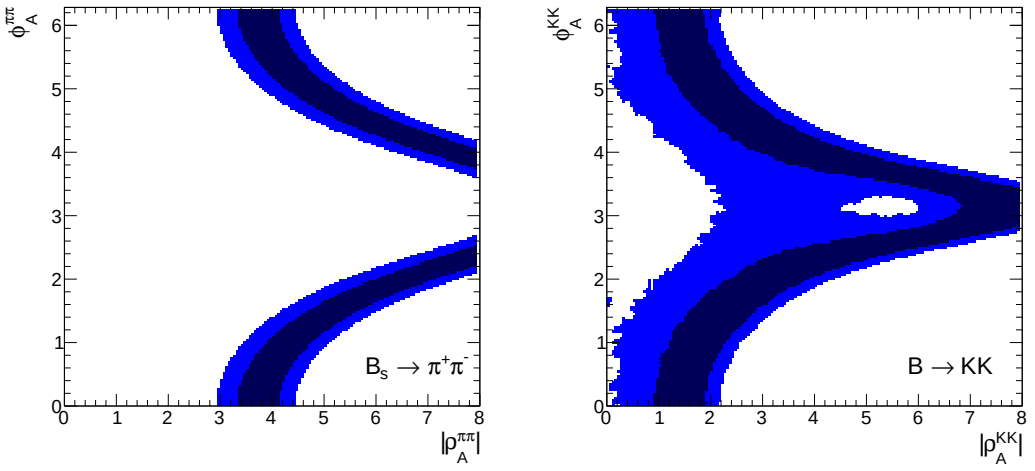

FIGURE 5.8: 68% and 95% CRs for the complex parameter $\rho_A^{\pi^+\pi^-}$ and $\rho_A^{K^+K^-}$ obtained from a branching-ratio fit assuming the SM.

5.2 Weak-annihilation dominated decays

5.2.1 $\bar{B}_s \to \pi^+\pi^-$ vs. $\bar{B}_d \to K^+K^-$

So far, we exclusively discussed decay amplitudes that are dominated by QCD-penguin topologies. These types of decays share the feature that the leading WA correction in $\beta_3^c(M_1M_2)$ is dominated by the building block A_3^f, originating from a gluon exchange between the final state quark currents. Further, we grouped those final state systems together that are related via the $(u \leftrightarrow d)$ quark exchange and assumed universality for their WA corrections. We extended our assumption to decay amplitudes with same final states, which was motivated and tested in Subsection 5.1.3. In view of our fit results, it is rather doubtful that universality holds in general along all decay amplitudes. It is even unclear if universality holds among PP, PV, VP or VV final states, although, being not completely forbidden from our fits.

Now we are interested in decay modes that solely receive contributions from WA topologies. The only so far measured systems are $\bar{B}_s \to \pi^+\pi^-$ and $\bar{B}_d \to K^+K^-$. Their amplitudes are parametrised by

$$\begin{aligned}\mathcal{A}_{\bar{B}_s\to\pi^+\pi^-} &= i\frac{G_F}{\sqrt{2}} f_{B_s} f_\pi^2 \sum_p \lambda_p^{(s)} \left(\delta_{pu} b_1 + 2b_4^p + \frac{1}{2} b_{4,\mathrm{EW}}^p\right), \\ \mathcal{A}_{\bar{B}_d\to K^+K^-} &= i\frac{G_F}{\sqrt{2}} f_{B_d} f_K^2 \sum_p \lambda_p^{(d)} \left(\delta_{pu} b_1 + 2b_4^p + \frac{1}{2} b_{4,\mathrm{EW}}^p\right),\end{aligned} \tag{5.14}$$

[4]We proved that the resulting relaxation in the WA fit is indeed a consequence of the additional degrees-of-freedom and was not caused by the fact that the observable $R_n^B(K\pi)$ was removed from the fit.

and are, apart from power corrections, not disturbed by parameters that usually cause large uncertainties like for example form factors or the inverse moment of the B-meson LCDA and $\rho_A^{M_1M_2}$ can be safely extracted. The involved coefficients $b_i(M_1M_2)$ exclusively depend on the building block $A_{1,2}^i$ (see Equation 3.25), where the gluon is emitted from the initial quark current (first two diagrams in Figure 3.5). The fit results for $\rho_A^{\pi^+\pi^-}$ (left) and $\rho_A^{K^+K^-}$ (right) are shown in Figure 5.8.

Their contours do not overlap within a probability of 95%, and at $\phi_A = 0$, the absolute value can be restricted to $|\rho_A^{\pi^+\pi^-}| \in [3.4; 4.1]$ and $|\rho_A^{K^+K^-}| \in [0.9; 1.9]$ at a probability of 68%. It is not surprising that the WA corrections for decays of different initial and final states differ from each other and confirms that universality is not valid in general. However, what might be remarkable is that $|\rho_A^{\pi^+\pi^-}|$ is much larger compared to all other fit results, whereas the contour from K^+K^- seem to be consistent, in particular, consistent with the contour of the QCD-penguin-dominated decays with also two kaons in the final state (upper panels in Figure 5.5). The power-suppressed ratio $\xi_3^A(M_1M_2)$ cannot be quoted, because the decay amplitudes do not depend on $\alpha_4^c(M_1M_2)$. Similar fits have been obtained in [140], whose results we confirm.

Apart from the misalignment of WA corrections in decays with different initial and final states, there might be another interesting aspect, which can be studied along pure WA decays. In the framework of QCDF, both decay amplitudes in Equation 5.14 solely depend on the building block A_1^i, which is the only source of strong phases. In order to observe CP violation, a relative strong phase between the CP-conserving and CP-violating part of the decay amplitude is needed, but since all coefficients $b_i(M_1M_2)$ obtain a common strong phase, no CP violation for these decay modes is predicted at all. This is a feature of the low-energy theory and also holds for NP contributions in general, which leads to the following implications: First, it is impossible within QCDF to extract information on neither $\phi_A^{K^+K^-}$ nor $\phi_A^{\pi^+\pi^-}$. Secondly, an observation of CP violation would cast doubt on the reliability of the right parametrisation of higher-order power corrections. This makes pure WA decays suitable to test the assumptions in QCDF. These effects might be also studied in the future through the corresponding neutral and for other spin (PV, VP, VV) final states.

Chapter 6

Exploring the structure of physics beyond the Standard Model

A large number of operators is involved in the phenomenology of hadronic B-meson decays. We already have to deal with 10 4-quark and two dipole operators in the SM and even many more can be considered beyond. We discussed in Chapter 5 that some isospin-sensitive observables like $\Delta A_{\mathrm{CP}}^{K\pi}$ and $R_n^B(K\pi)$ seem to elude from a consistent description in the SM, which, in particular for the former, attracted the attention of many works. The forthcoming sections shall be used to perform a model-independent analysis, in which we allow certain Wilson Coefficients, respectively SM couplings, to be enhanced. We would thereby like to understand, which class of operators is suitable to relax the aforementioned tensions and how well they can already be constrained by current data. The advantages of a model-independent analysis are manifold: Whereas a concrete model can in detail become rather complicated such as the Minimal Supersymmetric Standard Model (MSSM) with more than 100 free parameters, confining oneself to a finite subset of operators can account for several different models simultaneously and allow for a tremendous simplification of the analysis. Correlations between different kind of observables, as from direct vs. indirect searches, which automatically emerge in specific models, do not need to be considered, enabling oneself to focus the analysis on solving a particular problem. If it becomes clear what kind of operators are suitable for our purpose, one can extrapolate to the model in favour and see whether such effects are still allowed with respect to other constraints. Since no overwhelming hints from direct searches so far have appeared, a model-independent data-driven analysis seems to be a reasonable approach to search for physics beyond the SM.

We will investigate three effective realisations of potential NP scenarios. The first two analysis confine to the SM operator basis. In Section 6.1, we allow for non-standard Wilson Coefficients of the QED-penguin operators — a solution to the $\Delta A_{\mathrm{CP}}^{K\pi}$-puzzle that has already been suggested in the literature — and allow in Section 6.2 for arbitrary

contributions to the more fundamental, (at the Lagrangian level) flavour-violating SM coupling of the Z-boson. The latter also contributes to observables of the (semi-)leptonic decays $b \to s\ell^+\ell^-$ through dominant contributions to $\mathcal{C}_{10,A}$. The last analysis in Section 6.3 is dedicated to an extended operator basis. The operators with the flavour structure $\mathcal{O}^b = (\bar{s}b)\,(\bar{b}b)$ are discussed, with respect to an arbitrary Dirac and colour structure, in complete generality. They influence both hadronic and (semi-)leptonic observables through mixing effects; this time contributing to the vectorial QCD- and QED-penguin operators.

Each of the three above-mentioned scenarios are discussed along the same structure. First of all, we will set up our model and elaborate the most important features of the individual scenarios. The second part includes the actual analyse. We are mainly interested in contour regions and bounds on the individual effective couplings. They are obtained from a simultaneously fit of both NP and WA parameters, for which one $\rho_A^{M_1M_2}$ is assumed for each final state system. This ansatz is crucial for the fit and, to our knowledge, has not been applied so far in the literature. Compared to conventional QCDF, it leads to qualitative different results, as we will exemplary discuss later on. As a measure of the necessary amount of power corrections, we quote for each scenario and decay system the power-suppressed ratio $\xi_3^A(M_1M_2)$ at a probability of 68%, as described in Appendix A.5. In order to limit the amount of free parameters, we have to confine the fit to at most four to five hadronic decay systems, for which those with most experimental information available are chosen, in particular $B \to K\pi$, $K\rho$, $K^*\pi$, $K^*\rho$ and $B \to K^*\phi$. We only discuss $b \to s$ triggered decays because only insufficient experimental information from decay systems of $b \to d$ transition exist at the moment, which do not allow for an efficient simultaneous extraction of soft QCD and NP parameters. Since our main motivation to study contributions beyond the SM was to explain the discrepancy in $B \to K\pi$, we quantify the goodness of our fit through quoting significant pull values and comparing the χ^2 for the SM vs. NP-fit in $\Delta\chi^2(\text{SM})$. The last part discusses how additional contributions to the individual operators could be detected in future experiments as, for instance, at LHCb or Belle II. We predict, adapted to the respective scenarios, certain selected observables together with the mixing-induced CP asymmetries $\Delta S(M_1M_2)$. The latter are in principal part of the observable sets in those decay systems that also enter the fit, but are typically imprecisely measured and do not deliver further constraints. Those scenarios that also affect (semi-)leptonic decays can further be tested through the prediction of the CP-violating observables, described in Chapter 4.2.1.

6.1 Model-independent fits of the QED-penguin Coefficients $\mathcal{C}_7^{(\prime)}, \mathcal{C}_9^{(\prime)}$

The QED-penguin operators of the SM and their χ-flipped counterparts are isospin-violating and, if enhanced, suitable to affect the observables that have been constructed in Section 4.1. We expect that the encountered tensions in the SM, in particular, $\Delta A_{\text{CP}}^{K\pi}$ and $R_n^B(K\pi)$, can be relaxed through additional contributions to the Wilson Coefficients of these operators. It is interesting to study if such corrections are still allowed when taking observables of other decay systems into account. The observation that $\Delta A_{\text{CP}}^{K\pi}$ can be resolved through a modification of the QED-penguin Wilson Coefficients has already been made in [42] and motivated further studies [74, 141]. Many particular models exists that in fact imply corrections to these operators like, for instance, theories with an additional U(1) gauge group [142–145]. It is therefore well motivated to study the impact of an enhanced electroweak penguin sector on hadronic B-meson decays in a systematic, model-independent way.

In contrast to the hadronic decays in this work, which are mainly QCD-penguin-dominated, similar QED-penguin operators also occur in the EWH of (semi-)leptonic decays (see Equation 2.19), which constitute the leading contribution to the decay amplitude. If a particular model is constructed, in which either the flavour-violating couplings of the SM are enhanced or the new fields generate themselves flavour-violating transitions and do not couple hierarchical differently to quarks and leptons, it is very likely that effects in the observables of hadronic and (semi-)leptonic decays are correlated. A model-independent fit, as we are going to present it in the following subsection for the Wilson Coefficients of the 4-quark QED-penguin operators, was also performed for the corresponding semi-leptonic operators in [109, 110, 146, 147]. The qualitative results can be compared to our findings. In the following two NP scenarios, presented in Sections 6.2 and 6.3, we connect these systems practically through the enhancement of the SM coupling of the Z-boson to the $b \to s$ transition as well as an extended operator basis and, study their correlations in a combined fit.

6.1.1 Theory

The operator basis for hadronic B-meson decays consists among others out of four QED-penguin operators with non-vanishing Wilson Coefficients C_{7-10} (see Equation 2.14). They originate from box-, as well as photon-, and Z-penguin diagrams. The symmetry of the SM generates exclusively left-handed flavour-violating $b \to s$ transitions. The second quark-current transition in the QED-penguin operators receive different vectorial and axial-vectorial contributions, which is typically parametrised through purely left-handed ($C_{9,10}$) and purely right-handed ($C_{7,8}$) currents. Because the dominant contributions

for the vectorial and axial-vectorial part only differ by an overall sign, $C_{7,8}$ becomes accidentally small and $C_{9,10}$ enhanced. The even-numbered operators are defined in a colour-octet configuration and their Wilson Coefficients are suppressed by α_s compared to the Wilson Coefficients of the colour-singlet operators $C_{7,9}$. We therefore focus on the modification of the Wilson Coefficients $C_{7,9}$ and also include the possibility of right-handed flavour-violating currents through non-zero Wilson Coefficients of the χ-flipped operators: $C'_{7,9}$. Consequently, there are altogether maximally four complex parameters, modifying the physics at $\mu \sim M_W$, which we will concern in our fits. Since the Wilson Coefficients are proportional to the electromagnetic coupling constant α, it is useful to normalise the additional contributions to their SM counterparts. The primed Wilson Coefficients vanish in the SM and, as already mentioned, the parametrisation of the operator $\mathcal{O}_7$ leads to an accidentally small C_7, which suggests to use the absolute value of C_9 as the natural normalisation scale for all new contributions

$$C_i(M_W) = C_i^{\mathrm{SM}}(M_W) + |C_9^{\mathrm{SM}}(M_W)|\,\mathcal{C}_i, \qquad C'_i(M_W) = |C_9^{\mathrm{SM}}(M_W)|\,\mathcal{C}'_i, \tag{6.1}$$

where $\mathcal{C}_i^{(\prime)}$ are the parameters of interest and the numerical value for $C_9^{\mathrm{SM}}(M_W)$ is given in Table 2.1. The new contributions are introduced at the scale M_W, for which we adopt the RGE scheme from Section 2.1.

Although we will perform a simultaneous fit to all four complex Wilson Coefficients, it is sensible to study some limiting cases. First of all, the QED-penguin operators in the semi-leptonic sector can be related to those in the hadronic sector through a linear combination of the 4-quark operators after replacing the lepton current by according sum over quark currents

$$\begin{aligned} \mathcal{O}_{9V} &\sim \mathcal{O}_7 + \mathcal{O}_9, & \mathcal{O}_{10A} &\sim \mathcal{O}_7 - \mathcal{O}_9, \\ \mathcal{O}'_{9V} &\sim \mathcal{O}'_7 + \mathcal{O}'_9, & \mathcal{O}'_{10A} &\sim \mathcal{O}'_9 - \mathcal{O}'_7. \end{aligned} \tag{6.2}$$

The qualitative results that have been found for the fit of the semi-leptonic Wilson Coefficients in Subsection 4.2.2 and in the studies of for example [109, 110, 146, 147] can be compared to the results of our analysis and a common pattern might be observable. Secondly, we have discussed in Subsection 3.1.3 that parity symmetry arguments are useful to relate hadronic matrix elements of operators with their χ-flipped counterparts and shown in Equation 3.30 that they differ at most by an overall minus sign. This suggests to study the possibility of a *parity-symmetric* scenario, with $\bar{\mathcal{C}}_i \equiv \mathcal{C}_i + \mathcal{C}'_i$, and a *parity-anti-symmetric* scenario, $\Delta\mathcal{C}_i \equiv \mathcal{C}_i - \mathcal{C}'_i$. Depending on the spin of the final state,

the following generic pattern

$$\bar{\mathcal{C}}_i = \mathcal{C}_i + \mathcal{C}_i' \begin{cases} \text{PP, VV} & \text{blind} \\ \text{PV, VP} & \text{enhanced} \end{cases} \qquad \Delta\mathcal{C}_i = \mathcal{C}_i - \mathcal{C}_i' \begin{cases} \text{PP, VV} & \text{enhanced} \\ \text{PV, VP} & \text{blind} \end{cases} \tag{6.3}$$

can be observed. For the decays into two vector mesons, with either positive or negative polarisation, this relation is broken and can be tested in observables that depend on the helicity of the final state. As it is evident from Equation 6.3, one can expect that the decay systems with one pseudo-scalar and one vector meson will give orthogonal constraints to the decay systems with either two pseudo-scalar or two vector mesons.

Before going into the details of our results, we like to qualitatively argue on how isospin-violating observables are affected by the modification of the electroweak Wilson Coefficients, confining the discussion to the decay system $B \to K\pi$. Moreover, since similar fits with the conventional treatment of WA contributions have been performed in [74], we will emphasise the differences between both approaches. The QED-penguin operators mix neither into QCD-penguin[1] nor into tree-level operators and solely modify those hadronic matrix elements which contribute to the flavour amplitudes $\alpha^p_{3\,\mathrm{EW}}(K\pi)$, $\alpha^p_{4\,\mathrm{EW}}(\pi K)$. and $\beta^p_{3,4\,\mathrm{EW}}(\pi K)$. If the additional contributions do not generate corrections to the decay amplitude that are compatible in size to the leading order QCD-penguin amplitude $\hat{\alpha}^c_4$, the effects can be, as in the SM, parametrised through a modification of the three electroweak flavour-amplitude ratios, defined in Equation 4.15

$$r_i = r_i^{\mathrm{SM}} + \tilde{r}_i(|\mathcal{C}_i|)\, e^{i\delta_i}, \tag{6.4}$$

where the dependence on the potential weak phase δ_i in the Wilson Coefficients $\mathcal{C}_i = |\mathcal{C}_i|e^{i\delta_i}$ are kept explicit and the flavour-amplitude ratios depend on the absolute value of the modified Wilson Coefficients. It is then straight forward to expand Equations 4.18 and 4.16 in terms of the new flavour amplitudes $\tilde{r}_i$. We concentrate on the CP asymmetries of those decays that enter the definition of $\Delta A_{\mathrm{CP}}^{K\pi}$. In addition, since the CP asymmetry for $B^- \to \bar{K}^0\pi^-$ is fairly well measured and predicted to be close to zero in the SM, its dependence on the modification of the electroweak Wilson Coefficients is

[1] Actually, the QED- mix also into the QCD-penguin operators, but the effect is of higher order than considered here and numerically small.

also relevant for our analysis

$$\begin{aligned}
C(B^- \to K^-\pi^0) &\simeq 2\,\mathrm{Im}\,(\mathrm{r_T} + \mathrm{r_{T^C}})\,\sin\gamma - 2\sum_{i=7,9}\mathrm{Im}\Big(\tilde{\mathrm{r}}_{\mathrm{EW,i}} + \frac{2}{3}\tilde{\mathrm{r}}_{\mathrm{EW^C,i}} + \frac{2}{3}\tilde{\mathrm{r}}_{\mathrm{EW^A,i}}\Big)\,\sin\delta_{\mathrm{i}},\\
C(\bar{B}^0 \to K^-\pi^+) &\simeq 2\,\mathrm{Im}\,(\mathrm{r_T})\,\sin\gamma - 2\sum_{i=7,9}\mathrm{Im}\Big(\frac{2}{3}\tilde{\mathrm{r}}_{\mathrm{EW^C,i}} - \frac{1}{3}\tilde{\mathrm{r}}_{\mathrm{EW^A,i}}\Big)\,\sin\delta_{\mathrm{i}},\\
C(B^- \to \bar{K}^0\pi^-) &\simeq -2\sum_{i=7,9}\mathrm{Im}\Big(-\frac{1}{3}\tilde{\mathrm{r}}_{\mathrm{EW^C,i}} + \frac{2}{3}\tilde{\mathrm{r}}_{\mathrm{EW^A,i}}\Big)\,\sin\delta_{\mathrm{i}},
\end{aligned} \tag{6.5}$$

whereas the imaginary parts are given by the interference between the strong phase in $\hat{\alpha}_4^c(\pi K)$ and the ratios in Equation 6.4:

$$\mathrm{Im}(r_i) = -r_i^R \sin\hat{\phi}_4^c(\pi K) + r_i^I \cos\hat{\phi}_4^c(\pi K). \tag{6.6}$$

The numerical values for the ratios $r_i^{R,I}$ can be derived in terms of the enhanced Wilson Coefficients $\mathcal{C}_{7,9}^{(\prime)}$. Starting with the calculable QED-penguin amplitudes, we find

$$\begin{aligned}
\sum_{i=7,9}\tilde{r}_{\mathrm{EW}}^R e^{i\delta_i} &= -9.6^{+1.5}_{-1.4}\,\Delta\mathcal{C}_7 + 9.8^{+1.4}_{-1.5}\,\Delta\mathcal{C}_9, \quad \sum_{i=7,9}\tilde{r}_{\mathrm{EW^C}}^R e^{i\delta_i} = 9.3^{+0.4}_{-0.3}\,\Delta\mathcal{C}_7 + 2.6^{+2.1}_{-1.3}\,\Delta\mathcal{C}_9,\\
\sum_{i=7,9}\tilde{r}_{\mathrm{EW}}^I e^{i\delta_i} &= -0.2^{+0.4}_{-0.4}\,\Delta\mathcal{C}_7 + 0.2^{+0.3}_{-0.3}\,\Delta\mathcal{C}_9, \quad \sum_{i=7,9}\tilde{r}_{\mathrm{EW^C}}^I e^{i\delta_i} = -0.8^{+1.1}_{-1.1}\,\Delta\mathcal{C}_9,
\end{aligned} \tag{6.7}$$

with the numerical values quoted in %. The following observation can be made from the previous discussion:

- If $\Delta\mathcal{C}_{7,9} \sim \mathcal{O}(1)$, it appears from Equation 6.6 that the total amount of CP violation from these corrections cannot exceed the numerical values in front of the new Wilson Coefficients in Equation 6.7. This implies that the CP violation from the terms $\tilde{r}_{\mathrm{EW}}^I$ are negligible and $\tilde{r}_{\mathrm{EW^C}}^I$ can become at most 1% for $\Delta\mathcal{C}_9 \neq 0$.
- The typical order of magnitude in the SM for $\sin\hat{\phi}_4(\pi K) \sim 0.2$. This implies that for a moderate enhancement of the new Wilson Coefficients and a maximally CP-violating weak phase δ_i, the typical size of the additional CP violation achieves in $\tilde{r}_{\mathrm{EW}}^R$ and $\tilde{r}_{\mathrm{EW}}^{C,R}$ about 2%.
- The individual contribution to $\tilde{r}_{\mathrm{EW}}^R$ cancel each other, if $\Delta\mathcal{C}_7 \sim \Delta\mathcal{C}_9$.
- No CP violation can be expected from the contribution of $\Delta\mathcal{C}_7$ to the combination $\tilde{r}_{\mathrm{EW}}^R + \tilde{r}_{\mathrm{EW^C}}^R$.

As it was pointed in [74], also the WA contribution from QED-penguin operators, $\beta_{3,\mathrm{EW}}^c$, can contribute to the CP asymmetries. Their interplay is more involved because the flavour amplitude strongly depends on the WA parameter $\rho_A^{K\pi}$. Let us focus on two possible scenarios. First, we could set $\phi_A^{K\pi} = 0$, as it is done in the conventional

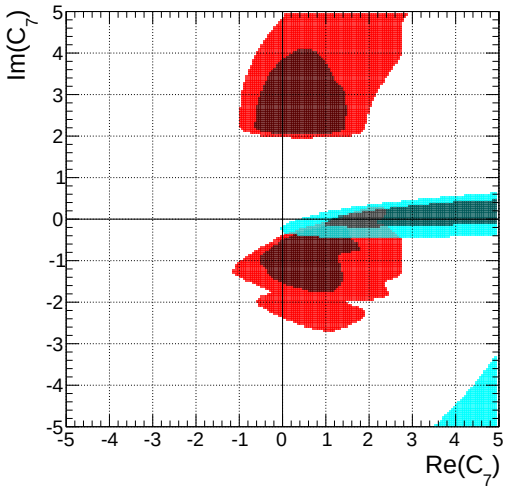

FIGURE 6.1: 68% and 95% CRs for a model-independent fit of an enhanced Wilson Coefficient $\mathcal{C}_7$. The contour regions are obtained from branching ratios and CP asymmetries of the decay system $B \to K\pi$, for which WA contributions have been either scanned (red) or fitted (cyan).

treatment of WA contributions, and no strong phase occurs in these flavour amplitudes. Second, $\rho_A^{K\pi}$ can be fixed to the solution of the SM fit, which implies large strong phases to $\beta^c_{3,\mathrm{EW}}$

$$\begin{aligned}
\sum_{i=7,9} \tilde{r}^R_{\mathrm{EW^A}} e^{i\delta_i} &= 7.6^{+0.5}_{-12.4}\,\Delta\mathcal{C}_7 + 0.9^{+0.1}_{-1.1}\,\Delta\mathcal{C}_9, \quad \sum_{i=7,9} \tilde{r}^I_{\mathrm{EW^A}} e^{i\delta_i} = \quad 0.0^{+5.4}_{-5.8}\Delta\mathcal{C}_7, \quad (\text{scan } \rho_{\mathrm{A}}^{\mathrm{K}\pi}) \\
\sum_{i=7,9} \tilde{r}^R_{\mathrm{EW^A}} e^{i\delta_i} &= 3.1^{+0.2}_{-0.3}\,\Delta\mathcal{C}_7 \; - 0.4^{+0.0}_{-0.0}\,\Delta\mathcal{C}_9, \quad \sum_{i=7,9} \tilde{r}^I_{\mathrm{EW^A}} e^{i\delta_i} = -7.2^{+0.6}_{-0.5}\,\Delta\mathcal{C}_7. \quad (\text{fit } \rho_{\mathrm{A}}^{\mathrm{K}\pi})
\end{aligned} \tag{6.8}$$

The amount of CP violation from $\Delta\mathcal{C}_9$ can be neglected in both cases, whereas the contributions from $\Delta\mathcal{C}_7$ can become large. The effect in $\tilde{r}^R_{\mathrm{EW^A}}$ is compatible in size to the corrections in $\tilde{r}^R_{\mathrm{EW}}$ and $\tilde{r}^R_{\mathrm{EW^C}}$. However, the corrections from $\tilde{r}^I_{\mathrm{EW^A}}$ depend on the considered scenario. In the first case, with vanishing strong phases, no CP violation can be observed at all. In the second case, the additional contribution is enhanced. A moderate modification of the Wilson Coefficient $\Delta\mathcal{C}_7$ would already imply a new source of CP violation of approximately 5% and can easily account for the tension in $\Delta A_{\mathrm{CP}}^{K\pi}$. But since the same flavour-amplitude ratio $\tilde{r}^A_{\mathrm{EW}}$ also occurs in $B^- \to \bar{K}^0\pi^-$, large CP-violating contributions would automatically be introduced to this decay, too. The measurement of its CP asymmetry is rather accurate, consistent with the SM prediction and therefore, actually forbids too large CP-violating corrections from $\Delta\mathcal{C}_7$.

In order to further analyse the difference between both approaches, we forestall the fit result of an enhanced Wilson Coefficient $\mathcal{C}_7$ in Figure 6.1. The red contour is obtained from scanning and the cyan contour from fitting WA contributions together with $\mathcal{C}_7$. The latter displays the exclusion of weak CP-violating phases in $\mathcal{C}_7$ and the

contour is restricted to an almost pure real solution, which approves our qualitative discussion above. The fit with scanned $\rho_A^{K\pi}$ allows for large complex corrections. Even the sign of the imaginary part of $\mathcal{C}_7$ is not dictated by the data ($\delta_7 \leftrightarrow -\delta_7$). This can be understood by the fact that the potential large CP-violating contribution in Equation 6.8 is included in the total error budget of the CP asymmetries through the variation of $\phi_A^{K\pi}$. Because the uncertainties enter the result uncorrelated, it is no problem in this approach to simultaneously explain large CP violation in $\Delta A_{\rm CP}^{K\pi}$, but no CP violation in $C(B^- \to \bar{K}^0\pi^-)$ from the same source. Such a scenario might be indeed realised in nature, but would require to explain, why the strong phase in $\bar{B}^0 \to K^-\pi^+$ and $B^- \to K^-\pi^0$ are equal, but different to the one in $B^- \to \bar{K}^0\pi^-$. Although any weak phase is excluded in the fit, resulting in the cyan contour, we still find a region in parameter space that can explain the observed CP-violating pattern. This effect originates from an enhancement of isospin-breaking, CP-violating terms in the SM. We have seen in Equation 6.8 that $\beta_{3,\rm EW}^c(\pi K)$ can become sizeable compared to the leading decay amplitude $\hat{\alpha}_4^c(\pi K)$. If the fit of $\rho_A^{K\pi}$ prefers regions in parameter space that results in a purely imaginary decay amplitude $\beta_{3,\rm EW}^c(\pi K)$, we obtain a decay-specific correction to $\hat{\phi}_4^c(\pi K)$, which cannot be neglected anymore

$$\hat{\phi}_4^c(M_aM_b) = \begin{cases} \arg\left(\hat{\alpha}_4^c(\pi K) - \frac{1}{2}\beta_{3,\rm EW}^c(\pi K)\right) & \text{for } \bar{B}^0 \to K^-\pi^+, \\ \arg\left(\hat{\alpha}_4^c(\pi K) + \beta_{3,\rm EW}^c(\pi K)\right) & \text{for } B^- \to K^-\pi^0, \end{cases} \tag{6.9}$$

and the approximation in Equation 6.6 must be modified through

$$\text{Im}(r_i) = -r_i^R \sin\,\hat{\phi}_4^c(M_aM_b) + r_i^I \cos\,\hat{\phi}_4^c(M_aM_b). \tag{6.10}$$

It turns out in the fit that the phases $\hat{\phi}_4^c(M_aM_b)$ are typically small and the relative change of $\cos\hat{\phi}_4^c(M_aM_b)$ will be moderate, but enhanced for terms proportional to $\sin\hat{\phi}_4^c(M_aM_b)$. The difference in $\sin\hat{\phi}(K^-\pi^0)$ and $\sin\hat{\phi}^c(K^+\pi^-)$, which enters the determination of $\Delta A_{\rm CP}^{K\pi}$, is of the order of 7%, when limiting WA contributions to the SM fit, and the CP-violating terms from the large colour-allowed tree-level flavour amplitude do not cancel any longer

$$\Delta A_{\rm CP}^{K\pi} \simeq \Delta A_{\rm CP}^{K\pi}(\text{SM}) - 2r_{\rm T}^{\rm R}\left[\sin\hat{\phi}_4^c(K^-\pi^0) - \sin\hat{\phi}_4^c(K^-\pi^+)\right]\sin\gamma. \tag{6.11}$$

At the same time, $C(B^- \to \bar{K}^0\pi^-)$ is not affected from NP in $\mathcal{C}_7$, because it receives no CP-violating contributions in the SM that could be enhanced by the above-described mechanism.

6.1.2 Fit results

We study the scenario of a modified electroweak sector by a model-independent fit of the enhanced Wilson Coefficients $\mathcal{C}_{7,9}^{(\prime)}$. The present section will be used to summarise the final results of our analysis by contour plots of the fit parameters, collections of significant pull values and the modification of the power-suppressed ratios $\xi_3^A(M_1M_2)$. The definitions and statistical treatment of these quantities can be found in Appendix A. The Wilson Coefficients are simultaneously fitted with one WA parameter $\rho_A^{M_1M_2}$ for each decay system, as tabulated in Chapter 4.1.1. In order to obtain reliable constraints on $\mathcal{C}_{7,9}^{(\prime)}$, only those decay systems are suitable for which sufficient experimental information are available. In that sense, we will use observables from $B \to (K\pi,\, K\rho,\, K^*\pi,\, K^*\rho)$ in our fits, for which four branching ratio and four direct CP asymmetry measurements exist. As described in Chapter 4.1, ratios of branching ratios and CP asymmetry differences, which are sensitive to isospin-breaking corrections, can be constructed and are included in the observable set SII, which will be used. Moreover, the decay system $B \to K^*\phi$, though only two decay modes exist, is also considered because two branching ratios, six direct CP asymmetries, four polarisation fractions, and four strong amplitude phases can be utilised. At the moment, it is the only hadronic decay system for which a full angular analysis could be performed by experimenters. In order to study individual constraints, the 68% CR is presented for each decay system separately and their combination at 68% and 95% probability. Measurements on some mixing-induced CP asymmetries $\Delta S(M_1M_2)$ exist, but they are removed from the fit and will be instead predicted in the forthcoming subsection.

We divide the analyses into the following sub-scenarios:

- **single dominant operator scenario**
  $\mathcal{C}_i : \mathcal{C}_i \in \mathbb{C},\ \mathcal{C}_{j\neq i} = 0.$
- **parity-(anti-)symmetric scenario**
  $\mathcal{C}_{77'} :\ \mathcal{C}_7, \mathcal{C}_7' \ \in \mathbb{C},\ \mathcal{C}_9 = \mathcal{C}_9' = 0,$
  $\mathcal{C}_{99'} :\ \mathcal{C}_9, \mathcal{C}_9' \ \in \mathbb{C},\ \mathcal{C}_7 = \mathcal{C}_7' = 0.$
- **(axial-)vector coupling scenario**
  $\mathcal{C}_{79} :\ \mathcal{C}_7, \mathcal{C}_9 \ \in \mathbb{C},\ \mathcal{C}_7' = \mathcal{C}_9' = 0,$
  $\mathcal{C}_{7'9'} :\ \mathcal{C}_7', \mathcal{C}_9' \ \in \mathbb{C},\ \mathcal{C}_7 = \mathcal{C}_9 = 0.$
- **generic modification scenario**
  $\mathcal{C}_{77'99'} : \mathcal{C}_i \in \mathbb{C}.$

The single dominant operator scenario allows only one Wilson Coefficient to be varied simultaneously within a certain range. It will be clearly useful to qualitative discuss which region of parameter space is preferred by the individual Wilson Coefficients and

how well each additional degree-of-freedom can contribute to resolve the tensions in the data. The next two scenarios enhance the number of parameters by two. They probe certain combinations of QED-penguin operators. The (axial-)vector coupling scenario is sensitive to the spin structure of the $\bar{q} \to q$ transition and can be related to the semi-leptonic operators. The parity-(anti-)symmetric scenario probes the spin structure of the flavour-violating $b \to s$ transition. As mentioned in Equation 6.3, depending on the resulting correlation among the Wilson Coefficients in the fits, certain decay systems might be unaffected and constraints from their observables can be easily circumvented. At last, all Wilson Coefficients are kept free and modified simultaneously in the generic modification scenario.

1. Single dominant operator scenario

Significant pull values, which have been encountered in the analysis, are collected in Table 6.1. Figure 6.2 shows the individual 68% CRs for the real and imaginary part of $\mathcal{C}_7^{(\prime)}$ in the upper and $\mathcal{C}_9^{(\prime)}$ in the lower panel from the decay systems $B \to K\pi$ (cyan), $B \to K\rho$ (blue), $B \to K^*\pi$ (green), $B \to K^*\rho$ (purple), and $B \to K^*\phi$ (brown). All observables have then been used to perform a combined fit with 2+10 real degrees-of-freedom, accounting for NP in $\mathcal{C}_i^{(\prime)}$, respectively for WA for the individual decay systems, from which the red contour follows after marginalising over all $\rho_A^{M_1 M_2}$. The plots show the 68% and 95% CRs. The correlation between a single Wilson Coefficient and its χ-flipped counterpart can be studied by inspecting the panels from left to right. It can be seen that the contours from $B \to K\rho$ and $B \to K^*\pi$ are unchanged under the transformation $\mathcal{C}_i \leftrightarrow \mathcal{C}_i'$, whereas those from $B \to K\pi$, $B \to K^*\rho$, and $B \to K^*\phi$ are mirrored. This observation is slightly broken for decays with two vector modes in the final state. The contour regions of $\mathcal{C}_7^{(\prime)}$ from $B \to K\pi$, which give the tightest constraint, is restricted to the real axis of the complex plane. This observation was qualitatively discussed in the previous section. Nevertheless, the contour from $B \to K\pi$ only does not confine the Wilson Coefficient to small, SM-like values and still allows $|\mathcal{C}_7^{(\prime)}| > 5$. The observation that a single decay system cannot refuse solutions of the fit that implies large corrections to the SM is present in almost all scenarios. Once, taking data from all decay systems into account, these solutions become unlikely and the fit contracts to a region near the SM. The pull values at the best-fit point of the $\mathcal{C}_7$, respectively $\mathcal{C}_{7'}$ scenario are for $\delta(R_n^B(K\pi)) = -0.9\sigma\,(-0.9\sigma)$ and for $\delta(\Delta A_{\mathrm{CP}}^{K\pi}) = -1.0\sigma\,(-0.9\sigma)$. They can indeed significantly be improved by the fit, which implies that the mechanism of decay-specific enhancement of SM CP violation sufficiently explains the $\Delta A_{\mathrm{CP}}^{K\pi}$ puzzle. This is achieved without any additional source of CP violation and implies that decay modes with vanishing CP asymmetries in the SM are not affected by this scenario. We will come back to this point in the following subsection. The constraints from $B \to K\rho$, $B \to K^*\pi$ and $B \to K^*\rho$ are, as expected, compatible with the SM and restrict $|\mathcal{C}_7^{(\prime)}| \lesssim 1$.

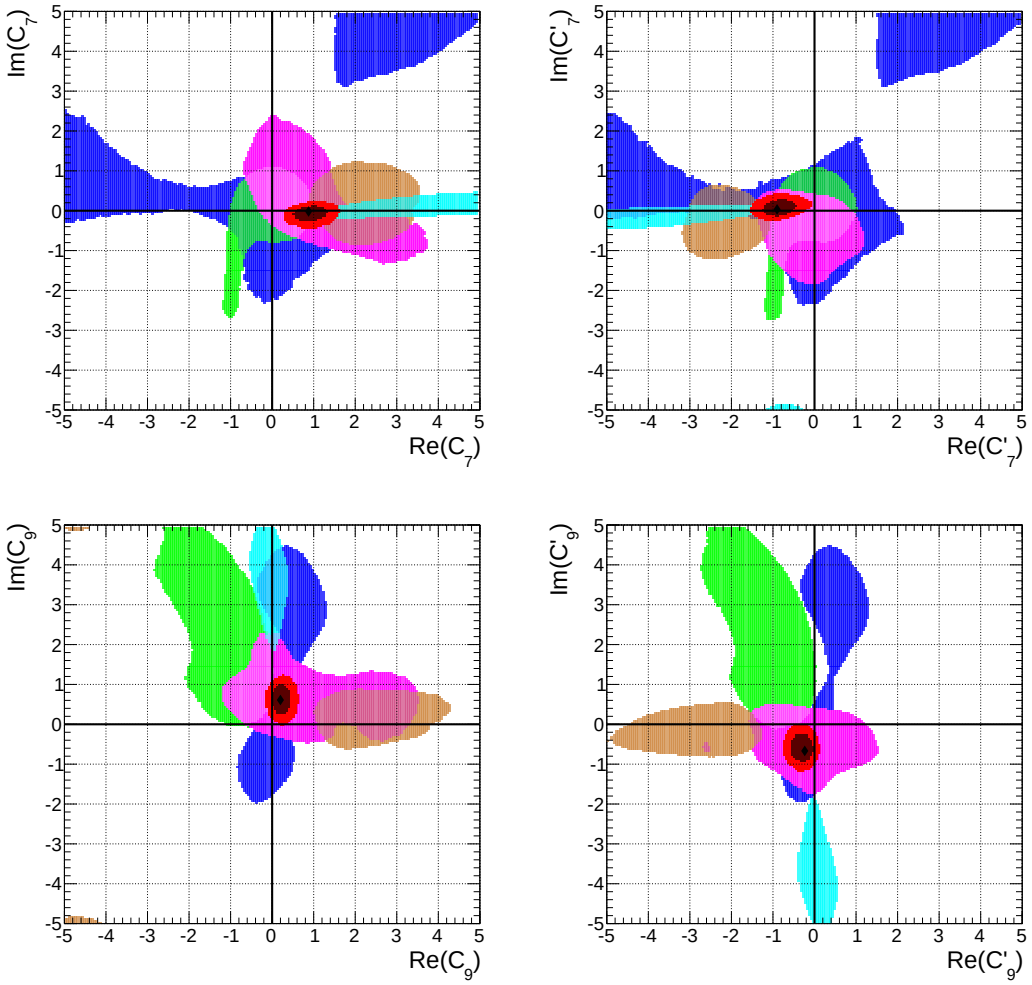

FIGURE 6.2: 68% CR for the complex Wilson Coefficients $\mathcal{C}_{7,9}^{(\prime)}$ in the single dominant operator scenario. Constraints are obtained from the decay systems $B \to K\pi$ (cyan), $B \to K\rho$ (blue), $B \to K^*\pi$ (green), $B \to K^*\rho$ (purple), and $B \to K^*\phi$ (brown). The combined contour (red) is shown for a probability of 68% and 95%. The ♦ corresponds to the best-fit point of the combined fit.

The data for $B \to K^*\phi$ favours, in agreement with $B \to K\pi$, also large, real contributions to $\mathcal{C}_7^{(\prime)}$ and shifts the brown contour away from zero, which increases $\mathcal{B}(\bar{B} \to \bar{K}^{*0}\phi)$ and $\phi_\perp(B^- \to K^{*-}\phi)$. We discussed in Subsection 3.1.3 that additional contributions to χ-flipped operators enhances the positive polarised decay amplitude. This implies that observables which depend on the helicity of the final states are affected differently. Unfortunately, in the case of $\mathcal{C}_{7'}$, we observe that the corrections to the strong amplitude phases tend to decrease $\phi_\perp(B^- \to K^{*-}\phi)$ and increase $\phi_\parallel(B^- \to K^{*-}\phi)$, contrary to the measurements, resulting in a weak preference for the scenario $\mathcal{C}_7$ ($\Delta\chi^2(\text{SM}) = 15\,(13)$).

The situation for the fit of $\mathcal{C}_9^{(\prime)}$ is very different. The contour obtained from $B \to K\pi$ exclusively prefers large imaginary contributions, inevitably implying additional contributions to the CP asymmetries of the other decay systems. In particular, constraints

from $B \to K^*\phi$ and $B \to K^*\rho$ are in conflict with such large contributions, which explains why the pull in $\Delta A_{\rm CP}^{K\pi}$ can be decreased to $= -1.8\sigma\,(-1.9\sigma)$, but not completely resolved. The contour of the combined fit still preferentially lies at the imaginary axis in the complex plane, but shrinks to $|\mathcal{C}_9^{(\prime)}| \sim 1$. Nevertheless, such moderate corrections in $\mathcal{C}_9^{(\prime)}$ are sufficient to significantly improve on $\delta(R_n^B(K\pi)) = -0.3\sigma\,(-0.1\sigma)$. Since the data in $B \to K^*\phi$ also prefers, as in the fit of $\mathcal{C}_7^{(\prime)}$, large real contributions to $\mathcal{C}_9^{(\prime)}$, the combined fit cannot improve the tensions in $\mathcal{B}(\bar{B}^0 \to K^{*0}\phi)$ and $B^- \to \phi_\perp(K^{*-}\phi)$. Compared to the modification of $\mathcal{C}_7^{(\prime)}$, these scenarios are less well suited to improve on the tensions, resulting only into a $\Delta\chi^2(\mathrm{SM}) = 7\,(9)$.

The influence of the fit on the power-suppressed corrections is presented by the power-suppressed ratio $\xi_3^A(M_1M_2)$, which we accumulate for the decay systems $B \to K\pi$, $K\rho$, $K^*\pi$, $K^*\rho$ at the probability of 68% in Table 6.2. The best-fit points for $\rho_A(M_1M_2)$ are also shown. Within all four scenarios, they are compatible with one of the two solutions from the SM fit. The values for the power-suppressed ratio, however, can still differ from the SM value. The ratio for $B \to K\pi$ and $B \to K^*\pi$ can only be slightly decreased, and a minimal amount of $\xi_3^A(K\pi) \sim 0.35$, respectively $\xi_3^A(K^*\pi) \sim 0.74$ is still required to explain the data. Nevertheless, the large WA scenario is still excluded. This is not true for the decays $B \to K\rho$ and $B \to K^*\rho$, in which power-suppressed correction can become even larger as the leading amplitude, but also, compared to the SM value, much smaller, $\xi_3^A(K\rho) \sim 0.27$, respectively $\xi_3^A(K^*\rho) \sim 0.55$.

The results of the single dominant operator scenario can be summarised by the following two statements:

- The modification of the Wilson Coefficients $\mathcal{C}_7^{(\prime)}$ and $\mathcal{C}_9^{(\prime)}$ can significantly improve on the observed tension in the SM, whereas the scenarios $\mathcal{C}_{7^{(\prime)}}$ are preferred. At the moment, the data does neither prefer the modification of $\mathcal{C}_{7,9}$ nor of their χ-flipped counterparts, $\mathcal{C}'_{7,9}$. Both fits yield similar results with a parity-anti-symmetric configuration, caused by the dominance of the precise data in $B \to K\pi$. In order to break this symmetry, more accurate measurements on decay systems with one pseudo-scalar and one vector meson in the final state are needed.

- The additional corrections to the Wilson Coefficients are already confined to the size of the SM contribution $|\mathcal{C}_i| \sim 1$. $\mathcal{C}_9^{(\prime)}$ is found to be almost imaginary and $\mathcal{C}_7^{(\prime)}$ real.

One of the main motivation for introducing additional contributions to the QED-penguin operators was to explain the long-standing discrepancy of $\Delta A_{\rm CP}^{K\pi}$. We have shown that, in fact, all Wilson Coefficients can be sufficiently enlarged to decrease the tension without spoiling data from other decay systems. However, we also proposed a solution of the tension within the SM, assigned to an enhanced power correction of the HS contribution in Chapter 5.1.4. An unavoidable consequence of this scenario was an

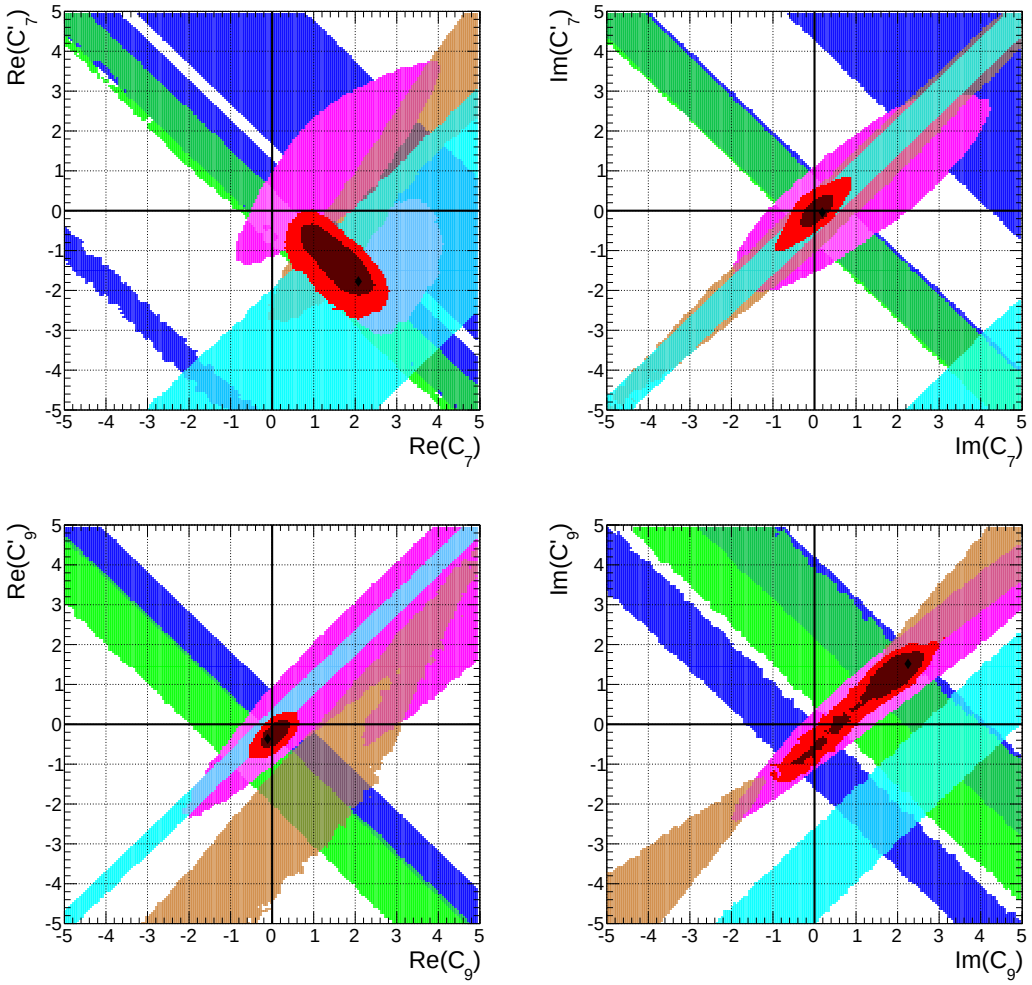

FIGURE 6.3: 68% CR for the complex Wilson Coefficients $\mathcal{C}_{7,9}^{(\prime)}$ in the scenarios $\mathcal{C}_{77'}$ (upper) and $\mathcal{C}_{99'}$ (lower). Constraints are obtained from the decay systems $B \to K\pi$ (cyan), $B \to K\rho$ (blue), $B \to K^*\pi$ (green), $B \to K^*\rho$ (purple), and $B \to K^*\phi$ (brown). The combined contour (red) is shown for 68% and 95% CRs. The ♦ corresponds to the best-fit point of the combined fit.

enhanced CP asymmetry in $C(\bar{B}^0 \to \bar{K}^0\pi^0) = 0.14^{+0.06}_{-0.05}$. Fortunately, an enhancement of $\mathrm{Re}\,\mathcal{C}_7^{(\prime)}$ does not change its SM prediction and both scenarios can be clearly distinguished. This CP asymmetry, however, receives contributions from the $\mathcal{C}_{9^{(\prime)}}$ scenarios and is given at the best-fit points to be $C(\bar{B}^0 \to \bar{K}^0\pi^0) = 0.03^{+0.04}_{-0.04}$. The prediction only overlaps with the one from the enhanced HS scenario within a probability of 95% and the additional information from $\bar{B}_s \to K^0\pi^0$ might be needed to distinguish between the two possibilities if we neglect NP in $b \to d$ transitions, or at least assume different contribution than for $b \to s$.

2. Parity-(anti-)symmetric scenario

Figure 6.3 shows the contour regions for the two scenarios $\mathcal{C}_{77'}$ (upper panel) and $\mathcal{C}_{99'}$

(lower panel), whereas we confine to show the correlations among the real (left) and imaginary (right) parts of the fitted Wilson Coefficients. The colour coding is the same as for the previous scenarios above and significant pull values are again collected in Table 6.1. All plots nicely reveal the orthogonality between constraints from $B \to K\rho\,(K^*\pi)$ and $B \to K\pi\,(K^*\rho,\, K^*\phi)$. Even the breaking of parity symmetry, $\bar{C}_i = const.$, in VV final state systems can be observed in the plots. The parity symmetry implies that all observables for PV and VP modes are equal at all parameter points along the line $\Delta\mathcal{C} = const.$ (line with gradient 1) and for PP and VV modes at parameter points along the line $\bar{\mathcal{C}} = const.$ (line with gradient -1).

The contour regions from $B \to K^*\pi$ is in the scenario $\mathcal{C}_{77'}$ tightly restricted to a line crossing the SM point in both the real as well as in the imaginary plane. The same is true for $B \to K\pi$ in the imaginary plane and the combined fit results into a SM-like solution. Also the contour from $B \to K^*\phi$ already delivers almost equally well constraints on $\mathrm{Im}\,\mathcal{C}_7 - \mathrm{Im}\,\mathcal{C}_7'$ as $B \to K\pi$, consistent with vanishing weak phases. However, an offset from zero in the real plane, as we already encountered in the $\mathcal{C}_7$ and $\mathcal{C}_{7'}$ scenarios, is also present here and because $\Delta\mathcal{C} = 0$ does not affect observables of $B \to K^*\pi$, $(K\rho)$, the fit allows for rather large contributions of $|\mathrm{Re}\,\mathcal{C}_{7(\prime)}| \sim 2$. All tensions, apart from an arising discrepancy in $R_n^B(K^*\rho)$ of 1.6σ, can be resolved and compared to all other scenarios with the same amount of degrees-of-freedom, $\mathcal{C}_{77'}$ is the most-likely and bares the largest $\Delta\chi^2(\mathrm{SM})$ of 20.

The fit for $\mathcal{C}_{99'}$ shows a similar dilemma as observed in the single dominant operator analysis. The contour of $B \to K\pi$ strictly lies on a SM compatible line and does not allow for large contributions to the real part of $\Delta\mathcal{C}_9$, but the data of $B \to K^*\phi$ prefers an offset of at least $\mathrm{Re}\,\Delta\mathcal{C}_9 \sim 1$. However, the combined plot is dictated by $B \to K\pi$ and results into a region near the SM point. The situation for the imaginary plane is turned upside down. Data from $B \to K^*\phi$ and $B \to K^*\rho$ lies on a SM compatible line, whereas $B \to K\pi$ needs an offset from SM of at least $\mathrm{Im}\,\Delta\mathcal{C}_9 \sim 3$. The constraints from CP asymmetries of the former decays dictate the combined plot and $\Delta A_{\mathrm{CP}}^{K\pi}$ can only be relaxed to a pull value of -1.2σ. The orthogonal contour from $B \to K^*\pi$, as already found in the single dominant operator scenarios, also prefers an offset for the imaginary part of $\bar{\mathcal{C}}_9$, such that the SM is excluded from the 68% CR. Though, a solution to the $\Delta A_{\mathrm{CP}}^{K\pi}$ puzzle is already quite limited, the tension for the ratio of branching ratios $R_n^B(K\pi)$ can be resolved and the fit can be improved compared to the SM by $\Delta\chi^2(\mathrm{SM}) = 12$.

Both scenarios allow for large contributions to the modification of the Wilson Coefficients, which implies visible effects for the power-suppressed ratio ξ_3^A, listed in Table 6.2. The ratio for $B \to K\pi$ and $B \to K^*\pi$ can be decreased by a factor of 2–3 compared to the SM value, such that for example a relative amount of power corrections $\xi_3^A(K\pi) = 0.13$ for the scenario $\mathcal{C}_{77'}$ can already be sufficient to explain the data

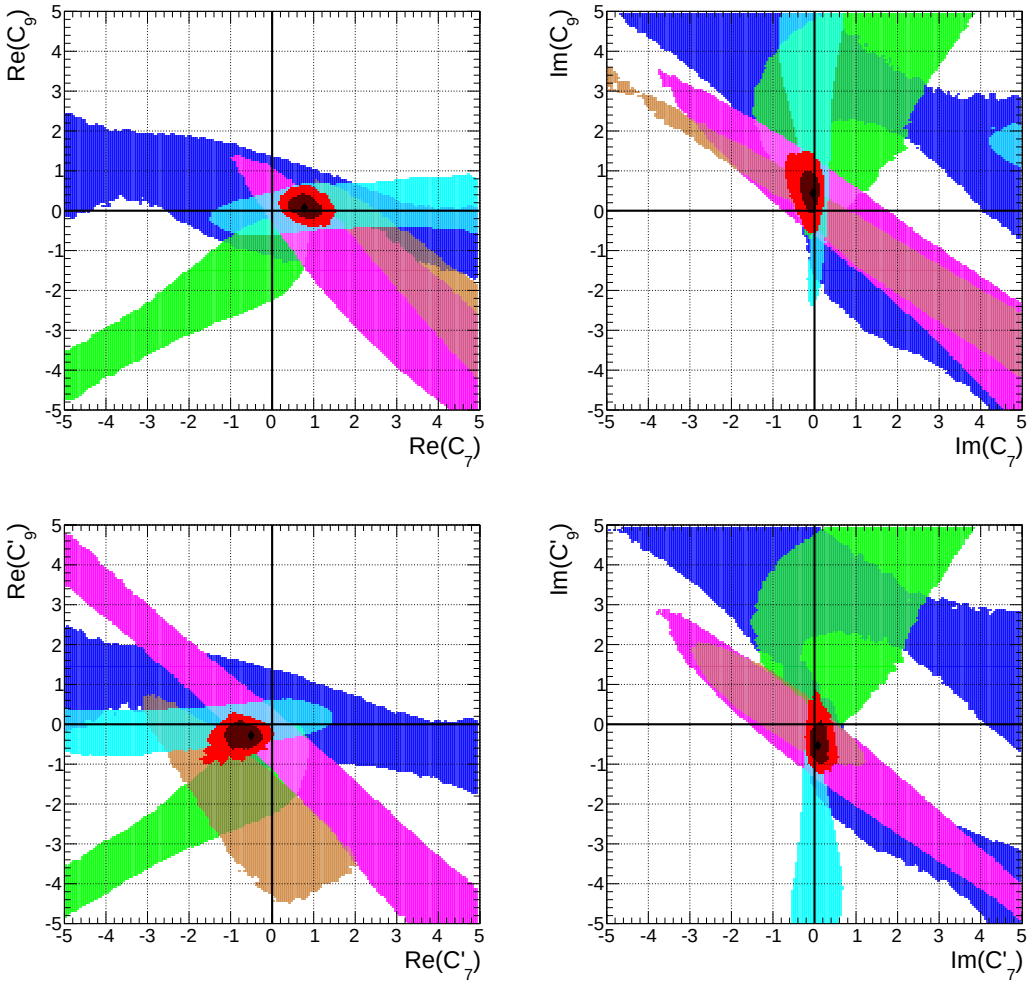

FIGURE 6.4: 68% CR for the complex Wilson Coefficients $\mathcal{C}_{7,9}^{(\prime)}$ in the scenarios $\mathcal{C}_{79}$ (upper) and $\mathcal{C}_{7'9'}$ (lower). Constraints are obtained from the decay systems $B \to K\pi$ (cyan), $B \to K\rho$ (blue), $B \to K^*\pi$ (green), $B \to K^*\rho$ (purple), and $B \to K^*\phi$ (brown). The combined contour (red) is shown for a probability of 68% and 95%. The ⧫ corresponds to the best-fit point of the combined fit.

in $B \to K\pi$. For $B \to K\rho$ and $B \to K^*\rho$ there might be even no contribution from power correction needed at all, but, the additional freedom also allows for the large WA scenario in each decay system.

3. The (axial-)vector coupling scenario

The results of the fit for the (axial-)vector coupling scenario are displayed in Figure 6.4 and significant pull values are again collected in Table 6.1. The combined contour regions for $\mathcal{C}_{79}$ (upper panels) are almost mirrored at the SM axis for the χ-flipped $\mathcal{C}_{7'9'}$ scenario (lower panels), which demonstrates the statistical dominance of the data in $B \to K\pi$. We find for the real part of the Wilson Coefficients $|\mathrm{Re}\,\mathcal{C}_7^{(\prime)}| \sim 1$, whereas $|\mathrm{Re}\,\mathcal{C}_9^{(\prime)}| \sim 0$, and vice versa for the imaginary contribution, $|\mathrm{Im}\,\mathcal{C}_7^{(\prime)}| \sim 0$, whereas $|\mathrm{Im}\,\mathcal{C}_9^{(\prime)}| \sim 1$. Although the number of fitted Wilson Coefficients increased by one, the solutions of the

$B \to M_1M_2$					[84]	[84]				
	$\mathrm{Re}\,\mathcal{C}_i^{(\prime)}$, $\mathrm{Im}\,\mathcal{C}_i^{(\prime)}$	$\Delta A_{\mathrm{CP}}^{K\pi}$	$R_n^B(K\pi)$	$C_L(K^{*-}\phi)$	$C(\bar{K}^{*0}\phi)$	$\mathcal{B}(\bar{K}^{*0}\phi)$	$\phi_\perp(K^{*-}\phi)$	$R_n^B(K^*\pi)$	$R_n^B(K^*\rho)$	$\Delta\chi^2$(SM)
SM		$\mathbf{-2.8}\sigma$	$\mathbf{-1.9}\sigma$	-1.5σ	0.3σ	1.7σ	1.4σ	0.6σ	0.6σ	
$\mathcal{C}_7$	0.88, −0.02	-0.9σ	-0.9σ	$\mathbf{-1.6}\sigma$	0.2σ	0.8σ	0.3σ	0.0σ	1.0σ	15
$\mathcal{C}_7'$	−0.90, 0.03	-1.0σ	-0.9σ	-1.5σ	0.2σ	1.2σ	1.2σ	0.1σ	0.8σ	13
$\mathcal{C}_9$	0.20, 0.61	$\mathbf{-1.8}\sigma$	-0.3σ	-0.7σ	1.4σ	$\mathbf{1.8}\sigma$	1.4σ	1.0σ	0.7σ	7
$\mathcal{C}_9'$	−0.24, −0.67	$\mathbf{-1.7}\sigma$	-0.1σ	-0.7σ	$\mathbf{1.6}\sigma$	$\mathbf{1.8}\sigma$	1.4σ	0.3σ	0.6σ	9
$\mathcal{C}_{77'}$	2.06, 0.20 −1.77, −0.05	0.0σ	0.0σ	-1.3σ	0.4σ	0.0σ	0.0σ	0.2σ	$\mathbf{1.6}\sigma$	20
$\mathcal{C}_{99'}$	−0.12, 2.22 −0.35, 1.53	-1.2σ	-0.1σ	-0.3σ	0.9σ	$\mathbf{1.8}\sigma$	1.4σ	$\mathbf{1.6}\sigma$	0.7σ	12
$\mathcal{C}_{79}$	0.78, −0.04 0.07, 0.44	-0.5σ	-0.4σ	-1.0σ	1.1σ	0.9σ	0.7σ	0.3σ	0.9σ	17
$\mathcal{C}_{7'9'}$	−0.51, 0.08 −0.28, −0.53	-0.4σ	0.0σ	-1.0σ	1.2σ	1.3σ	1.1σ	0.8σ	0.8σ	15
$\mathcal{C}_{77'99'}$	1.70, 0.25 −0.97, 0.09 0.33, 1.66 −0.62, 1.61	-0.1σ	0.0σ	-1.1σ	0.0σ	0.0σ	0.0σ	0.7σ	$\mathbf{1.6}\sigma$	25

TABLE 6.1: Compilation of best-fit points and pull values with $|\delta| \geq 1.6$ and for $\phi_\perp(K^{*+}\phi)$ for the model-independent fits of QED-penguin operators.

combined plots can be restricted to likewise small corrections as in the single dominant operator analysis. This can be understood since the additional degrees-of-freedom cannot be utilised to avoid constraints of a certain group of decay systems as it was the case in the parity-(anti-)symmetric scenario. The individual benefits of the $\mathcal{C}_{7(\prime)}$ and $\mathcal{C}_{9(\prime)}$ scenarios then combines into a significant improvement of the tensions. The pull values for $\Delta A_{\mathrm{CP}}^{K\pi}$ decreases to $-0.5\sigma\,(-0.4\sigma)$ and for $R_n^B(K\pi)$ to $-0.1\sigma\,(-0.4\sigma)$. The tensions in $\mathcal{B}(\bar{B}^0 \to K^{*0}\phi)$ can be relaxed to $0.9\sigma\,(1.3\sigma)$ and for $\phi_\perp(B^- \to K^{*-}\phi)$ to $0.7\sigma\,(1.1\sigma)$, resulting altogether into $\Delta\chi^2(\mathrm{SM}) = 17\,(15)$.

The observed pattern of purely real $\mathcal{C}_7^{(\prime)}$ and purely imaginary $\mathcal{C}_9^{(\prime)}$ does not favour a specific linear combination which could be related to the semi-leptonic operators. These would imply contour regions near a line in the real and imaginary plane with gradient 1, respectively -1, which are not the favoured regions in the plots.

The necessary amount of power corrections can be decreased in both scenarios. In particular, $\xi_3^A(K\pi) = 0.22$ for $\mathcal{C}_{79}$ and $\xi_3^A(K\pi) = 0.29$ for $\mathcal{C}_{7'9'}$ and the large WA scenario is unlikely, which is not true for the residual decay systems. The largest impact on $\xi_3^A(M_1M_2)$ can be observed in the decay $B \to K\rho$ for the scenario $\mathcal{C}_{79}$, for which maybe no contributions from WA are needed at all.

4. Generic modification scenario

In the last scenario, we allow all four Wilson Coefficients to be modified simultaneously. The pull values and the best-fit point are listed in Table 6.1. It turns out that this scenario shares the feature of a combination of the two $\mathcal{C}_{77'}$ and $\mathcal{C}_{99'}$ scenarios. The

	$K\pi$		$K^*\pi$		$K\rho$		$K^*\rho$	
	$\lvert\rho_A\rvert,\ \phi_A$	ξ_3^A	$\lvert\rho_A\rvert,\ \phi_A$	ξ_3^A	$\lvert\rho_A\rvert,\ \phi_A$	ξ_3^A	$\lvert\rho_A\rvert,\ \phi_A$	ξ_3^A
SM	3.34, 2.71	0.39	1.61, 5.84	0.89	2.69, 2.68	0.78	1.56, 5.66	1.33
$\mathcal{C}_7$	3.61, 2.68	[0.34, 0.62]	1.79, 5.89	[0.89, 1.47]	1.79, 5.55	[0.39, 1.76]	2.23, 2.77	[0.68, 1.75]
$\mathcal{C}_{7'}$	3.62, 2.67	[0.35, 0.66]	3.77, 1.84	[0.74, 2.78]	3.11, 2.63	[0.73, 1.47]	2.15, 2.76	[0.55, 1.63]
$\mathcal{C}_9$	2.42, 5.39	[0.35, 0.73]	1.66, 5.85	[0.82, 1.53]	1.70, 5.38	[0.27, 1.63]	1.54, 5.63	[0.55, 2.08]
$\mathcal{C}_{9'}$	2.43, 5.39	[0.36, 0.71]	1.63, 5.88	[0.76, 1.40]	1.23, 5.59	[0.33, 1.53]	1.55, 5.63	[0.56, 1.92]
$\mathcal{C}_{77'}$	2.03, 5.72	[0.13, 2.24]	1.70, 5.87	[0.38, 2.93]	1.51, 5.44	[0.00, 3.23]	1.75, 6.00	[0.10, 2.50]
$\mathcal{C}_{99'}$	3.77, 2.63	[0.19, 0.80]	3.34, 2.99	[0.52, 3.33]	1.44, 0.03	[0.02, 3.09]	1.52, 5.63	[0.02, 3.93]
$\mathcal{C}_{79}$	2.25, 5.43	[0.22, 0.75]	3.07, 2.92	[0.84, 1.76]	2.41, 2.89	[0.06, 2.61]	1.51, 5.64	[0.46, 2.11]
$\mathcal{C}_{7'9'}$	2.23, 5.43	[0.29, 0.69]	1.55, 5.87	[0.64, 2.93]	1.92, 5.52	[0.24, 1.67]	2.29, 2.73	[0.34, 2.30]
$\mathcal{C}_{77'99'}$	2.26, 5.57	[0.06, 1.31]	1.65, 6.07	[0.06, 4.21]	1.45, 0.02	[0.00, 4.73]	1.81, 5.90	[0.01, 2.86]

TABLE 6.2: Compilation of best-fit points for $\rho_A^{M_1M_2}$ and ξ_3^A at the probability of 68%. The various results are given for $B \to K\pi$, $K\rho$, $K^*\pi$, $K^*\rho$ and specified for the modified QED-penguin operator scenarios. As explained in Appendix A.5, the interval of ξ_3^A(NP) should be compared to ξ_3^A(SM) at the best-fit point of $\rho_A^{M_1M_2}$, listed in the first row.

best-fit point of the parameters $\mathrm{Re}\,\mathcal{C}_7 - \mathrm{Re}\,\mathcal{C}_7'$ prefer a parity-anti-symmetric solution with rather large contributions of $|\mathrm{Re}\ \mathcal{C}_7^{(\prime)}| \sim 1 - -1.7$, whereas the imaginary parts of $\mathrm{Im}\,\mathcal{C}_9 - \mathrm{Im}\,\mathcal{C}_9'$ favours a parity-symmetric solution with similar large contributions to $|\mathrm{Im}\,\mathcal{C}_9^{(\prime)}| \sim 1.6$. The latter implies $\mathrm{Im}\,\Delta\mathcal{C}_9 \sim 0$ and $\mathrm{Im}\,\bar{\mathcal{C}}_9 \sim 3.2$, leaving the observables in $B \to K\pi\,(K^*\rho,\, K^*\phi)$ almost unaffected and satisfying the required offset from $B \to K^*\pi$ data, which we have seen in the lower right panel of Figure 6.3.

Inspecting the pull values in Table 6.1, it is evident that if we allow for arbitrary additional contributions to all colour-singlet QED-penguin operators, the fit supports a complete solution of all encountered tensions in the SM. However, because these contributions can become very large, some predictions that were consistent with the measurement in the SM, become problematic in the fit. As for the $\mathcal{C}_{77'}$ scenario, the pull value of, e.g, $R_n^B(K^*\rho)$, increases to 1.6σ. It is not surprising that the additional freedom in the fit manifests in a huge range for the power-suppressed ratio ξ_3^A (see Table 6.2). All data for each decay systems can be explained both with and without large contributions from WA. However, the best-fit points for $\rho_A^{M_1M_2}$ are still in agreement with one of the two regions that have been found in the SM fit, except for the decay $B \to K\rho$. The absolute value decreases to $|\rho_A^{K\rho}| = 1.45$ and the strong phases vanishes, $\phi_A^{K\rho} = 0.02$.

After the discussion of the individual scenarios, let us summaries the main results of our analysis, which have been obtained so far:

- All introduced scenarios can explain the tensions in $\Delta A_{\mathrm{CP}}^{K\pi}$ and $R_n^B(K\pi)$, whereat contributions beyond the SM to $\mathcal{C}_7^{(\prime)}$ are, in view of current data, more likely as to $\mathcal{C}_9^{(\prime)}$. We find that $\mathcal{C}_7^{(\prime)}$ has to be almost purely real and $\mathcal{C}_9^{(\prime)}$ imaginary. A very

interesting observation is that $\Delta A_{\rm CP}^{K\pi}$ can be explained without any new source of CP violation in $\mathcal{C}_7^{(\prime)}$. Such contributions will be challenging to detect in future measurements, leaving many promising CP asymmetries to find NP unaffected.

- The statistical dominance of data from $B \to K\pi$ forces those scenarios in which both primed and unprimed Wilson Coefficients are fitted into a parity-anti-symmetric configuration. This qualitative results have also been found for model-independent fits of (semi-)leptonic data (see discussion in Chapter 4.2.2). Unfortunately, such a pattern is not observed for the specific linear combination of hadronic operators that relates to the semi-leptonic operators. Since this combination has explicitly been kept free in the scenarios $\mathcal{C}_{79}$ and $\mathcal{C}_{7'9'}$, it would be interesting to impose it through a different choice of the operator basis

$$\big((\bar{s}\,b)_{V\pm A}(\bar{q}\,q)_{V+A},\,(\bar{s}\,b)_{V\pm A}(\bar{q}\,q)_{V-A}\big) \to \big((\bar{s}\,b)_{V\pm A}(\bar{q}\,q)_{V},\,(\bar{s}\,b)_{V\pm A}(\bar{q}\,q)_{A}\big)$$

  in a subsequent study.

- In order to reject or to find further evidence for the parity-anti-symmetric pattern, improved measurements on decay modes with VV final states are needed. Concerning the single dominant operator scenarios, no preference can be assigned to either the left-handed or right-handed operators. This could be tested through improved measurements of $B \to PV\,(VP)$ decay modes.

- Our approach of fitting WA simultaneously with NP contributions lead to qualitative different results as for conventional QCDF.

At last, we like to quote the allowed ranges of the NP fit parameters. Since the actual bounds on the individual Wilson Coefficients indeed vary within certain scenarios, we quote the results of both the single dominant operator scenarios and of the parity-(anti-)symmetric scenarios (curly brackets). The former already leads to rather restricted constraints, whereas the additional degrees-of-freedom in the latter can be utilised to allow for significantly larger corrections. The bounds are obtained from the respective 1-dimensional posterior probability

$$\begin{aligned}
&\mathrm{Re}\,\mathcal{C}_7 \in [\ \ 0.40;\ \ 1.50]\,,\ \{\,[-1.45;\ \ 2.70]\,\},\quad \mathrm{Im}\,\mathcal{C}_7 \in [-0.35;\ \ 0.20]\,,\ \{\,[-0.85;\ 0.65]\,\},\\
&\mathrm{Re}\,\mathcal{C}_7' \in [-1.40;\ -0.25]\,,\ \{\,[-2.45;\ -0.20]\,\},\quad \mathrm{Im}\,\mathcal{C}_7' \in [-0.15;\ \ 0.35]\,,\ \{\,[-0.95;\ 0.65]\,\},\\
&\mathrm{Re}\,\mathcal{C}_9 \in [-0.05;\ \ 0.35]\,,\ \{\,[-0.40;\ \ 0.55]\,\},\quad \mathrm{Im}\,\mathcal{C}_9 \in [\ \ 0.10;\ \ 1.10]\,,\ \{\,[-0.95;\ 2.65]\,\},\\
&\mathrm{Re}\,\mathcal{C}_9' \in [-0.65;\ \ 0.05]\,,\ \{\,[-0.75;\ \ 0.20]\,\},\quad \mathrm{Im}\,\mathcal{C}_9' \in [-1.05;\ -0.10]\,,\ \{\,[-1.05;\ 1.95]\,\}.
\end{aligned}$$

6.1.3 Observable predictions

We will use the last section to work out measurable consequences of a modified electroweak sector. We confine to the single dominant operator scenarios in order to study

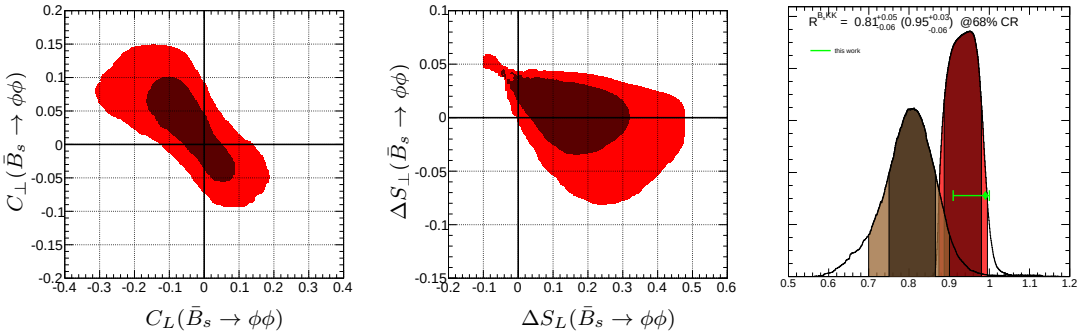

FIGURE 6.5: Correlations among the predictions for C_L vs. $C_\perp$ (left) and ΔS_L vs. $\Delta S_\perp$ (middle) in $\bar{B}_s \to \phi\phi$ for the scenario $\mathcal{C}_9$. The right panel shows the predictions for $R^{B_s KK}$ for the scenarios $\mathcal{C}_7$ (brown) and $\mathcal{C}_9$ (red), and the prediction from a SM fit is indicated by the green line at a probability of 68%. All residual predictions are given at a probability of 68% and 95%.

the sensitivity of particular observables to each Wilson Coefficients separately. The main task will be to find observables, respectively pattern of observables, that could help us to distinguish the individual scenarios.

The scenarios $\mathcal{C}_{7^{(\prime)}}$ and $\mathcal{C}_{9^{(\prime)}}$ are easily disentangled from each other. $\mathcal{C}_{7^{(\prime)}}$ is restricted to be real and does not introduce any new CP-violating phase. This implies that all vanishing CP asymmetries in the SM are not modified, contrary to the $\mathcal{C}_{9^{(\prime)}}$ scenarios. These considerations imply that $\mathcal{C}_{7^{(\prime)}}$ scenarios cannot be verified through these kind of CP asymmetries, but at least be refute if a non-vanishing CP asymmetry is measured. Suitable candidates are the direct and mixing-induced CP asymmetries in for instance $\bar{B}_s \to \phi_{L(\perp)}\,\phi_{L(\perp)}$, which will be probed by the LHCb experiment (see [90]). Their correlations for the $\mathcal{C}_9$ scenario are shown on the left and middle panel of Figure 6.5. The plots show that, although, $\mathcal{C}_9$ has been tightly constrained, it is in fact still possible to observe large effects in those observables. The corresponding predictions in the SM and for the $\mathcal{C}_{7^{(\prime)}}$ scenarios are approximately 0 and explicitly given in Appendix B.

More sensitive to the effects of an enhanced $\mathcal{C}_7^{(\prime)}$ are ratios of branching ratios, which have been used in the fit for the decay systems $B \to K\pi$, $K\rho$, $K^*\pi$, $K^*\rho$. However, we can also construct a corresponding ratio from the neutral and charged mode in $B_s \to KK$

$$R^{B_s KK} \equiv \frac{\mathcal{B}(\bar{B}_s \to K^+K^-)}{\mathcal{B}(\bar{B}_s \to \bar{K}^0K^0)} \simeq 1 - 2\mathrm{Re}\, r_\mathrm{T}\, \cos\gamma + 2\mathrm{Re}\, r_{\mathrm{EW^C}}, \tag{6.12}$$

with similar isospin-breaking corrections r_i as for the decay system $B \to K\pi$[2]. The branching ratio of $\bar{B}_s \to K^+K^-$ has already been measured quite accurately by the LHCb and CDF collaboration [148, 149] with a relative uncertainty of 7%. It was used

[2]The definitions for the flavour amplitude ratios are equivalent to those in Equation 4.14 with the replacements $(A_{\pi K}, A_{K\pi}) \to A_{KK}$ and $(\alpha((K\pi)), \beta(K\pi)) \to (\alpha((KK)), \beta(KK))$

$B \to M_1 M_2$	$\Delta S(K\pi)$	$\Delta S(K\rho)$	$\Delta S(K^*\pi)$	$\Delta S_L(K^*\rho)$	$\Delta S(K\eta')$	$\Delta S(K\omega)$	$\Delta S(K\phi)$	$\Delta S_L(K^*\phi)$	$\mathcal{B}(\phi\pi)$	$\mathcal{B}(\phi\rho)$
SM	[0.05, 0.13]	[−0.19, −0.04]	[0.06, 0.17]	[−0.15, 0.09]	[−0.01, 0.04]	[0.09, 0.17]	[0.01, 0.05]	[0.01, 0.04]	$0.24^{+0.07}_{-0.04}$	$0.68^{+0.19}_{-0.10}$
$\mathcal{C}_7$	$0.13^{+0.02}_{-0.12}$	$-0.16^{+0.10}_{-0.09}$	$0.09^{+0.09}_{-0.09}$	$0.08^{+0.06}_{-0.13}$	$0.05^{+0.03}_{-0.10}$	$0.15^{+0.04}_{-0.10}$	$0.05^{+0.04}_{-0.08}$	$0.04^{+0.05}_{-0.08}$	$0.78^{+0.26}_{-0.20}$	$0.33^{+0.11}_{-0.11}$
$\mathcal{C}'_7$	$0.12^{+0.02}_{-0.12}$	$-0.10^{+0.09}_{-0.10}$	$0.15^{+0.04}_{-0.12}$	$0.08^{+0.10}_{-0.15}$	$0.05^{+0.03}_{-0.11}$	$0.10^{+0.08}_{-0.09}$	$-0.02^{+0.09}_{-0.05}$	$0.04^{+0.06}_{-0.07}$	$0.06^{+0.04}_{-0.04}$	$0.26^{+0.09}_{-0.08}$
$\mathcal{C}_9$	$0.01^{+0.06}_{-0.08}$	$0.06^{+0.07}_{-0.09}$	$-0.04^{+0.08}_{-0.09}$	$-0.14^{+0.16}_{-0.16}$	$0.00^{+0.05}_{-0.05}$	$0.06^{+0.11}_{-0.08}$	$-0.06^{+0.10}_{-0.12}$	$-0.11^{+0.09}_{-0.12}$	$0.13^{+0.10}_{-0.05}$	$0.46^{+0.20}_{-0.13}$
$\mathcal{C}'_9$	$0.01^{+0.06}_{-0.08}$	$-0.31^{+0.09}_{-0.13}$	$0.21^{+0.04}_{-0.05}$	$-0.15^{+0.17}_{-0.17}$	$-0.01^{+0.06}_{-0.06}$	$0.18^{+0.03}_{-0.08}$	$0.06^{+0.08}_{-0.07}$	$-0.10^{+0.13}_{-0.12}$	$0.50^{+0.12}_{-0.05}$	$0.40^{+0.23}_{-0.12}$

TABLE 6.3: Predictions for the mixing-induced CP asymmetry of diverse B_d decays and for the purely isospin-breaking branching ratios $\mathcal{B}(\bar{B}_s \to \phi\pi,\, \phi\rho)$ within the single dominant operator scenarios and the SM.

in the fit to constrain ρ_A^{KK}, from which the prediction of $R^{B_s KK}$ was obtained, shown on the right panel of Figure 6.5. Both $\mathcal{C}_{9^{(\prime)}}$ and $\mathcal{C}_{7^{(\prime)}}$ predict a suppression of the ratio compared to the SM, whereas the effect is more significant for the latter.

Furthermore, we would also like to disentangle between contributions to $\mathcal{C}_{7,9}$ and to $\mathcal{C}'_{7,9}$. The fits are dominated by parity-anti-symmetric solutions. Hence, the observables $\hat{\mathcal{O}}$ for PV and VP final states are remarkably helpful and will follow the general pattern

$$\begin{aligned} \delta\hat{\mathcal{O}}(\mathcal{C}_i) &\simeq -\delta\hat{\mathcal{O}}(\mathcal{C}'_i) \qquad \text{for } VP, PV, \\ \delta\hat{\mathcal{O}}(\mathcal{C}_i) &\simeq \quad \delta\hat{\mathcal{O}}(\mathcal{C}'_i) \qquad \text{for } PP, VV, \end{aligned} \tag{6.13}$$

with $\delta\hat{\mathcal{O}}(\mathcal{C}_i) \equiv \hat{\mathcal{O}}^{(\mathrm{SM})} - \hat{\mathcal{O}}(\mathcal{C}_i)$.

We listed the predictions for certain mixing-induced CP asymmetries, ΔS_f and the branching ratios of the two purely isospin-violating decays $B_s \to \phi\pi,\, \phi\rho$ in Table 6.3. The fact that these branching ratios are sensitive to the modification of QED-penguin operators were already worked out in [74], in which QCDF with conventional treatment of WA contributions was used. However, as discussed in the introductory part of this section, this approach does not favour any particular region in the parameter space of the modified Wilson Coefficients, and only a relative enhancement/suppression can be observed. If our approach is reasonable, we can identify a particular pattern for the branching ratios among the corresponding scenarios and quote concrete predictions. We can summarise the main findings by the following statements:

- The impact from the scenarios $\mathcal{C}_{7^{(\prime)}}$ on the mixing-induced CP asymmetries ΔS_f are unfortunately inconclusive. The additional contributions could potentially become distinguishable from the SM background, but depend strongly on the underlying $\rho_A^{M_1 M_2}$ fit and are, within uncertainties, compatible with the SM predictions.

- The most significant effect on the mixing-induced CP asymmetries for the scenarios $\mathcal{C}_{9^{(\prime)}}$ is found for $\Delta S(B \to K\rho)$. In view of current data, $\Delta S(K\rho) = -0.15^{+0.18}_{-0.21}$ (HFAG) slightly prefers the primed scenario.

- The purely isospin-violating branching ratios obey significant contributions from all scenarios. The modification of $\mathcal{C}_{7^{(\prime)}}$ leads to a suppression for $\mathcal{B}(B_s \to \phi\rho)$ by a factor of two, and $\mathcal{B}(B_s \to \phi\pi)$ is suppressed for the primed and enhanced for the unprimed scenario by a factor of 3–4. $\mathcal{C}_{9^{(\prime)}}$ also predicts a suppression, albeit less significant, for $\mathcal{B}(\bar{B}_s \to \phi\rho)$ and the pattern for $\mathcal{B}(\bar{B}_s \to \phi\pi)$ is reversed compared to $\mathcal{C}_{7^{(\prime)}}$. Unfortunately, since most scenarios reveal a suppression of the branching ratios, it will be even more challenging to observe these very rare decays.

6.2 Enhanced Standard Model Z-penguin coupling Z^{sb}

We devoted the first analysis of potential contributions from physics beyond the SM to a generic, model-independent fit of the Wilson Coefficients in the electroweak sector. These effective couplings exclusively describe the physics of hadronic decays and no further relations among observables of, for instance (semi-)leptonic decays, must be considered. However, it is likely that a particular NP model relates these two systems, being triggered by the same flavour-violating quark transition $b \to s$. Such correlations are already present in the SM because leptons and quarks are given in the same representation of the SM gauge group $\mathrm{SU(2)_I} \times \mathrm{U(1)_Y}$ and hadronic and (semi-)leptonic decays receive a common contribution from for example Z-penguin diagrams. Instead of fitting the individual Wilson Coefficients in each system, we will now probe a potential enhancement of the Z-boson coupling, Z^{sb}, to the flavour-violating quark transition. This coupling is suppressed in the SM by both loop as well as the small coupling constant of the $\mathrm{SU(2)_I}$ gauge group and can be substantially modified through NP contributions. Several analysis, regarding an enhancement of the SM Z-penguin, were carried out with the phenomenological focus on either hadronic [74, 89, 150, 151] or (semi-)leptonic decays [146, 152]. As was pointed out in [152], such a NP scenario is particular interesting because the corresponding operator of the effective Z^{sb} coupling has mass dimension 4 and does not need not to decouple in the limit $\Lambda_{\mathrm{NP}} \to \infty$ from dimensional arguments alone, contrary to the Wilson Coefficients of the dimension 6 4-quark operators in the EWH. Typical examples are models with an extended fermionic spectrum by a fourth generation of sequential quarks[3].

Although we are not considering any specific model in this work, our scenario is nevertheless well motivated as a limiting case of several NP approaches. Supersymmetric models [154] with a dominant contribution from chargino-up-squarks penguin diagrams as well as composite Higgs, respectively Randall-Sundrum models [155, 156], in which flavour-violation can occur in the spectrum of the composite sector on their part mixing into the SM fields can effectively imitate the enhancement of the SM Z-penguin. Further examples are models with tree-level FCNCs, mediated through either the extension of the SM spectrum by additional non-sequential quarks [157] or an additional $U(1)$ gauge symmetry [142], in which the new gauge boson, Z', with potential flavour-violating couplings, mix into the SM Z-boson.

[3] The extension of the SM by only a $4^{\mathrm{th.}}$ generation of sequential quarks cannot accommodate the signal strength in $h \to \gamma\gamma$ and to less extend of $h \to \bar{b}b$ and $h \to \tau\tau$, measured at the LHC and Tevatron, and is excluded by more than 5 standard deviations [153]. Such a scenario could only be realised in nature accompanied by further assumptions.

6.2.1 Theory

Adopting the notations from [146] the part of the effective Lagrangian that describes the Z-boson coupling to the bottom and strange quarks can be parametrised in the following way

$$\mathcal{L}_{\text{eff}} = \mathcal{L}_{\text{eff}}^{\text{SM}} - \frac{G_F}{\sqrt{2}} \frac{e}{\pi^2} M_Z^2 c_{\text{w}} s_{\text{w}} \lambda_t^{(s)} \left[\overline{s} \gamma_\mu \left(P_L Z_L^{sb} + P_R Z_R^{sb} \right) b \right] Z^\mu + \text{h.c.}, \tag{6.14}$$

with $\lambda_t^{(s)} = V_{tb} V_{ts}^*$ and s_{w}, c_{w} the sine and cosine of the weak mixing angle θ_{w}. The Z-penguin contribution in the SM is implicitly included in $\mathcal{L}_{\text{eff}}^{\text{SM}}$ and can be parametrised analogue to the additional term on the right-hand side. The right-handed coupling $Z_R^{sb,\text{SM}}$ vanishes and, for $m_t = 173.2\,\text{GeV}$, we find

$$Z_L^{sb,\text{SM}}(M_W) = -C_0(x_t)/s_{\text{w}}^2 = -3.7, \qquad Z_R^{sb,\text{SM}}(M_W) = 0, \tag{6.15}$$

with the Inami-Lim function $C_0(x_t)$ [158]. As mentioned in [152], the Z-penguin amplitude in the SM itself is in general not gauge invariant, but the leading contribution in the limit $x_t \to \infty$. The modification of the effective SM Lagrangian will induce additional contributions to the $\Delta S = 1$ decay amplitudes of the B meson and, in particular, to the Wilson Coefficients of the 4-quark operators in Equation 2.15

$$\begin{aligned}
\mathcal{C}_3(M_W) &= -\frac{\alpha}{6\pi} Z_L^{sb}, & \mathcal{C}_5'(M_W) &= -\frac{\alpha}{6\pi} Z_R^{sb}, \\
\mathcal{C}_7(M_W) &= -\frac{2\alpha}{3\pi} s_{\text{w}}^2 Z_L^{sb}, & \mathcal{C}_7'(M_W) &= \frac{2\alpha}{3\pi} (1 - s_{\text{w}}^2) Z_R^{sb}, \\
\mathcal{C}_9(M_W) &= \frac{2\alpha}{3\pi} (1 - s_{\text{w}}^2) Z_L^{sb}, & \mathcal{C}_9'(M_W) &= -\frac{2\alpha}{3\pi} s_{\text{w}}^2 Z_R^{sb}.
\end{aligned} \tag{6.16}$$

The modification of the QCD-penguin Wilson Coefficients $\mathcal{C}_3$ and $\mathcal{C}_5'$ is a small correction compared to their SM contributions. In addition, the new Wilson Coefficients are introduced at the scale of the W-boson mass and, as shown in Equation 2.17, the relative effect of the high-scale on the on the low-scale QCD-penguin Wilson Coefficients through RG effects is marginal. Thus, an enhanced Z-penguin scenario can effectively be described by a modification of the electroweak penguin operators only. Furthermore, since $s_{\text{w}}^2 \ll 1$, an enhanced left-handed Z-penguin coupling mainly modifies $\mathcal{C}_9$ and an enhanced right-handed coupling $\mathcal{C}_7'$. Both scenarios share the features of the corresponding single dominant operator scenario. Because their explicit combination have not been tested so far and, in addition, no correlations to (semi-)leptonic observables had to be taken into account in the previous analysis, it is still interesting to study these scenarios in detail.

As mentioned, also the the Wilson Coefficients of the semi-leptonic operators in Equation 2.19 receive contributions

$$\begin{aligned} \mathcal{C}_{9,V}(M_W) &= -Z_L^{sb}(1-4s_{\mathrm{w}}^2), \quad & \mathcal{C}'_{9,V}(M_W) &= -Z_R^{sb}(1-4s_{\mathrm{w}}^2), \\ \mathcal{C}_{10,A}(M_W) &= \quad Z_L^{sb}, & \mathcal{C}'_{10,A}(M_W) &= \quad Z_R^{sb}. \end{aligned} \tag{6.17}$$

We discussed in Chapter 4.2.2 that the observed discrepancies in the semi-leptonic sector can actually be resolved through additional contributions to $\mathcal{C}_{9,V}^{(\prime)}$. Since the Z-penguin amplitude obeys an accidental cancellation for the vectorial Wilson Coefficients through $(1-4s_{\mathrm{w}}^2) \simeq 0.08$, an enhanced Z-penguin scenario predominantly modifies the $\mathcal{C}_{10,A}^{(\prime)}$. Although we can not expect to significantly relax the tension for these observables, they are still suitable to set further limits on the parameters $Z_{L,R}^{sb}$ in our fits.

The enhanced Z-penguin scenarios also contribute to the Wilson Coefficients of the operators in Equation 2.22, describing B^0-$\bar{B}^0$ mixing through a double insertion of the effective $\bar{s}bZ$ vertex

$$\begin{aligned} \mathcal{C}_V^{LL}(M_W) &= \frac{4}{\sqrt{2}G_F}\left(\frac{\alpha}{M_W}\right)^2\left(Z_L^{sb}\right)^2, \quad \mathcal{C}_V^{RR}(M_W) = \frac{4}{\sqrt{2}G_F}\left(\frac{\alpha}{M_W}\right)^2\left(Z_R^{sb}\right)^2, \\ \tilde{\mathcal{C}}_S^{LR}(M_W) &= -4\frac{4}{\sqrt{2}G_F}\left(\frac{\alpha}{M_W}\right)^2 Z_L^{sb} Z_R^{sb}. \end{aligned} \tag{6.18}$$

In the SM, the contribution to M_{12}^s is dominated by box diagrams with virtual top quarks. However, a correction to $\mathcal{C}_V^{LL}$ as above is also present from the SM Z-penguin, but can typically be completely neglected. If the new couplings Z_L^{sb} and Z_R^{sb} can be restricted to SM-like values, $|Z_{L,R}^{sb}| \sim Z_L^{sb,\mathrm{SM}}$, their corrections are negligible, too.

The actual analysis of an enhanced Z-penguin scenario will be performed in the forthcoming section, in which we will focus on the following assumptions

- **Enhanced left-handed Z-penguin** $Z_L^{sb} \in \mathbb{C},\ Z_R^{sb} = 0.$
- **Enhanced right-handed Z-penguin** $Z_L^{sb} = 0,\ Z_R^{sb} \in \mathbb{C}.$
- **Enhanced generic Z-penguin** $Z_L^{sb},\ Z_R^{sb} \in \mathbb{C}.$

6.2.2 Fit results

The fitting procedure for the enhanced Z-penguin scenarios is equivalent to the one in the previous section and as described in Appendix A. The plots in Figure 6.6 and Figure 6.7 show the 68% and 95% CRs for the complex parameters Z_L^{sb} and Z_R^{sb} in the case of the enhanced left-handed (left panel), respectively right-handed (right panel) Z-penguin scenario for the former and the generic enhanced Z-penguin for the latter. The blue contour regions are obtained from only observables in the (semi-)leptonic sector, listed in Table 4.4, whereas the red region is the combination of constraints from (semi-)leptonic

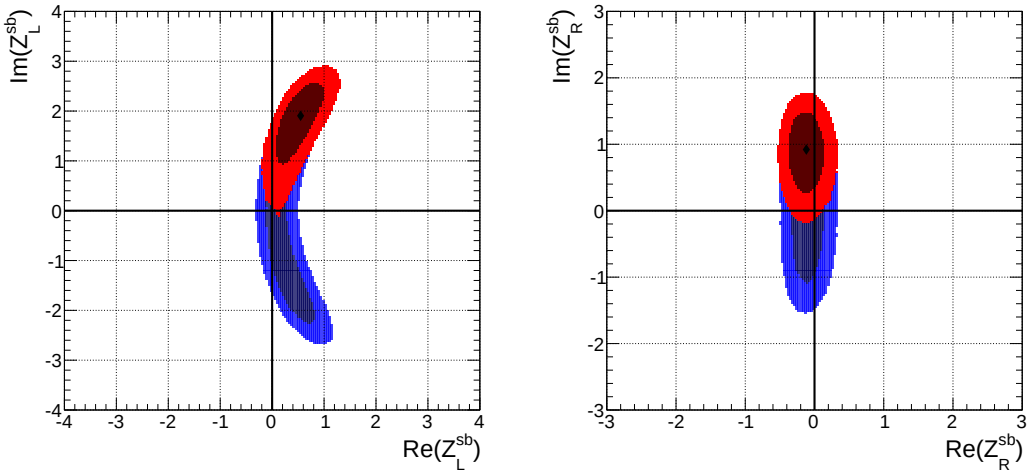

FIGURE 6.6: 68% and 95% CRs for the complex couplings Z_L^{sb} (left) and Z_R^{sb} (right) in the scenario with only one coupling being modified. Constraints are obtained from observables of (semi-)leptonic only (blue) and from the combination of (semi-)leptonic and hadronic B-meson decays (red), whereas the decay systems $B \to K\pi$, $K\rho$, $K^*\pi$, $K^*\rho$ are used. The ♦ corresponds to the best-fit point of the combined fit.

and hadronic decays. As we will discus below and can be seen from the plots, observables of the decays $B \to K^{(*)}\ell^+\ell^-$ are already rather restrictive, such that the additional contributions to the Wilson Coefficients of the 4-quark QED-penguin operators cannot exceed the contours that have been found in the model-independent analysis. Therefore, we excluded observables of the decay system $B \to K^*\phi$ from the fit, which mainly forbid too large contributions to the imaginary part of $\mathcal{C}_9^{(\prime)}$. This task will now be handled by the constraints from (semi-)leptonic decays and, the CP asymmetries in $B \to K^*\phi$ can be instead predicted. Apart from the discussed exception, the residual hadronic decay systems from the previous section $B \to K\pi$, $K\rho$, $K^*\pi$, $K^*\rho$ are used in the fit.

One of the main results of our analyse is to find limits on the enhanced Z-penguin couplings. Inspecting the diverse contour regions, a qualitative difference between the single (in Figure 6.6) and generic (upper panels in Figure 6.7) enhanced Z-penguin scenarios cannot be observed. Due to the additional degrees-of-freedom in the latter, its contour regions slightly smear out. Being conservative, we assume the generic enhanced Z-penguin scenario to find the following bounds on the effective couplings $Z_{L,R}^{sb}$ at 95% probability

$$\begin{aligned} \mathrm{Re}\, Z_L^{sb} &\in [\ \ 0.0;\, 1.2]\,, \quad \mathrm{Re}\, Z_R^{sb} \in [-0.5;\, 0.6]\,, \\ \mathrm{Im}\, Z_L^{sb} &\in [-0.4;\, 2.7]\,, \quad \mathrm{Im}\, Z_R^{sb} \in [-0.2;\, 1.9]\,. \end{aligned}$$

The allowed ranges for the real parts of the Z-penguin coupling are roughly 2–3 times smaller than for the imaginary part. This is mainly caused by constraints from semi-leptonic decays. The branching ratios of $B \to K^*\ell^+\ell^-$ and $B \to K\ell^+\ell^-$ as well as the forward-backward asymmetry, $A_{\mathrm{FB}}(B \to K^*\ell^+\ell^-)$, are most restricting. In the

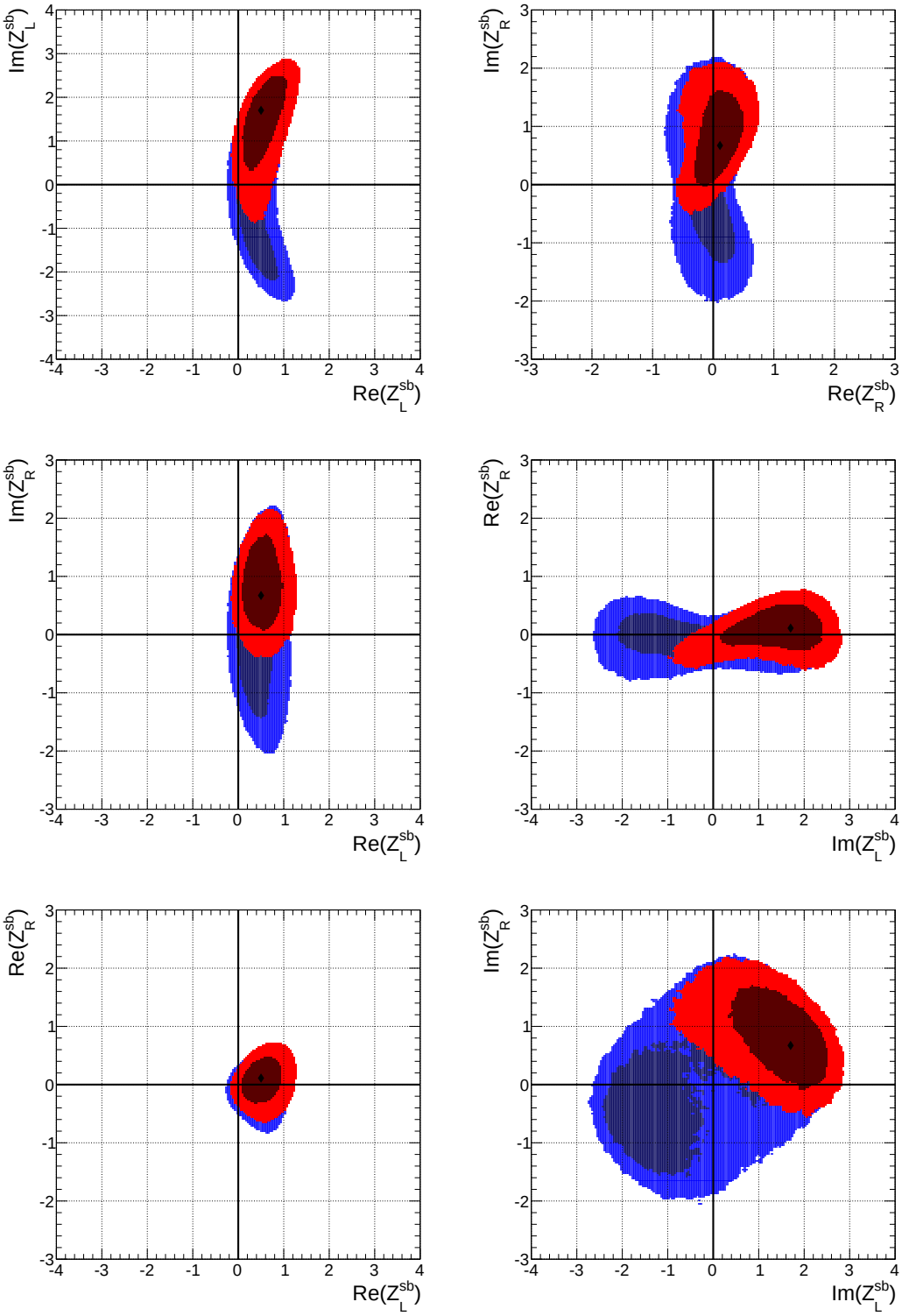

FIGURE 6.7: 68% and 95% CRs for the complex couplings Z_L^{sb} (left) and Z_R^{sb} (right) in the scenario with both couplings being simultaneously modified. Constraints are obtained from observables of (semi-)leptonic only (blue) and from the combination of (semi-)leptonic and hadronic B-meson decays (red), whereas the decay systems $B \to K\pi$, $K\rho$, $K^*\pi$, $K^*\rho$ are used. The ♦ corresponds to the best-fit point of the combined fit.

case in which Z_L^{sb} is enhanced, contour regions from the individual branching ratios are given as a rather small expanded ring with centre (at the real axis) and radius of about 4. However, the contour from the forward-backward asymmetry give a circle that is centred at the SM and does not allow for larger values than $\left|Z_L^{sb}\right| \sim 2$ and the ring contour from the branching ratios is cut, leaving the observed bean-like blue region. For an enhancement of Z_R^{sb}, we obtain a similar contour from $\mathcal{B}(B \to K\ell^+\ell^-)$ as before, but the ring from $\mathcal{B}(B \to K^*\ell^+\ell^-)$ is now mirrored at the imaginary axis (centre at -4), such that the combination of both contours does not obey a curved form as for Z_L^{sb}, but is roughly symmetric about both axis. Because the information from the branching ratios are orthogonal now, it is not surprising that $\mathrm{Im}\, Z_R^{sb}$ is better constrained as $\mathrm{Im}\, Z_L^{sb}$.

The dominance of the (semi-)leptonic observables in constraining the real parts of $Z_{L,R}^{sb}$ can be seen in the lower left panel in Figure 6.7. The additional information from hadronic decays influence the confidence level region of $\mathrm{Re}\, Z_L^{sb} - \mathrm{Re}\, Z_R^{sb}$ only marginal. Nevertheless, all (semi-)leptonic observables which enter our fit are insensitive to the imaginary part of the enhanced Z-penguin. Hence, the resulting blue contours are all symmetric about the real axis and information from hadronic decays are still suitable to further restrict the parameter space. If constraints from hadronic decays are taken into account, we can exclude $\mathrm{Im}\, Z_{L,R}^{sb} \leq 0$ and with it the SM at more than 68% probability. This will be important for those observables that are predicted in the following subsection, being sensitive to the sign of the imaginary part of $Z_{L,R}^{sb}$.

A third class of constraints can be obtained from B_s–$\bar{B}_s$ mixing, respectively the off-diagonally mass matrix element, M_{12}^s. Coinciding with our naive expectation that contributions from an enhanced Z-penguin to neutral meson mixing can be neglected as long as $Z_{L,R}^{sb} \sim Z_L^{sb,\mathrm{SM}}$, we found the following bounds:

$$|\mathrm{Re}\, Z_{L,R}| \sim |\mathrm{Im}\, Z_{L,R}| \leq 6\,(22) \text{ at } 68\,(95)\% \text{ probability.} \tag{6.19}$$

With regard to the gained contours from (semi-)leptonic and hadronic decays, M_{12}^s cannot further constrain the parameter space, for which reason we refrain from showing its contour regions in the plots. If deviations from the SM prediction will appear in future measurements, any concrete model will need an additional source of triggering $B_s - \bar{B}_s$ mixing apart from the effect of an enhanced Z-penguin.

We already mentioned that the individual scenarios can effectively be described by a modification of a single electroweak Wilson Coefficient, as it was analysed in the previous section. In order to relate the results of both analysis to each other, we have to take care of the different normalisation factors that enter the modification of the Wilson Coefficients

$$\left|C_9^{\mathrm{SM}}(M_W)\right| : \frac{2\alpha}{3\pi}(1 - s_{\mathrm{w}}^2) \qquad 6:1, \tag{6.20}$$

$B \to M_1 M_2$ & $B \to K^* \ell^+ \ell^-$					[104]	
	$\mathrm{Re}\, Z_A^{sb}$, $\mathrm{Im}\, Z_A^{sb}$	$\Delta A_{\mathrm{CP}}^{K\pi}$	$R_n^B(K\pi)$	$C(\bar{K}^0\pi^-)$	$\langle P_5' \rangle_{[1,6]}$	$\Delta\chi^2(SM)$
SM		$\mathbf{-2.8\sigma}$	$\mathbf{-1.9\sigma}$	1.0σ	$\mathbf{2.2\sigma}$	
Z_L	0.55, 1.90	$\mathbf{-1.6\sigma}$	-0.8σ	1.2σ	$\mathbf{2.1\sigma}$ ($\mathbf{2.1\sigma}$)	9
Z_R	−0.12, 0.92	-1.5σ	-1.2σ	1.5σ	$\mathbf{2.3\sigma}$ ($\mathbf{2.3\sigma}$)	8
$Z_L - Z_R$	0.50, 1.70 0.11, 0.67	-0.7σ	-0.8σ	$\mathbf{1.7\sigma}$	$\mathbf{2.0\sigma}$ ($\mathbf{2.0\sigma}$)	12

TABLE 6.4: Compilation of best-fit points and pull values with $|\delta| \geq 1.6$ for the enhanced left-handed, right-handed, and generic Z-coupling scenarios. Pull values for a fit with (semi-)leptonic data only are shown in parentheses.

and bounds and contour regions for the Wilson Coefficients $\mathcal{C}_7^{(\prime)}$ and $\mathcal{C}_9^{(\prime)}$, obtained in the model-independent fit, can be compared to the bounds and contour regions from the enhanced Z-penguin scenarios, when rescaled by a factor of 6.

The enhanced right-handed Z-penguin scenario, respectively the effective coupling Z_R^{sb}, is correlated to $\mathcal{C}_7'$, which contour region was found to be purely real in the previous subsection. The constraints on $\mathrm{Re}\, Z_R^{sb}$ from observables of (semi-)leptonic decays are already tightly restricting and do not allow for the proposed real solution, such that Z_R^{sb} receive instead almost imaginary contributions. In fact, the pull value for $\Delta A_{\mathrm{CP}}^{K\pi}$ decreases to -1.5σ, listed in Table 6.4, but this solution induces also CP-violating contributions to other decay modes, raising a tension in $C(B^- \to \bar{K}^0\pi^-)$ of 1.5σ. A solution to the discrepancy in $R_n^B(K\pi)$ is also less effective than for the $\mathcal{C}_7'$ scenario and leaves a pull of -1.2σ. An enhanced left-handed Z-penguin can effectively be described through the $\mathcal{C}_9$ scenario, for which purely imaginary contributions were preferred. Because $\mathrm{Im}\, Z_L^{sb}$ is less restricted, the contour for Z_L^{sb} can still become half as large as for $\mathcal{C}_9$ and shares, apart from a slight inclination due to the bean-like contour from (semi-)leptonic decays, similar features. The pull values are comparable to the Z_R^{sb} scenario, and both models, Z_L^{sb} as well as Z_R^{sb}, are similar suited to resolve the tensions, resulting into $\Delta\chi^2(\mathrm{SM}) = 9$, respectively $\Delta\chi^2(\mathrm{SM}) = 8$. We also studied the generic enhanced Z-penguin scenario, in which the left- and right-handed coupling were fitted simultaneously. The results can be considered as the combination of the individual scenarios discussed above. Although Z_L^{sb} as well as Z_R^{sb} individually relax the tensions in $\Delta A_{\mathrm{CP}}^{K\pi}$ to -0.7σ and in $R_n^B(K\pi)$ to -0.8σ and the quality of the fit increases to $\Delta\chi^2(\mathrm{SM}) = 12$, an increasing tension for the CP asymmetry $C(B^- \to \bar{K}^0\pi^-)$ of -1.7σ restrict the possibility of a complete resolution.

So far, we did not discus the encountered discrepancy for observables in $B \to K^*\ell^+\ell^-$. As mentioned in Chapter 4.2.2, the tensions in $\langle A_{\mathrm{FB}} \rangle_{[>16]}$ and $\langle F_{\mathrm{L}} \rangle_{[14,16]}$ are caused by inconsistent, individual measurements, whereas $\langle A_{\mathrm{CP}} \rangle_{[14,16]}$ and $\langle P_4' \rangle_{[14,16]}$

	$K\pi$		$K^*\pi$		$K\rho$		$K^*\rho$	
	$\lvert\rho_A\rvert,\ \phi_A$	ξ_3^A	$\lvert\rho_A\rvert,\ \phi_A$	ξ_3^A	$\lvert\rho_A\rvert,\ \phi_A$	ξ_3^A	$\lvert\rho_A\rvert,\ \phi_A$	ξ_3^A
SM	$3.34, 2.71$	0.39	$1.61, 5.84$	0.89	$2.69, 2.68$	0.78	$1.56, 5.66$	1.33
Z_L^{sb}	$2.29, 5.41$	[0.37, 0.62]	$1.63, 5.87$	[0.82, 1.41]	$2.79, 2.67$	[0.44, 1.52]	$1.57, 5.63$	[0.88, 1.90]
Z_R^{sb}	$2.17, 5.43$	[0.34, 0.62]	$1.64, 5.87$	[0.82, 1.34]	$2.75, 2.69$	[0.50, 1.42]	$2.39, 2.73$	[1.03, 1.97]
Z_L^{sb}, Z_R^{sb}	$2.17, 5.43$	[0.30, 0.67]	$1.64, 5.87$	[0.63, 1.81]	$2.78, 2.68$	[0.12, 2.85]	$2.38, 2.73$	[0.48, 2.50]

TABLE 6.5: Compilation of the best-fit points for $\rho_A^{M_1M_2}$ and ξ_3^A at the probability of 68%. The results are given for $B \to K\pi$, $K\rho$, $K^*\pi$, $K^*\rho$ and specified for the enhanced left-handed, right-handed, and generic Z-coupling scenarios. As explained in Appendix A.5, the interval of ξ_3^A(NP) should be compared to ξ_3^A(SM) at the best-fit point of $\rho_A^{M_1M_2}$, listed in the first row.

could be explained through very large corrections to the semi-leptonic Wilson Coefficients, which are, however, forbidden from constraints of other observables. For that reason, we pass on showing their pull values in Table 6.4. It was also discussed that $\langle P_5' \rangle_{[1,6]}$ cannot be explained within a modification of $\mathcal{C}_{10,A}^{(\prime)}$ only, (see [122]), which we can confirm through almost stagnating pull values for any of the three Z-penguin scenarios. To summarise, although now further improvements on tensions in (semi-)leptonic decays can be expected from an enhanced Z-penguin scenario, the parameter space can indeed be tightly restricted.

As for the model-independent analysis in the previous section, we again quantify the necessarily amount of power corrections for each decay system and scenario through the power-suppressed ratio $\xi_3^A(M_1M_2)$, collected together with the best-fit points for the WA parameter $\rho_A^{M_1M_2}$ in Table 6.5. We can see that the largest decrease of the power-suppressed ratio is encountered for the generic enhanced Z-penguin scenario. For instance, the power corrections in $B \to K\rho$ might be almost negligible, $\xi_3^A(K\rho) = 0.12$, compared to its SM value, and even the data for $B \to K\pi$ might be explained with a correction of only $\xi_3^A(K\pi) = 0.30$. In addition, the large weak-annihilation scenario is still excluded for $B \to K\pi$. Similar to the results of the model-independent analysis, all best-fit points for $\rho_A^{M_1M_2}$ lie within the 68% CR of the SM fit. This emphasis that the unknown soft QCD interaction still behaves as in the SM, in spite of the modification of QED-penguin Wilson Coefficients.

Let us summarise the results that have been obtained from the discussion so far:

- Whereas the tensions in observables of (semi-)leptonic decays cannot be explained in any of the analysed scenarios, the discrepancy in $\Delta A_{\rm CP}^{K\pi}$ and $R_n^B(K\pi)$ can significantly be relaxed, favouring the generic enhanced Z-penguin scenario.

- $\mathrm{Re}\, Z_{L,R}^{sb}$ are tightly restricted from constraints of (semi-)leptonic decays, whereas the bounds for $\mathrm{Im}\, Z_{L,R}^{sb}$ are weaker. In addition, the contours are symmetric about

the real axis, such that the sign of $\mathrm{Im}\, Z^{sb}_{L,R}$, which is important for CP-violating observables, cannot be determined from (semi-)leptonic observables only. Further information from hadronic decays are suitable to break this symmetry implying substantially consequences for the predictions of observables.

- Taking all constraints into account, the effective couplings Z^{sb}_L and Z^{sb}_R can still receive a relative correction of 80%, respectively 51%, compared to $Z^{sb,\mathrm{SM}}_L$ at the probability of 95%.

6.2.3 Observable predictions

We will now work out how a Z-penguin scenario could be detected in various observables and whether it is possible to distinguish the individual scenarios from each other. As for the model-independent analysis, we again quote the predictions for the purely isospin-violating branching ratios of $\bar{B}_s \to \phi\pi$, $\phi\rho$ and for mixing-induced CP asymmetries of various B_d decays, $\Delta S(M_1 M_2)$, in the upper part of Table 6.6. Because the effective Z-penguin couplings are already tightly constrained from (semi-)leptonic decays, large contributions to the branching ratios cannot be expect. The impact from Z^{sb}_R is completely negligible, but at least, an enhanced left-handed Z-penguin could decrease the branching ratios about $10 - 20\%$. Regarding the uncertainties, it might be rather tough to achieve the necessarily experimental precision in the near future that would be required to resolve a contribution from Z^{sb}_L from the SM background in these observables. Though the effective couplings are quite well restricted, the fits prefer almost pure imaginary contributions, which will especially influence CP asymmetries. All predictions for $\Delta S(M_1 M_2)$ coincide within their errors with the SM, but the uncertainties, which also include a weighted contribution from the NP and WA parameter space (see Appendix A.4), are large, such that deviations form SM predictions are not unlikely and detectable. Nevertheless, based on the current status on the limits for $Z^{sb}_{L,R}$, an experimental precision of at least a few percent will be needed for the mixing-induced CP asymmetries in B_d decays.

More suitable to find NP that enhances the SM Z-penguin might be the CP asymmetries in $B \to K^*_L \phi_L$ and $\bar{B}_s \to \phi_L \phi_L$. We plotted the correlated predictions for the direct and mixing-induced CP asymmetry in the upper panels for the former and the direct CP asymmetry for the neutral and charged mode of the latter decay in the middle panels of Figure 6.8. The plots are obtained from left to right for the left-, right-handed, and the generic enhanced Z-penguin scenario. The SM predicts vanishing CP violation in these decays, but significant deviations from zero can still occur, especially for new contributions to Z^{sb}_L. Additionally, the impact on the observables from Z^{sb}_L and Z^{sb}_R are anti-correlated, such that it is possible to distinguish the individual contributions from each other.

$B \to M_1 M_2$	$\Delta S(K\pi)$	$\Delta S(K\rho)$	$\Delta S(K^*\pi)$	$\Delta S_L(K^*\rho)$	$\Delta S(K\eta')$	$\Delta S(K\omega)$	$\Delta S(K\phi)$	$\Delta S_L(K^*\phi)$	$\mathcal{B}(\phi\pi)$	$\mathcal{B}(\phi\rho)$
SM	$[0.05, 0.13]$	$[-0.19, -0.04]$	$[0.06, 0.17]$	$[-0.15, 0.09]$	$[-0.01, 0.04]$	$[0.09, 0.17]$	$[0.01, 0.05]$	$[0.01, 0.04]$	$0.24^{+0.07}_{-0.04}$	$0.68^{+0.19}_{-0.10}$
Z_L^{sb}	$0.08^{+0.03}_{-0.11}$	$-0.07^{+0.10}_{-0.06}$	$0.06^{+0.05}_{-0.12}$	$0.04^{+0.06}_{-0.19}$	$0.04^{+0.02}_{-0.08}$	$0.13^{+0.09}_{-0.06}$	$-0.01^{+0.05}_{-0.07}$	$-0.03^{+0.05}_{-0.07}$	$0.19^{+0.04}_{-0.07}$	$0.60^{+0.13}_{-0.15}$
Z_R^{sb}	$0.14^{+0.00}_{-0.14}$	$-0.06^{+0.04}_{-0.16}$	$0.12^{+0.07}_{-0.07}$	$0.00^{+0.08}_{-0.17}$	$0.06^{+0.01}_{-0.11}$	$0.15^{+0.02}_{-0.11}$	$0.03^{+0.03}_{-0.08}$	$0.04^{+0.04}_{-0.06}$	SM	SM
Z_L^{sb}, Z_R^{sb}	$0.07^{+0.04}_{-0.10}$	$-0.08^{+0.10}_{-0.07}$	$0.09^{+0.05}_{-0.09}$	$0.06^{+0.05}_{-0.19}$	$0.04^{+0.02}_{-0.10}$	$0.13^{+0.07}_{-0.09}$	$-0.02^{+0.05}_{-0.07}$	$0.03^{+0.03}_{-0.09}$	$0.20^{+0.05}_{-0.05}$	$0.60^{+0.14}_{-0.10}$
$B \to K^*\ell^+\ell^-$	$\langle A^{\rm im}\rangle_{[1,6]}$	$\langle A^{\rm im}\rangle_{[14,16]}$	$\langle A^{\rm im}\rangle_{[>16]}$	$\langle H_{\rm T}^{4,5}\rangle_{[14,16]}$	$\langle H_{\rm T}^{4,5}\rangle_{[>16]}$	$\langle P_3^{\rm CP}\rangle_{[1,6]}$	$\langle P_6'^{\rm CP}\rangle_{[1,6]}$	$\langle P_8'^{\rm CP}\rangle_{[1,6]}$		
SM	$\mathcal{O}(10^{-4})$	$\mathcal{O}(10^{-3})$	$\mathcal{O}(10^{-3})$	$\mathcal{O}(10^{-5})$	$\mathcal{O}(10^{-5})$	$\mathcal{O}(10^{-4})$	$\mathcal{O}(10^{-3})$	$0.01^{+0.00}_{-0.01}$		
Z_L^{sb}	SM	SM	SM	SM	SM	SM	$-0.37^{-0.08}_{+0.06}$	$0.01^{+0.04}_{-0.00}$		
Z_R^{sb}	$0.03^{+0.01}_{-0.01}$	$0.07^{+0.02}_{-0.02}$	$0.05^{+0.02}_{-0.02}$	$-0.31^{+0.09}_{-0.07}$	$-0.29^{+0.08}_{-0.08}$	$-0.16^{+0.05}_{-0.04}$	$0.17^{+0.05}_{-0.05}$	$0.30^{+0.07}_{-0.09}$		
Z_L^{sb}, Z_R^{sb}	$0.03^{+0.01}_{-0.01}$	$0.08^{+0.03}_{-0.03}$	$0.06^{+0.02}_{-0.02}$	$-0.35^{+0.13}_{-0.11}$	$-0.33^{+0.11}_{-0.11}$	$-0.15^{+0.03}_{-0.04}$	$-0.15^{+0.10}_{-0.13}$	$0.28^{+0.10}_{-0.04}$		

TABLE 6.6: Compilation of predictions for the enhanced left-handed, right-handed, and generic Z-coupling scenarios.

In contrast to the model-independent analysis in the previous section, we can now make use of the correlations to (semi-)leptonic decays and also predict for example observables for $B \to K^*\ell^+\ell^-$. Large corrections are present for the modification of the right-handed coupling for the CP asymmetries $H_T^{4,5}$ at mid and high q^2 and for the CP asymmetries $P_{6,8}^{\prime\rm CP}$ and $P_3^{\rm CP}$ at low q^2, listed in the lower part of Table 6.6. Apart from $\langle P_6^{\prime\rm CP}\rangle_{[1,6]}$, these observables behave SM-like for a modification of the left-handed coupling. Therefore, $\langle P_6^{\prime\rm CP}\rangle_{[1,6]}$ is the most important observable to distinguish Z_L^{sb} from Z_R^{sb} because both scenarios cause large corrections with respectively opposite sign. Once $\langle P_6^{\prime\rm CP}\rangle_{[1,6]}$ is measured, one of the two scenarios in which only one coupling is predominantly enhanced can be ruled out, but a simultaneously enhancement of both couplings could still explain the data, too. In order to distinguish these two options, the contrary information from for instance $\langle P_8^{\prime\rm CP}\rangle_{[1,6]}$ is needed. The correlation of the two observables is presented in the lower panels of Figure 6.8, where we plotted $\langle P_6^{\prime\rm CP}\rangle_{[1,6]}$ vs. $\langle P_8^{\prime\rm CP}\rangle_{[1,6]}$ from left to right for left-, right-handed, and the generic enhanced Z-penguin scenario. Corresponding to the colour coding of the contour plots, the blue predictions are obtained from a fit of only (semi-)leptonic observables and the red from the combined fit. It can be seen that the additional information from hadronic decays are indeed beneficial to shrink the prediction range considerably.

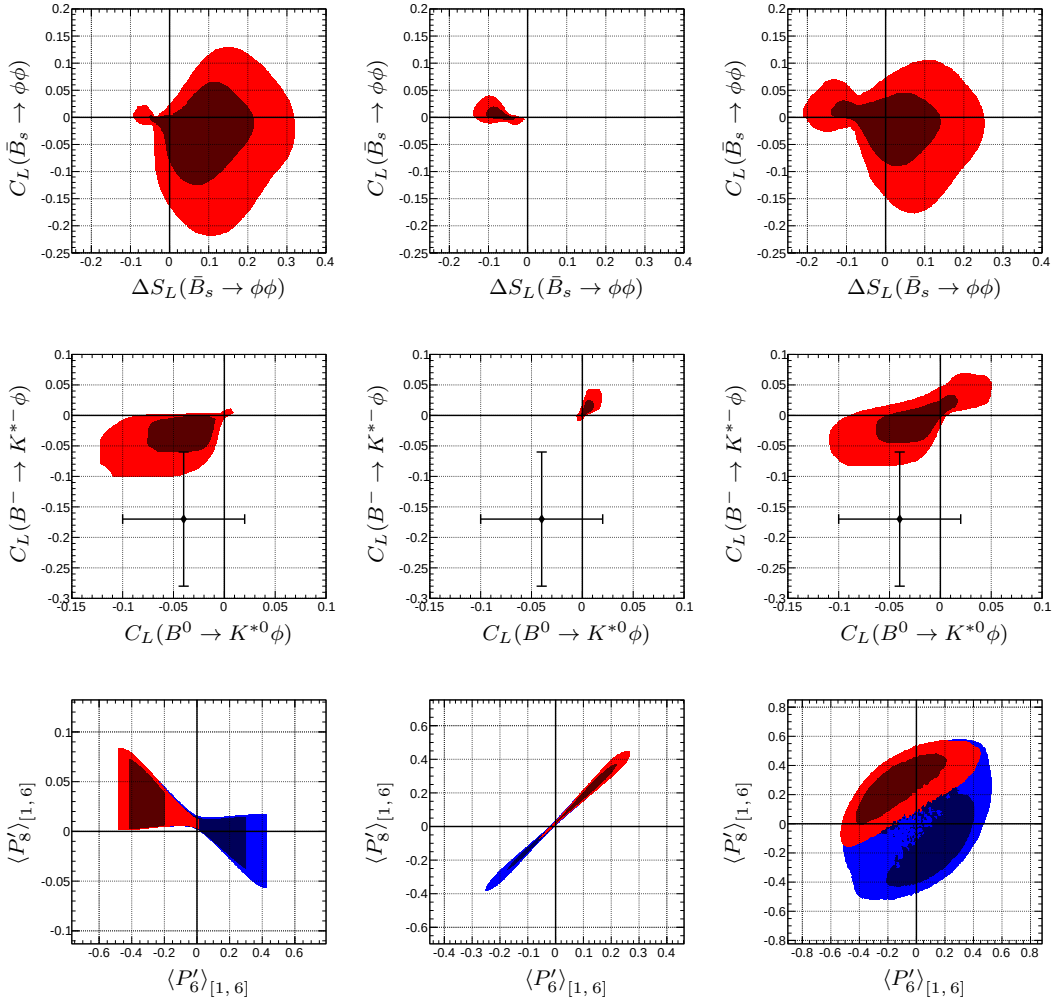

FIGURE 6.8: Correlations among the predictions for C_L vs. S_L in $\bar{B}_s \to \phi\phi$ (upper panels), C_L in $\bar{B}^0 \to \bar{K}^{*0}\phi$ vs. $B^- \to K^{*-}\phi$ (middle panels), and $\langle P_6' \rangle_{[1,6]}$ vs. $\langle P_8' \rangle_{[1,6]}$ (lower panels) at the probability of 68% and 95%. The results are obtained from left to right for modifications of the left-handed, the right-handed, and for both Z-coupling(s). Experimental central values and 1σ uncertainty interval from HFAG are shown for those observables that have already been measured — represented by black lines.

6.3 Extended operator basis through $\mathcal{O}^b = (\bar{s}b)\,(\bar{b}b)$

The last NP analysis is dedicated to the phenomenological consequences of an extended operator basis in which we allow for model-independent additional contributions to 4-quark operators with the general flavour structure $\mathcal{O}^b = (\bar{s}b)\,(\bar{b}b)$. Such operators can occur in models with an extended Higgs sector as, for example, the two-Higgs Doublet Models (2HDM) or the Minimal Supersymmetric Standard Model (MSSM) [159, 160]. In general, a flavour-changing neutral Higgs-exchange generates scalar-penguin operators of the form $\mathcal{O}_S^q = (\bar{s}b)_{S\pm P}\,(\bar{q}q)_{S\pm P}$, which might be enhanced by the ratio of the two vacuum expectation values of the scalar fields, parametrised through $\tan\beta$. Many analysis were performed regarding contributions to the lighter down-type quarks $q = d, s$ in the penguin operator [161–167]. These operators already contribute at leading order to certain decay classes such as $q = d$ in $B \to K^{(*)}(\pi, \rho, \omega)$ and for $q = s$ in $B \to K^{(*)}(\eta^{(\prime)}, \phi)$. Since the b quark sticks out through its large Yukawa coupling, respectively mass, in the down quark sector, $m_b \gg m_s \gg m_d$, it might be reasonable that the leading contributions should be assigned to the penguin operators with $q = b$. These operators do not generate a leading order correction to any hadronic matrix element, but contribute through mixing effects to the SM Wilson Coefficients, and therefore, in principle to all decays which are triggered by the same $b \to s$ transition. By this reason, we can again, as for the enhanced Z-penguin scenarios, study correlation between (semi-)leptonic and hadronic decays, whereas this time, only $\mathcal{C}_{9,V}^{(\prime)}$ are modified, offering a solution to the tension in $\langle P_5' \rangle_{[1,6]}$. The specific flavour structure in $\mathcal{O}^b$ can be utilised to reduce the number of independent operators out of all potential operators with generic Dirac and colour structure to $5+5'$ (χ-flipped), making an analysis in complete generality rather compact. Model-independent analysis of these class of operators with focus on (semi-)leptonic observables have been performed in [168, 169] and including hadronic decays within the context of the MSSM in [170]. The authors in [171] tried to explain some discrepancy in the absorptive part of the off-diagonal B_s–$\bar{B}_s$ matrix element, Γ_{12}^s, accompanied with constraints from (semi-)leptonic observables, through analogue operators, with the b quarks exchanged through the heaviest leptons in the SM, $\mathcal{O}^\tau = (\bar{s}b)\,(\bar{\tau}\tau)$.

Another interesting aspect is that, contrary to the previous NP analysis, both QED- and QCD-penguin Wilson Coefficients can receive contributions. This leads to appreciable correlations between the new Wilson Coefficients and the WA parameters $\rho_A^{M_1 M_2}$ and implies $\xi_3^A(M_1 M_2)$, which have been introduced as a credibility-measure of the m_b/Λ_{QCD} expansion in QCDF, to be strongly affected.

6.3.1 Theory

The phenomenological impact of all 4-quark operators with the flavour structure $\mathcal{O}^b = (\bar{s}b)\,(\bar{b}b)$ will be discussed in the following. With respect to a general Dirac as well as colour structure, we can think of 14 possible operators

$$\begin{aligned} \mathcal{O}_S^b &= (\bar{s}_\alpha P_A b_\beta)(\bar{b}_\gamma P_B b_\delta), & \mathcal{O}_V^b &= (\bar{s}_\alpha \gamma_\mu P_A b_\beta)(\bar{b}_\gamma \gamma^\mu P_B b_\delta), \\ \mathcal{O}_T^b &= (\bar{s}_\alpha \sigma_{\mu\nu} P_A b_\beta)(\bar{b}_\gamma \sigma^{\mu\nu} P_B b_\delta), \end{aligned} \tag{6.21}$$

where $\sigma_{\mu\nu} = \frac{1}{2}[\gamma_\mu, \gamma_\nu]$, $P_{A,B} \in P_L, P_R$ the chiral projectors of the quark fields and $(\alpha, \beta, \gamma, \delta)$ are colour indices, which can occur in an either colour-singlet $\delta_{\alpha\beta}\delta_{\gamma\delta}$ or colour-octet $\delta_{\alpha\delta}\delta_{\gamma\beta}$ configuration. Because the tensor operators with mixed chirallity vanish in $D = 4$ dimensions, they do not need to be considered. In addition, we can make use of the Fierz identities

$$\begin{aligned} (\bar{f}_\alpha \sigma_{\mu\nu} P_{L(R)} f_\beta)(\bar{f}_\gamma \sigma^{\mu\nu} P_{L(R)} f_\delta) &= 4\,(\bar{f}_\alpha P_{L(R)} f_\beta)(\bar{f}_\gamma P_{L(R)} f_\delta) + 8\,(\bar{f}_\alpha P_{L(R)} f_\delta)(\bar{f}_\gamma P_{L(R)} f_\beta), \\ (\bar{f}_\alpha \gamma_\mu P_{L(R)} f_\beta)(\bar{f}_\gamma \gamma^\mu P_{L(R)} f_\delta) &= \quad (\bar{f}_\alpha \gamma_\mu P_{L(R)} f_\delta)(\bar{f}_\gamma \gamma^\mu P_{L(R)} f_\beta), \\ 2\,(\bar{f}_\alpha P_{L(R)} f_\beta)(\bar{f}_\gamma P_{R(L)} f_\delta) &= -(\bar{f}_\alpha \gamma_\mu P_{R(L)} f_\delta)(\bar{f}_\gamma \gamma^\mu P_{L(R)} f_\beta), \end{aligned} \tag{6.22}$$

to further reduce the total number of independent operators to five: The residual tensor operators can be replaced through a linear combination of both purely left-handed scalar operators, whereas the scalar operators with mixed chirallity are related to the corresponding vector operators. At last, all purely left-handed vector operators in a colour-octet configuration can be replaced by their colour-singlet counterparts. Apart from the tensor operators, each operator in Equation 6.21 can be mapped to only one other single operator, such that the results of our analysis, are, with respect to some overall factor from Fierz transformations, applicable. It is therefore sufficient to confine our analysis to the operators

$$\begin{aligned} \mathcal{O}_{11}^b &= (\bar{s}_\alpha\, b_\alpha)_{V-A}(\bar{b}_\beta\, b_\beta)_{V-A}, \\ \mathcal{O}_{12}^b &= (\bar{s}_\alpha\, b_\beta)_{V-A}(\bar{b}_\beta\, b_\alpha)_{V+A}, & \mathcal{O}_{13}^b &= (\bar{s}_\alpha\, b_\alpha)_{V-A}(\bar{b}_\beta\, b_\beta)_{V+A}, \\ \mathcal{O}_{14}^b &= (\bar{s}_\alpha\, b_\beta)_{S+P}(\bar{b}_\beta\, b_\alpha)_{S+P}, & \mathcal{O}_{15}^b &= (\bar{s}_\alpha\, b_\alpha)_{S+P}(\bar{b}_\beta\, b_\beta)_{S+P}, \end{aligned} \tag{6.23}$$

and their χ-flipped counterparts. Analogue considerations also apply for operators with the flavour structure $\mathcal{O}^s = (\bar{s}b)\,(\bar{s}s)$. For the residual discussion, we will focus on NP in $\mathcal{O}^b$ and, if we do not explicitly comment on $\mathcal{O}^s$, omit the superscript from both operators and Wilson Coefficients.

In order to take new contributions from these operators into account, the EWH in Equations 2.14 and 2.18 has to be extended

$$\mathcal{H}_{\text{eff}} = \mathcal{H}_{\text{eff}}^{\text{SM}} + \frac{G_F}{\sqrt{2}} \sum_{p=u,c} \lambda_p^s \left(\sum_{i=11}^{15} \mathcal{C}_i \mathcal{O}_i + \mathcal{C}_i' \mathcal{O}_i' \right) + \text{h.c.}\,. \tag{6.24}$$

Although all terms are included in our numerical analysis, the contributions proportional to the suppressed CKM-matrix elements in λ_u, which includes the CP-violating phase γ of the SM, can be neglected. Due to their flavour structure, the new operators do not contribute at leading order to neither hadronic nor (semi-)leptonic decays, but mix into the SM operators via the one-loop diagrams, shown in Figure 6.9. After solving the RGE, the SM Wilson Coefficients at the scale m_b are modified

$$C_i^{(\prime)}(m_b) = |C_j^{\text{SM}}(m_b)| \left(1 + \kappa_i(\mathcal{C}_{11}^{(\prime)}, \ldots, \mathcal{C}_{15}^{(\prime)})\right) \begin{cases} j = i+2 & \text{for } i = 7, 8, \\ j = i & \text{for others.} \end{cases} \tag{6.25}$$

The large Wilson Coefficient, $|C_{9,10}^{\text{SM}}|$, were used as normalisation constant for $\kappa_{7,9}$, analogue to the model-independent analysis of QED-penguin operators.

The mixing effects can be classified in the following way: The scalar operators $\mathcal{O}_{14,15}$ exclusively mix into the dipole operators $\mathcal{O}_{7\gamma,8g}$, such that their impact is confined to a modification of

$$\kappa_{7\gamma} = 0.08\,\mathcal{C}_{14} + 0.03\,\mathcal{C}_{15}, \qquad \kappa_{8g} = -0.25\,\mathcal{C}_{15}, \tag{6.26}$$

The matrix elements of the dipole operators occur in QCDF first at NLO, such that it is sufficient to calculate their ADM at LO. As recently studied model-independently in [172], the Wilson Coefficient of the electromagnetic dipole operator, $C_{7\gamma}$, is best constrained by observables from $b \to s(\gamma)\ell^+\ell^-$ decays, and we won't further discus contributions from $\mathcal{C}_{14}^{(\prime)}$. The Wilson Coefficient of the chromo-magnetic dipole operator, C_{8g}, solely contributes to the QCD-penguin amplitude $\hat{\alpha}_4$ and, as we will see, has similar phenomenological consequences as a modification of the Wilson Coefficient $\mathcal{C}_{12}^{(\prime)}$, such that it is also unnecessary to discuss a modification of $\mathcal{C}_{14}^{(\prime)}$ explicitly. Therefore, our analysis will be confined to a modification of $\mathcal{C}_{11-13}^{(\prime)}$. In contrast to the scalar operators, the vector operators $\mathcal{O}_{11-13}^{(\prime)}$ do not mix into the dipole, but into the QCD- and QED-penguin operators. Their ADM have been calculated at NLO accuracy in α_s to reduce the uncertainty from scale variation, which could spoil our fits. To be consistent, we also have to incorporate the NLO corrections of these operators to the hadronic matrix elements in QCDF, which, together with the ADM, are presented in Appendix C.

Due to the Dirac, respectively colour structure of the operators $\mathcal{O}_{13}^{(\prime)}$, their contribution to the left, respectively right diagram in Figure 6.9, with the exchange of a gluon,

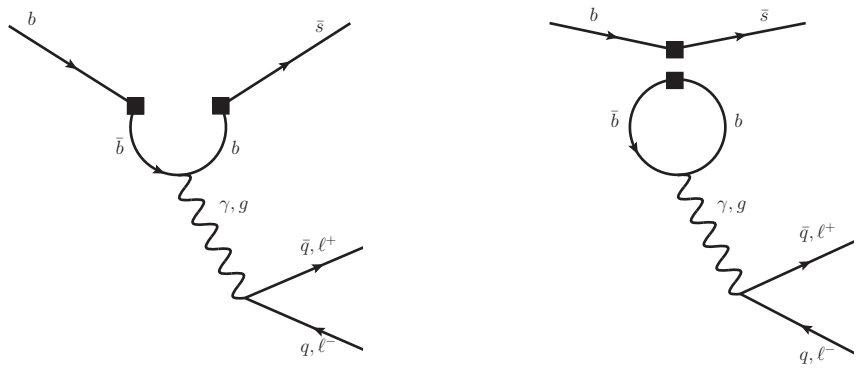

FIGURE 6.9: Open and closed QCD- (gluon exchange) and QED-penguin (photon exchange) diagrams with $(\bar{s}b)\,(\bar{b}b)$ operator insertions, where the lower fermion current can be either quarks or leptons. The diagram with an off-shell gluon, respectively photon, contributes to the dipole operators.

vanishes and modifies the SM QCD-penguin Wilson Coefficients only at NLO. However $\mathcal{O}^{(\prime)}_{11,12}$ already contribute at LO, explaining the hierarchy $\kappa_i(\mathcal{C}^{(\prime)}_{11}) \sim \kappa_i(\mathcal{C}^{(\prime)}_{12}) \gg \kappa_i(\mathcal{C}^{(\prime)}_{13})$

$$\begin{aligned} \kappa_3 &= 0.49\,\mathcal{C}_{11} + 1.20\,\mathcal{C}_{12} + 0.37\,\mathcal{C}_{13}, \quad \kappa_4 = -0.83\,\mathcal{C}_{11} - 0.95\,\mathcal{C}_{12} - 0.06\,\mathcal{C}_{13}, \\ \kappa_5 &= 1.32\,\mathcal{C}_{11} + 0.75\,\mathcal{C}_{12} - 0.43\,\mathcal{C}_{13}, \quad \kappa_6 = -0.82\,\mathcal{C}_{11} - 1.21\,\mathcal{C}_{12} - 0.08\,\mathcal{C}_{13}. \end{aligned} \tag{6.27}$$

The QED-penguin Wilson Coefficients receive corrections from all three operators already at LO and now the hierarchy changes, $\kappa_i(\mathcal{C}^{(\prime)}_{11}) \sim \kappa_i(\mathcal{C}^{(\prime)}_{13}) \gg \kappa_i(\mathcal{C}^{(\prime)}_{12})$

$$\begin{aligned} \kappa_7 &= 0.20\,\mathcal{C}_{11} + 0.07\,\mathcal{C}_{12} + 0.17\,\mathcal{C}_{13}, \quad \kappa_8 = \quad 0.28\,\mathcal{C}_{11} + 0.14\,\mathcal{C}_{12} + 0.18\,\mathcal{C}_{13}, \\ \kappa_9 &= 0.22\,\mathcal{C}_{11} + 0.08\,\mathcal{C}_{12} + 0.18\,\mathcal{C}_{13}, \quad \kappa_{10} = -0.21\,\mathcal{C}_{11} - 0.09\,\mathcal{C}_{12} - 0.13\,\mathcal{C}_{13}. \end{aligned} \tag{6.28}$$

Since the diagrams that are responsible for the mixing into the semi-leptonic operators $\mathcal{O}_{9,V}$ are obtained by replacing the quarks through leptons in the lower current of Figure 6.9, we sustain the same hierarchy and even the same proportions among the individual contributions as for the QED-penguin operators in $\kappa_{9,V}$

$$\kappa_{9,V} = -1.21\,\mathcal{C}_{11} - 0.43\,\mathcal{C}_{12} - 0.98\,\mathcal{C}_{13}. \tag{6.29}$$

This implies that the relative effects between the QED-penguin and semi-leptonic Wilson Coefficients are equal for each scenario and the phenomenological difference manifests exclusively in the relative effects between QCD- and QED-penguin Wilson Coefficients. We therefore listed in Table 6.7 the corrections to the QCD- and QED-penguin amplitudes normalised to the corresponding SM amplitude for all four hadronic decay systems. In order to identify the leading correction, we also quote the relative weight between QCD and QED-penguin amplitudes for the SM by the ratio $|\alpha_4^{\mathrm{SM}}|/|\alpha_i^{\mathrm{SM}}|$. We can see

	$B \to K\pi$			$B \to K\rho$			$B \to K^*\pi$			$B \to K_L^*\rho_L$		
	c_4	$c_3^{\rm EW}$	$c_4^{\rm EW}$	c_4	$c_3^{\rm EW}$	$c_4^{\rm EW}$	c_4	$c_3^{\rm EW}$	$c_4^{\rm EW}$	c_4	$c_3^{\rm EW}$	$c_4^{\rm EW}$
$\mathcal{C}_{11}$	0.53	0.00	1.12	0.44	0.47	0.33	0.56	0.00	0.29	0.56	0.47	0.26
$\mathcal{C}_{12}$	0.89	0.00	0.43	1.17	0.16	0.16	0.67	0.00	0.09	0.71	0.16	0.08
$\mathcal{C}_{13}$	0.06	0.00	0.89	0.16	0.39	0.22	0.01	0.00	0.26	0.01	0.39	0.24
$\lvert\alpha_4^{\rm SM}\rvert/\lvert\alpha_i^{\rm SM}\rvert$	1	12	52	1	3	14	1	5	13	1	4	17

TABLE 6.7: We list the relative change $c_i = |\alpha_i(\mathcal{C}_j)|/|\alpha_i^{\rm SM}|$ of the decay amplitudes α_4, $\alpha_3^{\rm EW}$,and $\alpha_4^{\rm EW}$ for decay systems $B \to K\pi$, $K\rho$, $K^*\pi$, $K^*\rho$ depending on the modification of the Wilson Coefficients $\mathcal{C}_{11-13}$. In order to figure out the main contribution to the decay amplitudes, we compare in the last row the electroweak with the QCD-penguin amplitudes for the SM.

that a modification of both Wilson Coefficients $\mathcal{C}_{11}^{(\prime)}$ and $\mathcal{C}_{12}^{(\prime)}$ leads to a dominating contribution to the QCD-penguin amplitude α_4. Whereas corrections to the electroweak amplitude are completely negligible for the latter, they can still become relevant for the former. It is worth to mention, that from Equation 6.29 we can expect the most stringent bounds from (semi-)leptonic observables for $\mathcal{C}_{11}^{(\prime)}$ and loosest for $\mathcal{C}_{12}^{(\prime)}$. The situation for an enhanced $\mathcal{C}_{13}^{(\prime)}$ is different. The QCD-penguin amplitude only receive corrections at NLO, but due to its relative weight compared to the QED-penguin amplitudes, it can still become the leading correction. In addition, the individual decay amplitudes for $B \to PP$, (PV, VP, VV) depend on a different linear combination of Wilson Coefficient, such that those decay amplitudes that receive the leading correction varies for each decay system. Inspecting the last two rows of Table 6.7, the new contribution dominates in α_4 for $B \to K\pi$, $B \to K\rho$ receive leading corrections to α_4 and $\alpha_3^{\rm EW}$, and the corrections in $B \to K^*\pi$ and $B \to K_L^*\rho_L$ predominantly contribute to $\alpha_4^{\rm EW}$, respectively $\alpha_3^{\rm EW}$.

These considerations motivates to study the phenomenological consequences for each Wilson Coefficient separately. We introduce the following scenarios, which will be analysed in the following section

- **Scenario I: QCD- with pollution from QED-penguin $\mathcal{C}_{11}$, $\mathcal{C}'_{11} \in \mathbb{C}$.**
- **Scenario II: QCD-penguin $\mathcal{C}_{12}$, $\mathcal{C}'_{12} \in \mathbb{C}$.**
- **Scenario III: QCD- and QED-penguin $\mathcal{C}_{13}$, $\mathcal{C}'_{13} \in \mathbb{C}$.**

Our main motivation for introducing contributions beyond the SM was to explain the observed discrepancy in $\Delta A_{\rm CP}^{K\pi}$ and $R_n^B(K\pi)$. These observables are sensitive to isospin-violating corrections, but $B \to K\pi$ is dominated for each scenario by corrections to $\alpha_4^c(K\pi)$

$$\hat{\alpha}_4^c(\pi K) = \hat{\alpha}_4^{c,\rm SM}(\pi K)\left(1 + \tilde{r}_{\rm QCD}\left(|\mathcal{C}_i|\right)e^{i\delta_i}\right), \qquad \tilde{r}_{\rm QCD} \equiv \frac{\hat{\alpha}_4^c(\pi K)(|\mathcal{C}_i|)}{\hat{\alpha}_4^{c,\rm SM}(\pi K)}, \tag{6.30}$$

which are isospin-conserving. However, these observables can still be modified and, before going into the details of our analysis, preceding analytically considerations are assistant to better understand our fit results. The additional Wilson Coefficients are complex and can obtain a CP-violating phase, given by δ_i in Equation 6.30. Because $\mathrm{Re}\,\mathcal{C}_i$ basically yield an additional CP-conserving contribution to the leading decay amplitude, which is also the main task of the WA parameter, $\mathrm{Re}\,\mathcal{C}_i$ and $\rho_A^{M_1 M_2}$ can always be compensated by each other. This implies that we can expect significant differences for the WA fit, but no substantially constraints to the real part of the Wilson Coefficients. Here we have to rely on data from (semi-)leptonic decays. From a phenomenological point of view, the CP-violating part $\mathrm{Im}\,\mathcal{C}_i$ are more interesting for hadronic decays. Since $\tilde{r}_{\mathrm{QCD}}$ occurs in each decay mode, all four CP asymmetries obtain a universal shift of

$$\delta C(B \to K\pi) \simeq -2\,\mathrm{Im}\,\tilde{r}_{\mathrm{QCD}}\,\sin(\delta_i), \tag{6.31}$$

which cancels when taking the difference of two CP asymmetries. However, because the new contribution can reduce the necessarily amount of CP violation from the SM tree-level amplitudes in for example $C(\bar{B}^0 \to K^-\pi^+)$, the WA fit and, in particular, the determination of $\hat{\alpha}_4^c(K\pi)$, can be relaxed in favour of $\Delta A_{\mathrm{CP}}^{K\pi}$ (see Equation 5.3). Such a solution is limited by the experimentally allowed CP asymmetry in $B^- \to \bar{K}^0\pi^-$, which vanishes in the SM. This implies that an accurate measurement of this CP asymmetry, consistent with zero, would forbid a solution to the $\Delta A_{\mathrm{CP}}^{K\pi}$ puzzle for scenarios that predominantly enhance the QCD-penguin amplitude, or reworded: The scenarios $\mathcal{C}_{11^{(\prime)}-13^{(\prime)}}$ with a non-vanishing weak phase imply a clean signature of $C(B^- \to \bar{K}^0\pi^-) \neq 0$. These effects can only be observed if $\rho_A^{K\pi}$ is simultaneously fitted with the NP contributions. A conventional treatment of power-suppressed corrections would, on the one hand, not change the prediction for $\Delta A_{\mathrm{CP}}^{K\pi}$ and, on the other hand, lead to overestimated constraints for $\mathrm{Re}\,\mathcal{C}_i$. This confirms the usefulness of our approach.

The ratio of branching ratios, $R_n^B(K\pi)$, is affected by several aspects: The correlation between $\mathrm{Re}\,\mathcal{C}_i$ and $\rho_A^{K\pi}$ changes the strong phase in $\hat{\alpha}_4^c(K\pi)$ and, implicitly the SM contribution to this observable (see Equation 4.16). Further, a modification of the electroweak decay amplitude, even though suppressed, also contributes and solely depends on $\mathrm{Im}\,\mathcal{C}_i$. The most important correction originates from the interference of the SM tree-level with the new contribution to the QCD-penguin amplitude

$$\delta R_n^B(K\pi) \simeq -2\,\mathrm{Re}\,\tilde{r}_{\mathrm{QCD}}\,\mathrm{Re}\,r_{\mathrm{T}}\cos(\gamma + \delta_i)\,. \tag{6.32}$$

Such corrections do not occur in the expansion in Equation 4.16. Quadratic terms of the amplitude ratios r_i are small in the SM due to a suppression by either $\cos\gamma$ or the

colour-suppressed tree ratio r_{TC}, but the interference with the new corrections can be enhanced if δ_i is adjusted.

Before going into the details of our analysis, we like to comment on the similarity between operators with the flavour structure $\mathcal{O}^b = (\bar{s}b)\,(\bar{b}b)$ and $\mathcal{O}^s = (\bar{s}b)\,(\bar{s}s)$. Their analytic solutions to the RGE are equivalent and both operator classes lead to the same phenomenological observations. The only exception are decays that contain at least one ϕ or $\eta^{(\prime)}$ meson in the final state with either a $K^{(*)}$ for B_d or yet another ϕ or $\eta^{(\prime)}$ for B_s decays. These modes already receive leading order corrections to their hadronic matrix elements from the operators $\mathcal{O}^s$. Since we do not use data from these decays, the results of our analysis are applicable to the Wilson Coefficients of the operator $\mathcal{O}^s$, too.[4]

6.3.2 Fit results

We are now presenting the outcome of our model-independent fits, regarding an potential enhancement of the operators $\mathcal{O}^b = (\bar{s}b)\,(\bar{b}b)$. We focus on $\mathcal{O}_{11-13}$ and their χ-flipped counter parts, but all results can be applied, with respect to the Fierz transformations to all operators in Equation 6.21. Even an analysis with the operators $\mathcal{O}^s$ would lead to equivalent results. As in the case for the Z-penguin scenarios, we can make use of information from both (semi-)leptonic and hadronic decays. The results are presented by contour plots, in which we compare constraints from (semi-)leptonic observables (blue) with constraints from the combination of (semi-)leptonic and hadronic observables (red) at 68% and 95% probability. Due to the different dependence of the four potential spin configurations in the final state ($B \to PP, PV, VP, VV$), we use the hadronic decay system $B \to K\pi$, $K\rho$, $K^*\pi$, $K^*\rho$ in our fits. Significant pull values, ($|\delta| \geq 1.6$) and $\Delta\chi^2(\mathrm{SM})$ are collected in Table 6.8 and the key parameter $\xi_3^A(M_1M_2)$ to judge on the validity of the $\Lambda_{\mathrm{QCD}}/m_b$ expansion is listed for each scenario and decay system individually in Table 6.9.

The contour plots in which only one additional Wilson Coefficient was modified are shown in Figure 6.10 for the scenarios $\mathcal{C}_{11}$, $\mathcal{C}_{12}$, and $\mathcal{C}_{13}$ from top to down and for $\mathcal{C}_i$ vs. $\mathcal{C}_i'$ from left to right. The hierarchical impact of the individual Wilson Coefficients to the (semi-)leptonic decays, as was found in Equation 6.29, can be inferred from the blue contours. Compared to the red contours, it is evident that the real part of $\mathcal{C}_i$ is best constrained from (semi-)leptonic observables. Even for the $\mathcal{C}_{12}$ scenario, in which the contributions to $\alpha_4(M_1M_2)$ are largest and bounds from $b \to s(\gamma)\ell^+\ell^-$ are weakest, $\mathrm{Re}\,\mathcal{C}_{12}$ cannot be sufficiently restricted from hadronic decays alone. This confirms that $\mathrm{Re}\,\mathcal{C}_i$ can always be compensated through the additional degrees-of-freedom in the fit

[4] Due to $m_s \neq m_b$, the operators $\mathcal{O}^s$ and $\mathcal{O}^b$ also generate different contributions to all hadronic matrix elements at NLO. However, the higher-order corrections have mainly been introduced to reduce uncertainties from scale variation, which are equivalent for both operator insertions and their difference at NLO is phenomenological irrelevant. However, if one is interested in a sustainable analysis of these operators, constraints from the other decay modes should be included.

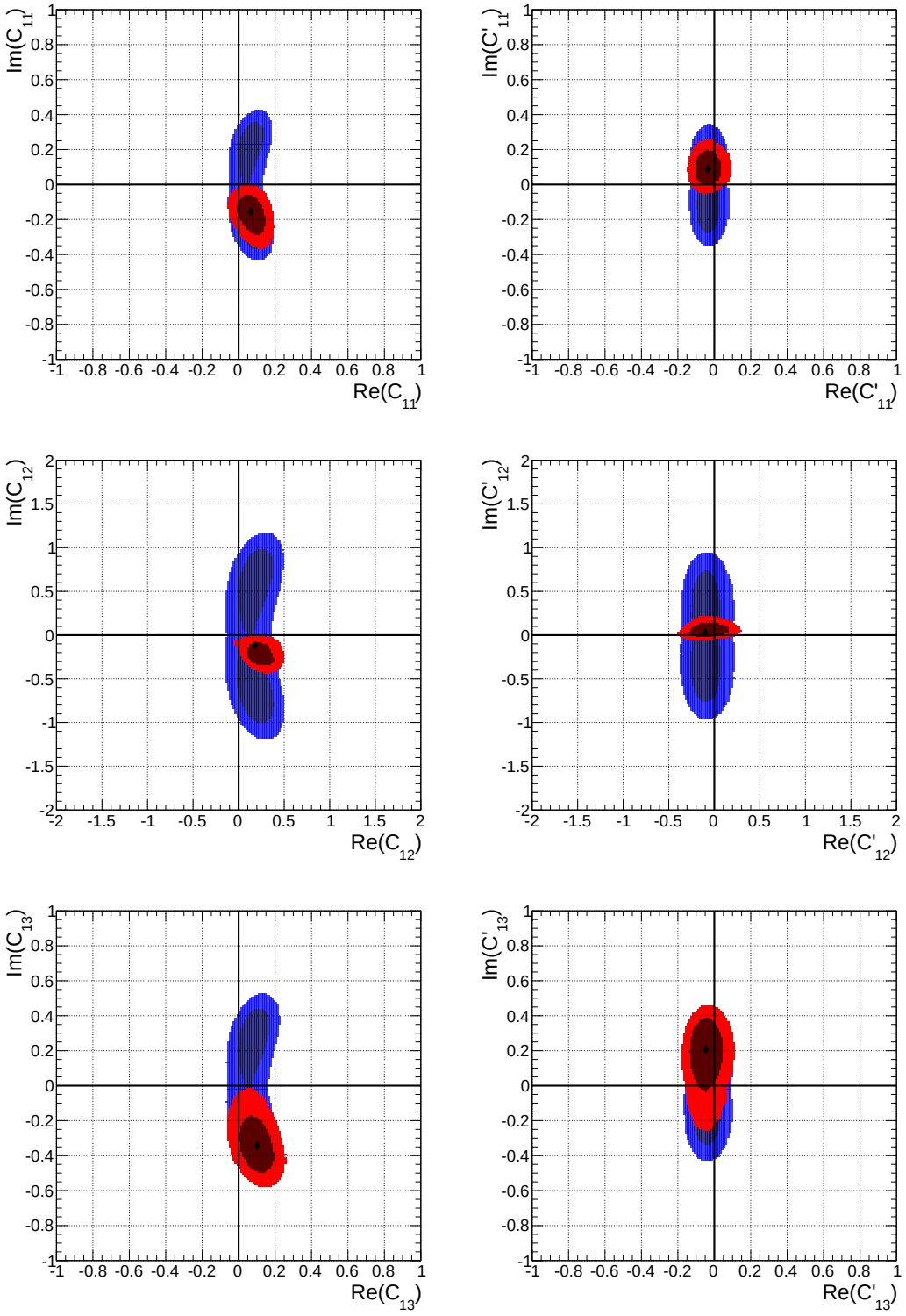

FIGURE 6.10: 68% and 95% CRs for the complex Wilson Coefficients $\mathcal{C}_{11}^{(\prime)}$, $\mathcal{C}_{12}^{(\prime)}$, and $\mathcal{C}_{13}^{(\prime)}$ in the scenarios with only one coefficient being modified. Constraints are obtained from observables of (semi-)leptonic only (blue) and from the combination of (semi-)leptonic and hadronic B-meson decays (red), whereas the decay systems $B \to K\pi$, $K\rho$, $K^*\pi$, $K^*\rho$ have been used. The ♦ corresponds to the best-fit point of the combined fit.

— the WA parameter $\rho_A^{M_1 M_2}$. The imaginary part of $\mathcal{C}_i$, however, is CP-violating and cannot be compensated by power-suppressed corrections. In particular, it is found that, at the probability of 68%, $\mathrm{Im}\,\mathcal{C}_i < 0$ and $\mathrm{Im}\,\mathcal{C}_i' > 0$, whereas for $\mathcal{C}_{11}$ and $\mathcal{C}_{13}$ the residual allowed region in the upper, respectively lower half of the imaginary plane coincide with the contour from $b \to s(\gamma)\ell^+\ell^-$. $\mathcal{C}_{12}$ is more restricting, as suggested by the hierarchy in Equation 6.27, and hadronic decays allow to further cut significantly on the parameter space. In addition, it seems to be that the χ-flipped Wilson Coefficients are stronger bounded. This pattern can be explained through the statistical dominance of the data in $B \to K\pi$, preferring a parity-anti-symmetric solution $\Delta\mathcal{C}_i = const.$, as described in Chapter 6.1.1. Constraints from $B \to K^*\pi$ and $B \to K\rho$ are contrary and prefer parity-symmetric configuration $\bar{\mathcal{C}}_i = const.$. Since the data for these decay systems favour $\mathrm{Im}\,\mathcal{C}_i < 0$, they are in conflict with $\mathrm{Im}\,\mathcal{C}_i' > 0$.

The contour plots in which both $\mathcal{C}_i$ and $\mathcal{C}_i'$ have been fitted together are displayed in Figure 6.11 for the scenario $\mathcal{C}_{11-11'}$, in Figure 6.12 for $\mathcal{C}_{12-12'}$, and in Figure 6.13 for $\mathcal{C}_{13-13'}$. The statistical importance of the (semi-)leptonic observables for $\mathrm{Re}\,\mathcal{C}_i^{(\prime)}$ is evident from the $\mathrm{Re}\,\mathcal{C}_i - \mathrm{Re}\,\mathcal{C}_i'$ correlation plot in the respective lower left panels. The suggested solution to solve the tension in $\langle P_5' \rangle_{[1,6]}$, $\mathrm{Re}\,\bar{\mathcal{C}}_i = 0$, presented by a line through zero with gradient -1, is apparent. The parity-anti-symmetric solution for $\mathrm{Im}\,\bar{\mathcal{C}}_i$ is also presented by a line with gradient -1, but for the correlation plot $\mathrm{Im}\,\mathcal{C}_i - \mathrm{Im}\,\mathcal{C}_i'$ in the lower right panel. Contrary to the single dominant operator scenarios, rather crossing the SM point, $\mathrm{Im}\,\bar{\mathcal{C}}_i = 0$, the data prefer some offset δ, which implies that the sign of $\mathrm{Im}\,\mathcal{C}_i'$ is not fixed any longer. This can be explained by the fact that the additional degree-of-freedom is used to explain the data in $B \to K\pi$ with large effects in $\mathcal{C}_i$ and a compensating effect in $\mathcal{C}_i'$, to avoid tensions in the decay systems $B \to K\rho$ and $B \to K^*\pi$. These two observations explains why $\mathrm{Re}\,\mathcal{C}_i - \mathrm{Im}\,\mathcal{C}_i$ plots (upper left panels) are qualitative similar, but the $\mathrm{Re}\,\mathcal{C}_i' - \mathrm{Im}\,\mathcal{C}_i'$ plots tilted, compared to contour regions in the single dominant operator analysis.

We give bounds on the individual Wilson Coefficients, which have been obtained from the 1-dimensional posterior probability at the probability of 95%. To be conservative, we used the combined operator scenarios, which, in general, lead to larger allowed parameter regions than the single dominant operator scenarios, to find the following bounds

$$
\begin{aligned}
&\mathrm{Re}\,\mathcal{C}_{11} \in [\ \ 0.01;\ \ 0.23]\,, \quad \mathrm{Re}\,\mathcal{C}_{12} \in [\ \ 0.02;\ 0.56]\,, \quad \mathrm{Re}\,\mathcal{C}_{13} \in [\ \ 0.00;\ 0.22]\,,\\
&\mathrm{Im}\,\mathcal{C}_{11} \in [-0.41;\ -0.01]\,, \quad \mathrm{Im}\,\mathcal{C}_{12} \in [-0.46;\ 0.00]\,, \quad \mathrm{Im}\,\mathcal{C}_{13} \in [-0.59;\ 0.05]\,,\\
&\mathrm{Re}\,\mathcal{C}_{11}' \in [-0.25;\ \ 0.04]\,, \quad \mathrm{Re}\,\mathcal{C}_{12}' \in [-0.52;\ 0.14]\,, \quad \mathrm{Re}\,\mathcal{C}_{13}' \in [-0.29;\ 0.12]\,,\\
&\mathrm{Im}\,\mathcal{C}_{11}' \in [-0.16;\ \ 0.24]\,, \quad \mathrm{Im}\,\mathcal{C}_{12}' \in [-0.20;\ 0.34]\,, \quad \mathrm{Im}\,\mathcal{C}_{13}' \in [-0.21;\ 0.38]\,.
\end{aligned}
$$

The qualitative features, which have been discussed above, can be confirmed. The

allowed interval in Equation 6.33 approve in particular that $\mathrm{Im}\,\mathcal{C}_i'$ is stronger constrained than $\mathrm{Im}\,\mathcal{C}_i$ and $\mathrm{Re}\,\mathcal{C}_i^{(\prime)}$ is stronger constrained as $\mathrm{Im}\,\mathcal{C}_i^{(\prime)}$, whereas $\mathrm{Re}\,\mathcal{C}_i^{(\prime)}$ follows the pattern, dictated by observables from (semi-)leptonic decays and $\mathrm{Im}\,\mathcal{C}_i \leq 0$ is almost fulfilled for all three Wilson Coefficients and at the probability of 95%.

The χ-flipped scenarios $\mathcal{C}_i'$ are less well suited to accommodate the data. That is reflected in the individual $\Delta\chi^2(\mathrm{SM})$, listed in Table 6.8. Although no large pull values in neither $B \to K\rho$ nor $B \to K^*\pi$ occur, the allowed parameter range is tightly restricted, such that other tensions cannot be resolved, leading to substantially smaller improvement compared to $\Delta\chi^2(\mathrm{SM})$ for the $\mathcal{C}_i$ scenarios.

In detail, the most serious tension for the (semi-)leptonic decay system occurs for the observable $\langle P_5' \rangle_{[1,6]}$, which indeed can be relaxed within the $\mathcal{C}_i$ and $\mathcal{C}_i - \mathcal{C}_i'$ scenarios, though for the price of an increasing discrepancy in $\mathcal{B}(B \to K^*\ell^+\ell^-)$. If in addition the polarisation fraction measurements from the BaBar and Atlas collaboration, which in order to be conservative were removed as constraints (see Chapter 4.2.1), are taken into account, the parity-anti-symmetric solution would be pushed to larger values and the pull value of $\langle P_5' \rangle_{[1,6]}$ would decrease to roughly 1.0σ, but for the branching ratio of $B \to K^*\ell^+\ell^-$ further increase to worrying 2.0σ.

The hadronic decay systems, in particular $B \to K\pi$, suffers from the tension in $\Delta A_{\mathrm{CP}}^{K\pi}$. The solution suggested in the theory section (see Equation 6.31) is limited due to an universal shift in all CP asymmetries and especially for the asymmetry in $B^- \to \bar{K}^0\pi^-$, which is rather well measured and compatible with zero. In order to display the limitation of explaining $\Delta A_{\mathrm{CP}}^{K\pi}$, we quote $C(B^- \to \bar{K}^0\pi^-)$ at the best-fit point for the $\mathcal{C}_{12}$ and $\mathcal{C}_{12}'$ scenarios, together with the corresponding asymmetry in $B \to K^*\pi$

$$
\begin{aligned}
C(B^- \to \bar{K}^0\pi^-) &= 1.5^{+1.9}_{-1.9}\,\%, & C(B^- \to \bar{K}^{*0}\pi^-) &= 3.8^{+4.2}_{-4.2}\,\%, & &\text{HFAG,}\\
C(B^- \to \bar{K}^0\pi^-) &= -0.7^{+0.2}_{-0.2}\,\%, & C(B^- \to \bar{K}^{*0}\pi^-) &= -0.6^{+0.3}_{-0.3}\,\%, & &\text{SM,}\\
C(B^- \to \bar{K}^0\pi^-) &= 4.1^{+1.5}_{-1.4}\,\%, & C(B^- \to \bar{K}^{*0}\pi^-) &= 2.8^{+2.1}_{-1.5}\,\%, & &\mathcal{C}_{12},\\
C(B^- \to \bar{K}^0\pi^-) &= 0.8^{+0.5}_{-0.5}\,\%, & C(B^- \to \bar{K}^{*0}\pi^-) &= -2.0^{+0.4}_{-0.7}\,\%, & &\mathcal{C}_{12}',
\end{aligned}
\tag{6.33}
$$

On the one hand, it can be seen that the anti-correlation due to χ-flipped operators among $B \to PP$ and $B \to PV$ modes is responsible for the unprimed scenarios being favoured compared to the primed scenarios. On the other hand, the allowed amount of CP violation in the QCD-penguin amplitude is limited through the precise measurement of $C(B^- \to \bar{K}^0\pi^-)$, such that the $\Delta A_{\mathrm{CP}}^{K\pi}$ puzzle cannot be fully resolved. However, it is still not unlikely that a combination of an enhanced power-suppressed correction in HS amplitudes together with NP contributions is at work. The tension for the ratio of

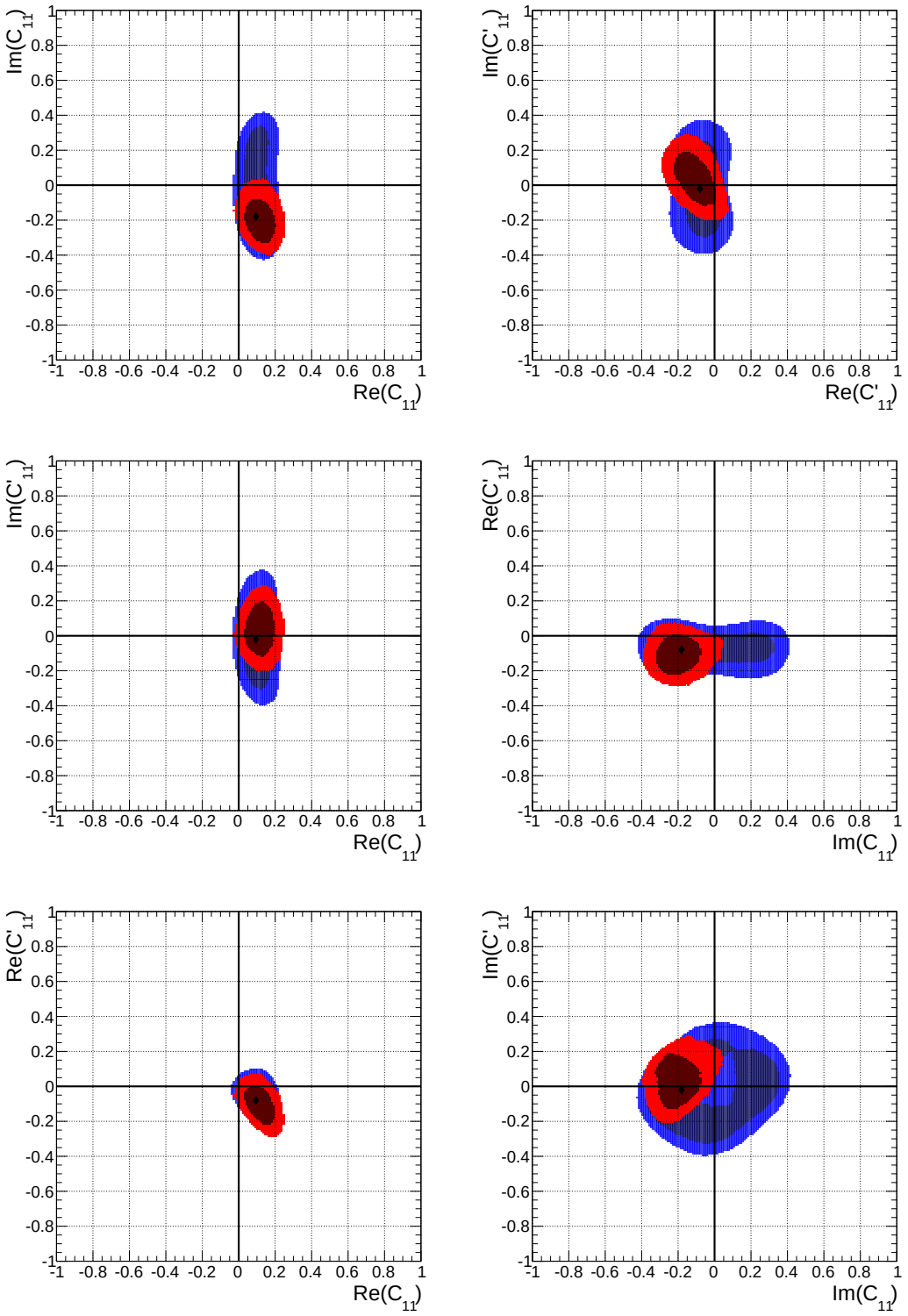

FIGURE 6.11: 68% and 95% CRs for the complex Wilson Coefficients $\mathcal{C}_{11}^{(\prime)}$ in the scenarios with both coefficients being simultaneously fitted. Constraints are obtained from observables of (semi-)leptonic only (blue) and from the combination of (semi-)leptonic and hadronic B-meson decays (red), whereas the decay systems $B \to K\pi$, $K\rho$, $K^*\pi$, $K^*\rho$ are used. The ♦ corresponds to the best-fit point of the combined fit.

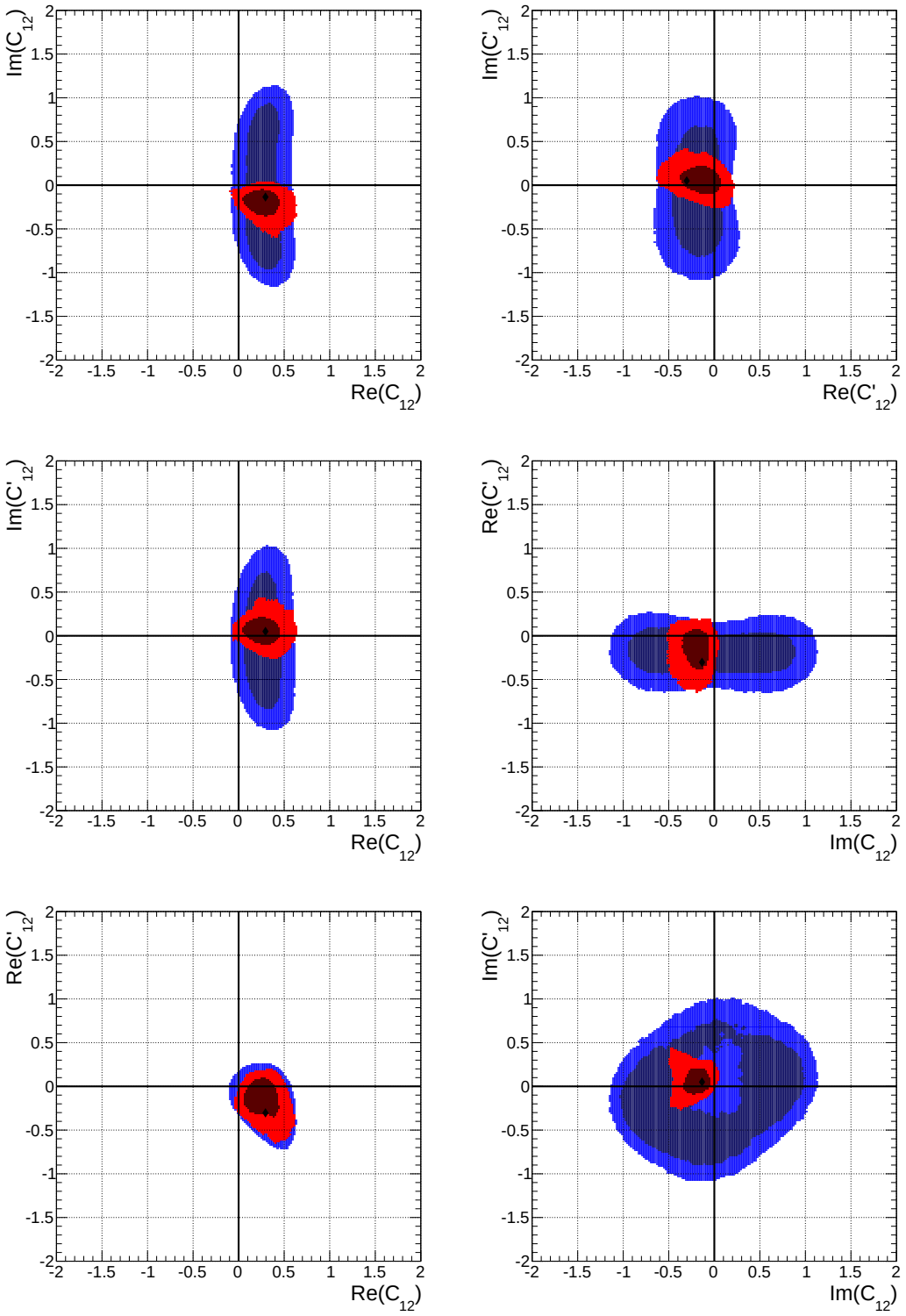

FIGURE 6.12: 68% and 95% CRs for the complex Wilson Coefficients $\mathcal{C}_{12}^{(\prime)}$ in the scenarios with both coefficients being simultaneously fitted. Constraints are obtained from observables of (semi-)leptonic only (blue) and from the combination of (semi-)leptonic and hadronic B-meson decays (red), whereas the decay systems $B \to K\pi$, $K\rho$, $K^*\pi$, $K^*\rho$ are used. The ♦ corresponds to the best-fit point of the combined fit.

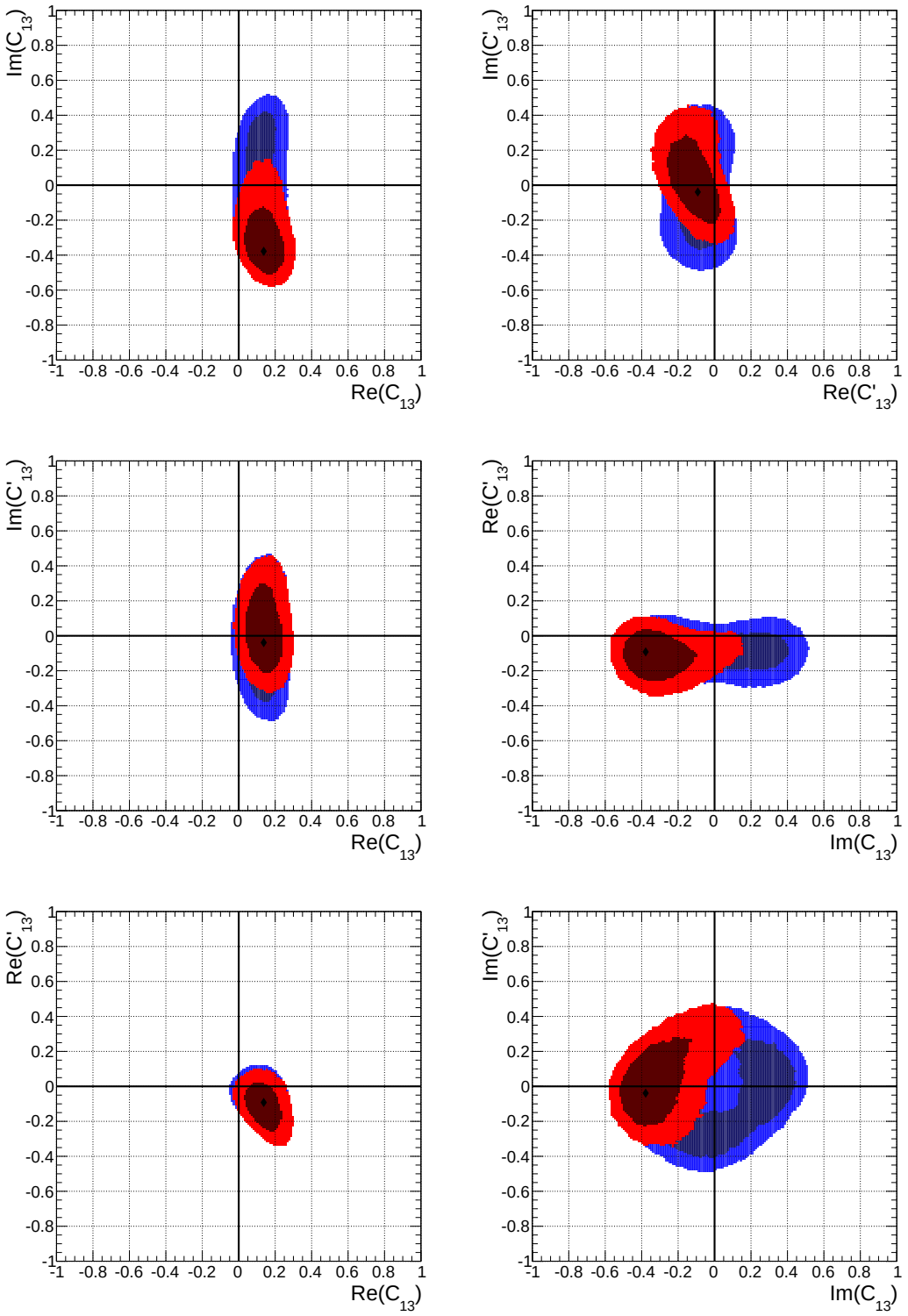

FIGURE 6.13: 68% and 95% CRs for the complex Wilson Coefficients $\mathcal{C}_{13}^{(\prime)}$ in the scenarios with both coefficients being simultaneously fitted. Constraints are obtained from observables of (semi-)leptonic only (blue) and from the combination of (semi-)leptonic and hadronic B-meson decays (red), whereas the decay systems $B \to K\pi$, $K\rho$, $K^*\pi$, $K^*\rho$ are used. The ♦ corresponds to the best-fit point of the combined fit.

$B \to M_1 M_2$ & $B \to K^* \ell^+ \ell^-$							
	$\mathrm{Re}\,\mathcal{C}_i^{(\prime)}$, $\mathrm{Im}\,\mathcal{C}_i^{(\prime)}$	$\Delta A_{\mathrm{CP}}^{K\pi}$	$R_n^B(K\pi)$	$\langle A_{\mathrm{FB}}\rangle_{[1,6]}$ [97]	$\langle P_5'\rangle_{[1,6]}$ [104]	$\mathcal{B}(K^* ll)_{[>16]}$ [95]	$\Delta\chi^2(SM)$
SM		$\mathbf{-2.8\sigma}$	$\mathbf{-1.9\sigma}$	-1.4σ	$\mathbf{2.2\sigma}$	0.5σ	
$\mathcal{C}_{11}$	0.07, −0.16	$\mathbf{-2.2\sigma}$	-0.3σ	$-1.5\sigma\,(-1.5\sigma)$	$\mathbf{1.8\sigma}\,(\mathbf{1.7\sigma})$	$0.8\sigma\,(0.7\sigma)$	11
$\mathcal{C}_{11'}$	−0.04, 0.09	$\mathbf{-2.4\sigma}$	-0.6σ	$-1.4\sigma\,(-1.4\sigma)$	$\mathbf{2.2\sigma}\,(\mathbf{2.2\sigma})$	$0.7\sigma\,(0.6\sigma)$	7
$\mathcal{C}_{11-11'}$	0.09, −0.18 −0.08, −0.02	$\mathbf{-2.2\sigma}$	-0.2σ	$\mathbf{-1.6\sigma}\,(-1.5\sigma)$	$\mathbf{1.6\sigma}\,(1.5\sigma)$	$1.4\sigma\,(1.2\sigma)$	13
$\mathcal{C}_{12}$	0.18, −0.12	$\mathbf{-2.2\sigma}$	-0.2σ	$-1.5\sigma\,(-1.5\sigma)$	$\mathbf{1.8\sigma}\,(\mathbf{1.7\sigma})$	$1.0\sigma\,(0.7\sigma)$	11
$\mathcal{C}_{12'}$	−0.10, 0.03	$\mathbf{-2.5\sigma}$	-0.8σ	$-1.4\sigma\,(-1.4\sigma)$	$\mathbf{2.2\sigma}\,(\mathbf{2.2\sigma})$	$0.7\sigma\,(0.6\sigma)$	5
$\mathcal{C}_{12-12'}$	0.29, −0.14 −0.30, 0.05	$\mathbf{-1.8\sigma}$	0.1σ	$\mathbf{-1.6\sigma}\,(-1.5\sigma)$	$1.5\sigma\,(1.5\sigma)$	$\mathbf{1.8\sigma}\,(\mathbf{1.2\sigma})$	14
$\mathcal{C}_{13}$	0.10, −0.34	$\mathbf{-2.2\sigma}$	-0.8σ	$-1.5\sigma\,(-1.5\sigma)$	$\mathbf{1.6\sigma}\,(\mathbf{1.7\sigma})$	$0.7\sigma\,(0.7\sigma)$	11
$\mathcal{C}_{13'}$	−0.05, 0.21	$\mathbf{-2.4\sigma}$	-0.9σ	$-1.4\sigma\,(-1.4\sigma)$	$\mathbf{2.2\sigma}\,(\mathbf{2.2\sigma})$	$0.5\sigma\,(0.6\sigma)$	7
$\mathcal{C}_{13-13'}$	0.14, −0.38 −0.09, −0.04	$\mathbf{-2.2\sigma}$	-0.7σ	$\mathbf{-1.6\sigma}\,(-1.5\sigma)$	$1.4\sigma\,(1.5\sigma)$	$1.2\sigma\,(1.2\sigma)$	13

TABLE 6.8: Compilation of best-fit points and pull values with $|\delta| \geq 1.6$ for the model-independent fits of the new operators $\mathcal{O}^b$. Pull values for fits with (semi-)leptonic data only are shown in parentheses.

branching fractions, $R_n^B(K\pi)$, cannot be accommodated through any enhanced power-corrections and, need to be explained through physics beyond the SM. This is indeed possible for scenarios with predominant contribution to the QCD-penguin amplitude. Both $\mathcal{C}_{11}$ and $\mathcal{C}_{12}$ scenarios are in spite of further constraints from $b \to s(\gamma)\ell^+\ell^-$, suitable to explain the discrepancy. Even the $\mathcal{C}_{13}$ scenarios can decrease the pull value below one standard deviations.

The difference between the $\mathcal{C}_{11^{(\prime)}}$, $\mathcal{C}_{12^{(\prime)}}$, and the $\mathcal{C}_{13^{(\prime)}}$ scenarios is also notably visible through the allowed ranges of the power-suppressed ratio $\xi_3^A(M_1M_2)$, listed in Table 6.9. Whereas it is possible that contributions from WA in, for instance $B \to K\pi$, become negligible for the former, they still need to be of the order $\xi_3^A(K\pi) \sim 0.30$ for the latter scenarios, which is comparable with the results of the model-independent and the enhanced Z-penguin analysis. The most significant effects are encountered for $\mathcal{C}_{12-12'}$ in which $\xi_3^A(K^*\pi) = 0.41$ could be reduced by a factor of 2, $\xi_3^A(K\rho) = 0.12$ by a factor of 7, and $\xi_3^A(K^*\rho) = 0.44$ by a factor of 3 compared to their SM values. As noted before, the lower limit for $\xi_3^A(K\pi) = 0$. Though $\hat{\alpha}_4^c(M_1M_2)$ is significantly modified, the large WA scenario in $B \to K\pi$ is still disfavoured. We have seen that the single dominant operator fits of the unprimed Wilson Coefficients are more suitable to explain the data than of the primed Wilson Coefficients. This preference is additionally supported from a stronger suppression of the power-suppressed ratios for the former scenarios. The best-fit points for the WA parameter obey for all decay systems and each scenario similar features as in SM. The phase is found to coincide with one of the two solutions, suggested by the SM fit and only the absolute value seems to vary, notably for $B \to K\pi$ and $B \to K\rho$. The only exception is $\rho_A^{K\pi}$ in $\mathcal{C}_{12-12'}$. Due to the large contributions from $\mathrm{Re}\,\Delta\mathcal{C}_{12} \sim 0.6$

	$K\pi$		$K^*\pi$		$K\rho$		$K^*\rho$	
	$\lvert\rho_A\rvert,\ \phi_A$	ξ_3^A	$\lvert\rho_A\rvert,\ \phi_A$	ξ_3^A	$\lvert\rho_A\rvert,\ \phi_A$	ξ_3^A	$\lvert\rho_A\rvert,\ \phi_A$	ξ_3^A
SM	$3.34, 2.71$	0.39	$1.61, 5.84$	0.89	$2.69, 2.68$	0.78	$1.56, 5.66$	1.33
$\mathcal{C}_{11}$	$2.79, 2.85$	[0.14, 0.42]	$1.48, 5.89$	[0.71, 1.28]	$1.30, 5.45$	[0.42, 1.35]	$2.32, 2.73$	[0.98, 1.82]
$\mathcal{C}_{11'}$	$3.04, 2.80$	[0.22, 0.48]	$1.72, 5.86$	[0.86, 1.49]	$2.70, 2.74$	[0.46, 1.32]	$1.56, 5.64$	[0.97, 1.92]
$\mathcal{C}_{11-11'}$	$2.53, 2.78$	[0.00, 0.43]	$1.54, 5.92$	[0.65, 1.47]	$2.59, 2.75$	[0.30, 1.69]	$2.28, 2.76$	[0.75, 2.03]
$\mathcal{C}_{12}$	$2.19, 2.71$	[0.00, 0.27]	$1.25, 5.85$	[0.47, 0.91]	$2.19, 2.68$	[0.21, 0.90]	$1.32, 5.66$	[0.86, 1.74]
$\mathcal{C}_{12'}$	$2.89, 2.70$	[0.14, 0.57]	$1.87, 5.90$	[0.72, 1.61]	$2.10, 5.57$	[0.41, 1.63]	$1.53, 5.67$	[0.75, 2.25]
$\mathcal{C}_{12-12'}$	$2.15, 2.07$	[0.00, 0.44]	$1.61, 5.92$	[0.41, 1.69]	$2.64, 2.75$	[0.12, 1.96]	$2.00, 2.86$	[0.44, 1.91]
$\mathcal{C}_{13}$	$3.15, 2.79$	[0.29, 0.48]	$1.64, 5.87$	[0.41, 1.42]	$2.58, 2.76$	[0.84, 1.36]	$1.55, 5.63$	[0.99, 2.03]
$\mathcal{C}_{13'}$	$3.24, 2.77$	[0.32, 0.52]	$1.65, 5.86$	[0.45, 1.44]	$2.76, 2.69$	[0.79, 1.37]	$1.57, 5.63$	[0.94, 1.94]
$\mathcal{C}_{13-13'}$	$3.10, 2.79$	[0.26, 0.52]	$1.62, 5.89$	[0.77, 1.48]	$1.50, 5.44$	[0.34, 1.52]	$1.53, 5.63$	[0.78, 2.11]

TABLE 6.9: Compilation of the best-fit points for $\rho_A^{M_1M_2}$ and ξ_3^A at the probability of 68%. The results are given for $B \to K\pi$, $K\rho$, $K^*\pi$, $K^*\rho$ and specified for the scenarios with additional operators, $\mathcal{O}^b$. As explained in Appendix A.5, the interval of ξ_3^A(NP) should be compared to ξ_3^A(SM) at the best-fit point of $\rho_A^{M_1M_2}$, listed in the first row.

to the QCD-penguin amplitude, $\phi_A^{K\pi} = 2.15$ leads to destructive interference between $\mathrm{Re}\,\alpha_4^c(K\pi)$ and $\mathrm{Re}\,\beta_3^c(K\pi)$, contrary to all other scenarios.

A further particularity for these models arises because of the strong interference between the power-suppressed corrections and NP contributions. We mentioned in Chapter 5.2.1 that the SM fit of the two pure WA-dominated decays $\bar{B}_d \to K^+K^-$ and $\bar{B}_s \to \pi^+\pi^-$ reveals completely different solutions. Although we do not doubt that WA effects could be different for these decays, it is interesting to study how the fit would change if the QCD-penguin Wilson Coefficients are modified. We therefore fitted $\rho_A^{\pi\pi}$ for $\bar{B}_s \to \pi^+\pi^-$ ($b \to s$ transition) again, whereas the Wilson Coefficients $\mathcal{C}_{11}^{(\prime)} - \mathcal{C}_{13}^{(\prime)}$ were fixed at their best-fit point of the combined scenarios. Since the strong phase cannot be extracted within QCDF for these modes, neither in SM nor in any NP models, we confine ourselves to quote the resulting 95% CR of $|\rho_A^{\pi\pi}|$ at $\phi_A^{\pi\pi} = 0$, compared to the result of the SM fit of $|\rho_A^{KK}|$ at $\phi_A^{KK} = 0$ ($b \to d$ transition)

$\bar{B}_d \to K^+K^-$	$\bar{B}_s \to \pi^+\pi^-$			
SM	SM	$\mathcal{C}_{11-11'}$	$\mathcal{C}_{12-12'}$	$\mathcal{C}_{13-13'}$
[0.0; 2.20]	[2.95; 4.45]	[2.55; 4.15]	[1.70; 2.80]	[2.90; 4.50]

The solution for the $\mathcal{C}_{13-13'}$ scenario does not change the fit significantly. The interval in $\mathcal{C}_{11-11'}$ and $\mathcal{C}_{12-12'}$ indeed strongly decreases and the latter actually overlaps with the SM interval of $\bar{B}_d \to K^+K^-$.

Before going into the details of phenomenological consequences of the above-discussed scenarios, we like to summarise our main results:

- The $\Delta A_{\rm CP}^{K\pi}$ puzzle cannot satisfactorily be explained in any of the scenarios. Further assumptions on power-corrections in HS amplitudes are needed. The tensions in $\langle P_5' \rangle_{[1,6]}$ and $R_n^B(K\pi)$ are, in particular for the unprimed and combined scenarios, well described, implying a strong preference for $\mathcal{C}_i$ compared to $\mathcal{C}_i'$.
- The largest contributions to hadronic decays can be expected from $\mathcal{C}_{11}^{(\prime)}$, $\mathcal{C}_{12}^{(\prime)}$ and to (semi-)leptonic decays from $\mathcal{C}_{11}^{(\prime)}$, $\mathcal{C}_{13}^{(\prime)}$. Although the effects from the latter Wilson Coefficients to for instance $B \to K\pi$ are small, information from hadronic decays are still suitable to constrain the imaginary part of the complex parameter space.
- The modification of $\mathcal{C}_{11}^{(\prime)}$ and $\mathcal{C}_{12}^{(\prime)}$ implies corrections to the QCD-penguin amplitude $\alpha_4^c(M_1M_2)$ and thereby a strong correlation between $\beta_3^c(M_1M_2)$ and the new Wilson Coefficients. These scenarios enforce a simultaneously fit of NP and WA parameters, supporting our approach.

6.3.3 Observable predictions

We are making predictions for several different kind of observables, which will help us to distinguish the individual scenarios through future measurements. We listed some CP asymmetries for $B \to K^*\ell^+\ell^-$ in the lower part of Table 6.10. It can be seen that all observables, except for $\langle P_8'^{\rm CP} \rangle_{[1,6]}$, behave SM-like for contributions to the unprimed Wilson Coefficients. Contributions to the primed Wilson Coefficients can lead to significant deviations, especially for $\langle H_{\rm T}^{4,5} \rangle$. The respective extent of the effects to the individual observables, $\hat{\mathcal{O}}$, mainly follows the pattern

$$\hat{\mathcal{O}}(\mathcal{C}_{13}^{(\prime)}) > \hat{\mathcal{O}}(\mathcal{C}_{11}^{(\prime)}) > \hat{\mathcal{O}}(\mathcal{C}_{12}^{(\prime)}), \tag{6.34}$$

as anticipated in the theory section (see Equation 6.27 and Equation 6.29) and confirmed by our fits. The pattern for hadronic observables is different. We listed in the upper part of Table 6.10 the mixing-induced CP asymmetries $\Delta S(M_1M_2)$ for several B_d decays. The effects from $\mathcal{C}_{13}^{(\prime)}$ are small. Indeed, the predictions can exceed within uncertainties the interval of the SM prediction, but their central values are indistinguishable from the SM background. However, the effects from $\mathcal{C}_{11}^{(\prime)}$ and $\mathcal{C}_{12}^{(\prime)}$ can become significant and we find

$$\Delta S(\mathcal{C}_{11}^{(\prime)}) \sim \Delta S(\mathcal{C}_{12}^{(\prime)}) \gg \Delta S(\mathcal{C}_{13}^{(\prime)}). \tag{6.35}$$

This means that scenarios with a modification of either $\mathcal{C}_{11}^{(\prime)}$ or $\mathcal{C}_{12}^{(\prime)}$ will be hard to distinguish from each other when studying hadronic observables and we have to rely on data from (semi-)leptonic decays. Fortunately, the mentioned anti-correlation between different spin configurations in the final state can be utilised to at least distinguish scenarios with right-handed from left-handed flavour violation. According to the dominance

$B \to M_1 M_2$	$\Delta S(K\pi)$	$\Delta S(K\rho)$	$\Delta S(K^*\pi)$	$\Delta S_L(K^*\rho)$	$\Delta S(K\eta')$	$\Delta S(K\omega)$	$\Delta S(K\phi)$	$\Delta S_L(K^*\phi)$
SM	[0.05, 0.13]	[−0.19, −0.04]	[0.06, 0.17]	[−0.15, 0.09]	[−0.01, 0.04]	[0.09, 0.17]	[0.01, 0.05]	[0.01, 0.04]
$\mathcal{C}_{11}$	$0.19^{+0.03}_{-0.05}$	$-0.02^{+0.06}_{-0.09}$	$0.23^{+0.03}_{-0.05}$	$0.06^{+0.19}_{-0.13}$	$0.07^{+0.08}_{-0.07}$	$0.19^{+0.07}_{-0.07}$	$0.10^{+0.07}_{-0.07}$	$0.08^{+0.08}_{-0.07}$
$\mathcal{C}_{11'}$	$0.15^{+0.05}_{-0.05}$	$-0.19^{+0.09}_{-0.10}$	$0.00^{+0.09}_{-0.11}$	$0.04^{+0.08}_{-0.17}$	$0.15^{+0.07}_{-0.09}$	$-0.05^{+0.17}_{-0.15}$	$-0.28^{+0.12}_{-0.12}$	$0.10^{+0.09}_{-0.04}$
$\mathcal{C}_{12}$	$0.23^{+0.03}_{-0.04}$	$0.09^{+0.08}_{-0.08}$	$0.26^{+0.02}_{-0.03}$	$0.14^{+0.06}_{-0.11}$	$0.10^{+0.16}_{-0.10}$	$0.21^{+0.03}_{-0.11}$	$0.24^{+0.01}_{-0.22}$	$0.08^{+0.09}_{-0.05}$
$\mathcal{C}_{12'}$	$0.15^{+0.05}_{-0.06}$	$-0.23^{+0.10}_{-0.11}$	$0.01^{+0.10}_{-0.11}$	$0.04^{+0.08}_{-0.17}$	$0.21^{+0.04}_{-0.18}$	$0.11^{+0.08}_{-0.08}$	$-0.90^{+0.88}_{-0.20}$	$0.16^{+0.06}_{-0.12}$
$\mathcal{C}_{13}$	$0.08^{+0.10}_{-0.03}$	$-0.07^{+0.06}_{-0.12}$	$0.08^{+0.12}_{-0.02}$	$0.00^{+0.10}_{-0.15}$	$0.05^{+0.03}_{-0.11}$	$0.14^{+0.06}_{-0.06}$	$0.03^{+0.06}_{-0.05}$	$-0.02^{+0.10}_{-0.02}$
$\mathcal{C}_{13'}$	$0.07^{+0.09}_{-0.03}$	$-0.09^{+0.04}_{-0.15}$	$0.06^{+0.10}_{-0.05}$	$0.02^{+0.06}_{-0.19}$	$0.05^{+0.02}_{-0.12}$	$0.13^{+0.04}_{-0.10}$	$0.00^{+0.07}_{-0.04}$	$-0.03^{+0.10}_{-0.02}$
$B \to K^*\ell^+\ell^-$	$\langle A^{\rm im}\rangle_{[1,6]}$	$\langle A^{\rm im}\rangle_{[14,16]}$	$\langle A^{\rm im}\rangle_{[>16]}$	$\langle H_{\rm T}^{4,5}\rangle_{[14,16]}$	$\langle H_{\rm T}^{4,5}\rangle_{[>16]}$	$\langle P_3^{\rm CP}\rangle_{[1,6]}$	$\langle P_6'^{\rm CP}\rangle_{[1,6]}$	$\langle P_8'^{\rm CP}\rangle_{[1,6]}$
SM	$\mathcal{O}(10^{-4})$	$\mathcal{O}(10^{-3})$	$\mathcal{O}(10^{-3})$	$\mathcal{O}(10^{-5})$	$\mathcal{O}(10^{-5})$	$\mathcal{O}(10^{-4})$	$\mathcal{O}(10^{-3})$	$0.01^{+0.00}_{-0.01}$
$\mathcal{C}_{11}$	SM	SM	SM	SM	SM	SM	SM	$-0.16^{+0.05}_{-0.06}$
$\mathcal{C}_{11'}$	$-0.01^{+0.01}_{-0.00}$	$0.03^{+0.02}_{-0.01}$	$0.03^{+0.01}_{-0.01}$	$-0.16^{+0.06}_{-0.06}$	$-0.15^{+0.06}_{-0.06}$	$0.01^{+0.01}_{-0.00}$	$0.00^{+0.00}_{-0.01}$	$0.05^{+0.02}_{-0.02}$
$\mathcal{C}_{12}$	SM	SM	SM	SM	SM	SM	SM	$-0.08^{+0.02}_{-0.02}$
$\mathcal{C}_{12'}$	$0.00^{+0.00}_{-0.00}$	$0.01^{+0.00}_{-0.00}$	$0.01^{+0.00}_{-0.00}$	$-0.04^{+0.02}_{-0.02}$	$-0.04^{+0.02}_{-0.02}$	$0.00^{+0.00}_{-0.00}$	$-0.01^{+0.01}_{-0.01}$	$0.02^{+0.01}_{-0.01}$
$\mathcal{C}_{13}$	SM	SM	SM	SM	SM	SM	SM	$-0.24^{+0.06}_{-0.05}$
$\mathcal{C}_{13'}$	$-0.01^{+0.00}_{-0.00}$	$0.05^{+0.02}_{-0.02}$	$0.05^{+0.02}_{-0.02}$	$-0.25^{+0.10}_{-0.08}$	$-0.25^{+0.09}_{-0.08}$	$0.01^{+0.02}_{-0.00}$	$-0.01^{+0.01}_{-0.01}$	$0.08^{+0.03}_{-0.03}$

TABLE 6.10: Compilation of predictions for the $\mathcal{C}_{11}^{(\prime)}$, $\mathcal{C}_{12}^{(\prime)}$, and $\mathcal{C}_{13}^{(\prime)}$ scenarios

of the data in $B \to K\pi$ in the fit, we find the following pattern

$$\begin{aligned} \delta(\Delta S(\mathcal{C}_i)) &\sim \quad \delta(\Delta S(\mathcal{C}_i')) \qquad \text{for PP, VV,} \\ \delta(\Delta S(\mathcal{C}_i)) &\sim -\delta(\Delta S(\mathcal{C}_i')) \qquad \text{for PV, VP,} \end{aligned} \tag{6.36}$$

in which δ represents the difference between the SM and NP predictions. In some cases the predictions for $\Delta S(M_1M_2)$, as it is the case for $\Delta S(K\phi)$ or $\Delta S(K\eta')$ within the $\mathcal{C}_{12}'$ scenario, allow for huge ranges. However, $\rho_A^{M_1M_2}$ is loosely constrained in these decay modes, as one can see from the SM fits in Appendix B. If these observables are instead used as constraint in the fit, they would not lead to further restrictions of the NP parameter space, but rather for $\rho_A^{M_1M_2}$, as we have tested. More suitable are decay systems in which the power-suppressed corrections can be robustly extracted. With respect to this, $\Delta S(K\pi)$ and $\Delta S(K\rho)$ are promising candidates to identify NP contributions to the QCD-penguin decay amplitude. Their correlation is presented in the histograms, shown in the upper panel of Figure 6.14, where we plotted from left to right the predictions from the $\mathcal{C}_{11^{(\prime)}}$, $\mathcal{C}_{12^{(\prime)}}$ and, $\mathcal{C}_{13^{(\prime)}}$ scenarios, comparing contributions from left-handed (red) against right-handed (blue) flavour violation. The lower two panels show the prediction of the so far unmeasured direct and mixing-induced CP asymmetries in $\bar{B}_s \to \phi_L\phi_L$ and $\bar{B}_s \to \bar{K}_L^{*0}K_L^{*0}$. Since decays into purely longitudinal-polarised vector modes do not distinguish between left- and right-handed flavour violation, we confine to the former scenarios as had been favoured by the data. Furthermore, we decided to predict observables from longitudinal-polarised modes because of their scaling property, implying less sensitivity to power corrections. We can see that the predictions, at least from the $\mathcal{C}_{11^{(\prime)}}$ and $\mathcal{C}_{12^{(\prime)}}$ scenarios, can significantly vary from their SM value because

WA is only inferred from branching-ratio and polarisation-fraction measurements and not well constrained for these decay modes. Power corrections for, e.g., $\bar{B}_s \to \bar{K}^{*0}K^{*0}$, as quantified for the SM in Table 5.2, can become larger as the QCD-penguin amplitude, which complicates a accurate determination of the strong phase in $\hat{\alpha}_4(K^*K^*)$ and causes two solutions to the direct CP asymmetry, though the fit reveals a defined weak phase. Such a phenomena does not occur for the decay $\bar{B}_s \to \phi_L\phi_L$, for which WA contributions are less important. Although the impact on those observables are large, the scenarios $\mathcal{C}_{11}$ and $\mathcal{C}_{12}$ could be clearly verified, but not falsified. The predictions from all three scenarios also allow for the possibility of no CP violation, which, if experimentally established, would rather constrain WA than NP.

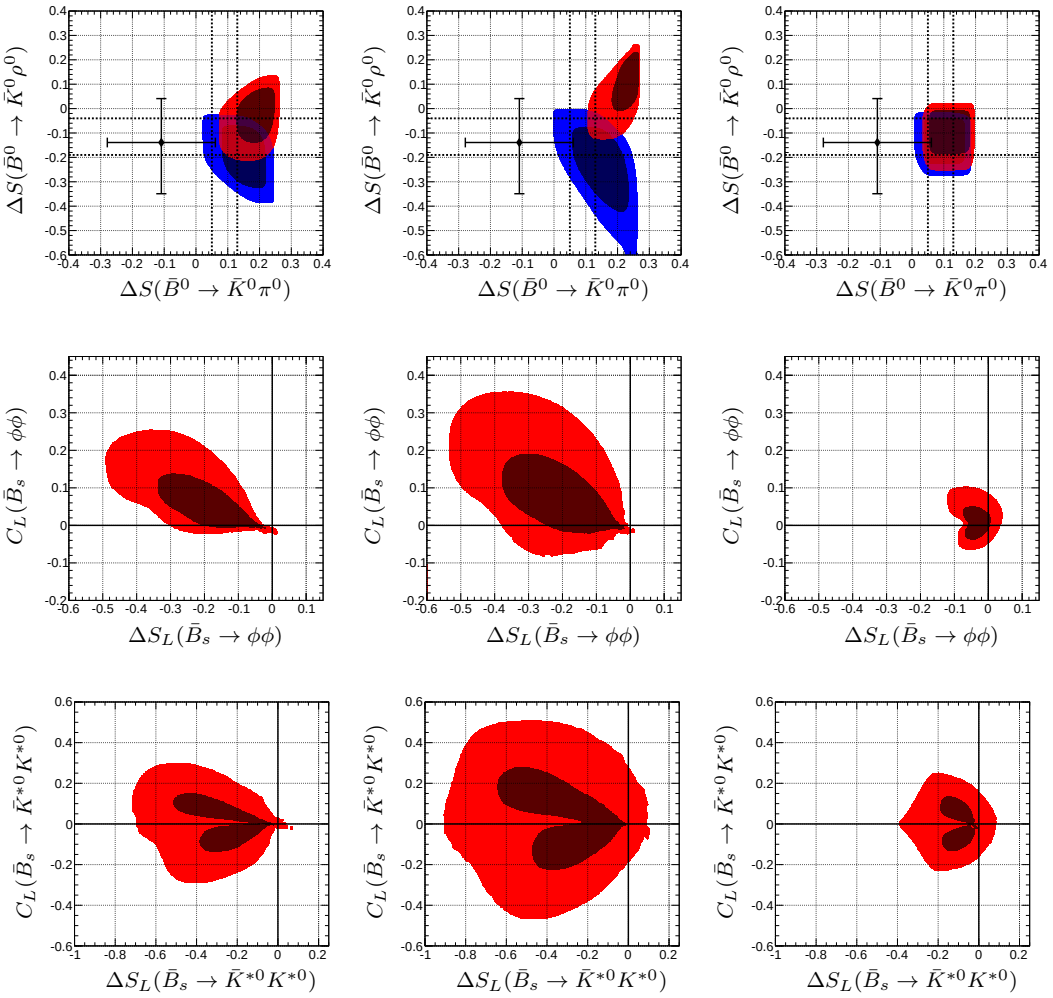

FIGURE 6.14: Correlations among the predictions for ΔS in $\bar{B}^0 \to \bar{K}^0\pi^0$ vs. $\bar{B}^0 \to \bar{K}^0\rho^0$ (upper panels), ΔS_L vs. C_L in both $\bar{B}_s \to \phi\phi$ (middle panels) as well as in $\bar{B}_s \to \bar{K}^{*0}K^{*0}$ (lower panels) at the probability of 68% and 95%. The results are obtained from left to right for modifications of $\mathcal{C}_{11}$, $\mathcal{C}_{12}$, and $\mathcal{C}_{13}$ (red) and for their χ-flipped counterparts (blue). Experimental central values and 1σ uncertainty interval from HFAG are shown for those observables that have already been measured — represented by solid black lines. The dotted black lines show the prediction interval at 68% probability obtained from a SM fit.

Part III

Conclusions

Chapter 7

Outlook & Conclusions

Calculating the matrix elements of the decay of a B meson into two light hadronic final states is a rather complicated problem due to the current incalculability of the QCD interaction at low-energy scales. The development of QCD factorisation by Beneke, Buchalla, Neubert, and Sachrajda, as a systematic approach to calculate these from first principles to arbitrary order in the strong gauge coupling α_s and to leading order in the expansion of the b-quark mass, was a substantial progress and led to for example many phenomenological studies ([28] more than 1000 citations). Predictions for hadronic observables are thereby mainly limited through power corrections, which naively scale like $\Lambda_{\rm QCD}/m_b \sim 10{-}20\,\%$. The largest contributions originate from hard-spectator scattering and weak annihilation. Their consideration became indeed indispensable for a sensible description of the data. About 15 years after the development of QCD factorisation, further effort were put into the calculation of higher-order radiative corrections to the tree-level and QCD-penguin matrix elements, whereas the latter is still work in progress. However, a reliable approach to consistently incorporate power corrections is still lacking. The impact of these corrections on the individual observables are typically uncorrelated included in the total error budget, even for those that stem from the same decay mode, and might be estimated too large. So far, the abundance of hadronic observables has mostly been measured during the last decade by the BaBar and Belle collaborations and, since a few years and for certain decay modes, also from the LHCb experiment at the LHC. Forthcoming experiments, as Belle II, and the upgrades of the LHCb detector will allow to push these measurements to a rather high precision. To gain further benefits from hadronic observables, a more suitable way to approximate these power corrections is mandatory.

We suggested in this work to extract weak annihilation contribution from experimental data, whereas one universal weak annihilation parameter was assumed for those QCD-penguin-dominated decay amplitudes whose initial and final states are related via $(u \leftrightarrow d)$ quark exchange. The tremendous reduction of uncertainty thereby allows us,

on the one hand, to test QCD factorisation within the Standard Model and our assumption about universality and, on the other hand, to effectively search for indirect hints of physics beyond the Standard Model. The former aspect was studied in the first part of the phenomenological section of this thesis. Although, extracting weak annihilation from data have already been studied in the literature for certain decay modes and observables, a detailed analysis of all measured QCD-penguin-dominated decay modes, systematically classified among final state systems, have not been performed so far. Their weak annihilation contributions are numerically dominated by the same topology due to the hierarchy of Wilson Coefficients in $\beta_3^c(M_1M_2)$ and one might expect similar results of the individual fits. This could indeed be confirmed. Especially, the results for the decay modes $B \to K\pi$, $K\rho$, $K^*\pi$, $K^*\rho$ reveal two solutions with almost equal phases and similar absolute values for $\rho_A^{M_1M_2}$. Their contour regions overlap at the probability of 68% — even for $B \to K^*\rho$, for which, contrary to the others, the combination of branching and polarisation fractions, instead of branching fractions and CP asymmetries, dominate the combined fit. Furthermore, the upper range for the prior probability of $|\rho_A^{M_1M_2}|$ was only limited to be smaller than 8 and in principle allowed for huge corrections to the decay amplitude (more than twice as large as the leading QCD-penguin decay amplitude). It is all the more notable that the fits preferred solutions in which the decay amplitudes from weak annihilation are still reasonable small. This is a non-trivial outcome of our fits. We quantified the relative amount of power corrections, needed to explain the data, by the ratio $\xi_3^A(M_1M_2)$. Since $\alpha_4^c(M_1M_2)$ with at least one vector meson in the final state is accidentally smaller, the best-measured $B \to PP$ decay mode, $B \to K\pi$, seems to be most suitable to define a benchmark whether the expansion in $\Lambda_{\rm QCD}/m_b$ is reliable. We found $\xi_3^A(K\pi) \in [0.37; 0.54]$ at the probability of68%, which can yet significantly decrease by the upcoming NNLO calculations of the QCD-penguin amplitude.

Our assumption that final state systems that are related via $(u \leftrightarrow d)$ quark exchange obey similar hadronisation dynamics was then further tested. If the approach of universal weak annihilation contribution to these decay groups would not have been justified, we should have seen discrepancy in the data. However, the only system, in which we have found tensions, was $B \to K\pi$, reproducing the well-known $\Delta A_{\rm CP}^{K\pi}$ puzzle. This problem also occurs in QCD factorisation with conventional error estimation or within other approaches, which avail itself of symmetry arguments, and is unlikely to be caused by wrongly interpreted weak annihilation contributions. We showed a further alternative to solve this tension in the Standard Model through enhanced hard-spectator scattering interactions. This possibility could be approved in the future through large effects for the CP asymmetries $C(\bar{B}^0 \to \bar{K}^0\pi^0)$ and $C(\bar{B}_s \to K^0\pi^0)$. The ratio of branching ratio $R_n^B(K\pi)$ is less sensitive to other sources of power corrections and also obeys a small discrepancy, which was not discussed in the literature, so far. This observable will be

a suitable candidate to search for new-physics contributions as soon as the discrepancy will be confirmed by more data.

Although, universality might be valid under the above-described conditions or can even be expanded to the case of same final state decays, connecting certain B_s with B_d modes, universality is not expected in general. One example are the pure weak annihilation decays $\bar{B}_s \to \pi^+\pi^-$ and $\bar{B}_d \to K^+K^-$. Contrary to $|\rho_A^{KK}| \leq 2.20$, we have seen that $|\rho_A^{\pi\pi}| \geq 2.95$, need to be rather large and typically proposed values of $|\rho_A^{M_1M_2}| \sim 1.5 - 2.0$ cannot accommodate the data. This confirms our approach of fitting $\rho_A^{M_1M_2}$ rather than remaining to a fixed value and including power corrections as a potentially overestimated error.

The second part of this thesis considered the possibility of solving the previous detected tensions through additional contributions beyond the Standard Model. We did not study any particular model, but rather tried to find the structure of new-physics through model-independent fits, thereby, allowing certain effective couplings like Wilson Coefficients of the effective weak Hamiltonian or more fundamental Standard Model couplings to be enhanced. Such a procedure has the advantage that the effects of several concrete models can consequently be described simultaneously and bounds on effective couplings are easily projected onto any favoured model. At the same time, we do not have to bother about other constraints, which automatically arise in any particular model, and focus on a specific problem.

Since an adequate number of $b \to d$ triggered decay modes that would allow to extract the new-physics and weak annihilation parameter together, does not exist, we exclusively probed the possibility of additional contributions in $b \to s$ transition. Contrary to the Standard Model, we permit both left- and right-handed flavour violation. At the moment, the most accurate data is available for $B \to K\pi$ and due to the observed discrepancy, all considered scenarios were dominated by this decay system. The relation between, for instance, enhanced Wilson Coefficients therefore follows the pattern

$$\mathcal{C}_i \simeq -\mathcal{C}_i'.$$

In order to either approve or refute this hypothesis, more precise measurements are needed from other decay modes, especially from the $B \to VV$ modes like, $B \to K^*\phi$ and $B \to K^*\rho$. Whereas models with either preferred left- or right-handed flavour violation should effect all hadronic observables, the parity-anti-symmetric pattern with left- and right-handed flavour violation does not influence $B \to VP$ and $B \to PV$ decay modes, as $B \to K\rho$ and $B \to K^*\pi$, explaining the importance of decays with two vector mesons in the final state.

Our first analysis was dedicated to an enhancement of the QED-penguin Wilson Coefficients. At the beginning, we showed that our approach indeed imply qualitative

different results compared to conventional QCD factorisation. The latter approach yield a contour region for a $\mathcal{C}_7$ fit that allowed for two different CP-violating phases. This seems to be suspicious, considering that we tried to solve a discrepancy in only one CP asymmetry. Indeed, taking power corrections uncorrelated into account covers the effects from physics beyond the Standard Model and their contributions can only be sharply extracted in a combined fit, supporting our ansatz. We further fitted systematically new-physics corrections to $\mathcal{C}_7$, $\mathcal{C}_9$ and their counterparts $\mathcal{C}_7'$, $\mathcal{C}_9'$. We found that new-physics in these Wilson Coefficients could still be as large as the Standard Model contribution to C_9. Most scenarios could properly account for the two discrepancies, whereas the data prefers models with new-physics in $\mathcal{C}_7$ and $\mathcal{C}_7'$. Surprisingly, these Wilson Coefficients were found to be almost purely real, which will be hard to approve by other, especially CP-violating, observables. At last, the amount of power corrections for the $\mathcal{C}_{77'}$ scenario could remarkably decrease to $\xi_3^A(K\pi) = 0.13$.

We further studied two new-physics scenarios that also affect decay modes triggered by $b \to s(\gamma)\ell^+\ell^-$. On the one hand, we allowed for contributions to the Standard Model Z-coupling to the $b \to s$ quark transition and, on the other hand, introduced new operators, $\mathcal{O}^b = (\bar{s}b)\,(\bar{b}b)$, contributing via mixing effects. Because (semi-)leptonic observables are dominated by QED-penguin operators, their observables reveal stronger constraints, but at the moment, most measured observables are insensitive to a CP-violating phase making hadronic constraints complementary. In detail, there is tension between semi-leptonic data and the SM prediction for $\langle P_5' \rangle\,(B \to K^*\ell^+\ell^-)$ in the bin $q^2 = [1,\,6]\,\mathrm{GeV}^2$, which could be resolved by additional contributions to the vectorial Wilson Coefficients. This discrepancy can be addressed within the extended operator basis scenarios, exclusively contributing to $\mathcal{C}_{9,V}$, but not for the enhanced Z-penguin model, contributing mainly to $\mathcal{C}_{10,A}$. The situation for $\Delta A_{\mathrm{CP}}^{K\pi}$ is unfortunately turned around. The new operators O^b mainly influence the QCD-penguin operators and are not well suited to solve this tensions, which is not the case for the Z-penguin scenario, modifying the QED-penguin Wilson Coefficients. Since $R_n^B(K\pi)$ can be resolved in both scenarios, $\Delta A_{\mathrm{CP}}^{K\pi}$ might also originate from enhanced power corrections in hard-spectator scattering interactions – even in the presence of certain new-physics scenarios.

The data prefers, on the one hand, a combination of left- and right-handed flavour-violating Z-couplings, for which the power correction ratio could decrease to $\xi_3^A(K\pi) = 0.30$ and, on the other hand, within the extended operator basis, a combined correction to $\mathcal{C}_{12}$ and $\mathcal{C}_{12}'$. The latter class of models dominantly change the QCD-penguin amplitude. Hence, tight correlations between new-physics and weak annihilation parameter are implied and actually even $\xi_3^A(K\pi) = 0$ is possible in this case.

For each of the three discussed classes of new-physics models, we exhaustively discussed at the end of each analysis, phenomenological implications of the sub-scenarios

under consideration and how they can be detected in prospective newly measured observables at the LHCb and Belle II. A data driven analysis, like the present one, need to be further tested in the future and assumptions might need to be adapted. Nevertheless, as long as it is not clear, how to incorporate power corrections from first principles, our approach, with eventually certain extended assumptions, is a suitable way to search for physics beyond the Standard Model in hadronic B-meson decays.

Appendix A

Statistical procedure

This appendix summarises the statistical methods that are used in order to obtain credibility regions for the parameters of interest, pull values of theory predictions and corresponding measurements of observables, and p-values as a measure of the goodness of fit. Further, we describe the determination of probability distributions of predictions for observables that were not included in the fit.

A.1 Credibility regions

For the purpose of parameter inference we use Bayes theorem to determine the posterior probability distribution, $P(\boldsymbol{\theta}|M, D)$, of the parameters of interest, $\boldsymbol{\theta} = (\theta_1, \theta_2, \ldots)$, given a model M and data D. Parameters of interest in our analysis are *i)* the phenomenological parameters of weak annihilation and hard spectator scattering $\rho_{A,H}^{M_1 M_2}$ and *ii)* parameters of new physics scenarios. Bayes theorem relates the posterior probability to the likelihood $\mathcal{L}(\boldsymbol{\theta}) = P(D|M, \boldsymbol{\theta})$, which is the probability of the data given the model M with parameter values $\boldsymbol{\theta}$ and the prior distributions, $P(M, \boldsymbol{\theta})$, which are the probability of model M with parameter values $\boldsymbol{\theta}$

$$P(\boldsymbol{\theta}|M, D) = \frac{P(D|M, \boldsymbol{\theta})\, P(M, \boldsymbol{\theta})}{Z} \qquad \text{and} \qquad Z \equiv \int P(D|M, \boldsymbol{\theta})\, P(M, \boldsymbol{\theta})\, d\boldsymbol{\theta}\,. \tag{A.1}$$

Here, the model-dependent normalisation factor Z is known as "evidence" or "marginal likelihood" that plays an important role in model comparison within the Bayesian approach. Throughout, the priors of the $\boldsymbol{\theta}$ are chosen as uniform within a certain interval.

It is common to introduce the likelihood function $\mathcal{L}(\boldsymbol{\theta})$ as the product of the probabilities $p(O_i = O_{i,\mathrm{th}}(\boldsymbol{\theta}))$ that each observable O_i in the data set takes the particular value $O_{i,\mathrm{th}}(\boldsymbol{\theta})$ predicted at the value of $\boldsymbol{\theta}$

$$\mathcal{L}(\boldsymbol{\theta}) = \prod_{i \in \text{data}} p\Big(O_i = O_{i,\mathrm{th}}(\boldsymbol{\theta})\Big) \sim \exp\left[-\frac{1}{2} \sum_{i \in \text{data}} \Big(\chi_i(\boldsymbol{\theta})\Big)^2\right]. \tag{A.2}$$

The probabilities p are given by the measured probability density functions pdf$[O_i]$ of each observable O_i and the second part of Equation A.2 indicates the special case of Gaussian distributed pdf's permitting to define a $\chi_i(\boldsymbol{\theta})$.

The expression of $\mathcal{L}(\boldsymbol{\theta})$ does not yet include the uncertainties due to nuisance parameters, $\boldsymbol{\nu} = (\nu_1, \nu_2, \ldots)$, which enter theoretical predictions of $B \to M_1 M_2$ decays as well as complementary constraints due to $b \to s(\gamma)\ell^+\ell^-$ decays. In this case, the nuisance parameters give rise to an interval for the theory prediction $[O_{i,\mathrm{th}} - \Delta^-_{i,\mathrm{th}},\, O_{i,\mathrm{th}} + \Delta^+_{i,\mathrm{th}}]$ with possibly asymmetric uncertainties $\Delta^\pm_{i,\mathrm{th}}$ around the central value $O_{i,\mathrm{th}}$ that is obtained for central values of all nuisance parameters. Usually, there is no unique or even no statistical interpretation of this interval. Here, the theoretical uncertainty $\Delta^\pm_{i,\mathrm{th}}$ is determined by adding in quadrature the uncertainties due to each nuisance parameter ν_a

$$\Delta^\pm_{i,\mathrm{th}} = \sqrt{\sum_a \left(\Delta^\pm_{i,a,\mathrm{th}}\right)^2}\,, \tag{A.3}$$

which arises from the minimal, central and maximal values $\nu_{a,\mathrm{min}}$, $\nu_{a,\mathrm{cen}}$ and $\nu_{a,\mathrm{max}}$, respectively,

$$\Delta^{+(-)}_{i,a,\mathrm{th}} = \left|O_{i,\mathrm{th}}(\nu_{a,\mathrm{max(min)}}) - O_{i,\mathrm{th}}(\nu_{a,\mathrm{cen}})\right|, \tag{A.4}$$

while keeping all others at their central values. Clearly, this is an approximation that neglects more complicated interdependence of observables on several parameters and also possible correlations among different nuisance parameters. The nuisance parameters are listed in Table 3.1 for $B \to M_1 M_2$ decays and further details concerning $b \to s(\gamma)\ell^+\ell^-$ are given in Chapter 4.2.1.

In the presence of nuisance parameters, we will adopt the simple procedure to use the maximal value of the pdf inside the interval of the theory prediction, hence replacing in Equation A.2

$$p\Big(O_i = O_{i,\mathrm{th}}(\boldsymbol{\theta})\Big) \quad \to \quad \max\left[p\Big(O_i \in [O_{i,\mathrm{th}} - \Delta^-_{i,\mathrm{th}},\, O_{i,\mathrm{th}} + \Delta^+_{i,\mathrm{th}}]\Big)\right], \tag{A.5}$$

where the dependence of $O_{i,\mathrm{th}}$ and $\Delta^\pm_{i,\mathrm{th}}$ on $\boldsymbol{\theta}$ and $\boldsymbol{\nu}$ is not explicitly shown. This procedure is implemented easily for Gaussian distributed pdf's by the modification of

the definition of

$$\chi_i(\boldsymbol{\theta},\boldsymbol{\nu}) = \begin{cases} \dfrac{\left|O_{i,\mathrm{th}}(\boldsymbol{\theta},\boldsymbol{\nu}) - O_{i,\mathrm{exp}}\right| - \Delta^{+}_{i,\mathrm{th}}(\boldsymbol{\theta},\boldsymbol{\nu})}{\sigma^{-}_{i,\mathrm{exp}}} & \text{if} \quad O_{i,\mathrm{exp}} \geq O_{i,\mathrm{th}} + \Delta^{+}_{i,\mathrm{th}}, \\ \dfrac{\left|O_{i,\mathrm{th}}(\boldsymbol{\theta},\boldsymbol{\nu}) - O_{i,\mathrm{exp}}\right| - \Delta^{-}_{i,\mathrm{th}}(\boldsymbol{\theta},\boldsymbol{\nu})}{\sigma^{+}_{i,\mathrm{exp}}} & \text{if} \quad O_{i,\mathrm{exp}} \leq O_{i,\mathrm{th}} - \Delta^{-}_{i,\mathrm{th}}, \\ 0 & \text{else.} \end{cases} \tag{A.6}$$

where $O_{i,\mathrm{exp}}$ and $\sigma^{\pm}_{i,\mathrm{exp}}$ denote the central value and the left and right standard deviation of the pdf$[O_i]$, respectively. The central value of the theoretical prediction $O_{i,\mathrm{th}}$ is obtained at the particular value of the parameters of interest $\boldsymbol{\theta}$ and the $\boldsymbol{\nu}$ are set to their central values.

Obviously, the modification of Equation A.6 is tailored to Gaussian pdf's, which is our interpretation of experimental world averages given by the Particle Data Group (PDG) [63] or Heavy Flavour Averaging Group (HFAG) [3]. However, the ratios of Gaussian distributed observables — like the ones defined in Equation 4.3: $R = \mathcal{B}_1/\mathcal{B}_2$ — follow a Gaussian ratio distribution. In the absence of experimental results of these ratios, one has to resort to the combination of the two Gaussian distributions of numerator and denominator. In all relevant cases, the $\mathcal{B}_i$ are Gaussian distributed with symmetric errors (from HFAG) and assuming that their errors are uncorrelated, the analytic expression of $p(R)$ is known [173]. Because it is monotonic rising till its maximum at $R_{\mathrm{max}} = \mathcal{B}_1/\mathcal{B}_2$ and then monotonic falling, the maximal value of the probability in the theory interval can be easily found by evaluating $p(R)$ at

$$R = \begin{cases} R_{i,\mathrm{th}} + \Delta^{+}_{i,\mathrm{th}} & \text{if} \quad \dfrac{\mathcal{B}_{1,\mathrm{exp}}}{\mathcal{B}_{2,\mathrm{exp}}} \geq R_{i,\mathrm{th}} + \Delta^{+}_{i,\mathrm{th}}, \\ R_{i,\mathrm{th}} - \Delta^{-}_{i,\mathrm{th}} & \text{if} \quad \dfrac{\mathcal{B}_{1,\mathrm{exp}}}{\mathcal{B}_{2,\mathrm{exp}}} \leq R_{i,\mathrm{th}} - \Delta^{-}_{i,\mathrm{th}}, \\ \dfrac{\mathcal{B}_{1,\mathrm{exp}}}{\mathcal{B}_{2,\mathrm{exp}}} & \text{else.} \end{cases} \tag{A.7}$$

The probability value is converted to $\chi = -2\log p(R)$. Let us finally note that the difference between the Gaussian ratio distribution and a Gaussian distribution with central value R and $\sigma(R)$ determined from simple uncertainty propagation calculus, is numerically negligible unless large deviations of experimental and theoretical values probe the tails of the distributions, which are "heavier" for the Gaussian ratio distribution.

Concerning the evaluation of the posterior probability, it is determined numerically with the help of the Markov Chain Monte Carlo (MCMC) implementation of the Bayesian Analysis Tool (BAT) [174]. One and two-dimensional posterior distributions

are obtained in turn by marginalisation over the remaining parameters of interest. The best-fit points are identified with the help of Minuit that is initialised with the point of the highest posterior found during the MCMC run.

A.2 Pull value

The deviation of a single measurement of an observable O_i from its prediction $O_{i,\mathrm{th}} \pm \Delta^{\pm}_{i,\mathrm{th}}$ for a particular value of the parameters of interest $\boldsymbol{\theta}_*$ will be given in terms of the pull value, taking into account the theoretical uncertainty. Here, we define the pull value as the integral over those regions of the pdf$[O_i]$, which have higher probability as the maximal probability value $p^{\max}(O_{i,\mathrm{th}}(\boldsymbol{\theta}_*))$ appearing in the interval spanned by the theory prediction $[O_{i,\mathrm{th}} - \Delta^{-}_{i,\mathrm{th}},\, O_{i,\mathrm{th}} + \Delta^{+}_{i,\mathrm{th}}]$ due to variation of the nuisance parameters

$$\delta = \int_{-\infty}^{+\infty} dO_i \, p(O_i) \, \theta[p(O_i) - p^{\max}] \tag{A.8}$$

where $\theta(x)$ denotes the step function. Consequently, the pull value is zero if the maximum of the pdf is inside this theory interval. In the case of a normally distributed pdf (with $\sigma^{+}_{i,\mathrm{exp}} = \sigma^{-}_{i,\mathrm{exp}}$), a non-zero pull implies a symmetric integration interval around the central value $O_{i,\mathrm{exp}}$ of the distribution and the integrated fraction of probability can be converted into the distance between the lower or upper boundary of the theory uncertainty interval to $O_{i,\mathrm{exp}}$ in terms of its standard deviation $\sigma_{i,\mathrm{exp}}$ depending on whether the theory prediction is above or below $O_{i,\mathrm{exp}}$. In the case of non-Gaussian pdf's, the pull value gives a measure of the probability fraction that corresponds to those values of O_i that have higher experimental probability than the ones contained in the interval of the theory prediction[1]. The pull value is simply calculated by drawing values for O_i that are distributed according to the pdf$[O_i]$ and taking the ratio of the cases in which $p(O_i) > p^{\max}(O_{i,\mathrm{th}}(\boldsymbol{\theta}_*))$ and the total number of draws.

A.3 p Value

As a measure of the goodness of fit, we will use p values in order to compare within the same theoretical model at some point $\boldsymbol{\theta}_*$ — usually the best-fit point(s) — the quality of the fit for different sets of data. For this purpose we will assume the model with the specific choice $\boldsymbol{\theta}_*$, allowing us to produce frequencies of possible outcomes within the model. We will use two ways to calculate p values.

[1] For very non-Gaussian pdf's with several disconnected regions of probability, the pull value might give rise to misleading interpretations, however, all measurements at hand are Gaussian or Gaussian ratio distributed.

The common definition is used as a first possibility, assuming the validity of normal and all independent pdf's. It consists in the evaluation of the cumulative of the χ^2-distribution — the latter denoted by $f(x, N_{\text{dof}})$, with N_{dof} number of degrees-of-freedom — starting from the value $\chi^2_* = -2 \log \mathcal{L}(\boldsymbol{\theta}_*)$

$$p = \int_{\chi^2_*}^{\infty} dx\, f(x, N_{\text{dof}})\,, \tag{A.9}$$

and corresponds to the probability of observing a test statistic at least as extreme in a χ^2 distribution with N_{dof}. Values of $p < 5\%$ are usually referred to as "statistical significant" deviation from the null hypothesis, i.e., the validity of the model with parameters $\boldsymbol{\theta}_*$. As usual, the number of degrees-of-freedom is given as $N_{\text{dof}} = (N_{\text{meas}} - \dim(\boldsymbol{\theta}))$, with N_{meas} denoting the number of measurements.

As a second possibility we calculate the p value defining a test statistics based on the likelihood [105]. The according frequency distribution is determined from 10^6 pseudo experiments in the lack of raw data and experimental efficiency corrections that require dedicated detector simulations. For this purpose, the pdf of each observable O_i is shifted such that the position of it's maximum at $O_i = O_{i,\text{exp}}$ coincides with the prediction $O_{i,\text{th}}(\boldsymbol{\theta}_*)$ at the point $\boldsymbol{\theta}_*$ of interest. In this way, the uncertainties of the measurement with central value $O_{i,\text{exp}}$ are adopted for $O_{i,\text{th}}(\boldsymbol{\theta}_*)$, neglecting possibly different experimental efficiency corrections. In each pseudo experiment, possible experimental outcomes are drawn for all measurements in the data set from the shifted pdf's and the likelihood value is compared to that of the observed data set, determining this way the fraction of pseudo experiments with smaller likelihood values. The p value is identified with this fraction, however for the number of degrees-of-freedom that corresponds to the number of measurements N_{meas} in the data set. Subsequently, we correct the p value by converting it to a χ^2 value with the help of the inverse cumulative distribution with N_{meas} degrees-of-freedom and recalculate it for the actual N_{dof} [175] using Equation A.9.

A.4 Probability distributions of observables

If certain observables are not yet measured or despite an existing measurement are not included in the data set D of the fit, one might obtain a prediction of its probability distribution given the data D and model M [105]. In the case of MCMC, we calculate the considered observables at each point of the Markov Chain for the current value of $\boldsymbol{\theta}$ and determine the interval of the theory uncertainty $[O_{i,\text{th}} - \Delta^-_{i,\text{th}},\, O_{i,\text{th}} + \Delta^+_{i,\text{th}}]$ due to nuisance parameters as described in Chapter A.1. The obtained intervals are subsequently normalised to their width $|\Delta^+_{i,\text{th}} + \Delta^-_{i,\text{th}}|$ and used to fill a histogram that is normalised eventually to obtain a probability distribution.

A.5 Size of power-suppressed corrections in new-physics models

The amount of power corrections in hadronic B-meson decays can be calculated in the Standard Model at each parameter point in the $\rho_{A,H}$ plane. Fitting these corrections to the data, we obtain a best-fit point $\boldsymbol{\theta}_*$ and the most likely value for the ratios $\xi^{A,H}(\boldsymbol{\theta}_*, \nu = \nu_{\text{cen}})$[2] in Equation 3.36. Even contour lines can easily be drawn into the 2 dimensional parameter plane $|\rho_{A,H}| - \phi_{A,H}$. Once, additional degrees-of-freedom are taken into account, the exercise to find the most likely values for these ratios to a given credibility region of the new parameters becomes more involved. The parameter space can be split into

$$\boldsymbol{\theta} = \boldsymbol{\theta}_1 \otimes \boldsymbol{\theta}_2 = \{\rho_A, \rho_H\} \otimes \{\chi_{\text{fund.}}\}, \tag{A.10}$$

where $\chi_{\text{fund.}}$ contains n parameters, necessary to characterise some non-standard effects. The power correction ratios are defined in terms of the fit parameters $\xi = \xi(\boldsymbol{\theta}_1, \boldsymbol{\theta}_2)$. We then introduce the *reduced* power correction ratio ξ_{ij} to obtain a measure for the relative amount of power corrections at each point of a certain combination of two new-physics parameters $\boldsymbol{\theta}_{2,i}$, $\boldsymbol{\theta}_{2,j}$

$$\xi_{ij}(a,b) = \xi(\boldsymbol{\theta}_{1*}, \boldsymbol{\theta}_{2*}^{\text{red.}}, \boldsymbol{\theta}_{2i} = a, \boldsymbol{\theta}_{2j} = b), \qquad i,j \leq n, \tag{A.11}$$

where $\boldsymbol{\theta}_{1*}$ and $\boldsymbol{\theta}_{2*}^{\text{red.}} \in \{\chi_{\text{fund.}}\} \backslash \{\boldsymbol{\theta}_{2i}, \boldsymbol{\theta}_{2j}\}$ are defined by the best-fit point of the reduced Likelihood

$$\mathcal{L}^{\text{red.}}(\boldsymbol{\theta}_1, \boldsymbol{\theta}_2^{\text{red.}}) \equiv \mathcal{L}(\boldsymbol{\theta}_1, \boldsymbol{\theta}_2^{\text{red.}}, \boldsymbol{\theta}_{2i} = a, \boldsymbol{\theta}_{2j} = b). \tag{A.12}$$

In order to study how the power-suppressed ratio changes within a certain new-physics model, we quote in the phenomenological part of this work (see Chapter 6) the minimal/maximal value for the reduced power-suppressed ratios $\underset{i,j}{min}\ \xi_{ij}(a,b)$, for which $a, b \in 68\%$ CR of the marginalised 2D histograms. These values should be than compared to ξ_3^A at the best-fit point from the SM fit.

[2] For the sake of clearness, we omit the superscript A,H and the argument ν from ξ for the following discussion. The nuisance parameter ν are understood to be evaluated at their central value.

Appendix B

Standard Model fits

B.1 Fit results for other $B \to PP$, PV, VV

We collect here the SM fits of the residual QCD-penguin-dominated decay modes that were not shown in Chapter 5. Several plots reveal that certain observables are unsuitable to constrain the parameters of WA, which is caused by insufficient sensitivity to $\rho_A^{M_1 M_2}$. For instance, the direct CP asymmetry of $B \to K\phi$ is, because of absent tree-level decay amplitudes, predicted to vanish in the SM and cannot be enhanced — even in presents of large power corrections, due to which we observe the less well-defined green contour. In case of the four decay systems $B \to K^{(*)}\eta^{(\prime)}$ the reason for the inability of constraining WA mainly originate from lacking experimental precision and large theoretical uncertainties. The only exception is $B \to K^*\eta'$, for which still five disjoint CRs can be found to explain the data. Contrary to these decay modes, $B_s \to K\pi$ allows for an precise extraction of $\rho_A^{K\pi}$. We already tested in Subsection 5.1.3 that the direct CP asymmetry of $\bar{B}_s \to K^+\pi^-$ can be correctly predicted from a fit of the corresponding decay of the B_d meson and the comparison of their combined contours in Figures B.1 and 5.1 bare similar areas in parameter space. The contours from $B \to K^*\omega$, $B_s \to K^*\phi$, and $B_s \to \phi\phi$ reveal the typical features of two vector mesons in the final state, for which only data of branching and polarisation fractions are available: Two solution with comparably small $|\rho_A|$ at $\phi_A = 0 \pm \delta$ and $\phi_A \simeq \pi \pm \delta$, with some small correction δ.

B.2 Predictions of CP violation in $B \to K^*\phi$, $\bar{B}_s \to \phi\phi$, and $\bar{B}_s \to \bar{K}^{*0}K^{*0}$

We have shown that CP violation in various decay modes can receive significant contributions from the NP scenarios considered in our analysis. Their SM predictions have been obtained from a fit of $\rho_A^{M_1 M_2}$. Apart from the direct and mixing-induced CP asymmetries, we included all available data of each system and summarised the results in

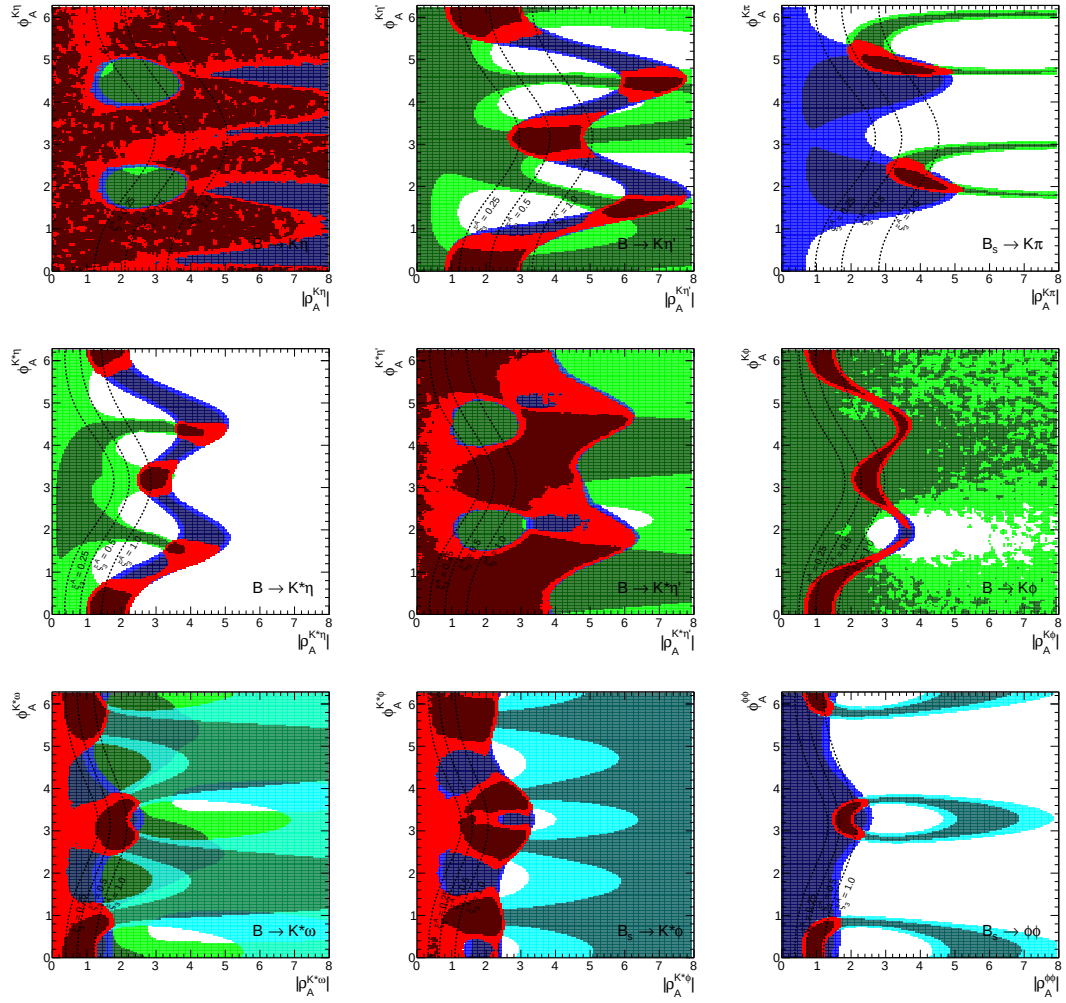

FIGURE B.1: 68% and 95% CRs for the complex parameters $\rho_A^{M_1 M_2}$ for QCD-penguin-dominated B-meson decays $B \to K^{(*)}\eta^{(\prime)}$, $B_s \to K\pi$, $B \to K\phi$, $B \to K^*\omega$, $B_s \to K^*\phi$, and $B_s \to \phi\phi$ in the SM. Allowed regions are separately shown for branching ratios (blue), CP asymmetries (green), polarisation fraction (cyan), and the combination (red). The dashed lines correspond to $\xi_3^A(M_1 M_2) = 0.25\,(0.5,\, 1.0)$.

Table B.1. It turns out that the amount of CP violation in these decays that can be accommodated in the SM is small, due to which we did not indicate their values in our plots.

	ΔS_L	$\Delta S_\perp$	C_L	$C_\perp$
$\bar{B}_s \to \phi\phi$	$-0.03^{+0.00}_{-0.00}$	$+0.04^{+0.00}_{-0.00}$	10^{-3}	10^{-3}
$\bar{B}_s \to \bar{K}^{*0}K^{*0}$	$-0.03^{+0.00}_{-0.02}$	$+0.04^{+0.00}_{-0.00}$	$0.00^{+0.01}_{-0.00}$	10^{-3}
$\bar{B}^0 \to \bar{K}^{*0}\phi$	$[0.01, 0.04]$	$[-0.04, -0.01]$	10^{-3}	10^{-3}
$B^- \to K^{*-}\phi$	–	–	$0.00^{+0.00}_{-0.01}$	$-0.01^{+0.01}_{-0.00}$

TABLE B.1: Predictions for the direct and mixing-induced CP asymmetries in $B \to K^*\phi$, $\bar{B}_s \to \phi\phi$, and $\bar{B}_s \to \bar{K}^{*0}K^{*0}$ from a SM fit.

Appendix C

NLO calculations for the new operators $\mathcal{O}^b = (\bar{s}b)(\bar{b}b)$

This Appendix collects all relevant ADMs and higher-order QCDF corrections, which have been used for the NP scenarios in Chapter 6.3. The SM operator basis is defined in Equation 2.15 for the 4-quark and in Equation 2.19 for the semi-leptonic operators and extended by the $(\bar{s}b)(\bar{b}b)$ operators in Equation 6.23. The full EWH is given as a sum of the individual contributions in Equation 2.14, Equation 2.18 and Equation 6.24

$$\mathcal{H}_{\text{eff}} = \frac{G_F}{\sqrt{2}} \sum_{p=u,c} \lambda_p^s \left(\sum_{i=1}^{10} C_i O_i^{(p)} + C_{7\gamma} O_{7\gamma} + C_{8g} O_{8g} + \sum_{i=11}^{15} \mathcal{C}_i^{(\prime)} \mathcal{O}_i^{(\prime)} + 4 C_{9V} \mathcal{O}_{9V} \right) + \text{h.c.}, \tag{C.1}$$

C.1 Anomalous dimension matrix

To lowest order in $\mathcal{O}(\alpha_s)$ we obtain the self-mixing of the operators $Q_{11} - Q_{15}$ [176]

$$\left[\gamma_{s,cc}^{(0)}\right]_{11-15} = \frac{\alpha_s}{4\pi} \begin{pmatrix} 6 - \frac{6}{N} & 0 & 0 & 0 & 0 \\ 0 & -12C_F & 0 & 0 & 0 \\ 0 & -6 & \frac{6}{N} & 0 & 0 \\ 0 & 0 & 0 & 8C_F & 4C_F \\ 0 & 0 & 0 & C_F & -7C_F \end{pmatrix} \tag{C.2}$$

as well as the self-mixing to the order $\mathcal{O}(\alpha_e)$

$$\left[\gamma_{e,cc}^{(0)}\right]_{11-15} = \frac{\alpha}{4\pi} \begin{pmatrix} \frac{4}{3} & 0 & 0 & 0 & 0 \\ 0 & -\frac{4}{3} & 0 & 0 & 0 \\ 0 & 0 & -\frac{4}{3} & 0 & 0 \\ 0 & 0 & 0 & \frac{-4}{9} & \frac{16}{9} \\ 0 & 0 & 0 & \frac{16}{9} & \frac{-4}{9} \end{pmatrix} \tag{C.3}$$

The ADM, which is responsible for the mixing into the QCD-penguin $Q_3 - Q_6$ and the chromo-magnetic operators are given at lowest order in α_s [168, 176]

$$\left[\gamma^{(0)}_{s,p}\right]_{3-6,11-13} = \frac{\alpha_s}{4\pi}\frac{2}{3}\begin{pmatrix} -\frac{1}{N} & 1 & -\frac{1}{N} & 1 \\ -\frac{1}{N} & 1 & -\frac{1}{N} & 1 \\ 0 & 0 & 0 & 0 \end{pmatrix}, \qquad \left[\gamma^{(0)}_{s,p}\right]_{8g,15} = \frac{\alpha_s}{4\pi}(1) \tag{C.4}$$

and at NLO, we only include the mixing of $Q_{11} - Q_{13}$ into the Standard Model QCD-penguin operators $Q_3 - Q_6$ [176]

$$\left[\gamma^{(1)}_{s,p}\right]_{3-6,11-13} = \frac{1}{2}\left(\frac{\alpha_s}{4\pi}\right)^2$$
$$\begin{pmatrix} 6N_c - \frac{64}{27} - \frac{16}{3N_c} + \frac{172}{27N_c^2} & \frac{352}{27}N_c - \frac{2}{3} - \frac{460}{27N_c} & -6N_c - \frac{244}{27} + \frac{20}{3N_c} - \frac{188}{27N_c^2} & \frac{172}{27}N_c - \frac{2}{3} + \frac{260}{27N_c} \\ -\frac{112}{27} - \frac{356}{27N_c^2} & -\frac{32}{27}N_c + \frac{500}{27N_c} & \frac{140}{27} + \frac{148}{27N_c^2} & \frac{220}{27}N_c - \frac{508}{27N_c} \\ -6N_c + \frac{40}{3N_c} & -\frac{22}{3} & 6N_c + \frac{4}{3N_c} & -\frac{22}{3} \end{pmatrix} \tag{C.5}$$

At last, we need the mixing of $Q_{11}-Q_{13}$ into the Standard Model QED-penguin operators $Q_7 - Q_{10}$ and of Q_{14}, Q_{15} into the electro-magnetic dipole operator [168]

$$\left[\gamma^{(0)}_{e,p}\right]_{7-10,11-13} = -\frac{8}{27}\frac{\alpha}{4\pi}\begin{pmatrix} 1+N_c & 0 & 1+N_c & 0 \\ 1 & 0 & 1 & 0 \\ N_c & 0 & N_c & 0 \end{pmatrix}, \quad \left[\gamma^{(0)}_{e,p}\right]_{7\gamma,14-15} = \frac{\alpha}{4\pi}\begin{pmatrix} -\frac{1}{3}N_c \\ -\frac{1}{3} \end{pmatrix},$$
$$\left[\gamma^{(0)}_{e,p}\right]_{9V,11-13} = \frac{4}{9}\frac{\alpha}{4\pi}\begin{pmatrix} 1+N_c \\ 1 \\ N_c \end{pmatrix}. \tag{C.6}$$

C.2 Hadronic matrix elements

Because we incorporated the RGE for the mixing of the operators $\mathcal{O}_{11-13}$ into the QCD-penguin operators of the SM at next-to leading order precision, we need to take care of next-to leading order corrections to hadronic matrix elements for a proper cancellation of the scale dependence. The decay amplitude $a_{4,6}(M_1M_2)$ receive contributions from penguin topologies parametrised through $P_{4,6}(M_2)$ in Equation 3.22, which get modified by contributions from $\mathcal{C}_{11,12}$

$$\begin{aligned} \delta P_4^p(M_2) &= \frac{C_F\alpha_s}{4\pi N_c}\left(\left[\frac{4}{3}\ln\frac{m_b}{\mu} + \frac{2}{3} - G_{M_2}(1)\right]\mathcal{C}_{11} + \left[\frac{4}{3}\ln\frac{m_b}{\mu} - G_{M_2}(1)\right]\mathcal{C}_{12}\right), \\ \delta P_6^p(M_2) &= \frac{C_F\alpha_s}{4\pi N_c}\left(\left[\frac{4}{3}\ln\frac{m_b}{\mu} + \frac{2}{3} - \hat{G}_{M_2}(1)\right]\mathcal{C}_{11} + \left[\frac{4}{3}\ln\frac{m_b}{\mu} - \hat{G}_{M_2}(1)\right]\mathcal{C}_{12}\right). \end{aligned} \tag{C.7}$$

The definition of the penguin functions $G(s)$ and $\hat{G}(s)$ can be found in [36, 53].

Bibliography

[1] M. Beneke, G. Buchalla, M. Neubert, and C. T. Sachrajda, "QCD factorization for exclusive, nonleptonic B meson decays: General arguments and the case of heavy light final states," *Nucl.Phys.* **B591** (2000) 313–418, arXiv:hep-ph/0006124 [hep-ph].

[2] M. Beneke, T. Huber, and X.-Q. Li, "NNLO vertex corrections to non-leptonic B decays: Tree amplitudes," *Nucl.Phys.* **B832** (2010) 109–151, arXiv:0911.3655 [hep-ph].

[3] **Heavy Flavor Averaging Group** Collaboration, Y. Amhis *et al.*, "Averages of b-hadron, c-hadron, and tau-lepton properties as of early 2012," arXiv:1207.1158 [hep-ex].

[4] P. Ball and R. Zwicky, "New results on $B \to \pi, K, \eta$ decay formfactors from light-cone sum rules," *Phys.Rev.* **D71** (2005) 014015, arXiv:hep-ph/0406232 [hep-ph].

[5] S. Glashow, J. Iliopoulos, and L. Maiani, "Weak Interactions with Lepton-Hadron Symmetry," *Phys.Rev.* **D2** (1970) 1285–1292.

[6] S. Weinberg, "A Model of Leptons," *Phys.Rev.Lett.* **19** (1967) 1264–1266.

[7] A. Salam, "Weak and Electromagnetic Interactions," *Conf.Proc.* **C680519** (1968) 367–377.

[8] P. W. Higgs, "Broken symmetries, massless particles, and gauge fields," *Phys.Lett.* **12** (1964) 132–133.

[9] P. W. Higgs, "Broken Symmetries and the Masses of Gauge Bosons," *Phys.Rev.Lett.* **13** (1964) 508–509.

[10] P. W. Higgs, "Spontaneous Symmetry Breakdown without Massless Bosons," *Phys.Rev.* **145** (1966) 1156–1163.

[11] F. Englert and R. Brout, "Broken Symmetry and the Mass of Gauge Vector Mesons," *Phys.Rev.Lett.* **13** (1964) 321–323.

[12] G. Guralnik, C. Hagen, and T. Kibble, "Global Conservation Laws and Massless Particles," *Phys.Rev.Lett.* **13** (1964) 585–587.

[13] T. Kibble, "Symmetry breaking in non-Abelian gauge theories," *Phys.Rev.* **155** (1967) 1554–1561.

[14] **D0 Collaboration** Collaboration, S. Abachi *et al.*, "Search for high mass top quark production in $p\bar{p}$ collisions at $\sqrt{s} = 1.8$ TeV," *Phys.Rev.Lett.* **74** (1995) 2422–2426, arXiv:hep-ex/9411001 [hep-ex].

[15] **CDF Collaboration** Collaboration, F. Abe *et al.*, "Observation of top quark production in $\bar{p}p$ collisions," *Phys.Rev.Lett.* **74** (1995) 2626–2631, arXiv:hep-ex/9503002 [hep-ex].

[16] **DONUT Collaboration** Collaboration, K. Kodama *et al.*, "Observation of tau neutrino interactions," *Phys.Lett.* **B504** (2001) 218–224, arXiv:hep-ex/0012035 [hep-ex].

[17] **CMS Collaboration** Collaboration, S. Chatrchyan *et al.*, "Observation of a new boson at a mass of 125 GeV with the CMS experiment at the LHC," *Phys.Lett.* **B716** (2012) 30–61, arXiv:1207.7235 [hep-ex].

[18] **ATLAS Collaboration** Collaboration, G. Aad *et al.*, "Observation of a new particle in the search for the Standard Model Higgs boson with the ATLAS detector at the LHC," *Phys.Lett.* **B716** (2012) 1–29, arXiv:1207.7214 [hep-ex].

[19] F. Bezrukov, M. Y. Kalmykov, B. A. Kniehl, and M. Shaposhnikov, "Higgs Boson Mass and New Physics," *JHEP* **1210** (2012) 140, arXiv:1205.2893 [hep-ph].

[20] A. Sakharov, "Violation of CP Invariance, C Asymmetry, and Baryon Asymmetry of the Universe," *Pisma Zh.Eksp.Teor.Fiz.* **5** (1967) 32–35.

[21] K. G. Wilson, "Nonlagrangian models of current algebra," *Phys.Rev.* **179** (1969) 1499–1512.

[22] S. Weinberg, "Phenomenological Lagrangians," *Physica* **A96** (1979) 327.

[23] J. Gasser and H. Leutwyler, "Chiral Perturbation Theory: Expansions in the Mass of the Strange Quark," *Nucl.Phys.* **B250** (1985) 465.

[24] E. Fermi, "An attempt of a theory of β radiation. 1," *Z. Phys.* **88** (1934) 161–177.

[25] V. Cirigliano, G. Ecker, H. Neufeld, A. Pich, and J. Portoles, "Kaon Decays in the Standard Model," *Rev.Mod.Phys.* **84** (2012) 399, arXiv:1107.6001 [hep-ph].

[26] N. Cabibbo, "Unitary Symmetry and Leptonic Decays," *Phys.Rev.Lett.* **10** (1963) 531–533.

[27] M. Kobayashi and T. Maskawa, "CP Violation in the Renormalizable Theory of Weak Interaction," *Prog.Theor.Phys.* **49** (1973) 652–657.

[28] M. Beneke, G. Buchalla, M. Neubert, and C. T. Sachrajda, "QCD factorization for $B \to \pi\pi$ decays: Strong phases and CP violation in the heavy quark limit," *Phys.Rev.Lett.* **83** (1999) 1914–1917, arXiv:hep-ph/9905312 [hep-ph].

[29] M. Beneke, G. Buchalla, M. Neubert, and C. T. Sachrajda, "QCD factorization in $B \to \pi K$, $\pi\pi$ decays and extraction of Wolfenstein parameters," *Nucl.Phys.* **B606** (2001) 245–321, arXiv:hep-ph/0104110 [hep-ph].

[30] D. B. Kaplan, "Five lectures on effective field theory," arXiv:nucl-th/0510023 [nucl-th].

[31] A. Pich, "Effective field theory: Course," arXiv:hep-ph/9806303 [hep-ph].

[32] A. J. Buras, "Weak Hamiltonian, CP violation and rare decays," arXiv:hep-ph/9806471 [hep-ph].

[33] G. Buchalla, A. J. Buras, and M. E. Lautenbacher, "Weak decays beyond leading logarithms," *Rev.Mod.Phys.* **68** (1996) 1125–1144, arXiv:hep-ph/9512380 [hep-ph].

[34] J. Virto, *Topics in Hadronic B Decays*. PhD thesis, 2008. arXiv:0712.3367 [hep-ph].

[35] D. Becirevic, V. Gimenez, G. Martinelli, M. Papinutto, and J. Reyes, "B parameters of the complete set of matrix elements of $\Delta B = 2$ operators from the lattice," *JHEP* **0204** (2002) 025, arXiv:hep-lat/0110091 [hep-lat].

[36] M. Beneke and M. Neubert, "QCD factorization for $B \to PP$ and $B \to PV$ decays," *Nucl.Phys.* **B675** (2003) 333–415, arXiv:hep-ph/0308039 [hep-ph].

[37] N. Cabibbo and L. Maiani, "Two-Body Decays of Charmed Mesons," *Phys.Lett.* **B73** (1978) 418.

[38] D. Fakirov and B. Stech, "F and D Decays," *Nucl.Phys.* **B133** (1978) 315–326.

[39] M. Melcher, *B decays from QCD sum rules*. PhD thesis, 2006. available from: http://dokumentix.ub.uni-siegen.de/opus/volltexte/2006/212/.

[40] A. Khodjamirian, T. Mannel, M. Melcher, and B. Melic, "$B \to \pi\pi$ hadronic amplitudes from QCD light-cone sum rules," *PoS* **HEP2005** (2006) 194.

[41] A. Khodjamirian, T. Mannel, M. Melcher, and B. Melic, "Annihilation effects in $B \to \pi\pi$ from QCD light-cone sum rules," *Phys.Rev.* **D72** (2005) 094012, arXiv:hep-ph/0509049 [hep-ph].

[42] A. J. Buras, R. Fleischer, S. Recksiegel, and F. Schwab, "Anatomy of prominent B and K decays and signatures of CP violating new physics in the electroweak penguin sector," *Nucl.Phys.* **B697** (2004) 133–206, arXiv:hep-ph/0402112 [hep-ph].

[43] R. Fleischer and R. Knegjens, "In Pursuit of New Physics with $B_s^0 \to K^+K^-$," *Eur.Phys.J.* **C71** (2011) 1532, arXiv:1011.1096 [hep-ph].

[44] D. London, J. Matias, and J. Virto, "$B_d^0(t) \to \pi^+\pi^-$ and $B_s^0(t) \to K^+K^-$ decays: A Tool to measure new-physics parameters," *Phys.Rev.* **D71** (2005) 014024, arXiv:hep-ph/0410011 [hep-ph].

[45] S. Descotes-Genon, J. Matias, and J. Virto, "Exploring $B_{(d,s)} \to KK$ decays through flavour symmetries and QCD-factorisation," *Phys.Rev.Lett.* **97** (2006) 061801, arXiv:hep-ph/0603239 [hep-ph].

[46] J. D. Bjorken, "Topics in B Physics," *Nucl.Phys.Proc.Suppl.* **11** (1989) 325–341.

[47] M. J. Dugan and B. Grinstein, "QCD basis for factorization in decays of heavy mesons," *Phys.Lett.* **B255** (1991) 583–588.

[48] M. Beneke and T. Feldmann, "Symmetry breaking corrections to heavy to light B meson form-factors at large recoil," *Nucl.Phys.* **B592** (2001) 3–34, arXiv:hep-ph/0008255 [hep-ph].

[49] J. Charles, A. Le Yaouanc, L. Oliver, O. Pene, and J. Raynal, "Heavy to light form-factors in the final hadron large energy limit,".

[50] V. M. Braun and I. Filyanov, "Conformal Invariance and Pion Wave Functions of Nonleading Twist," *Z.Phys.* **C48** (1990) 239–248.

[51] P. Ball, V. M. Braun, Y. Koike, and K. Tanaka, "Higher twist distribution amplitudes of vector mesons in QCD: Formalism and twist-three distributions," *Nucl.Phys.* **B529** (1998) 323–382, arXiv:hep-ph/9802299 [hep-ph].

[52] A. Grozin and M. Neubert, "Asymptotics of heavy meson form-factors," *Phys.Rev.* **D55** (1997) 272–290, arXiv:hep-ph/9607366 [hep-ph].

[53] M. Beneke, J. Rohrer, and D. Yang, "Branching fractions, polarisation and asymmetries of $B \to VV$ decays," *Nucl.Phys.* **B774** (2007) 64–101, arXiv:hep-ph/0612290 [hep-ph].

[54] M. Bartsch, G. Buchalla, and C. Kraus, "$B \to V_L V_L$ Decays at Next-to-Leading Order in QCD," arXiv:0810.0249 [hep-ph].

[55] A. L. Kagan, "Right-handed currents, CP violation, and $B \to VV$," arXiv:hep-ph/0407076 [hep-ph].

[56] V. Braun, D. Y. Ivanov, and G. Korchemsky, "The B meson distribution amplitude in QCD," *Phys.Rev.* **D69** (2004) 034014, arXiv:hep-ph/0309330 [hep-ph].

[57] M. Beneke and J. Rohrwild, "B meson distribution amplitude from $B \to \gamma l \nu$," *Eur.Phys.J.* **C71** (2011) 1818, arXiv:1110.3228 [hep-ph].

[58] **CLEO Collaboration** Collaboration, T. Browder *et al.*, "Search for $B \to \mu \bar{\nu}_\mu \gamma$ and $B \to e \bar{\nu}_e \gamma$," *Phys.Rev.* **D56** (1997) 11–16.

[59] **BaBar Collaboration** Collaboration, B. Aubert *et al.*, "Search for the radiative leptonic decay $B^+ \to \gamma \ell^+ \nu_l$," arXiv:0704.1478 [hep-ex].

[60] **BaBar Collaboration** Collaboration, B. Aubert *et al.*, "A Model-independent search for the decay $B^+ \to l^+ \bar{\nu}_l \gamma$," *Phys.Rev.* **D80** (2009) 111105, arXiv:0907.1681 [hep-ex].

[61] P. Ball and R. Zwicky, "$B_{d,s} \to \rho, \omega, K^*, \phi$ decay form-factors from light-cone sum rules revisited," *Phys.Rev.* **D71** (2005) 014029, arXiv:hep-ph/0412079 [hep-ph].

[62] **UTFit Collaboration** Collaboration, M. Bona *et al.*, "Fit results from Summer 2013,". available from: http://www.utfit.org.

[63] **Particle Data Group** Collaboration, J. Beringer *et al.*, "Review of particle physics," *Phys. Rev.* **D86** (2012) 010001 and 2013 partial update for the 2014 edition.

[64] S. Bethke, "The 2009 World Average of α_s," *Eur.Phys.J.* **C64** (2009) 689–703, arXiv:0908.1135 [hep-ph].

[65] **CDF Collaboration, D0 Collaboration** Collaboration, T. Aaltonen *et al.*, "Combination of the top-quark mass measurements from the Tevatron collider," *Phys.Rev.* **D86** (2012) 092003, arXiv:1207.1069 [hep-ex].

[66] M. Beneke and S. Jäger, "Spectator scattering at NLO in non-leptonic B decays: Leading penguin amplitudes," *Nucl.Phys.* **B768** (2007) 51–84, arXiv:hep-ph/0610322 [hep-ph].

[67] M. Beneke and M. Neubert, "Flavor singlet B decay amplitudes in QCD factorization," *Nucl.Phys.* **B651** (2003) 225–248, arXiv:hep-ph/0210085 [hep-ph].

[68] A. Bharucha, "Two-loop Corrections to the B $\to \pi$ Form Factor from QCD Sum Rules on the Light-Cone and $|V_{ub}|$," *JHEP* **1205** (2012) 092, arXiv:1203.1359 [hep-ph].

[69] G. Duplancic and B. Melic, "B, $B_s \to$ K form factors: An Update of light-cone sum rule results," *Phys.Rev.* **D78** (2008) 054015, arXiv:0805.4170 [hep-ph].

[70] P. Ball, V. Braun, and A. Lenz, "Higher-twist distribution amplitudes of the K meson in QCD," *JHEP* **0605** (2006) 004, arXiv:hep-ph/0603063 [hep-ph].

[71] P. Ball, G. W. Jones, and R. Zwicky, "$B \to V\gamma$ beyond QCD factorisation," *Phys.Rev.* **D75** (2007) 054004, arXiv:hep-ph/0612081 [hep-ph].

[72] P. Ball, V. Braun, and A. Lenz, "Twist-4 distribution amplitudes of the K^* and ϕ mesons in QCD," *JHEP* **0708** (2007) 090, arXiv:0707.1201 [hep-ph].

[73] R. Fleischer and T. Mannel, "Constraining the CKM angle γ and penguin contributions through combined $B \to \pi K$ branching ratios," *Phys.Rev.* **D57** (1998) 2752–2759, arXiv:hep-ph/9704423 [hep-ph].

[74] L. Hofer, D. Scherer, and L. Vernazza, "$B_s \to \phi\rho^0$ and $B_s \to \phi\pi^0$ as a handle on isospin-violating New Physics," *JHEP* **1102** (2011) 080, arXiv:1011.6319 [hep-ph].

[75] Y. Nir, "CP violation in meson decays," arXiv:hep-ph/0510413 [hep-ph].

[76] **LHCb** Collaboration, R. Aaij *et al.*, "First measurement of time-dependent *CP* violation in $B_s^0 \to K^+K^-$ decays," *JHEP* **1310** (2013) 183, arXiv:1308.1428 [hep-ex].

[77] **Belle Collaboration** Collaboration, K. Chen *et al.*, "Measurement of branching fractions and polarization in $B \to \phi K^{(*)}$ decays," *Phys.Rev.Lett.* **91** (2003) 201801, arXiv:hep-ex/0307014 [hep-ex].

[78] **CDF Collaboration** Collaboration, D. Acosta *et al.*, "First evidence for $B_s^0 \to \phi\phi$ decay and measurements of branching ratio and A_{CP} for $B^+ \to \phi K^+$," *Phys.Rev.Lett.* **95** (2005) 031801, arXiv:hep-ex/0502044 [hep-ex].

[79] **BaBar Collaboration** Collaboration, J. Lees *et al.*, "Study of CP violation in Dalitz-plot analyses of $B^0 \to K^+K^-K_S^0$, $B^+ \to K^+K^-K^+$, and $B^+ \to K_S^0K_S^0K^+$," *Phys.Rev.* **D85** (2012) 112010, arXiv:1201.5897 [hep-ex].

[80] **LHCb collaboration** Collaboration, R. Aaij *et al.*, "Measurement of the charge asymmetry in $B^\pm \to \phi K^\pm$ and search for $B^\pm \to \phi\pi^\pm$ decays," *Phys.Lett.* **B728** (2014) 85–94, arXiv:1309.3742 [hep-ex].

[81] **Belle Collaboration** Collaboration, V. Chobanova *et al.*, "Measurement of Branching Fractions and CP Asymmetries in $B \to \omega K$ Decays and First Evidence of CP Violation in $B^0 \to \omega K^0_S$," arXiv:1311.6666 [hep-ex].

[82] **BaBar Collaboration** Collaboration, B. Aubert *et al.*, "Branching fraction and CP-violation charge asymmetry measurements for B-meson decays to $\eta K^\pm$, $\eta\pi^\pm$, $\eta' K$, $\eta'\pi^\pm$, ωK, and $\omega\pi^\pm$," *Phys.Rev.* **D76** (2007) 031103, arXiv:0706.3893 [hep-ex].

[83] **BaBar Collaboration** Collaboration, B. Aubert *et al.*, "Time-Dependent and Time-Integrated Angular Analysis of $B \to \phi K_s \pi^0$ and $B \to \phi K^+\pi^-$," *Phys.Rev.* **D78** (2008) 092008, arXiv:0808.3586 [hep-ex].

[84] **Belle Collaboration** Collaboration, M. Prim *et al.*, "Angular analysis of $B^0 \to \phi K^*$ decays and search for CP violation at Belle," *Phys.Rev.* **D88** (2013) 072004, arXiv:1308.1830 [hep-ex].

[85] **LHCb Collaboration** Collaboration, R. Aaij *et al.*, "First observation of the decay $B^0_s \to K^{*0}\bar{K}^{*0}$," *Phys.Lett.* **B709** (2012) 50–58, arXiv:1111.4183 [hep-ex].

[86] T. Aushev, W. Bartel, A. Bondar, J. Brodzicka, T. Browder, *et al.*, "Physics at Super B Factory," arXiv:1002.5012 [hep-ex].

[87] **Belle-II Collaboration** Collaboration, T. Abe *et al.*, "Belle II Technical Design Report," arXiv:1011.0352 [physics.ins-det].

[88] M. Beneke, "Corrections to $\sin(2\beta)$ from CP asymmetries in $B^0 \to (\pi^0, \rho^0, \eta, \eta', \omega, \phi)K_S$ decays," *Phys.Lett.* **B620** (2005) 143–150, arXiv:hep-ph/0505075 [hep-ph].

[89] G. Buchalla, G. Hiller, Y. Nir, and G. Raz, "The Pattern of CP asymmetries in $b \to s$ transitions," *JHEP* **0509** (2005) 074, arXiv:hep-ph/0503151 [hep-ph].

[90] **LHCb Collaboration** Collaboration, R. Aaij *et al.*, "Implications of LHCb measurements and future prospects," *Eur.Phys.J.* **C73** (2013) 2373, arXiv:1208.3355 [hep-ex].

[91] R. Fleischer and R. Knegjens, "Effective Lifetimes of B_s Decays and their Constraints on the B^0_s-$\bar{B}^0_s$ Mixing Parameters," *Eur.Phys.J.* **C71** (2011) 1789, arXiv:1109.5115 [hep-ph].

[92] K. De Bruyn, R. Fleischer, R. Knegjens, P. Koppenburg, M. Merk, *et al.*, "Branching Ratio Measurements of B_s Decays," *Phys.Rev.* **D86** (2012) 014027, arXiv:1204.1735 [hep-ph].

[93] **LHCb Collaboration** Collaboration, R. Aaij *et al.*, "Measurement of the $B^0_s \to \mu^+\mu^-$ branching fraction and search for $B^0 \to \mu^+\mu^-$ decays at the LHCb experiment," *Phys.Rev.Lett.* **111** (2013) 101805, arXiv:1307.5024 [hep-ex].

[94] **CMS Collaboration** Collaboration, S. Chatrchyan *et al.*, "Measurement of the $B_s \to \mu^+\mu^-$ branching fraction and search for $B^0 \to \mu^+\mu^-$ with the CMS Experiment," *Phys.Rev.Lett.* **111** (2013) 101804, arXiv:1307.5025 [hep-ex].

[95] **BELLE Collaboration** Collaboration, J.-T. Wei *et al.*, "Measurement of the Differential Branching Fraction and Forward-Backword Asymmetry for $B \to K^{(*)}\ell^+\ell^-$," *Phys.Rev.Lett.* **103** (2009) 171801, arXiv:0904.0770 [hep-ex].

[96] **BABAR Collaboration** Collaboration, J. Lees *et al.*, "Measurement of Branching Fractions and Rate Asymmetries in the Rare Decays $B \to K^{(*)}\ell^+\ell^-$," *Phys.Rev.* **D86** (2012) 032012, arXiv:1204.3933 [hep-ex].

[97] **CDF Collaboration** Collaboration, H. Miyaki, "Branching Ratio Measurements of Exclusive $b \to s\mu^+\mu^-$ Decays and Angular Analysis in $B \to K^*\mu^+\mu^-$ Decays," (2012) . CDF public note 10894, available from: http://www-cdf.fnal.gov/physics/new/bottom/bottom.html.

[98] **LHCb Collaboration** Collaboration, R. Aaij *et al.*, "Differential branching fraction and angular analysis of the $B^+ \to K^+\mu^+\mu^-$ decay," *JHEP* **1302** (2013) 105, arXiv:1209.4284 [hep-ex].

[99] **LHCb Collaboration** Collaboration, R. Aaij *et al.*, "Measurement of the *CP* asymmetry in $B^+ \to K^+\mu^+\mu^-$ decays," *Phys.Rev.Lett.* **111** (2013) 151801, arXiv:1308.1340 [hep-ex].

[100] **LHCb Collaboration** Collaboration, R. Aaij *et al.*, "Differential branching fraction and angular analysis of the decay $B^0 \to K^{*0}\mu^+\mu^-$," arXiv:1304.6325 [hep-ex].

[101] **CMS Collaboration** Collaboration, S. Chatrchyan *et al.*, "Angular analysis and branching fraction measurement of the decay $B^0 \to K^{*0}\mu^+\mu^-$," *Phys.Lett.* **B727** (2013) 77–100, arXiv:1308.3409 [hep-ex].

[102] **ATLAS Collaboration** Collaboration, G. Aad *et al.*, "Angular Analysis of $B_d \to K^{*0}\mu^+\mu^-$ with the ATLAS Experiment," ATLAS-CONF-2013-038, ATLAS-COM-CONF-2013-043.

[103] **LHCb Collaboration** Collaboration, R. Aaij *et al.*, "Measurement of the CP asymmetry in $B^0 \to K^{*0}\mu^+\mu^-$ decays," *Phys. Rev. Lett. 110,* **031801** (2013) 031801, arXiv:1210.4492 [hep-ex].

[104] **LHCb Collaboration** Collaboration, R. Aaij *et al.*, "Measurement of form-factor independent observables in the decay $B^0 \to K^{*0}\mu^+\mu^-$," *Phys.Rev.Lett.* **111** (2013) 191801, arXiv:1308.1707 [hep-ex].

[105] F. Beaujean, C. Bobeth, D. van Dyk, and C. Wacker, "Bayesian Fit of Exclusive $b \to s\bar{\ell}\ell$ Decays: The Standard Model Operator Basis," *JHEP* **1208** (2012) 030, arXiv:1205.1838 [hep-ph].

[106] C. Bobeth, G. Hiller, and D. van Dyk, "More Benefits of Semileptonic Rare B Decays at Low Recoil: CP Violation," *JHEP* **1107** (2011) 067, arXiv:1105.0376 [hep-ph].

[107] C. Bobeth, G. Hiller, D. van Dyk, and C. Wacker, "The Decay $B \to K\ell^+\ell^-$ at Low Hadronic Recoil and Model-Independent $\Delta B = 1$ Constraints," *JHEP* **1201** (2012) 107, arXiv:1111.2558 [hep-ph].

[108] R. R. Horgan, Z. Liu, S. Meinel, and M. Wingate, "Lattice QCD calculation of form factors describing the rare decays $B \to K^* \ell^+ \ell^-$ and $B_s \to \phi \ell^+ \ell^-$," arXiv:1310.3722 [hep-lat].

[109] R. R. Horgan, Z. Liu, S. Meinel, and M. Wingate, "Calculation of $B^0 \to K^{*0} \mu^+ \mu^-$ and $B_s^0 \to \phi \mu^+ \mu^-$ observables using form factors from lattice QCD," arXiv:1310.3887 [hep-ph].

[110] F. Beaujean, C. Bobeth, and D. van Dyk, "Comprehensive Bayesian Analysis of Rare (Semi)leptonic and Radiative B Decays," arXiv:1310.2478 [hep-ph].

[111] A. Khodjamirian, T. Mannel, A. Pivovarov, and Y.-M. Wang, "Charm-loop effect in $B \to K^{(*)} \ell^+ \ell^-$ and $B \to K^* \gamma$," *JHEP* **1009** (2010) 089, arXiv:1006.4945 [hep-ph].

[112] A. Khodjamirian, T. Mannel, and Y. Wang, "$B \to K \ell^+ \ell^-$ decay at large hadronic recoil," *JHEP* **1302** (2013) 010, arXiv:1211.0234 [hep-ph].

[113] **LHCb collaboration** Collaboration, R. Aaij *et al.*, "Differential branching fractions and isospin asymmetries of $B \to K^{(*)} \mu^+ \mu^-$ decays," arXiv:1403.8044 [hep-ex].

[114] M. Beneke, T. Feldmann, and D. Seidel, "Systematic approach to exclusive $B \to V \ell^+ \ell^-$, $V \gamma$ decays," *Nucl.Phys.* **B612** (2001) 25–58, arXiv:hep-ph/0106067 [hep-ph].

[115] C. Bobeth, G. Hiller, and G. Piranishvili, "Angular distributions of $\bar{B} \to \bar{K} \bar{\ell} \ell$ decays," *JHEP* **0712** (2007) 040, arXiv:0709.4174 [hep-ph].

[116] C. Bouchard, G. P. Lepage, C. Monahan, H. Na, and J. Shigemitsu, "Rare decay $B \to K \ \ell^+ \ell^-$ form factors from lattice QCD," *Phys.Rev.* **D88** (2013) 054509, arXiv:1306.2384 [hep-lat].

[117] C. Bouchard, G. P. Lepage, C. Monahan, H. Na, and J. Shigemitsu, "Standard Model predictions for $B \to K \ell^+ \ell^-$ with form factors from lattice QCD," arXiv:1306.0434 [hep-ph].

[118] C. Bobeth, G. Hiller, and D. van Dyk, "General Analysis of $\bar{B} \to \bar{K}^{(*)} \ell^+ \ell^-$ Decays at Low Recoil," *Phys.Rev.* **D87** (2013) 034016, arXiv:1212.2321 [hep-ph].

[119] U. Egede, T. Hurth, J. Matias, M. Ramon, and W. Reece, "New physics reach of the decay mode $\bar{B} \to \bar{K}^{*0} \ell^+ \ell^-$," *JHEP* **1010** (2010) 056, arXiv:1005.0571 [hep-ph].

[120] F. Kruger, L. M. Sehgal, N. Sinha, and R. Sinha, "Angular distribution and CP asymmetries in the decays $\bar{B} \to K^- \pi^+ e^- e^+$ and $\bar{B} \to \pi^- \pi^+ e^- e^+$," *Phys.Rev.* **D61** (2000) 114028, arXiv:hep-ph/9907386 [hep-ph].

[121] S. Descotes-Genon, T. Hurth, J. Matias, and J. Virto, "Optimizing the basis of $B \to K^* \ell^+ \ell^-$ observables in the full kinematic range," *JHEP* **1305** (2013) 137, arXiv:1303.5794 [hep-ph].

[122] W. Altmannshofer and D. M. Straub, "New physics in $B \to K^* \mu\mu$?," *Eur.Phys.J.* **C73** (2013) 2646, arXiv:1308.1501 [hep-ph].

[123] A. Lenz, U. Nierste, J. Charles, S. Descotes-Genon, A. Jantsch, *et al.*, "Anatomy of New Physics in $B - \bar{B}$ mixing," *Phys.Rev.* **D83** (2011) 036004, arXiv:1008.1593 [hep-ph].

[124] S. Baek, C.-W. Chiang, and D. London, "The $B \to \pi K$ Puzzle: 2009 Update," *Phys.Lett.* **B675** (2009) 59–63, arXiv:0903.3086 [hep-ph].

[125] M. Ciuchini, E. Franco, G. Martinelli, M. Pierini, and L. Silvestrini, "Searching For New Physics With $B \to K\pi$ Decays," *Phys.Lett.* **B674** (2009) 197–203, arXiv:0811.0341 [hep-ph].

[126] M. Gronau and J. L. Rosner, "Rates and asymmetries in $B \to K\pi$ decays," *Phys.Lett.* **B572** (2003) 43–49, arXiv:hep-ph/0307095 [hep-ph].

[127] S. Baek and D. London, "Is There Still a $B \to \pi K$ Puzzle?," *Phys.Lett.* **B653** (2007) 249–253, arXiv:hep-ph/0701181 [hep-ph].

[128] Q. Chang, X.-W. Cui, L. Han, and Y.-D. Yang, "Revisiting the Annihilation Corrections in Non-leptonic $\bar{B}_s^0$ Decays within QCD Factorization," *Phys.Rev.* **D86** (2012) 054016, arXiv:1205.4325 [hep-ph].

[129] M. Beneke, "Charmless Hadronic B Decays — Theory Status," (2014) . Talk given at the "3rd KEK Flavor Factory Workshop", held Tsukuba, Japan, Februrary 13 – 15, 2014, available from: http://kds.kek.jp/conferenceOtherViews.py?view=standard&confId=13910.

[130] **BaBar Collaboration** Collaboration, B. Aubert *et al.*, "Measurement of time dependent CP asymmetry parameters in B^0 meson decays to ωK_S^0, $\eta' K^0$, and $\pi^0 K_S^0$," *Phys.Rev.* **D79** (2009) 052003, arXiv:0809.1174 [hep-ex].

[131] **Belle Collaboration** Collaboration, Y. Chao *et al.*, "Measurements of time-dependent CP violation in $B^0 \to \omega K_S^0$, $f_0(980) K_S^0$, $K_S^0 \pi^0$ and $K^+ K^- K_S^0$ decays," *Phys.Rev.* **D76** (2007) 091103, arXiv:hep-ex/0609006 [hep-ex].

[132] **BaBar Collaboration** Collaboration, B. Aubert *et al.*, "Amplitude Analysis of the $B^\pm \to \phi K^*(892)^\pm$ Decay," *Phys.Rev.Lett.* **99** (2007) 201802, arXiv:0705.1798 [hep-ex].

[133] **BELLE Collaboration** Collaboration, K.-F. Chen *et al.*, "Measurement of polarization and triple-product correlations in $B \to \phi K^*$ decays," *Phys.Rev.Lett.* **94** (2005) 221804, arXiv:hep-ex/0503013 [hep-ex].

[134] M. Beneke, "Hadronic B decays," *eConf* **C0610161** (2006) 030, arXiv:hep-ph/0612353 [hep-ph].

[135] H. J. Lipkin, "Is observed direct CP violation in $B_d \to K^+ \pi^-$ due to new physics? Check standard model prediction of equal violation in $B_s \to K^- \pi^+$," *Phys.Lett.* **B621** (2005) 126–132, arXiv:hep-ph/0503022 [hep-ph].

[136] **CDF Collaboration** Collaboration, T. A. Aaltonen *et al.*, "Measurements of Direct CP-Violating Asymmetries in Charmless Decays of Bottom Baryons," arXiv:1403.5586 [hep-ex].

[137] **LHCb collaboration** Collaboration, R. Aaij *et al.*, "First observation of CP violation in the decays of B_s^0 mesons," *Phys.Rev.Lett.* **110** no. 22, (2013) 221601, arXiv:1304.6173 [hep-ex].

[138] H.-n. Li and S. Mishima, "Possible resolution of the $B \to \pi\pi$, πK puzzles," *Phys.Rev.* **D83** (2011) 034023, arXiv:0901.1272 [hep-ph].

[139] H.-Y. Cheng and C.-K. Chua, "Resolving B-CP Puzzles in QCD Factorization," *Phys.Rev.* **D80** (2009) 074031, arXiv:0908.3506 [hep-ph].

[140] K. Wang and G. Zhu, "Flavor dependence of annihilation parameters in QCD factorization," arXiv:1304.7438 [hep-ph].

[141] T. Feldmann, M. Jung, and T. Mannel, "Is there a non-Standard-Model contribution in non-leptonic $b \to s$ decays?," *JHEP* **0808** (2008) 066, arXiv:0803.3729 [hep-ph].

[142] P. Langacker and M. Plumacher, "Flavor changing effects in theories with a heavy Z' boson with family nonuniversal couplings," *Phys.Rev.* **D62** (2000) 013006, arXiv:hep-ph/0001204 [hep-ph].

[143] P. Langacker, "The Physics of Heavy Z' Gauge Bosons," *Rev.Mod.Phys.* **81** (2009) 1199–1228, arXiv:0801.1345 [hep-ph].

[144] A. J. Buras, F. De Fazio, and J. Girrbach, "The Anatomy of Z' and Z with Flavour Changing Neutral Currents in the Flavour Precision Era," *JHEP* **1302** (2013) 116, arXiv:1211.1896 [hep-ph].

[145] V. Barger, C.-W. Chiang, P. Langacker, and H.-S. Lee, "Solution to the $B \to \pi K$ puzzle in a flavor-changing Z-prime model," *Phys.Lett.* **B598** (2004) 218–226, arXiv:hep-ph/0406126 [hep-ph].

[146] W. Altmannshofer, P. Paradisi, and D. M. Straub, "Model-Independent Constraints on New Physics in $b \to s$ Transitions," *JHEP* **1204** (2012) 008, arXiv:1111.1257 [hep-ph].

[147] S. Descotes-Genon, J. Matias, and J. Virto, "Understanding the $B \to K^* \mu^+ \mu^-$ Anomaly," *Phys.Rev.* **D88** (2013) 074002, arXiv:1307.5683 [hep-ph].

[148] **CDF Collaboration** Collaboration, T. Aaltonen *et al.*, "Measurements of Direct CP Violating Asymmetries in Charmless Decays of Strange Bottom Mesons and Bottom Baryons," *Phys.Rev.Lett.* **106** (2011) 181802, arXiv:1103.5762 [hep-ex].

[149] **LHCb Collaboration** Collaboration, R. Aaij *et al.*, "Measurement of b-hadron branching fractions for two-body decays into charmless charged hadrons," *JHEP* **1210** (2012) 037, arXiv:1206.2794 [hep-ex].

[150] Y. Grossman, M. Neubert, and A. L. Kagan, "Trojan penguins and isospin violation in hadronic B decays," *JHEP* **9910** (1999) 029, arXiv:hep-ph/9909297 [hep-ph].

[151] D. Atwood and G. Hiller, "Implications of nonstandard CP violation in hadronic B decays," arXiv:hep-ph/0307251 [hep-ph].

[152] G. Buchalla, G. Hiller, and G. Isidori, "Phenomenology of nonstandard Z couplings in exclusive semileptonic $b \to s$ transitions," *Phys.Rev.* **D63** (2000) 014015, arXiv:hep-ph/0006136 [hep-ph].

[153] O. Eberhardt, G. Herbert, H. Lacker, A. Lenz, A. Menzel, *et al.*, "Impact of a Higgs boson at a mass of 126 GeV on the standard model with three and four fermion generations," *Phys.Rev.Lett.* **109** (2012) 241802, arXiv:1209.1101 [hep-ph].

[154] E. Lunghi, A. Masiero, I. Scimemi, and L. Silvestrini, "$B \to X_s \ell^+ \ell^-$-decays in supersymmetry," *Nucl.Phys.* **B568** (2000) 120–144, arXiv:hep-ph/9906286 [hep-ph].

[155] R. Contino, T. Kramer, M. Son, and R. Sundrum, "Warped/composite phenomenology simplified," *JHEP* **0705** (2007) 074, arXiv:hep-ph/0612180 [hep-ph].

[156] M. Bauer, S. Casagrande, U. Haisch, and M. Neubert, "Flavor Physics in the Randall-Sundrum Model: II. Tree-Level Weak-Interaction Processes," *JHEP* **1009** (2010) 017, arXiv:0912.1625 [hep-ph].

[157] Y. Grossman, Y. Nir, and R. Rattazzi, "CP violation beyond the standard model," *Adv.Ser.Direct.High Energy Phys.* **15** (1998) 755–794, arXiv:hep-ph/9701231 [hep-ph].

[158] T. Inami and C. Lim, "Effects of Superheavy Quarks and Leptons in Low-Energy Weak Processes $K_L \to \mu\bar{\mu}$, $K^+ \to \pi^+ \nu\bar{\nu}$, and K^0-$\bar{K}^0$," *Prog.Theor.Phys.* **65** (1981) 297.

[159] G. Isidori and A. Retico, "Scalar flavor changing neutral currents in the large $\tan\beta$ limit," *JHEP* **0111** (2001) 001, arXiv:hep-ph/0110121 [hep-ph].

[160] A. J. Buras, P. H. Chankowski, J. Rosiek, and L. Slawianowska, "$\Delta M_{d,s}, B^0_{d,s} \to \mu^+\mu^-$ and $B \to X_s\gamma$ in supersymmetry at large $\tan\beta$," *Nucl.Phys.* **B659** (2003) 3, arXiv:hep-ph/0210145 [hep-ph].

[161] V. Barger, C.-W. Chiang, P. Langacker, and H.-S. Lee, "Z' mediated flavor changing neutral currents in B meson decays," *Phys.Lett.* **B580** (2004) 186–196, arXiv:hep-ph/0310073 [hep-ph].

[162] P. K. Das and K.-C. Yang, "Data for polarization in charmless $B \to \phi K^*$: A Signal for new physics?," *Phys.Rev.* **D71** (2005) 094002, arXiv:hep-ph/0412313 [hep-ph].

[163] J.-F. Cheng, C.-S. Huang, and X.-H. Wu, "CP asymmetries in $B \to \phi K_S$ and $B \to \eta' K_S$ in MSSM," *Nucl.Phys.* **B701** (2004) 54–86, arXiv:hep-ph/0404055 [hep-ph].

[164] Y. Wu and C. Zhuang, "Exclusive $B \to PV$ Decays and CP Violation in the General two-Higgs-doublet Model," *Phys.Rev.* **D75** (2007) 115006, arXiv:hep-ph/0701072 [hep-ph].

[165] H. Hatanaka and K.-C. Yang, "Pseudoscalar and scalar operators of Higgs-penguins in the MSSM and $B \to \phi K^*$, $K\eta'$ decays," *Phys.Rev.* **D77** (2008) 035013, arXiv:0711.3086 [hep-ph].

[166] Q. Chang, X.-Q. Li, and Y.-D. Yang, "Revisiting $B \to \pi K, \pi K^*$ and ρK Decays: Direct CP Violation and Implication for New Physics," *JHEP* **0809** (2008) 038, arXiv:0807.4295 [hep-ph].

[167] S.-S. Bao, F. Su, Y.-L. Wu, and C. Zhuang, "Exclusive $B \to VV$ Decays and CP Violation in the General two-Higgs-doublet Model," *Phys.Rev.* **D77** (2008) 095004, arXiv:0801.2596 [hep-ph].

[168] G. Hiller and F. Kruger, "More model independent analysis of $b \to s$ processes," *Phys.Rev.* **D69** (2004) 074020, arXiv:hep-ph/0310219 [hep-ph].

[169] A. Datta, M. Duraisamy, and D. Ghosh, "Explaining the $B \to K^* \mu^+ \mu^-$ data with scalar interactions," arXiv:1310.1937 [hep-ph].

[170] M. Beneke, X.-Q. Li, and L. Vernazza, "Hadronic B decays in the MSSM with large $\tan(\beta)$," *Eur.Phys.J.* **C61** (2009) 429–438, arXiv:0901.4841 [hep-ph].

[171] C. Bobeth and U. Haisch, "New Physics in Γ_{12}^s: $(\bar{s}b)(\bar{\tau}\tau)$ Operators," *Acta Phys.Polon.* **B44** (2013) 127–176, arXiv:1109.1826 [hep-ph].

[172] M. König, M. Neubert, and D. M. Straub, "Dipole operator constraints on composite Higgs models," arXiv:1403.2756 [hep-ph].

[173] D. V. Hinkley, "On the ratio of two correlated normal random variables," *Biometrika* **56** no. 3, (1969) 635–639.

[174] A. Caldwell, D. Kollar, and K. Kroninger, "BAT: The Bayesian Analysis Toolkit," *Comput.Phys.Commun.* **180** (2009) 2197–2209, arXiv:0808.2552 [physics.data-an].

[175] F. Beaujean, A. Caldwell, D. Kollar, and K. Kroninger, "p-Values for model evaluation," *Phys.Rev.* **D83** (2011) 012004, arXiv:1011.1674 [physics.data-an].

[176] A. J. Buras, M. Misiak, and J. Urban, "Two loop QCD anomalous dimensions of flavor changing four quark operators within and beyond the standard model," *Nucl.Phys.* **B586** (2000) 397–426, arXiv:hep-ph/0005183 [hep-ph].

Acknowledgements

During the last three years at the Excellence Cluster of Universe I got the opportunity to work in a stimulating environment that allowed me to self-determined pursue my scientific research in a field I was interested in — always accompanied by a continuous profound support which I do not admit as self-evident in a typical professional life. Therefor, I am honestly grateful to my supervisor Martin Gorbahn. He always gave me the possibility to discuss about physics and enriched this time of my life with profound advises, which did not only exhibit the quality of the present thesis. I also like to thank him for giving me the chance of travelling to several fascinating conferences I gladly remember. Special thanks goes to my collaborator Christoph Bobeth for his patient and sustained kind of explaining me his insights of particle physics and his tirelessly effort he put into the significant improvement of this work through suitable comments. I am truly impressed of Martins and Christoph's fundamental and clear understanding of physics, which both of them always shared with me in lively discussions to enlighten my rather dim ideas. I like to thank them for the fruitful collaboration. I also like to thank Frederik Beaujean, Christoph Bobeth, and Daniel Greenwald for painful proofreading of my thesis, who helped me to remove many small errors from the manuscript and to improve its comprehensibility. Together with Joachim Brod, Emanuel Stamou, Sandro Casagrande, David Straub, Claudia Hagedorn, Christoph Niehoff, Peter Stangl, Jovan Mitrevski, Margarita Petkova, and Stefan Jahn, they were great colleagues and floor mates, with whom I enjoyed many discussions during lunch time and coffee breaks — also on topics that were not related to physics. During my engagements as tutor for the courses in Statistical Mechanics by Prof. Martin Zacharias and in Quantum Field Theory by Prof. Alejandro Ibarra, I had the pleasure of accompanying enquiring students in parts of their academic education in theoretical physics; thereby gaining myself deeper insights through active discussions and sensible comments. I like to thank these two for their confidence and the ability of being part of these successful lectures. I especially enjoyed the mutual organisation and preparation of the QFT tutorial with Alejandro, Emanuel, and Mathias Garny. I further like to express my gratitude to the administration of the Excellence Cluster of Universe for the pleasant surrounding, the organisation of countless stimulating scientific events, and not at least for taking over so many necessary, but painful administrative work. I am especially thankful to Dr. Birgit Schaffhauser whose insistent effort guaranteed my financial funding during the last period of this work as well as Andreas Weiss for his broad and helpful IT support. Last but not least many thanks goes to my friends, my family, my parents and my brother, who contributed individually in their personal way to the success of this work. In particular, I am deeply grateful for the endless patience and lovingly support of my wife, Janine, and my two children.